SIMULATION OF THE SEISMIC PERFORMANCE OF NONSTRUCTURAL SYSTEMS

NEES Nonstructural

EXPERIMENTAL SEISMIC EVALUATION, MODEL PARAMETERIZATION, AND EFFECTS OF COLD-FORMED STEEL-FRAMED GYPSUM PARTITION WALLS ON THE SEISMIC PERFORMANCE OF AN ESSENTIAL FACILITY

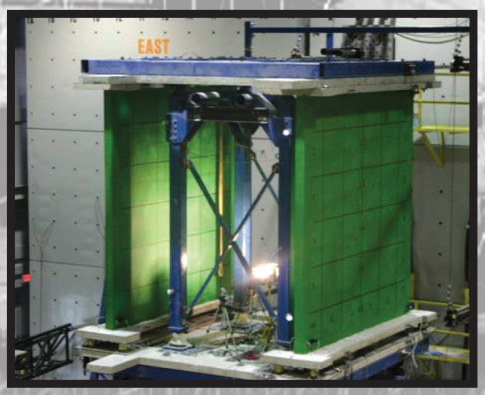

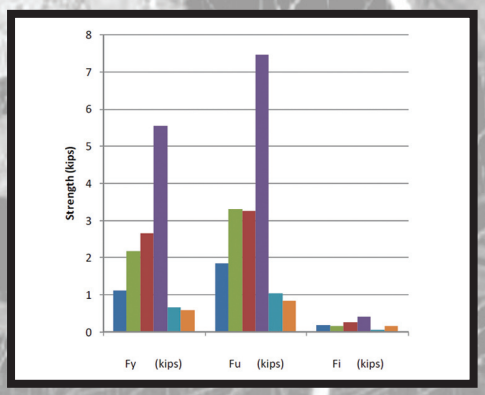

By
Ryan D. Davies, Rodrigo Retamales, Gilberto Mosqueda and Andre Filiatrault

Technical Report MCEER-11-0005 ■ October 12, 2011

This research was conducted at the University at Buffalo, State University of New York and was supported by the National Science Foundation under Grant No. CMMI-0721399.

Sponsored by the
National Science Foundation
NSF Grant Number CMMI-0721399

Project Title
Simulation of the Seismic Performance of
Nonstructural Systems

Project Team
University of Nevada Reno
University at Buffalo, State University of New York
Georgia Institute of Technology
Rutherford & Chekene
University of California, San Diego
Consortium of Universities for Research in Earthquake Engineering (CUREE)

Web Site
http://www.nees-nonstructural.org

DISCLAIMER

This report is based upon work supported by the National Science Foundation under Grant No. CMMI-0721399. Any opinions, findings, and conclusions or recommendations expressed in this material are those of the investigators and do not necessarily reflect the views of MCEER, the National Science Foundation, or other sponsors.

Experimental Seismic Evaluation, Model Parameterization, and Effects of Cold-Formed Steel-Framed Gypsum Partition Walls on the Seismic Performance of an Essential Facility

by

Ryan D. Davies,[1] Rodrigo Retamales,[2] Gilberto Mosqueda[3] and Andre Filiatrault[4]

Publication Date: October 12, 2011
Submittal Date: September 13, 2010

Technical Report MCEER-11-0005

NSF Grant Number CMMI-0721399

1 Design Engineer, Ehlert/Bryan, Inc.; former Graduate Student, Department of Civil, Structural and Environmental Engineering, University at Buffalo, State University of New York
2 Senior Structural Engineer, Ruben Boroschek & Associates; former Post Doctoral Researcher, Department of Civil, Structural and Environmental Engineering, University at Buffalo, State University of New York
3 Associate Professor, Department of Civil, Structural and Environmental Engineering, University at Buffalo, State University of New York
4 Professor, Department of Civil, Structural and Environmental Engineering, University at Buffalo, State University of New York

MCEER
University at Buffalo, State University of New York
Red Jacket Quadrangle, Buffalo, NY 14261
Phone: (716) 645-3391; Fax (716) 645-3399
E-mail: *mceer@buffalo.edu*; WWW Site: *http://mceer.buffalo.edu*

Project Overview

NEES Nonstructural: Simulation of the Seismic Performance of Nonstructural Systems

Nonstructural systems represent 75% of the loss exposure of U.S. buildings to earthquakes, and account for over 78% of the total estimated national annualized earthquake loss. A very widely used nonstructural system, which represents a significant investment, is the ceiling-piping-partition system. Past earthquakes and numerical modeling considering potential earthquake scenarios show that the damage to this system and other nonstructural components causes the preponderance of U.S. earthquake losses. Nevertheless, due to the lack of system-level research studies, its seismic response is poorly understood. Consequently, its seismic performance contributes to increased failure probabilities and damage consequences, loss of function, and potential for injuries. All these factors contribute to decreased seismic resilience of both individual buildings and entire communities.

Ceiling-piping-partition systems consist of several components and subsystems, have complex three-dimensional geometries and complicated boundary conditions because of their multiple attachment points to the main structure, and are spread over large areas in all directions. Their seismic response, their interaction with the structural system they are suspended from or attached to, and their failure mechanisms are not well understood. Moreover, their damage levels and fragilities are poorly defined due to the lack of system-level experimental studies and modeling capability. Their seismic behavior cannot be dependably analyzed and predicted due to a lack of numerical simulation tools. In addition, modern protective technologies, which are readily used in structural systems, have never been applied to these systems.

This project sought to integrate multidisciplinary system-level studies to develop, for the first time, a simulation capability and implementation process to enhance the seismic performance of the ceiling-piping-partition nonstructural system. A comprehensive experimental program using both the University of Nevada, Reno (UNR) and University at Buffalo (UB) NEES Equipment Sites was developed to carry out subsystem and system-level full-scale experiments. The E-Defense facility in Japan was used to carry out a payload project in coordination with Japanese researchers. Integrated with this experimental effort was a numerical simulation program that developed experimentally verified analytical models, established system and subsystem fragility functions, and created visualization tools to provide engineering educators and practitioners with sketch-based modeling capabilities. Public policy investigations were designed to support implementation of the research results.

The systems engineering research carried out in this project will help to move the field to a new level of experimentally validated computer simulation of nonstructural systems and establish a model methodology for future systems engineering studies. A system-level multi-site experimental research plan has resulted in a large-scale tunable test-bed with adjustable dynamic properties, which is useful for future experiments. Subsystem and system level experimental results have produced unique fragility data useful for practitioners.

The work included in this report enhances the understanding of the seismic behavior of nonstructural cold-formed steel framed gypsum partition walls. The test plan that included 50 full-scale partition walls, constructed and tested to both quasi-static and dynamic protocols developed for the University at Buf-

falo Nonstructural Component Simulator (UB-NCS), generated data regarding partition wall in-plane and out-of-plane seismic behavior and seismic fragility. Dynamic analyses that included the mechanical behavior of cold-formed steel gypsum partition walls in the structural frame of a four story steel building indicated a significant improvement in the collapse capacity of the building.

Project Management Committee

Manos Maragakis, Principal Investigator, University of Nevada Reno, Department of Civil Engineering, Reno, NV 89557; *maragaki@unr.edu.*

André Filiatrault, Co-Principal Investigator, University at Buffalo, State University of New York, Department of Civil, Structural and Environmental Engineering, Buffalo, NY 14260; *af36@buffalo.edu.*

Steven French, Co-Principal Investigator, Georgia Institute of Technology, College of Architecture, P.O. Box 0695, Atlanta, GA 30332; *Steve.French@ arch.gatech.edu*.

William Holmes, Rutherford & Chekene, 55 Second Street, Suite 600, San Francisco, CA 94105; *wholmes@ruthchek.com.*

Tara Hutchinson, Co-Principal Investigator, University of California, San Diego, Department of Structural Engineering, 9500 Gilman Drive, #0085, La Jolla, CA 92093; *tara@ucsd.edu*.

Robert Reitherman, Co-Principal Investigator, CUREE, 1301 S. 46th Street, Bldg. 420, Richmond, CA 94804; *reitherman@curee.org*.

Abstract

The contribution of nonstructural partition walls is often assumed to be negligible in the lateral response of common seismic force-resisting systems. However, this assumption may become nonconservative as the sum effect of individual wall systems is considered. The first phase of the NEES Nonstructural Grand Challenge Project tested full scale cold-formed steel-framed gypsum partition walls using the University at Buffalo Nonstructural Component Simulator (UB-NCS). A description and experimental results for 22 different partition wall configurations is given. Included in the wall variations is material type, connections, testing protocols, wall dimensions, and boundary conditions. Innovative designs to reduce the seismic fragility of partition walls were also developed as part of the testing program. The experimental data are used to populate an extensive seismic fragility database for cold-formed steel-framed gypsum partition walls. Parameters for a tri-linear hysteretic model, aimed at reproducing the in-plane mechanical behavior of partition walls, are determined from the experimentally obtained force-displacement curves. Recommended parameters for in-plane walls are given for individual configurations and cold-formed steel-framed nonstructural partition walls. The calibrated partition wall models are combined with the structural model of an existing four-story steel moment-resisting frame medical facility to demonstrate the effect on dynamic properties. As the period of the structure reduces due to the increased stiffness from the partition wall systems, reductions in drift and absolute floor accelerations are observed. The assumption that these wall systems have negligible impact is disproven by the use of incremental dynamic analyses performed according to the FEMA P695 methodology. These analyses show that including the contribution of steel stud gypsum partition walls to the lateral force-resisting system increases the building collapse safety margin by 32%.

Acknowledgements

Financial support for the work described in this report was provided by the National Science Foundation through the George E. Brown, Jr. Network for Earthquake Engineering Simulation Research (NEESR-GC) for Grand Challenge on Simulation of Seismic Performance of Nonstructural Components, award number CMMI 0721399 and by the Multidisciplinary Center for Earthquake Engineering Research through grants from New York State. This support is gratefully acknowledged.

Table of Contents

Section Title Page

Table of Contents (Cont'd)

Section Title Page

Table of Contents (Cont'd)

Section Title — Page

Table of Contents (Cont'd)

Section Title Page

List of Figures

List of Figures (Cont'd)

List of Figures (Cont'd)

List of Figures (Cont'd)

Figure **Title** **Page**

List of Figures (Cont'd)

List of Tables

Chapter 1
INTRODUCTION

The effect of seismic events on nonstructural components has been under -appreciated or neglected until recently. Following the 1994 Northridge earthquake, research relating to nonstructural components increased due to the development of the Performance Based Earthquake Engineering (PBEE) methodology. A document that has helped to further the research of nonstructural components was published by Taghavi and Miranda (2003). In this report, the cost estimate for different building components are estimated: 48-70 percent of commercial building costs are in the nonstructural components; 8-18 percent of the overall building cost is in the structural system; and 17-44 percent of the cost is dependent on building contents, as shown in Figure 1.1. These statistics along with the recent development of PBEE increased the need to have a better understanding of the dynamic response and degree of loss (economical or functional) of combined structural and nonstructural systems under potential earthquake scenarios. With the increased understanding of the seismic behavior of these systems, it is expected that more efficient and safer systems will be designed. These increased efforts in design will ensure buildings are more economical, considering their post-earthquake state, due to the anticipated reduction of losses. Along with cost benefits of reduced or controlled damage, important structures like hospitals can be designed to ensure the building maintains the PBEE level of "immediate occupancy" following a seismic event to handle medical emergencies.

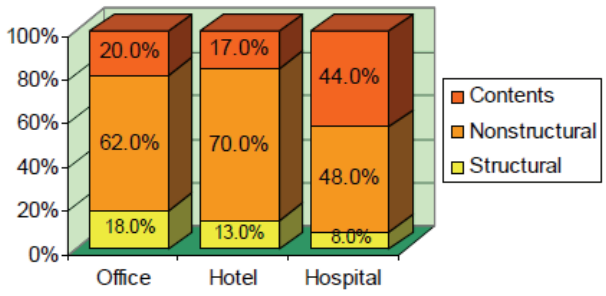

Figure 1.1 Typical Cost Estimates for Building Construction (taken from Whittaker et al. after Taghavi & Miranda, 2003)

1.1 Background

A building system is a structure that has a specific use (e.g., residential, commercial, etc.) and is designed to provide safety and comfort to the intended occupants. In commercial structures, the building architect is responsible for building planning to ensure comfort and useable spaces; meanwhile, occupant structural safety is primarily maintained through a sound structural design by the structural engineer of record. Often times building systems include subsystems or components that affect both of these areas of emphasis (i.e., occupant comfort and safety) and are known as nonstructural components. A design methodology for these components is given in Chapter 13 of *ASCE/SEI 7-05 - Minimum Design Loads for Buildings and Other Structures* (2006). The list of 'Architectural Components' requiring design in Table 13.5-1 in ASCE 7-05 includes 'Interior Nonstructural Walls and Partitions,' as shown in Figure 1.2.

TABLE 13.5-1 COEFFICIENTS FOR ARCHITECTURAL COMPONENT

Architectural Component or Element	a_p[a]	R_p[b]
Interior Nonstructural Walls and Partitions[b]		
Plain (unreinforced) masonry walls	1.0	1.5
All other walls and partitions	1.0	2.5
Cantilever Elements (Unbraced or braced to structural frame below its center of mass)		
Parapets and cantilever interior nonstructural walls	2.5	2.5
Chimneys and stacks where laterally braced or supported by the structural frame	2.5	2.5
Cantilever Elements (Braced to structural frame above its center of mass)		
Parapets	1.0	2.5
Chimneys and Stacks	1.0	2.5
Exterior Nonstructural Walls[b]	1.0[b]	2.5
Exterior Nonstructural Wall Elements and Connections[b]		
Wall Element	1.0	2.5
Body of wall panel connections	1.0	2.5
Fasteners of the connecting system	1.25	1.0
Veneer		
Limited deformability elements and attachments	1.0	2.5
Low deformability elements and attachments	1.0	1.5
Penthouses (except where framed by an extension of the building frame)	2.5	3.5
Ceilings		
All	1.0	2.5
Cabinets		
Storage cabinets and laboratory equipment	1.0	2.5
Access Floors		
Special access floors (designed in accordance with Section 13.5.7.2)	1.0	2.5
All other	1.0	1.5
Appendages and Ornamentations	2.5	2.5
Signs and Billboards	2.5	2.5
Other Rigid Components		
High deformability elements and attachments	1.0	3.5
Limited deformability elements and attachments	1.0	2.5
Low deformability materials and attachments	1.0	1.5
Other Flexible Components		
High deformability elements and attachments	2.5	3.5
Limited deformability elements and attachments	2.5	2.5
Low deformability materials and attachments	2.5	1.5

[a] A lower value for a_p shall not be used unless justified by detailed dynamic analysis. The value for a_p shall not be less than 1.00. The value of $a_p = 1$ is for rigid components and rigidly attached components. The value of $a_p = 2.5$ is for flexible components and flexibly attached components. See Section 11.2 for definitions of rigid and flexible.
[b] Where flexible diaphragms provide lateral support for concrete or masonry walls and partitions, the design forces for anchorage to the diaphragm shall be as specified in Section 12.11.2.

Figure 1.2 – Table of Seismic Coefficients for Architectural Components (ASCE 7-05, 2006)

1.2 Nonstructural Partition Walls

Large open areas in new commercial buildings are often due to: building owner requirements, architectural desires, heating-ventilating-air-conditioning needs, and economical structural designs. Whatever structural system is used (i.e., post and beam, shear wall, etc.), large open areas need to be separated into smaller more useable private spaces. The most common means for creating these separations are partition walls. These walls are required to resist the seismic loads as determined by ASCE 7-05 Chapter 13; however, these walls are considered a nonstructural component because they are designed to carry only limited gravity or lateral loads in addition to their own weight. Of the types of partition wall systems, the most common use wood and steel framing, which are covered with gypsum wall board in residential and commercial buildings, respectively.

1.2.1 Cold-formed Steel Framing

Wall systems in commercial structures are most often constructed using light-frame construction materials. Because of the low weight of cold-formed steel framing versus wood framing and the variability of the moisture content in the wood framing members, in large commercial structures steel framing is the preferred option. Steel is also the preferred option in many commercial structures because it is non-combustible. Although many different configurations are used to construct these walls, the strongest wall systems are generally constructed by attaching a base track, consisting typically of a U-shape, directly to the floor slab by using powder actuated fasteners. Another U-shaped track is located at the expected height of the wall with stud members placed vertically between the two tracks and attached using self drilling screws. The tracks along with the studs that are generally placed at 16-24 inches on center compose the frame of the wall. Gypsum wallboard panels, typically 1/2-5/8” in thickness, are then attached to the flanges of the steel tracks and studs to create the separation between areas. Depending on the use of the areas being created by the wall system, one or both sides of the wall will be sheathed with one or two layers of panels, designed to maintain a predetermined degree of fire protection. Several practices are used in the field for connecting perpendicular walls, screwing gypsum wallboards to steel framing and connecting framing elements. The most common of these procedures were considered when selecting the configurations for experimental studies.

1.2.2 Nonstructural Partition Wall Design

Partition wall systems, although designed for code-prescribed force levels, are considered negligible in the analysis of gravity and seismic force-resisting systems. In commercial structures using structural systems other than light-framed wall systems to resist lateral loads, design forces are much higher than the expected forces a partition wall system can resist. Another reason these systems are often neglected in design is that the structural engineer does not want to be liable for failures in the system, and they are usually designed by the architect and shown on the architectural rather than structural construction drawings. Common structural components have been researched for many years, whereas, the behavior of cold-formed steel-framed partition (nonstructural) walls has been the subject of limited research, and there is less information regarding static and dynamic behavior of these wall systems compared to structural systems. In order to improve the design philosophy of nonstructural partition walls, comprehensive studies on the cyclic and dynamic response of nonstructural components must be completed.

1.3 Current Research Efforts

The Network for Earthquake Engineering Simulation – Nonstructural Grand Challenge Project (NEES-NGC) entitled "Simulation of the Seismic Performance of Nonstructural Systems" (or NEES Nonstructural) is aimed at further understanding the seismic performance of ceiling, piping, and partition wall systems (CPP). This research is being conducted through laboratory testing of full-scale nonstructural systems and subsystems and highly intensive computer modeling. Further information on this project can be found at http://www.nees-nonstructural.org. This project will assist PBEE by developing designs of CPP systems that will enhance the seismic performance of primary and secondary systems in buildings.

The first experimental phase of this project was completed at the University at Buffalo on the new testing apparatus known as the Nonstructural Components Simulator (UB-NCS). The construction and testing of specimens began in the early spring of 2008 continuing through the spring of 2009. Fifty full-scale partition walls corresponding to twenty-two different construction configurations were built and tested on the UB-NCS. The designs of the wall systems were developed through coordination with the Practice Committee and Advisory Board of the NEES-NGC. Approximately 80 channels of data were recorded per wall during the testing program, including data from load cells, potentiometers, string pots, and accelerometers. Further information on the NEES-NGC partition wall testing program can be found in Chapter 3.

1.4 Objectives, Scope, and Report Organization

The experimentally obtained data from the NEES Nonstructural project partition wall specimens is used to develop a seismic fragility database for several configurations of cold-formed steel-framed gypsum partition walls. In addition, the experimental data and the performance observations were the key input needed for the research related to this report. The measured displacements imposed on the wall specimens and subsequent forces are parameterized to a hysteretic model closely resembling the lateral in-plane response of the wall systems. The hysteretic behavior is applied to a 2-D numerical model of a moment-resisting frame of a medical facility test structure. Drift ratios and absolute floor accelerations for building models including partition walls are monitored and compared to those of the original building model. An analysis based on the FEMA P695 methodology (FEMA, 2009) is completed to determine the change in collapse probability of the structure when the partition wall systems are included in the modeling. This report presents a combination of practical, experimental, and theoretical concepts in an effort to better clarify the effect of seismic events on the performance of nonstructural partition walls and the often neglected effect on the lateral behavior of a structure. The information is organized and presented in the following manner:

- A literature review of previous research related to nonstructural partition walls constructed using cold-formed steel framing and sheathed with gypsum wallboard panels is presented in Chapter 2.
- A description of the comprehensive testing program and an evaluation of the seismic performance of cold-formed steel-framed gypsum partition walls are given in Chapter 3.
- The assessment of the experimental seismic fragility of the partition walls and the development of a seismic fragility database are presented in Chapter 4.
- Within Chapter 5, the mechanical in-plane behavior of partition walls is examined, and wall behavior is analyzed and parameterized.
- The effect of nonstructural partition walls on the lateral response of a four story steel moment-resisting frame test structure is presented in detail in Chapter 6.
- The collapse probability of the test structure including partition walls is assessed using a FEMA P695 (FEMA 2009) methodology based analysis in Chapter 7.
- Conclusions, commentaries and recommendations for future research are presented in Chapter 8.

Chapter 2
LITERATURE REVIEW

The main objective of this research work report is to present results of a comprehensive testing program on nonstructural partition walls and study the effect of these walls on the lateral response of a four story steel moment-resisting structure. A secondary objective is to develop unique wall configurations that could improve seismic fragility by either shifting damage to higher displacements and/or completely removing damage states. A summary of research relating to lateral response of steel stud gypsum partition walls is given in this chapter. This review will demonstrate the need for an extensive testing program and highlight the importance of the current research being conducted as part of the NEES Nonstructural Grand Challenge Project.

2.1 Background

Nonstructural partition walls in commercial and institutional buildings are most often constructed using cold-formed steel framing and gypsum sheathing. The use of partition walls in this type of construction is to separate large open areas into smaller more useable spaces and are not considered to be structural elements. Because partition walls are anchored at the floor and ceiling concrete slabs, potential damage due to inter-story building displacements and absolute floor accelerations caused during a seismic event must be taken into account. The ASCE 7-05 standard states that "Every structure, and portion thereof, including nonstructural components, shall be designed and constructed to resist the effects of earthquake motions as prescribed by the seismic requirements of this standard" (ASCE 7-05, 2006). Design forces for nonstructural partition walls are considered in ASCE 7-05 under architectural elements, Section 13.5. Although the partition walls are designed for in- and out-of-plane forces and displacements, the partition walls are not considered as structural components or as a contributing member in the earthquake and gravitational force-resisting systems.

Because of the long history of using wood framing members in partition walls, most existing research examines the in-plane response of wood framed gypsum partition walls. Furthermore, research on out-of-plane seismic performance of partition walls has not been carried out so far due to the non-existence of testing facilities with the capability to impose simultaneously full scale inter-story drifts and floor

accelerations expected within multistory buildings during strong shaking on full scale testing specimens. In relation to the use of cold-formed steel framing in partition walls, minimal research relative to wood framed walls has been conducted. Even with the research that has been completed on cold-formed steel-framed gypsum partition walls, limitations still exist. For example, most commercial steel or reinforced concrete structures have floor to bottom of deck/framing dimensions greater than 8 feet. The size of most test specimens are only 8 feet in length by 8 feet tall, and in order to design wall systems in common commercial structures, extrapolation of the data are required for wall systems that are outside these dimensions. Also, most research on cold-formed steel-framed gypsum partition walls includes cross bracing straps or gypsum structural panels which are used for shear resistance. Another difference between existing research and actual wall construction details is the thickness of the gypsum panel. Most existing research considered 1/2-inch thick panels on each face, whereas panel thicknesses in most buildings is 5/8 in thick for suitable fire ratings.

The study of the effect of the nonstructural partition walls on the lateral response of a building model is an important goal of this project. Research has been conducted to better understand the effect of nonstructural components on the lateral stiffness of high rise structures (e.g., Su et al. (2005) and *Li* et al. (2009)). The nonstructural walls in these research projects however consist of concrete bricks, infill concrete walls, and precast panels. Although results for these projects were similar, showing increases in lateral stiffness, neither analyzed the cumulative effect of light-frame nonstructural partition walls, which walls have a much lower stiffness and strength capacity than concrete bricks, panels, or infill walls. Other studies address the effect of nonstructural components on the lateral behavior of light-frame residential structures (e.g., Gad et al. (1995)).

2.2 Lateral In-Plane Force-Displacement Response

In this section research related to the lateral in-plane response of partition walls constructed with cold-formed steel framing and gypsum wallboard panels is reviewed.

2.2.1 Study by Serrette et al. (1997)

This study conducted an extensive investigation into the racking behavior of steel-framed wall systems. Of the seventeen 8 feet tall by 8 feet long partition wall specimens, four considered 1/2-inch gypsum panels on both faces of 0.033” or 33 mil steel framing. Variations in the construction of the wall specimen

included: (1) a 20 gauge steel strap at mid-height of the wall for attaching gypsum panel edges; and (2) gypsum to framing connector spacing (i.e., 6 inches and 12 inches on center (o.c.) spacing at the edge and in the field, respectively; 7 inches o.c. at the edges and field; and 4 inches o.c. spacing at the edges and in the field). All gypsum panels were 1/2-inch thickness and fastened to the framing using #6 bugle head self-drilling screws 1-inch long.

Serrette et al. (1997) concluded that steel-framed walls with gypsum panels on both faces had relatively low shear values when compared to plywood or OSB sheathed walls. Serrette et al. also observed that walls with gypsum panels attached with their long axis perpendicular (horizontal) to the framing members had a higher stiffness than walls with panels attached parallel (vertical) to framing.

2.2.2 Study by Bersofsky (2004)

In this study Bersofsky constructed and tested 16 steel-framed gypsum partition walls to investigate how to best apply the PEER-PBEE methodology to this type of nonstructural component. The walls were 8 feet tall by 16 feet long and had perpendicular walls at each end 8 feet tall by 4 feet long, forming an "I" in plan view, as shown in Figure 2.1. Testing variables for the 16 wall specimen included:

(1) Doorframe in main wall, as shown in Figure 2.1;
(2) gypsum to framing connector spacing (8 inches and 12 inches);
(3) gypsum height (8 feet and 6-1/2 feet);
(4) slip tracks;
(5) gypsum panel thickness;
(6) steel framing thickness (25 gauge and 20 gauge.); and
(7) stud spacing (24 inches and 16 inches).

The specimens were tested quasi-statically using the CUREE loading/displacement protocol developed by Krawinkler et al. (2001). The protocol was paused at each peak displacement to record visual damage to the test specimens.

Because the primary objective of Bersofsky's research was developing fragility functions for typical interior wall partitions, three damage states were defined (i.e., DS1, DS2, and DS3). The difference between the damage states was superficial damage, repairable by mud, tape, and paint (DS1); non-superficial damage requiring removal and replacement of gypsum panel sections (DS2); and damage to the wall system requiring complete removal and replacement of wall (DS3). It was found that DS1 began

at drift ratios between 0.05 to 0.5%. DS2 did not occur in all specimens because of local failure at gypsum to framing connectors; and DS3 occurred at drift ratios of 1.5 to 3.0%. Walls constructed identically had similar behavior, however, mechanical response and damage varied between the configurations. Repetitive cycles had little impact on the fragility of the system as most damage was observed at the first peak cycle in each level.

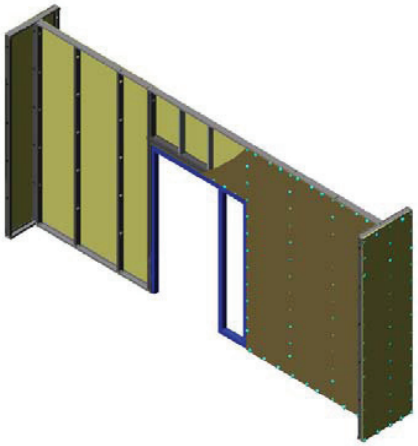

Figure 2.1. Rendering of Typical Testing Specimen (after Bersofsky, 2004)

2.2.3 Study by Lang & Restrepo (2005)

To investigate the seismic fragility of cold-formed steel gypsum sheathed partition walls common to modern commercial structures, this study constructed and tested two full scale specimens. The specimens were designed to be similar to a typical room found in an office building. Plan dimensions of the room were 15 feet by 12 feet and had a height of 14 feet, as shown in Figure 2.2.

The specimens were constructed using 20 gauge 3-5/8 inches steel framing members spaced at 24 inches on center. Gypsum panels with a thickness of 5/8-inch were attached to the face of the steel framing. Test protocols were different for each of the test specimens. Specimen 1 used the recommended protocol from the ATC-58 project, “Development of Next Generation Performance-Based Seismic Design Procedures for New and Existing Buildings” and the protocol for Specimen 2 was adjusted to lessen the total number of cycles, as shown in Figure 2.3.

The goal of this study was to serve as a model of how to best apply the PBEE methodology. Damage progression in the specimens was closely monitored and showed low cycle fatigue of the track fasteners.

The pre-peak behavior and damage progression between the two specimens were found to be dictated by the loading protocol. Through this study on seismic fragility, it was found that, the damage states previously defined and adopted by the Pacific Earthquake Engineering Research Center (Lang and Restrepo, 2005) were not well captured.

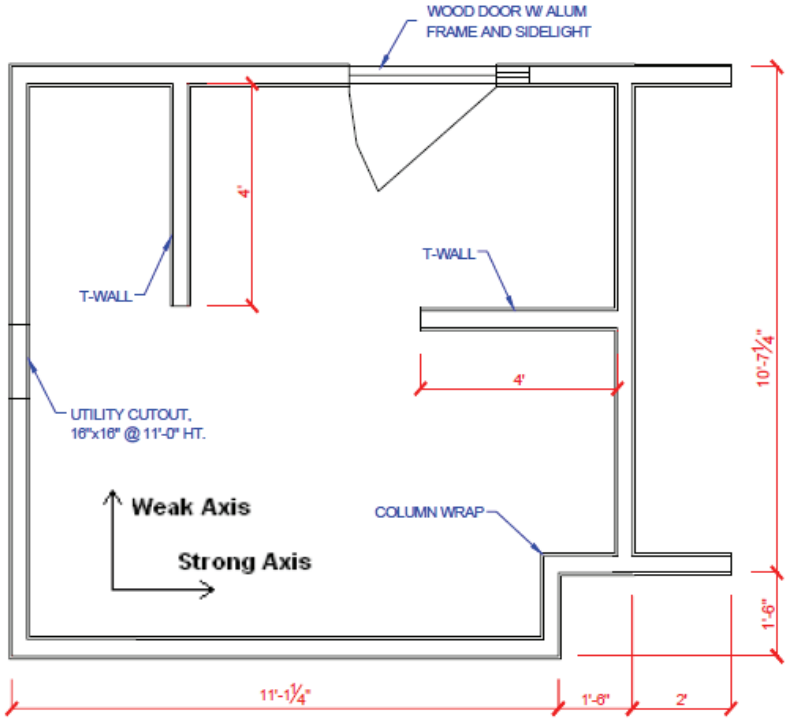

Figure 2.2 – Plan View of Test Specimen (after Lang and Restrepo, 2005)

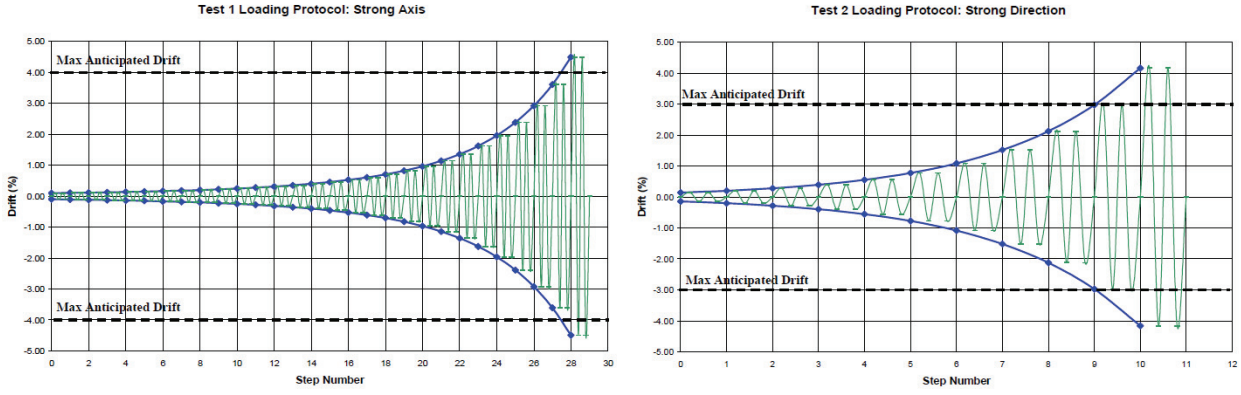

(a) **(b)**

Figure 2.3 – Test Protocol for (a) Specimen 1 and (b) Specimen 2 (after Lang & Restrepo, 2005)

2.2.4 Study by Lee et al. (2007)

Lee et al. (2007) tested four cold-formed steel-framed wall specimens with two layers of gypsum panels on both faces to characterize seismic performance and determine repair cost estimates. Two similar specimens were constructed with only a variance in the testing protocol (i.e., quasi-static and dynamic) with dimensions of approximately 13 feet long by over 9 feet tall. Another specimen constructed similar to those just described and tested according to the quasi-static protocol included an installed door. The fourth specimen was approximately 9 feet tall by almost 9-3/4 feet long with a return wall over 5 feet in length and subjected to the quasi-static protocol.

The cyclic response of the wall specimens showed pinching, and stiffness and strength degradation. Damage to gypsum panels was concentrated at the perimeter of the wall specimens. Little to no damage was observed up to a drift ratio of 0.01 radians (1% drift), whereas a drift ratio of 0.02 radians (2% drift) caused repair costs almost equal to the initial partition wall construction cost.

2.2.5 Study by Memari et al. (2008)

This research program performed nine in-plane tests on wall specimens constructed of wood (four specimens) and cold-formed steel stud (five specimens) framed with gypsum wallboard panels on both faces. The objective of this testing program was to better understand the difference in the lateral in-plane response of the two wall types, finished and unfinished. Of the five specimens using steel framing, one was subjected to monotonic loading, and the other four were tested using the CUREE testing protocol developed by Krawinkler et al. (2001). The five specimens were constructed using identical methods, however, two of the four specimens subjected to the cyclic protocol were finished using tape and joint compound whereas the other two cyclic and monotonic test specimens were left unfinished. The connection of the steel framing members to each other was done using #10-5/8 inches self drilling pan head screws; ½-inch gypsum panels were attached to steel framing using #8 by 1-1/4 inches coarse threaded drywall screws attached at 6 inches and 12 inches o.c. at the edge and in the field, respectively. To eliminate failure of the track to the test frame connections, wood blocking was inserted between studs. Conclusions of the study in relation to the steel-framed specimens showed:

- An increase of 45% in strength capacity for the finished walls versus the unfinished walls;
- Peak load occurred at 3 times the serviceability drift limit of *H/400* and approximately 40% of the ultimate allowable drift of *0.02H* allowed by ASCE 7 (ASCE, 2006), and;

- All specimens had an approximate ductility of 2.4.

2.3 Discussion

Although research has been conducted on nonstructural steel stud gypsum partition walls, limitations on wall dimensions and material specifications is limited in application to commercial structures. Top of slab to bottom of slab inter-story dimensions are often well over ten feet to allow for mechanical, plumbing, electrical, etc. equipment and runs above the suspended ceilings. Another limitation in regards to testing nonstructural systems is having a facility capable of reproducing expected drift ratios and accelerations for floors in high rise structures, as noted by Mosqueda et al. (2008). Analysis from Lang & Restrepo showed that a variation in mechanical response and seismic fragility can be observed based on the testing protocol; this is seen as another limitation and further discussion on this can be found in Retamales et al. (2008).

Although the wall specimens tested by Lee et al. were over 9 feet tall, construction details were based on common methods used in Japan in wall construction (i.e., double layer of gypsum panels on each face). The most applicable completed research to date for this type of wall system is the study by Bersofsky. Of the wall configurations tested only one considered ½-inch panel thickness with the remaining walls considering 5/8-inch thick gypsum panels. However the force-displacement response of these walls is only applicable to partition walls with a height of 8 feet.

Research on the influence of nonstructural components on the lateral behavior of buildings has been conducted. These projects, however, have emphases in only two key areas: the effect of stiff nonstructural walls (e.g., concrete panels, brick, or infill walls) on reinforced concrete structures (high seismic mass) and the effect of nonstructural components on cold-formed partition structures (low seismic mass). A combination of these two analyses would be helpful, and this would be to analyze the cumulative effect of light-frame partition walls on structures with higher seismic mass.

This literature review demonstrates the importance of the research on nonstructural steel stud gypsum partition walls as part of the NEES Grand Challenge Nonstructural Project. This study will evaluate the performance and damage states of partition walls constructed with similar details to current commercial and institutional construction. As described in this report, over sixteen configurations for in-plane partition walls will be tested and evaluated to give an in depth understanding of the force-displacement response of common commercial and institutional partition walls.

Chapter 3

FULL SCALE TESTING OF COLD-FORMED STEEL-FRAMED GYPSUM PARTITION WALLS

The first experimental phase of the NEES Nonstructural Grand Challenge Project "*Simulation of the Seismic Performance of Nonstructural Systems*" evaluated the seismic performance of cold-formed steel-framed gypsum partition wall subsystems, constructed following standard construction practices. The subsystem-level tests were performed using the University at Buffalo Nonstructural Components Simulator (UB-NCS), subjecting full-scale specimens to both dynamic and quasi-static test protocols. A total of 50 partition wall specimens were tested. The partition walls were installed parallel (36 specimens) and perpendicular (14 specimens) to the direction of the input motions, to study their in-plane and out-of-plane seismic performance, respectively. The main objective of the partition wall subsystem-level test series was to evaluate the seismic fragility of several configurations of cold-formed steel-framed gypsum partition walls.

3.1 The University at Buffalo Nonstructural Component Simulator (UB-NCS)

The UB-NCS, shown in Figure 3.1, provides the unique capability to replicate, under controlled laboratory conditions, the effects of strong seismic shaking on distributed nonstructural systems located at the upper levels of multistory buildings. Furthermore, this testing equipment allows for assessing the seismic interactions between displacement and acceleration sensitive nonstructural subsystems, providing a more realistic procedure for the seismic fragility assessment and seismic qualification of combined acceleration/displacement sensitive nonstructural systems. The UB-NCS testing facility can subject full-scale nonstructural specimens to accelerations of up to 3g, peak velocities of 100 in/s and displacements in the range of ±40 in, enveloping the peak seismic responses recorded at the upper levels of multistory buildings during historical earthquakes. The testing frame is activated by four identical high performance dynamic actuators with an individual load capacity of 22 kips. The frame is composed of two square 12.5 feet platforms with an inter-story height of 12 feet in the bottom level and 14 feet in the upper level. A more detailed description of the testing frame and its capabilities can be found in Mosqueda et al. (2008) and Retamales et al. (2008).

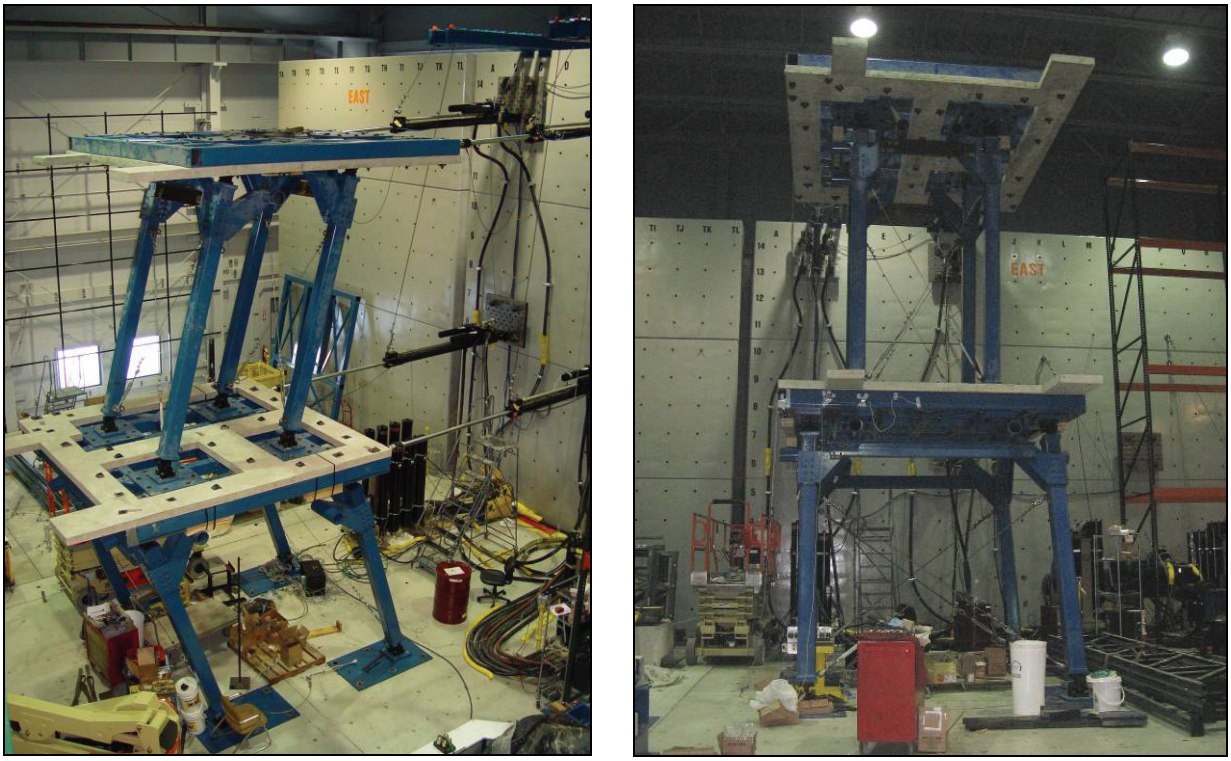

(a) Nonstructural Component Simulator (b) Front view

Figure 3.1 - Photograph of the UB-NCS at the University at Buffalo

3.2 Testing Protocols for the UB-NCS

Testing protocols currently used for the seismic performance assessment of nonstructural components and equipment, such as FEMA 461 (FEMA 2006) and AC156 (ICC-ES 2007), focus either on displacement or acceleration sensitive components, through quasi-static racking or shake table protocols. However, many nonstructural systems, like the Ceiling Piping and Partition (CPP) systems studied in the NEES Nonstructural Grand Challenge Project, are composed of subsystems that individually may be either acceleration or displacement sensitive, but when combined with other subsystems, may become sensitive to both accelerations and inter-story drifts. To this end, an innovative dynamic testing protocol has been developed for assessing the seismic fragility of nonstructural systems and evaluating dynamic interactions between nonstructural subsystems, taking full advantage of the UB-NCS testing capabilities. Previous research by Wilcoski et al. (1997) and Krawinkler et al. (2001) constitute the basis for this protocol.

The UB-NCS testing protocol consists of a pair of displacement histories for the bottom and top testing

platforms that simultaneously match: (1) a target floor (or ground) response spectrum, and (2) either a target generalized inter-story drift or a maximum inter-story drift, Δ_{Max}, based on the anticipated specimen deformation capacity. The input variables for the protocol are the local seismic hazard, in terms of the short-period and 1-second spectral accelerations defined in ASCE 7 (ASCE 2006), the normalized building height above grade where the nonstructural system is located, and optionally, the maximum drift Δ_{Max} to be imposed. For fragility assessment purposes, this test series has considered a generic site with spectral accelerations S_{DS}=1g and S_{D1}=0.6g, a generic nonstructural system located at a roof building level, and a maximum drift Δ_{Max}=3%. The protocol sweeps frequencies between 0.2 and 5 Hz, corresponding to the UB-NCS operating frequency range, which is sufficient to capture the first few modes of vibration that contribute to the seismic response of multistory buildings.

The testing protocol was calibrated to induce/impose the same number of "Rainflow" cycles (ASTM 1997) on acceleration/displacement sensitive nonstructural components as would be experienced during real building floor motions. Figure 3.2 shows the platform motions used as input for the UB-NCS during dynamic testing. Figure 3.2 also shows the inter-story drift protocol history. The motion histories in Figure 3.2 exhibit an instantaneous testing frequency transitioning from high to low frequencies, and then back again to high frequencies. The final high frequency sweep is intended to capture possible high frequency acceleration-induced failure modes of nonstructural systems damaged by low frequency inter-story drifts. Details on the derivation of the closed-form equations defining the dynamic fragility testing protocol can be found in Retamales (2008).

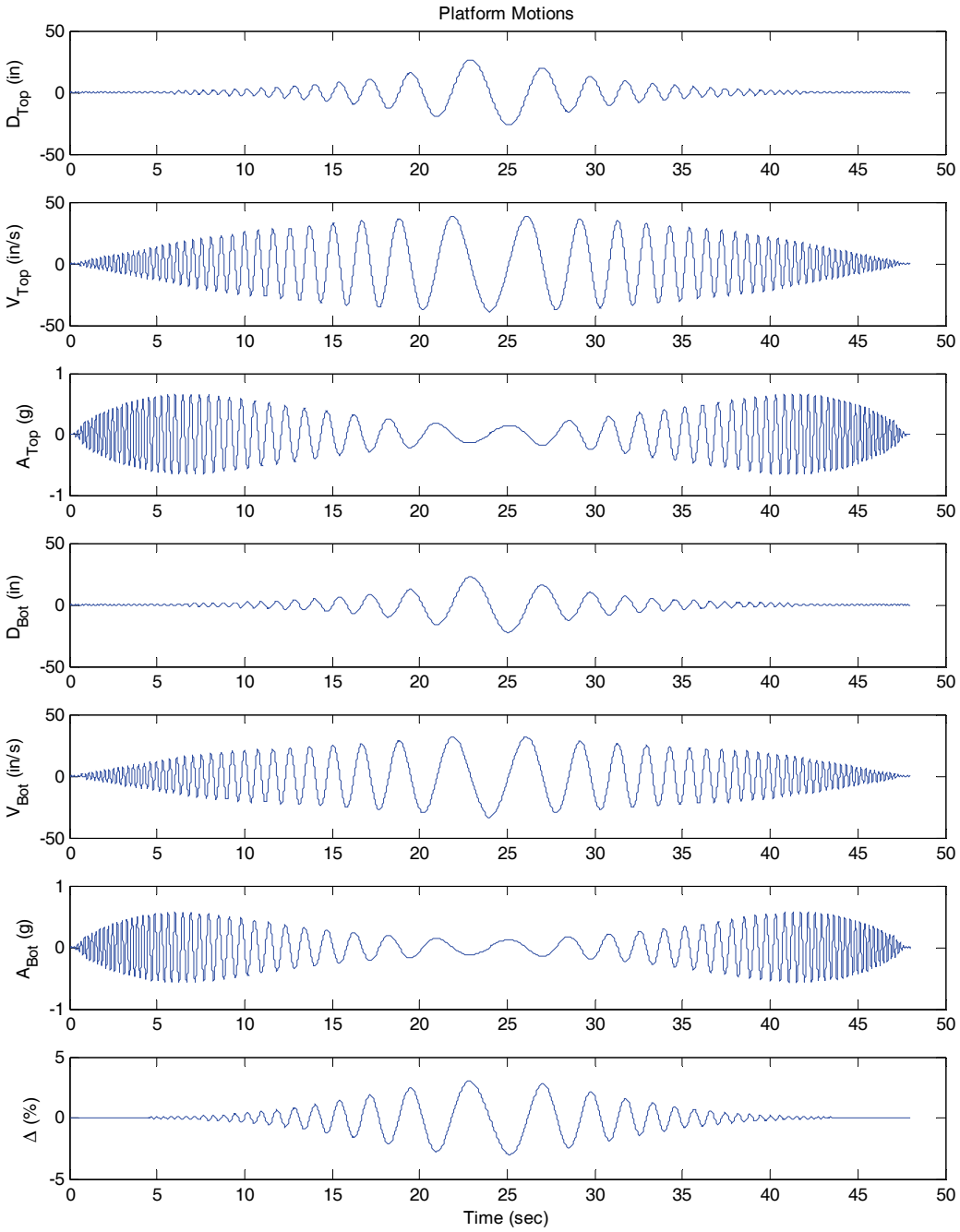

Figure 3.2 - Dynamic Fragility Testing Protocol

Table 3-1 summarizes the maximum seismic demands imposed by the dynamic fragility testing protocol to be considered in the test series.

Table 3-1 Peak Demands Imposed by Dynamic Fragility Testing Protocol

Peak Displacements		Peak Inter-story Drift		Peak Velocities		Peak Accelerations	
$D_{Max\ Bot}$ (in)	$D_{Max\ Top}$ (in)	Δ_{Max} (in)	δ_{Max} (%)	$V_{Max\ Bot}$ (in/s)	$V_{Max\ Top}$ (in/s)	$A_{Max\ Bot}$ (g)	$A_{Max\ Top}$ (g)
22.5	26.6	4.14	3.00	33.9	39.1	0.57	0.65

Complementarily, a quasi-static testing protocol was developed for evaluating the seismic fragility of nonstructural components purely sensitive to inter-story drifts. The quasi-static testing protocol used for the NEES Nonstructural Grand Challenge test series, shown in Figure 3.3b, captured the peak amplitudes of the testing protocol shown in Figure 3.3a. The quasi-static fragility testing protocol imposes a similar number of total and damaging cycles on drift sensitive nonstructural components and systems as the dynamic fragility testing protocol.

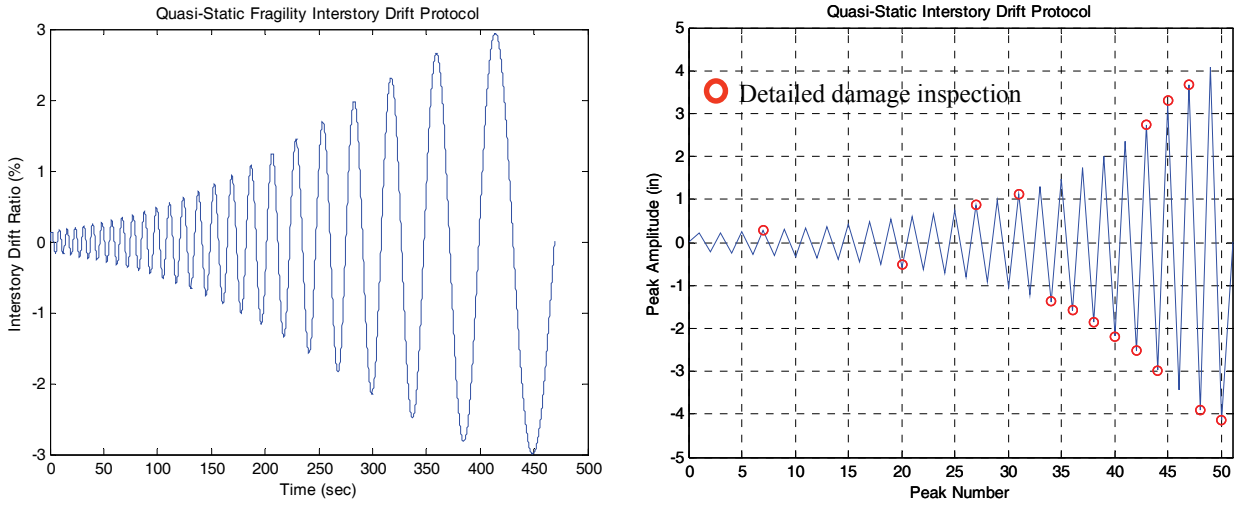

(a) **(b)**

Figure 3.3 - Quasi-static Fragility Testing Protocol (a) Low-rate Varying Quasi-static Testing Protocol and (b) Quasi-static Testing Protocol used in NEES Nonstructural Partition Walls Testing

The testing protocol shown in Figure 3.3b was applied at a loading rate of 2.4 inches/min. Table 3-2 summarizes the sequence of peaks imposed during testing. The highlighted values in Table 3-2 correspond to the steps at which a detailed inspection of the specimen's damage progression was performed.

Table 3-2 Quasi-static Testing Protocol Peaks

Step	Drift (in)	Drift Ratio (%)	Ramp Time (sec)
0	0.000	0.00	0
1	0.210	0.15	5
2	-0.219	0.16	5
3	0.230	0.17	6
4	-0.241	0.17	6
5	0.253	0.18	6
6	-0.265	0.19	7
7	**0.279**	**0.20**	**7**
8	-0.293	0.21	7
9	0.308	0.22	8
10	-0.324	0.23	8
11	0.341	0.25	9
12	-0.359	0.26	9
13	0.379	0.27	9
14	-0.399	0.29	10
15	0.422	0.31	11
16	-0.445	0.32	11
17	0.471	0.34	12
18	-0.498	0.36	12
19	0.527	0.38	13
20	**-0.559**	**0.40**	**14**
21	0.592	0.43	15
22	-0.629	0.46	16
23	0.668	0.48	17
24	-0.710	0.51	18
25	0.756	0.55	19
26	-0.805	0.58	20
27	**0.858**	**0.62**	**21**
28	-0.916	0.66	23
29	0.978	0.71	24
30	-1.046	0.76	26
31	**1.120**	**0.81**	**28**
32	-1.201	0.87	30
33	1.288	0.93	32
34	**-1.384**	**1.00**	**35**
35	1.488	1.08	37
36	**-1.601**	**1.16**	**40**
37	1.726	1.25	43
38	**-1.861**	**1.35**	**47**
39	2.009	1.46	50
40	**-2.171**	**1.57**	**54**
41	2.347	1.70	59
42	**-2.537**	**1.84**	**63**
43	**2.743**	**1.99**	**69**
44	**-2.963**	**2.15**	**74**
45	**3.196**	**2.32**	**80**
46	-3.435	2.49	86
47	**3.673**	**2.66**	**92**
48	**-3.893**	**2.82**	**97**
49	4.066	2.95	102
50	**-4.140**	**3.00**	**103**

3.3 General Specimens Description

In Phase 1 of the subsystem level test program, fifty specimens corresponding to twenty two different configurations of cold-formed steel-framed gypsum partition walls were tested. The partition walls were installed parallel (36 specimens) and perpendicular (14 specimens) to the direction of the input motions, to study their in-plane and out-of-plane seismic performance, respectively. Figure 3.4 shows the typical specimen configuration for in-plane testing.

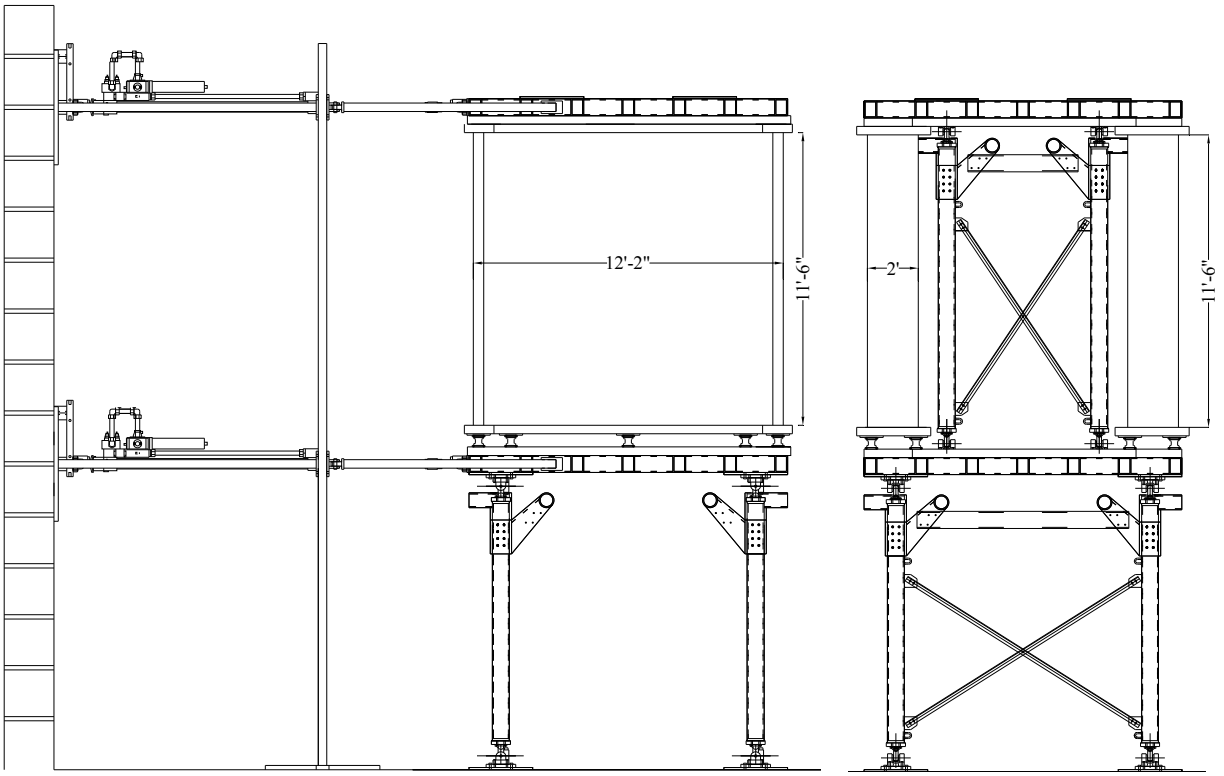

(a) Side view (b) Front view

Figure 3.4 - Typical In-plane Testing Configuration

3.3.1 Typical Specimen Geometry

The partition wall specimens were approximately 12 ft long by 11.5 ft tall. The typical length of return walls was 2’ for the first 30 specimens and 4’ for the last 20 specimens tested. Typical test layouts are shown in Figure 3.5 and Figure 3.6. Specimens were fastened to concrete slabs using standard powder driven 25 mm (1”) fasteners, using a Ramset gun model SA-270 and Ramset .27 caliber shots. When studs were screwed to bottom and top tracks and to adjacent studs at wall intersections, they were screwed using standard Phillips self-drilling #8 screws. A gap of approximately 1/8” was left in the connection between the top ends of studs and web of top tracks. The construction of the steel stud framing followed specifications in the Steel Stud Manufacturers Association manual (SSMA 2001) and in ASTM C754 (ASTM 2007).

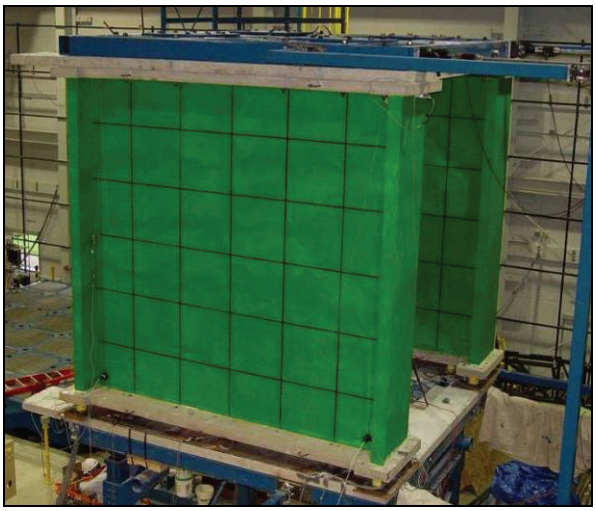

(a) For in-plane testing

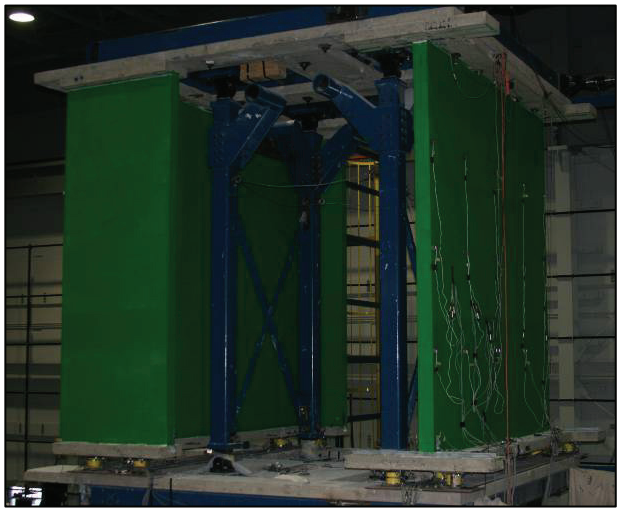

(b) For out-of-plane testing

Figure 3.5 - Photos of Typical Test Specimen Configurations

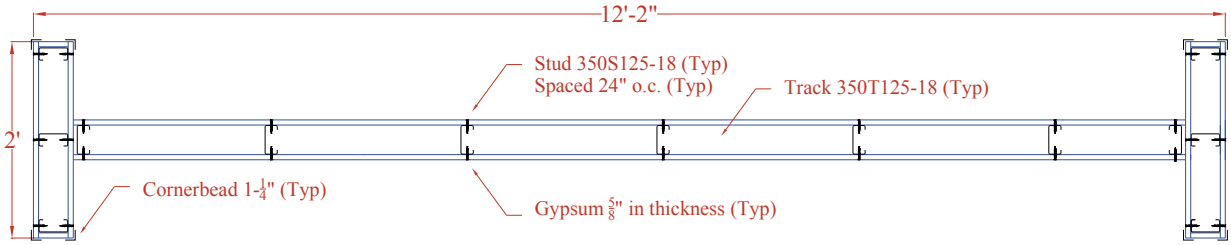

Figure 3.6 – Geometry of Typical Gypsum Partition Wall Specimens

The Practice Committee and the Advisory Board of the NEES Nonstructural Grand Challenge Project provided input into the proper selection of typical construction details for commercial and institutional buildings at the initial stages of the experimental program. The variables considered in the selection of the wall configurations included:

- Connectivity of sheathing and studs to bottom and top tracks (See Figure 3.7)
- Spacing of track-to-concrete fasteners (12 or 24” o.c.)
- Presence of transverse walls
- Detail of wall intersection (see Figure 3.8)
- Attachment of weights to the partition walls, such as bookshelves or equivalent un-braced rigid ceiling

- Height of the partition wall (total or partial height)
- Stud and track wall thickness (25 or 20 gauge)
- Spacing of the steel framing elements (16 or 24” o.c.)
- Direction of testing (in-plane or out-of-plane)
- Type of test (dynamic or quasi-static)

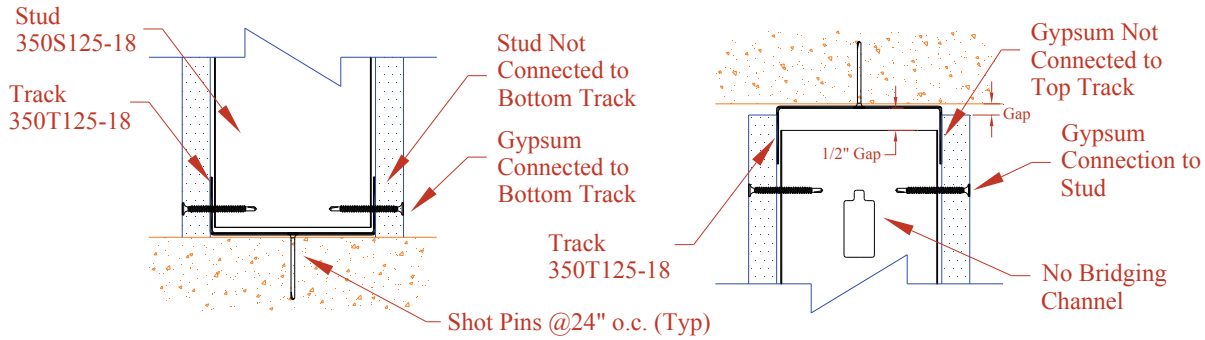

(a) Basic Connection (Slip Track)

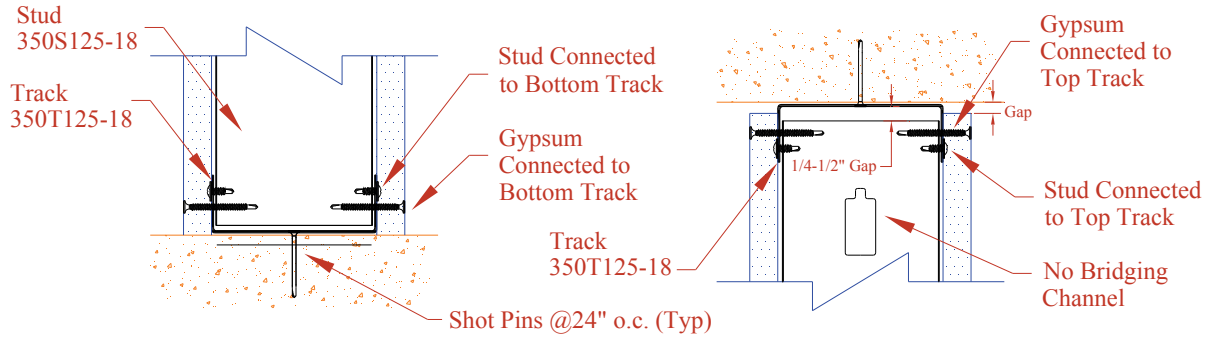

(b) Full Connection

Figure 3.7 - Typical Framing and Sheathing Connectivity Details

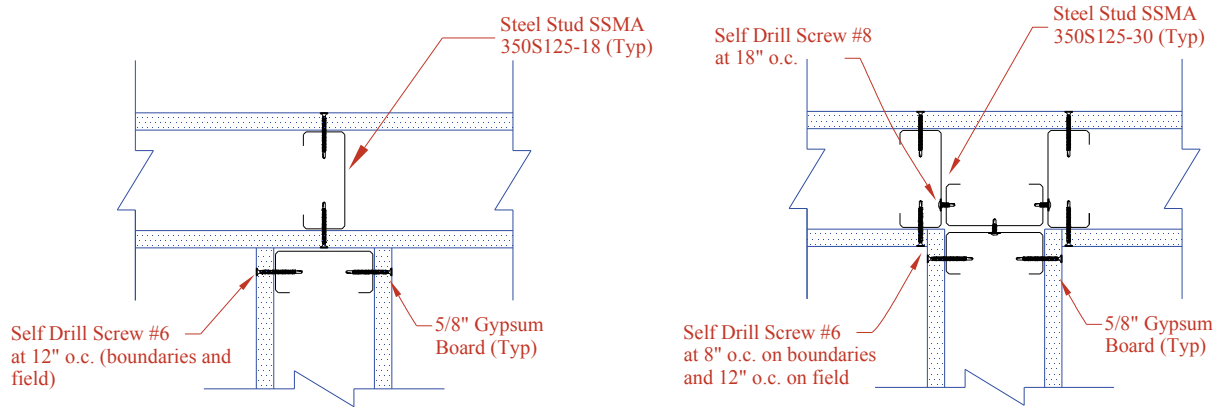

(a) Commercial construction (b) Institutional construction

Figure 3.8 - Typical Wall Intersection Details

Following a rigorous selection procedure, the nonstructural partition wall configurations listed in Table 3-3 were considered for testing.

Table 3-3 Summary of Gypsum Partition Wall Configurations

Config	Specimen ID	Specimen Description	Loading Direction/Rate	Steel Stud Type	Steel Frame and Sheathing Connectivity						
					Stud to Bottom Track	Stud to Top Track	Gypsum to Bottom Track	Gypsum to Top Track	Return Walls	Attached Mass	Ceiling Connected
1	1, 2 & 3	Basic (slip track)	In Plane/Static	350S125-18	No	No	Yes	No	Yes	No	No
2	4	Gypsum connected to top track	In Plane/Static	350S125-18	No	No	Yes	Yes	Yes	No	No
3	5, 6 & 10	No Return	In Plane/Static	350S125-18	No	No	Yes	Yes	No	No	No
4	7, 8 & 9	Full connection	In Plane/Static	350S125-18	Yes	Yes	Yes	Yes	Yes	No	No
5	11, 12 & 13	Bookshelf	In Plane/Dynamic	350S125-18	No	No	Yes	No	No	Yes	No
6	14, 15, & 16	Equivalent Ceiling	In Plane/Dynamic	350S125-18	Yes	No	Yes	No	No	Yes	Yes
7	17, 18 & 19	Partial height braced wall	In Plane/Static	350S125-18	Yes	Yes	Yes	Yes	Yes	No	No
8	20, 21 & 22	Institutional const./slip track	In Plane/Static	350S125-30	Yes	No	Yes	No	Yes	No	No
9	23, 24 & 26	Institutional const./Full Connection@24"	In Plane/Static	350S125-30	Yes	Yes	Yes	Yes	Yes	No	No
10	25, 27 & 28	Institutional const./Full Connection@12"	In Plane/static	350S125-30	Yes	Yes	Yes	Yes	Yes	No	No
11	29 & 30	No Return/Dynamic	In Plane/Dynamic	350S125-18	No	No	Yes	No	No	Yes	No
12	31 & 32	C-Shaped Walls	In Plane/Static	350S125-18	Yes	No	Yes	No	Yes	No	No
13	33	Solution to T corner damage/corner gaps	In Plane/Static	350S125-18	Yes	No	Yes	No	Yes	No	No
14	34	Solution to T corner damage/double slip track	In Plane/Static	350S125-18	No	No	No	No	Yes	No	No
15	35	Solution to L corner damage/corner gaps	In Plane/Static	350S125-18	Yes	No	Yes	No	Yes	No	No
16	36	Solution to T corner damage/slip track	In Plane/Static	350S125-18	Yes	No	Yes	No	Yes	No	No
17	37	Unloaded Wall w/ Returns	Out of Plane/Dynamic	350S125-18	No	No	Yes	No	Yes	No	No
18	38	Unloaded Wall w/o Returns	Out of Plane/Dynamic	350S125-18	No	No	Yes	No	No	No	No
19	39, 45 & 47	Bookshelf wall w/ returns	Out of Plane/Dynamic	350S125-18	No	No	Yes	No	Yes	Yes	No
20	40, 41 & 43	Bookshelf wall w/o returns	Out of Plane/Dynamic	350S125-18	No	No	Yes	No	No	Yes	No
21	42, 44 & 46	Equivalent Ceiling wall w/ returns	Out of Plane/Dynamic	350S125-18	Yes	No	Yes	No	Yes	Yes	Yes
22	48, 49 & 50	Partial height braced wall	Out of Plane/Dynamic	350S125-18	Yes	Yes	Yes	Yes	Yes	No	No

A detailed description of the test specimens, along with the detailed experimental results is presented in Appendix A.

In general, slight variations in the configurations were progressively introduced between consecutive tests. For fragility assessment purposes, 3 tests were conducted for each wall configuration, unless the

observed damage was similar to specimens already tested. All specimens without attached mass tested in-plane, except for configuration 11, were tested using the quasi-static testing protocol shown in Figure 3.3b. During the quasi-static tests, detailed inspections of the specimen's damage were performed at the peak drifts indicated in Figure 3.3b and highlighted in Table 3-2. The damage inspection involved visual screening of the outside of each wall, taking pictures to record damage, inspections by high definition cameras in the inside of each wall, and hand-written notes to accurately describe the type of damage occurring. Following the tests, most specimens were opened to assess damage in framing elements. Particularly, the specimen damage states triggered at each inspection and the damage progression were carefully monitored. All other specimens were tested using the dynamic testing protocol shown in Figure 3.2. During dynamic testing, visual inspections were not possible due to the high speed at which the tests elapsed, and therefore, the seismic demands triggering the damage states were estimated by tracking the time-stamped high-definition videos and the data recorded during the tests.

3.3.2 Materials used in Testing

This subsection describes the mechanical properties of the steels used in the studs and tracks of the specimens, and the concrete slabs used as boundary elements for the tested specimens.

3.3.2.1 Steel Studs and Tracks

The partition walls were constructed using standard steel studs and tracks selected from the SSMA catalog. Tests aiming at determining the effective material thickness, yield and tensile strength, and elongation at rupture were performed following the ASTM A370 (ASTM, 2003) procedures. Table 3-4 presents a summary of the experimental coupon test results. The minimum/reference values presented in Table 3-4 are given by ASTM A370. In Table 3-4, a significant difference in studs and tracks material properties is observed. A detailed description of the coupon test results is presented in Appendix B.

Table 3-4 Steel Stud and Track Material Properties

Description	Average Values Material Properties				
	Material Thickness e (mils)	Yielding Strength σ_y (ksi)	Ultimate Strength σ_u (ksi)	Rupture Elongation ε_u (in/in)	Elasticity Modulus E_s (ksi)
Studs SSMA 350S125-18	17	48	55	0.32	31830
Tracks SSMA 350S125-18	21	52	58	0.02	22216
Studs SSMA 350S125-30	31	38	49	0.22	26558
Tracks SSMA 350S125-30	36	52	57	0.31	23258
Tracks SSMA 350S125-18	25	27	43	0.36	14519
Minimum/Reference Values	Variable	33	45	0.20	29000

3.3.2.2 Concrete Slabs

The specimen's steel tracks were connected to the 4-inch-thick concrete platform slabs shown in Figure 3.9. The specified concrete strength was $f_c^{'}$ = 4 ksi, while the actual concrete strength, determined through testing of cylinders prepared when pouring the slabs, was in the range $f_c^{'} \approx$ 3.6-4.6 ksi, as described in Appendix B.

3.4 Test Program

Table 3-5 shows for reference the details of the partition wall testing program. Indicated in Table 3-5 are the fragility groups to which each specimen is associated. Details about the fragility analysis are presented in Chapter 4.

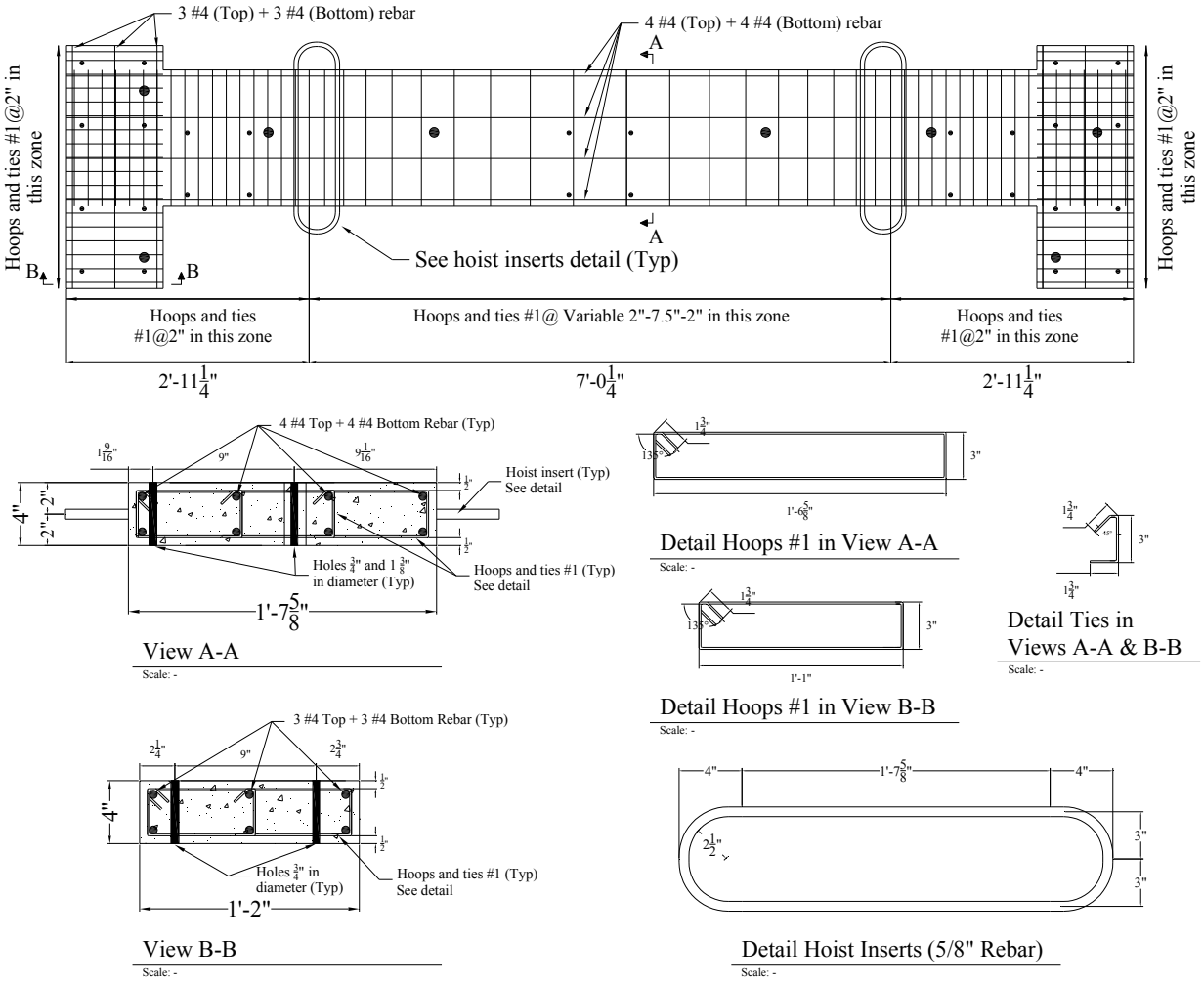

Figure 3.9 – Concrete Slab used as Boundary Elements for Test Specimens

Table 3-5 Experimental Testing Program

Specimen	Description	Date Test	Test Type	Fragility Group	Comment
1	Basic (slip track)	04-28-08	In Plane/Quasi Static	1a	
2	Basic (slip track)	04-28-08	In Plane/Quasi Static	1a	
3	Basic (slip track)	05-19-08	In Plane/Quasi Static	1a	
4	Gypsum connected to top track	05-19-08	In Plane/Quasi Static	1b	Field studs not connected to top track
5	No Return	05-23-08	In Plane/Quasi Static	1b	Field studs not connected to top track
6	No Return	05-23-08	In Plane/Quasi Static	1b	Field studs not connected to top track
7	Full connection	06-06-08	In Plane/Quasi Static	1b	
8	Full connection	06-06-08	In Plane/Quasi Static	1b	
9	Full connection	06-16-08	In Plane/Quasi Static	1b	
10	No Return	06-16-08	In Plane/Quasi Static	1b	Field studs not connected to top track
11	Bookshelf	06-23-08	In Plane/Dynamic	1a	Field studs not connected to top track
12	Bookshelf	06-23-08	In Plane/Dynamic	1a	Field studs not connected to top track
13	Bookshelf	07-03-08	In Plane/Dynamic	1a	Field studs not connected to top track
14	Equivalent Ceiling	07-03-08	In Plane/Dynamic	1a	Field studs not connected to top track
15	Equivalent Ceiling	07-10-08	In Plane/Dynamic	1a	Field studs not connected to top track
16	Equivalent Ceiling	07-10-08	In Plane/Dynamic	1a	Field studs not connected to top track
17	Partial height braced wall	07-17-08	In Plane/Quasi Static	3	
18	Partial height braced wall	07-17-08	In Plane/Quasi Static	3	
19	Partial height braced wall	08-19-08	In Plane/Quasi Static	3	
20	Institutional const./slip track	08-19-08	In Plane/Quasi Static	2a	
21	Institutional const./slip track	08-26-08	In Plane/Quasi Static	2a	
22	Institutional const./slip track	08-26-08	In Plane/Quasi Static	2a	
23	Institutional const./Full Connection@24"	09-08-08	In Plane/Quasi Static	2b	
24	Institutional const./Full Connection@24"	09-08-08	In Plane/Quasi Static	2b	
25	Institutional const./Full Connection@12"	09-19-08	In Plane/Quasi Static	2b	
26	Institutional const./Full Connection@24"	09-19-08	In Plane/Quasi Static	2b	
27	Institutional const./Full Connection@12"	10-02-08	In Plane/Quasi Static	2b	
28	Institutional const./Full Connection@12"	10-02-08	In Plane/Quasi Static	2b	
29	No Return/Dynamic	10-15-08	In Plane/Dynamic	1a	
30	No Return/Dynamic	10-15-08	In Plane/Dynamic	1a	
31	C-Shaped Walls	10-23-08	In Plane/Quasi Static	1a	
32	C-Shaped Walls	10-23-08	In Plane/Quasi Static	1a	
33	Solution to T corner damage/corner gaps	11-05-08	In Plane/Quasi Static	4	
34	Solution to T corner damage/double slip track	11-05-08	In Plane/Quasi Static	4	
35	Solution to L corner damage/corner gaps	11-14-08	In Plane/Quasi Static	4	
36	Solution to T corner damage/slip track	11-14-08	In Plane/Quasi Static	4	
37	Unloaded Wall w/ Returns	12-08-08	Out of Plane/Dynamic	1a	
38	Unloaded Wall w/o Returns	12-08-08	Out of Plane/Dynamic	1a	
39	Bookshelf wall w/ returns	01-08-09	Out of Plane/Dynamic	1a	
40	Bookshelf wall w/o returns	01-08-09	Out of Plane/Dynamic	1a	
41	Bookshelf wall w/o returns	01-26-09	Out of Plane/Dynamic	1a	
42	Equivalent Ceiling wall w/ returns	01-26-09	Out of Plane/Dynamic	1a	
43	Bookshelf wall w/o returns	02-02-09	Out of Plane/Dynamic	1a	
44	Equivalent Ceiling wall w/ returns	02-02-09	Out of Plane/Dynamic	1a	
45	Bookshelf wall w/ returns	02-09-09	Out of Plane/Dynamic	1a	
46	Equivalent Ceiling wall w/ returns	02-09-09	Out of Plane/Dynamic	1a	
47	Bookshelf wall w/ returns	02-16-09	Out of Plane/Dynamic	1a	
48	Partial height braced wall	02-16-09	Out of Plane/Dynamic	3	
49	Partial height braced wall	02-23-09	Out of Plane/Dynamic	3	
50	Partial height braced wall	02-23-09	Out of Plane/Dynamic	3	

3.5 Instrumentation

Extensive instrumentation was used for recording the displacements, forces and absolute accelerations imposed on the specimens by the motions of the UB-NCS platforms. Figure 3.10 shows the location of the load cells (Bracci et al. 1992), placed under the wall specimens, and used to measure the actual forces acting on the partition walls. Figure 3.11 shows the location of the potentiometers used to measure the

deformation fields within the specimens during in-plane testing, including relative displacements between tracks and concrete slabs, relative displacements between studs and tracks, relative displacements between perpendicular walls, and diagonal wall deformations. During dynamic testing, accelerometers were installed at each platform. In addition, for the out-of-plane tests, the grid of accelerometers shown schematically in Figure 3.12 was considered to record the amplification of accelerations within the wall plane. Figure 3.13 and Figure 3.14 show photographs with many of the instruments used for in-plane and out-of-plane testing, respectively. Figure 3.15 shows the location of the high definition cameras used to track the seismic demands triggering the different damage states. Table 3-6 and Table 3-7 list the instrumentation considered for in-plane and out-of-plane testing, respectively.

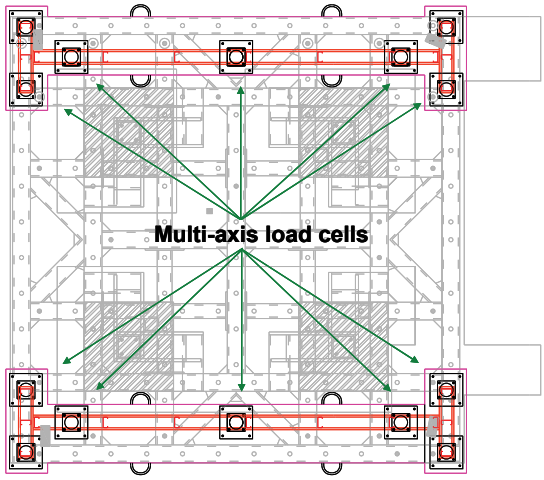

(a) General load cell layout

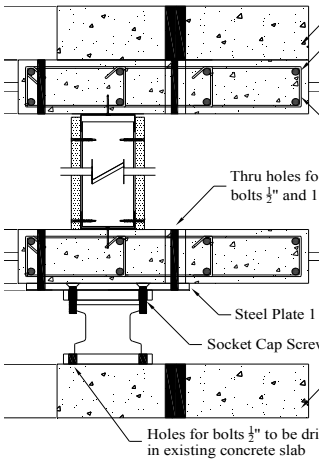

(b) Detail load cell under wall

(c) Boundary concrete slab mounted on top of (yellow) load cells

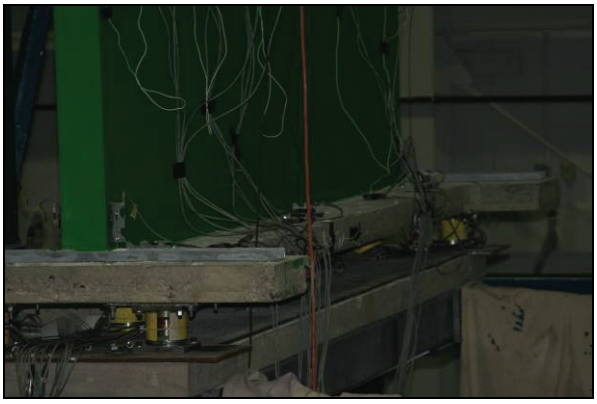

(d) Test specimen mounted on top of concrete slabs and (yellow) load cells

Figure 3.10 - Load Cell Instrumentation Under Partition Walls

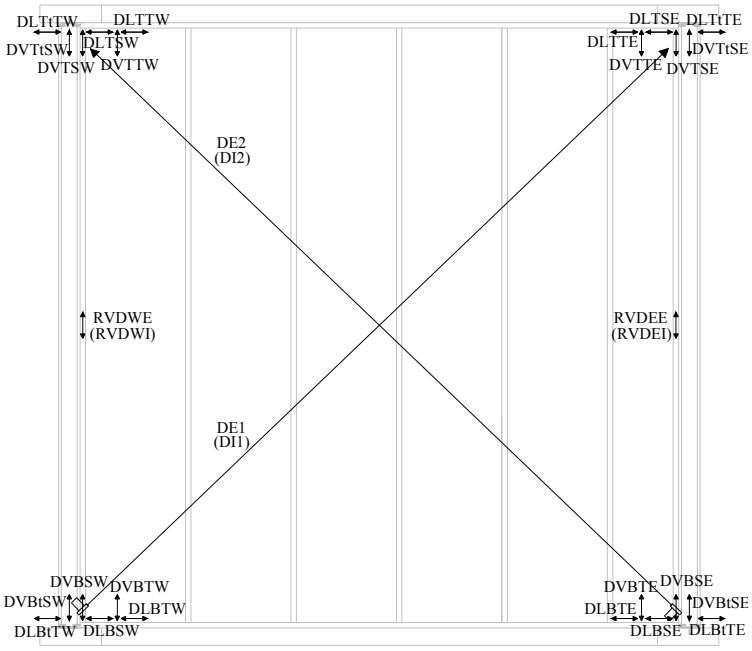

Figure 3.11 - Potentiometer Instrumentation in Partition Walls

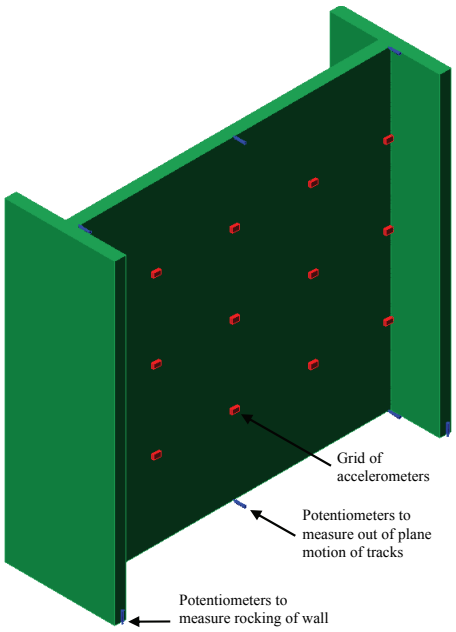

Figure 3.12 - Accelerometer Grid for Out-of-plane Tests

Slight variations to the instrumentation lists shown in Table 3-6 and Table 3-7 were introduced when testing specimens with attached equivalent rigid ceilings, specimens without return walls, in-plane dynamic testing, partial height walls, etc. The exact instrumentation list for each specimen has been made available in the World Wide Web through NEEShub (https://nees.org/myhub).

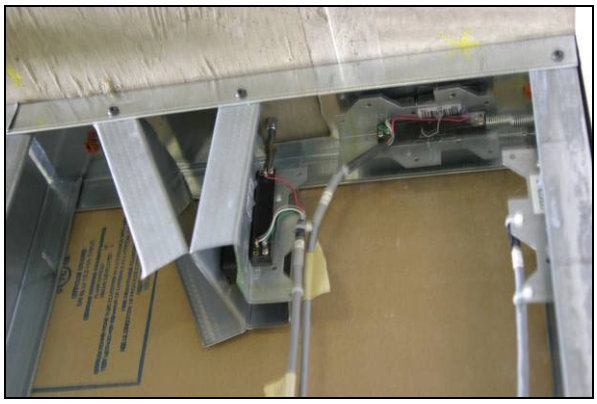

(a) Instruments used to measure relative vertical displacement between longitudinal wall top track and concrete slabs (DVTTE); and horizontal (DLTSE) and vertical (DVTSE) relative displacements between boundary stud and top track.

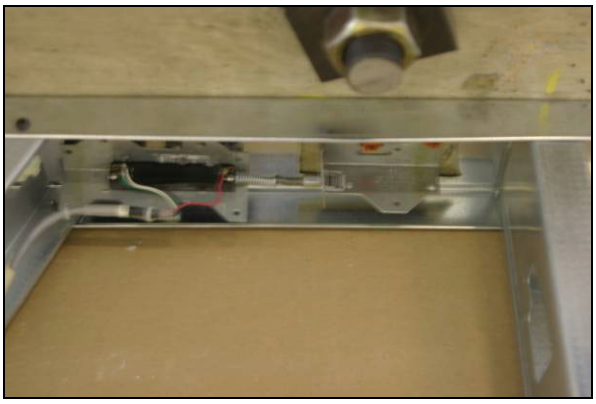

(b) Instruments used to measure relative horizontal displacement between longitudinal wall top track and concrete slabs (DLTTE).

(c) Instruments used to measure relative vertical displacement between longitudinal wall bottom track and concrete slabs (DLTTE).

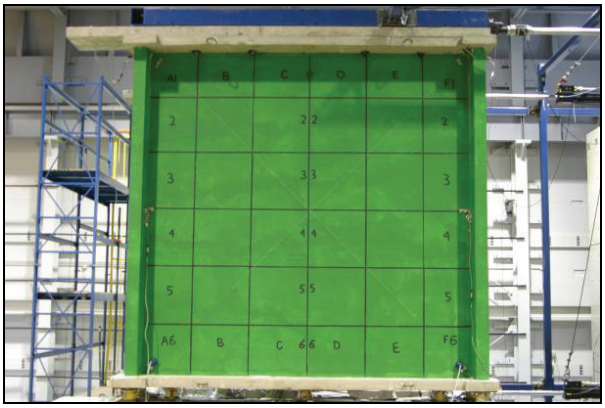

(d) Instruments used to measure diagonal deformations within the walls (DSWE1 and DSWE2); and relative vertical displacements between longitudinal and transverse walls (RVDWE and RVDEE).

Figure 3.13 - Typical Details of Instrumentation used to Measure Deformation Field within Specimen Walls During In-plane Testing.

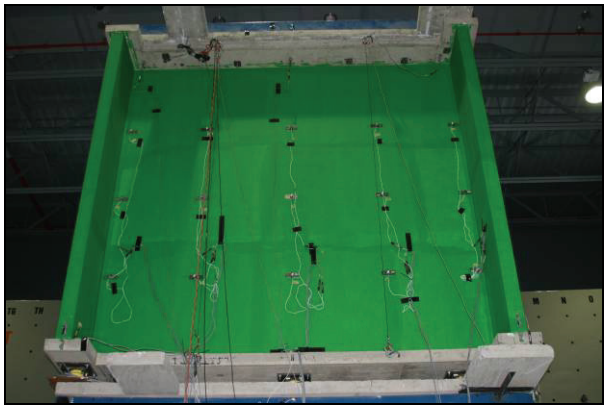

(a) Accelerometer grid used to measure acceleration field within full-height specimen.

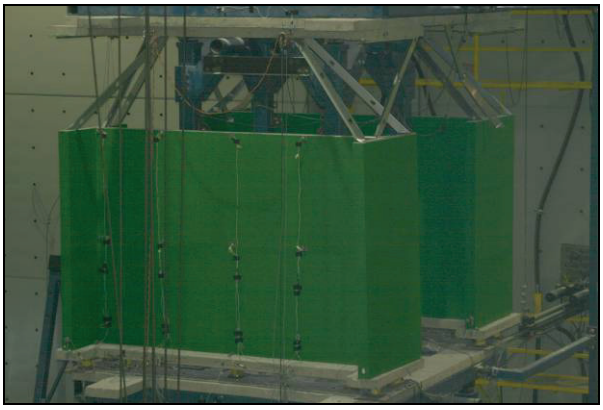

(b) Accelerometer grid used to measure acceleration field within partial-height specimen.

Figure 3.14 - Typical Details of Instrumentation used to Measure Acceleration Field within Specimen Walls during Out-of-plane Testing.

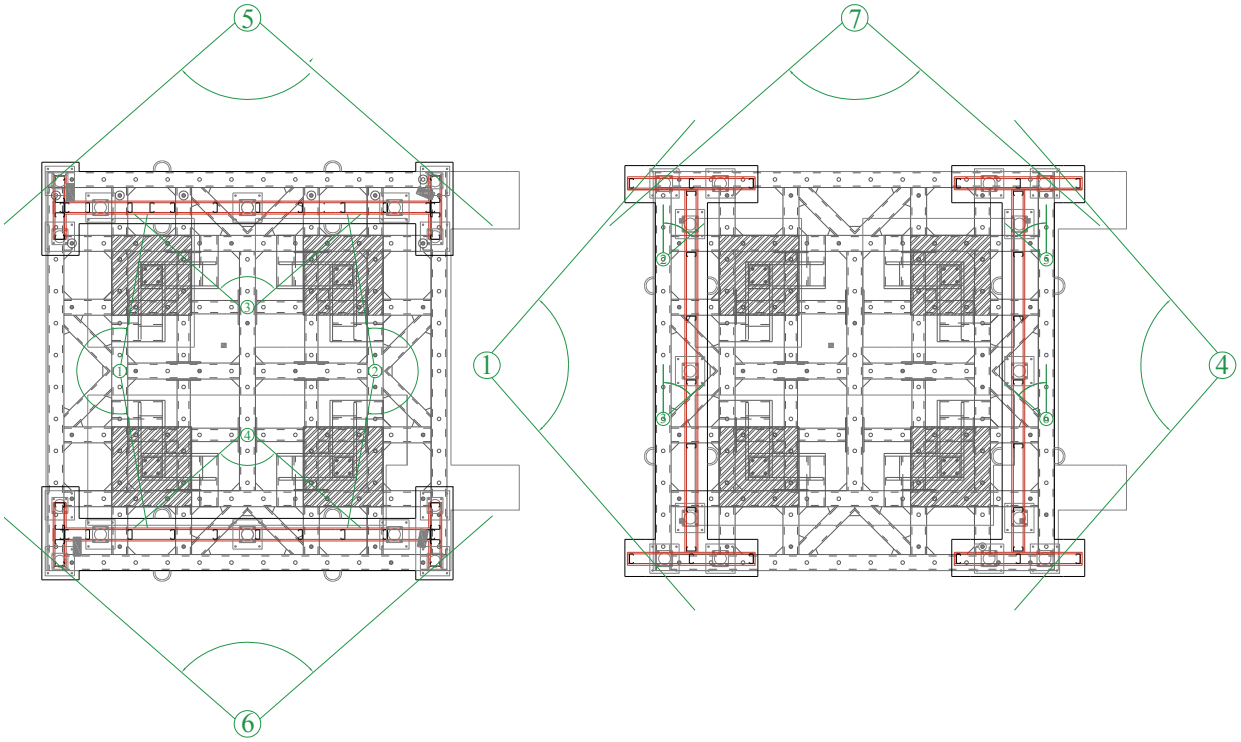

Figure 3.15 - Camera Location for In-plane and Out-of-plane Testing

Table 3-6 Instrumentation List for In-plane Testing

Channel	ID	Instrument	Response Quantity	Operation Limits	Orientation	Location/Comment
Data Acquired from UB-NCS Actuators						
1	Time		Time			
2	Com Top		Actuator Disp	± 40 in		Actuator A command
3	DisplA		Actuator Disp	± 40 in		Actuator A displacement
4	DisplB		Actuator Disp	± 40 in		Actuator B displacement
5	Com Bot		Actuator Disp	± 40 in		Actuator C command
6	DisplC		Actuator Force	± 40 in		Actuator C displacement
7	DisplD		Actuator Force	± 40 in		Actuator D displacement
Data Acquired from Load Cells						
8	LC4N	Load Cell	Vertical Force	± 5 kips	V	North Partition Wall
9	LC4Sx	Load Cell	Shear Force	± 5 kips	EW	North Partition Wall
10	LC1N	Load Cell	Vertical Force	± 5 kips	V	North Partition Wall
11	LC1Sx	Load Cell	Shear Force	± 5 kips	EW	North Partition Wall
12	LC3N	Load Cell	Vertical Force	± 5 kips	V	North Partition Wall
13	LC3Sx	Load Cell	Shear Force	± 5 kips	EW	North Partition Wall
14	LC15N	Load Cell	Vertical Force	± 5 kips	V	North Partition Wall
15	LC15Sx	Load Cell	Shear Force	± 5 kips	EW	North Partition Wall
16	LC5N	Load Cell	Vertical Force	± 5 kips	V	North Partition Wall
17	LC5Sx	Load Cell	Shear Force	± 5 kips	EW	North Partition Wall
18	LC2N	Load Cell	Vertical Force	± 5 kips	V	North Partition Wall
19	LC2Sx	Load Cell	Shear Force	± 5 kips	EW	North Partition Wall
20	LC8N	Load Cell	Vertical Force	± 5 kips	V	North Partition Wall
21	LC8Sx	Load Cell	Shear Force	± 5 kips	EW	North Partition Wall
22	LC6N	Load Cell	Vertical Force	± 5 kips	V	South Partition Wall
23	LC6Sx	Load Cell	Shear Force	± 5 kips	EW	South Partition Wall
24	LC11N	Load Cell	Vertical Force	± 5 kips	V	South Partition Wall
25	LC11Sx	Load Cell	Shear Force	± 5 kips	EW	South Partition Wall
26	LC14N	Load Cell	Vertical Force	± 5 kips	V	South Partition Wall
27	LC14Sx	Load Cell	Shear Force	± 5 kips	EW	South Partition Wall
28	LC9N	Load Cell	Vertical Force	± 5 kips	V	South Partition Wall
29	LC9Sx	Load Cell	Shear Force	± 5 kips	EW	South Partition Wall
30	LC10N	Load Cell	Vertical Force	± 5 kips	V	South Partition Wall
31	LC10Sx	Load Cell	Shear Force	± 5 kips	EW	South Partition Wall
32	LC12N	Load Cell	Vertical Force	± 5 kips	V	South Partition Wall
33	LC12Sx	Load Cell	Shear Force	± 5 kips	EW	South Partition Wall
34	LC13N	Load Cell	Vertical Force	± 5 kips	V	South Partition Wall
35	LC13Sx	Load Cell	Shear Force	± 5 kips	EW	South Partition Wall
Instrumentation South Wall						
36	DLBSW	Potentiometer	Displacement	± 1.5 in	EW	Longitudinal displacement bottom stud west corner
37	DVBSW	Potentiometer	Displacement	± 1.5 in	V	Vertical displacement bottom stud west corner
38	DLBTW	Potentiometer	Displacement	± 1.5 in	EW	Longitudinal displacement bottom track west corner
39	DVBTW	Potentiometer	Displacement	± 1.5 in	V	Vertical displacement bottom track west corner
40	DLBtTW	Potentiometer	Displacement	± 1.5 in	EW	Longitudinal displacement bottom transverse wall track west corner
41	DVBtSW	Potentiometer	Displacement	± 1.5 in	V	Vertical displacement bottom transverse wall stud west corner
42	DLBSE	Potentiometer	Displacement	± 1.5 in	EW	Longitudinal displacement bottom stud east corner
43	DVBSE	Potentiometer	Displacement	± 1.5 in	V	Vertical displacement bottom stud east corner
44	DLBTE	Potentiometer	Displacement	± 1.5 in	EW	Longitudinal displacement bottom track east corner
45	DVBTE	Potentiometer	Displacement	± 1.5 in	V	Vertical displacement bottom track east corner
46	DLBtTE	Potentiometer	Displacement	± 1.5 in	EW	Longitudinal displacement bottom transverse wall track east corner
47	DVBtSE	Potentiometer	Displacement	± 1.5 in	V	Vertical displacement bottom transverse wall stud east corner
48	DLTSW	Potentiometer	Displacement	± 1.5 in	EW	Longitudinal displacement top stud west corner
49	DVTSW	Potentiometer	Displacement	± 1.5 in	V	Vertical displacement top stud west corner
50	DLTTW	Potentiometer	Displacement	± 1.5 in	EW	Longitudinal displacement top track west corner
51	DVTTW	Potentiometer	Displacement	± 1.5 in	V	Vertical displacement top track west corner
52	DLTtTW	Potentiometer	Displacement	± 1.5 in	EW	Longitudinal displacement top transverse wall track west corner
53	DVTtSW	Potentiometer	Displacement	± 1.5 in	V	Vertical displacement top transverse wall stud west corner
54	DLTSE	Potentiometer	Displacement	± 1.5 in	EW	Longitudinal displacement top stud east corner
55	DVTSE	Potentiometer	Displacement	± 1.5 in	V	Vertical displacement top stud east corner
56	DLTTE	Potentiometer	Displacement	± 1.5 in	EW	Longitudinal displacement top track east corner
57	DVTTE	Potentiometer	Displacement	± 1.5 in	V	Vertical displacement top track east corner
58	DLTtTE	Potentiometer	Displacement	± 1.5 in	EW	Longitudinal displacement top transverse wall track east corner
59	DVTtSE	Potentiometer	Displacement	± 1.5 in	V	Vertical displacement top transverse wall stud east corner
60	DLBSC	Potentiometer	Displacement	± 1.5 in	EW	Longitudinal displacement bottom stud central zone
61	DLTSC	Potentiometer	Displacement	± 1.5 in	EW	Longitudinal displacement top stud central zone
62	RVDWE	Potentiometer	Displacement	± 1.5 in	V	Relative vertical displacement walls exterior west corner
63	RVDWI	Potentiometer	Displacement	± 1.5 in	V	Relative vertical displacement walls interior west corner
64	RVDEE	Potentiometer	Displacement	± 1.5 in	V	Relative vertical displacement walls exterior east corner
65	RVDEI	Potentiometer	Displacement	± 1.5 in	V	Relative vertical displacement walls interior east corner
Diagonal Instrumentation North Wall						
66	DNWE1	String Pot	Displacement	± 6 in	Diagonal	Deformation wall diagonal exterior
67	DNWI1	String Pot	Displacement	± 6 in	Diagonal	Deformation wall diagonal interior
68	DNWI2	String Pot	Displacement	± 6 in	Diagonal	Deformation wall diagonal interior
69	DNWE2	String Pot	Displacement	± 6 in	Diagonal	Deformation wall diagonal exterior
Diagonal Instrumentation South Wall						
70	DSWE1	String Pot	Displacement	± 6 in	Diagonal	Deformation wall diagonal exterior
71	DSWE2	String Pot	Displacement	± 6 in	Diagonal	Deformation wall diagonal exterior
72	DSWI1	String Pot	Displacement	± 6 in	Diagonal	Deformation wall diagonal interior
73	DSWI2	String Pot	Displacement	± 6 in	Diagonal	Deformation wall diagonal interior
UB-NCS Platform Accelerations						
74	ALevel1	Accelerometer	Acceleration	± 10 g	EW	Acceleration bottom UB-NCS platform
75	ALevel2	Accelerometer	Acceleration	± 10 g	EW	Acceleration top UB-NCS platform

Table 3-7 Instrumentation List for Out-of-plane Testing

Channel	ID	Instrument	Response quantity	Min Operation Limits	Orientation	Location and/or Comment
Data Acquired from Actuators						
1	Time		Time			
2	ComActA		Actuator Disp	±40in		Actuator A command
3	ComActB		Actuator Disp	±40in		Actuator B command
4	ComActC		Actuator Disp	±40in		Actuator C command
5	ComActD		Actuator Disp	±40in		Actuator D command
6	DispActA		Actuator Disp	±40in		Actuator A displacement
7	DispActB		Actuator Disp	±40in		Actuator B displacement
8	DispActC		Actuator Disp	±40in		Actuator C displacement
9	DispActD		Actuator Disp	±40in		Actuator D displacement
10	ForceA		Actuator Force	±50kip		Actuator A
11	ForceB		Actuator Force	±50kip		Actuator B
12	ForceC		Actuator Force	±50kip		Actuator C
13	ForceD		Actuator Force	±50kip		Actuator D
Data Acquired from Load Cells						
14	LC1	Load Cell	Shear Force	±5 kips	EW	East Partition Wall
15	LC1	Load Cell	Vertical Force	±5 kips	V	East Partition Wall
16	LC2	Load Cell	Shear Force	±5 kips	EW	East Partition Wall
17	LC2	Load Cell	Vertical Force	±5 kips	V	East Partition Wall
18	LC3	Load Cell	Shear Force	±5 kips	EW	East Partition Wall
19	LC3	Load Cell	Vertical Force	±5 kips	V	East Partition Wall
20	LC4	Load Cell	Shear Force	±5 kips	EW	East Partition Wall
21	LC4	Load Cell	Vertical Force	±5 kips	V	East Partition Wall
22	LC5	Load Cell	Shear Force	±5 kips	EW	East Partition Wall
23	LC5	Load Cell	Vertical Force	±5 kips	V	East Partition Wall
24	LC6	Load Cell	Shear Force	±5 kips	EW	East Partition Wall
25	LC6	Load Cell	Vertical Force	±5 kips	V	East Partition Wall
26	LC7	Load Cell	Shear Force	±5 kips	EW	East Partition Wall
27	LC7	Load Cell	Vertical Force	±5 kips	V	East Partition Wall
28	LC8	Load Cell	Shear Force	±5 kips	EW	West Partition Wall
29	LC8	Load Cell	Vertical Force	±5 kips	V	West Partition Wall
30	LC9	Load Cell	Shear Force	±5 kips	EW	West Partition Wall
31	LC9	Load Cell	Vertical Force	±5 kips	V	West Partition Wall
32	LC10	Load Cell	Shear Force	±5 kips	EW	West Partition Wall
33	LC10	Load Cell	Vertical Force	±5 kips	V	West Partition Wall
34	LC11	Load Cell	Shear Force	±5 kips	EW	West Partition Wall
35	LC11	Load Cell	Vertical Force	±5 kips	V	West Partition Wall
36	LC12	Load Cell	Shear Force	±5 kips	EW	West Partition Wall
37	LC12	Load Cell	Vertical Force	±5 kips	V	West Partition Wall
38	LC13	Load Cell	Shear Force	±5 kips	EW	West Partition Wall
39	LC13	Load Cell	Vertical Force	±5 kips	V	West Partition Wall
40	LC14	Load Cell	Shear Force	±5 kips	EW	West Partition Wall
41	LC14	Load Cell	Vertical Force	±5 kips	V	West Partition Wall
Platforms Accelerometers						
42	albot	Accelerometer	Accelerations	±10 g	EW	Acceleration bottom platform
43	altop	Accelerometer	Accelerations	±10 g	EW	Acceleration top platform
44	alce	Accelerometer	Accelerations	±10 g	EW	Acceleration concrete slab under east wall
45	alcw	Accelerometer	Accelerations	±10 g	EW	Acceleration concrete slab under west wall
Instrumentation East Wall						
46	alent	Accelerometer	Accelerations	±10 g	EW	Acceleration north top grid node
47	alenc	Accelerometer	Accelerations	±10 g	EW	Acceleration north center grid node
48	alenb	Accelerometer	Accelerations	±10 g	EW	Acceleration north bottom grid node
49	alecnt	Accelerometer	Accelerations	±10 g	EW	Acceleration center-north top grid node
50	alecnc	Accelerometer	Accelerations	±10 g	EW	Acceleration center-north center grid node
51	alecnb	Accelerometer	Accelerations	±10 g	EW	Acceleration center-north bottom grid node
52	alect	Accelerometer	Accelerations	±10 g	EW	Acceleration center top grid node
53	alecc	Accelerometer	Accelerations	±10 g	EW	Acceleration center center grid node
54	alecb	Accelerometer	Accelerations	±10 g	EW	Acceleration center bottom grid node
55	alecst	Accelerometer	Accelerations	±10 g	EW	Acceleration center-south top grid node
56	alecsc	Accelerometer	Accelerations	±10 g	EW	Acceleration center-south center grid node
57	alecsb	Accelerometer	Accelerations	±10 g	EW	Acceleration center-south bottom grid node
58	alest	Accelerometer	Accelerations	±10 g	EW	Acceleration south top grid node
59	alesc	Accelerometer	Accelerations	±10 g	EW	Acceleration south center grid node
60	alesb	Accelerometer	Accelerations	±10 g	EW	Acceleration south bottom grid node
61	dlettn	Potentiometer	Displacement	±1 in	EW	Displacement top track north
62	dlettc	Potentiometer	Displacement	±1 in	EW	Displacement top track center
63	dletts	Potentiometer	Displacement	±1 in	EW	Displacement top track south
64	dlebtn	Potentiometer	Displacement	±1 in	EW	Displacement bottom track north
65	dlebtc	Potentiometer	Displacement	±1 in	EW	Displacement bottom track center
66	dlebts	Potentiometer	Displacement	±1 in	EW	Displacement bottom track south
67	dventwe	Potentiometer	Displacement	±1 in	EW	Displacement vertical north transverse wall east end
68	dventww	Potentiometer	Displacement	±1 in	EW	Displacement vertical north transverse wall west end
69	dvestwe	Potentiometer	Displacement	±1 in	EW	Displacement vertical south transverse wall east end
70	dvestww	Potentiometer	Displacement	±1 in	EW	Displacement vertical south transverse wall west end
Instrumentation West Wall						
71	alwnt	Accelerometer	Accelerations	±10 g	EW	Acceleration north top grid node
72	alwnc	Accelerometer	Accelerations	±10 g	EW	Acceleration north center grid node
73	alwnb	Accelerometer	Accelerations	±10 g	EW	Acceleration north bottom grid node
74	alwcnt	Accelerometer	Accelerations	±10 g	EW	Acceleration center-north top grid node
75	alwcnc	Accelerometer	Accelerations	±10 g	EW	Acceleration center-north center grid node
76	alwcnb	Accelerometer	Accelerations	±10 g	EW	Acceleration center-north bottom grid node
77	alwct	Accelerometer	Accelerations	±10 g	EW	Acceleration center top grid node
78	alwcc	Accelerometer	Accelerations	±10 g	EW	Acceleration center center grid node
79	alwcb	Accelerometer	Accelerations	±10 g	EW	Acceleration center bottom grid node
80	alwcst	Accelerometer	Accelerations	±10 g	EW	Acceleration center-south top grid node
81	alwcsc	Accelerometer	Accelerations	±10 g	EW	Acceleration center-south center grid node
82	alwcsb	Accelerometer	Accelerations	±10 g	EW	Acceleration center-south bottom grid node
83	alwst	Accelerometer	Accelerations	±10 g	EW	Acceleration south top grid node
84	alwsc	Accelerometer	Accelerations	±10 g	EW	Acceleration south center grid node
85	alwsb	Accelerometer	Accelerations	±10 g	EW	Acceleration south bottom grid node
86	dlwttn	Potentiometer	Displacement	±1 in	EW	Displacement top track north
87	dlwttc	Potentiometer	Displacement	±1 in	EW	Displacement top track center
88	dlwtts	Potentiometer	Displacement	±1 in	EW	Displacement top track south
89	dlwbtn	Potentiometer	Displacement	±1 in	EW	Displacement bottom track north
90	dlwbtc	Potentiometer	Displacement	±1 in	EW	Displacement bottom track center
91	dlwbts	Potentiometer	Displacement	±1 in	EW	Displacement bottom track south
92	dvwntwe	Potentiometer	Displacement	±1 in	EW	Vertical displacement north transverse wall east end
93	dvwntww	Potentiometer	Displacement	±1 in	EW	Vertical displacement north transverse wall west end
94	dvwstwe	Potentiometer	Displacement	±1 in	EW	Vertical displacement south transverse wall east end
95	dvwstww	Potentiometer	Displacement	±1 in	EW	Vertical displacement south transverse wall west end

3.6 Specimens Performance Observations

This subsection presents a brief description of each test configuration along with the main damage mechanisms observed. Further details regarding the experimental observations, damage progression, and failure mechanisms can be found in the Appendix A and in the NEES Central Repository.

3.6.1 Performance Observations during In-plane Testing

A total of twenty-two light steel stud gypsum partition wall configurations were considered in the test series. Of the twenty-two configurations, sixteen configurations were tested in-plane. Variations in wall configurations and cyclic response are discussed in the following subsections.

3.6.1.1 Configuration 1

The test series began with testing Specimens 1, 2, and 3, which considered the most basic wall configuration. In these specimens, studs and gypsum wallboards were not screwed to the top track (slip track). The partition wall frame was constructed using steel studs model SSMA 362S125-18 with a typical spacing of 24" and standard tracks model SSMA 362T125-18. Two feet long perpendicular return walls were used to simulate typical wall boundary conditions. Gypsum wallboard panels (4'x8') with a thickness of 5/8" were laid perpendicular to the studs and screwed to the steel frame using standard Phillip self-drilling screws #6 spaced 12 inches on center at both perimeter and field. Drywall panel joints were offset on opposite faces of partition walls. The typical geometry of the specimens is shown in Figure 3.6, while a typical corner detail is presented in Figure 3.8a. Unintentionally, little to no gap was left between the top row of gypsum and the top concrete slab. The partition walls were finished with metal corner beads (1-1/4"), drywall paper joint tape (2-1/16" in width), two coats of mud, and water-based semi-gloss green paint, chosen in order to better contrast pictures. This type of construction was practically used for the construction of all specimens. Particular deviations from this construction scheme are described later for each specimen.

For specimens 1, 2 and 3, little to no damage was observed in the longitudinal walls. Only slight crushing of longitudinal wall corners was observed at relatively large drift ratios (up to 2%), as shown in Figure 3.16. The damage was mainly concentrated in the top tracks of the transverse walls and in the vertical joints between perpendicular walls, as shown in Figure 3.17 through Figure 3.19. Shown in Figure 3.20 is

the Force-Displacement curve for Specimen 3. The mean capping force (F_u) for Specimens 1 thru 3 is 1.75 kips at a mean drift ratio (Δ_u) of 0.58% with respective standard deviations of 0.51 kips and 0.20%.

Figure 3.16 – Crushing of Longitudinal Wall Corner at Large Drifts.

Figure 3.17 – Damage in Transverse Wall Top Track. The Connection to Concrete Slab of this Track did not Fail.

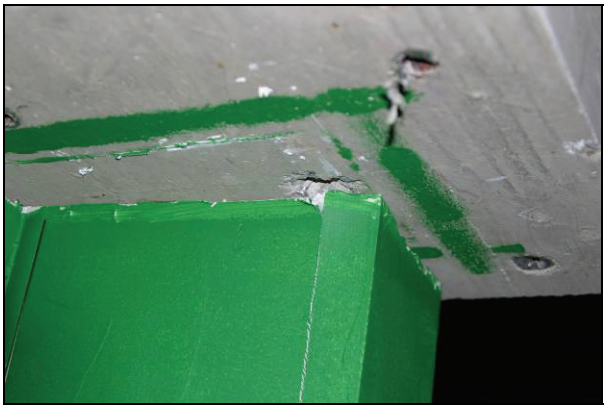

Figure 3.18 – Failure of Transverse Wall Top Track Fastener to Concrete Slab.

Figure 3.19 – Damage in Vertical Joint of Transverse and Longitudinal Walls

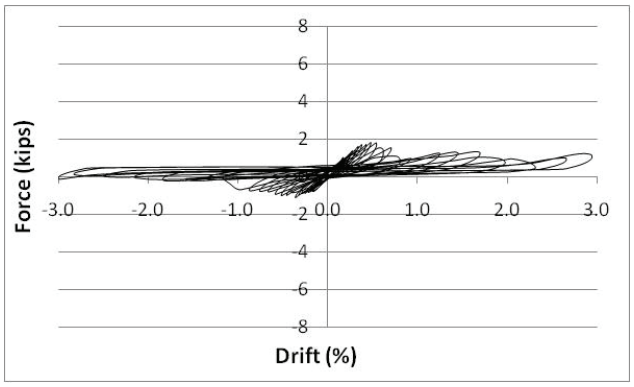

Figure 3.20 – Hysteretic Behavior of Specimen 3

3.6.1.2 Configuration 2

Specimen 4 is constructed using the same material as Specimens 1, 2, and 3, yet had the gypsum boards screwed to the top and bottom tracks. Damage similar to specimens 1, 2, and 3 was observed in the corners of the in-plane wall and at perpendicular wall joints. Previous to the damage at the edges of the gypsum board, crushing of the gypsum was observed around screws connecting wall panels to the top track, as shown in Figure 3.21 and Figure 3.22. As the drift increased, an increase in force surpassing the capping force was observed, this increase is caused by "ratcheting" effects.

Figure 3.21 – Damage at Gypsum to Top Track Screw Connectors

Figure 3.22 – Ratcheting of Partition Wall

Ratcheting occurs as drift ratios are increased because the sheathing is rotating as a rigid body. The gap between gypsum panels and concrete platforms go to zero, as shown in Figure 3.22, and increased forces

begin to be imposed on the walls. In Figure 3.23 a plot of the hysteretic behavior of specimen 4 is given. Because of the connection of the gypsum board to the top and bottom tracks, resulting in a 'stiffer wall', a higher capping force of 3.34 kips at a lower drift of Δ_u = 0.42% occurred.

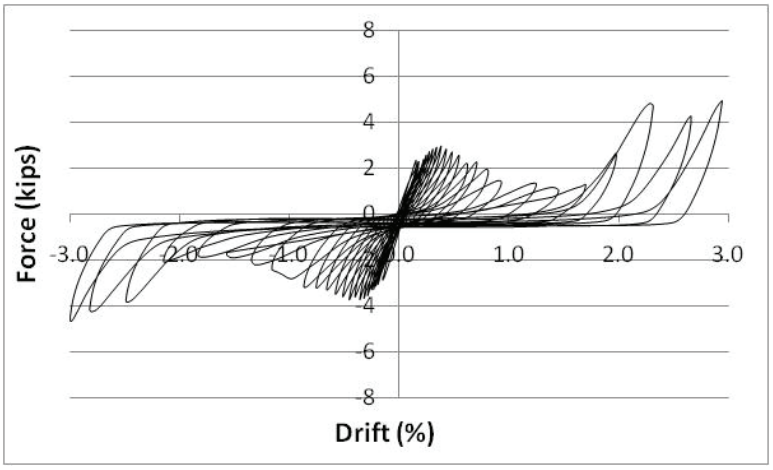

Figure 3.23 – Hysteretic Behavior of Specimen 4

3.6.1.3 Configuration 3

The following configuration includes test specimens 5, 6, and 10, and had the perpendicular walls removed to investigate the performance of the longitudinal walls alone, as shown in Figure 3.24 and Figure 3.25. For these specimens, the gypsum panels were attached to the top track and used 25 gauge steel material, most of the damage consisted of structural damage to the boundary stud. Also, extensive superficial damage to the gypsum board attached to the wall edges and the corner beads occurred, as shown in Figure 3.26. In these specimens, it was also observed that the top tracks moved from their original location. This happened as the top track slipped because of tearing in the steel track around the pin connections attaching the track to the concrete, as shown in Figure 3.27. The mean capping force is F_u = 2.66 kips with a standard deviation of 1.07 kips. The capping drift had a mean value of 0.52% and a standard deviation of 0.25%. The high deviation for this group demonstrates the range of failure mechanisms for this configuration. Figure 3.28 and Figure 3.29 are respectively the hysteretic behavior for specimens 5 and 10. In specimen 5, in the negative drift axis, a continuous increase in forces is observed, with only a slight change in the backbone at about 1.0% drift. In this specimen failure of the top track pin connectors was observed, whereas, in specimen 10, damage was concentrated in the gypsum panels and connectors.

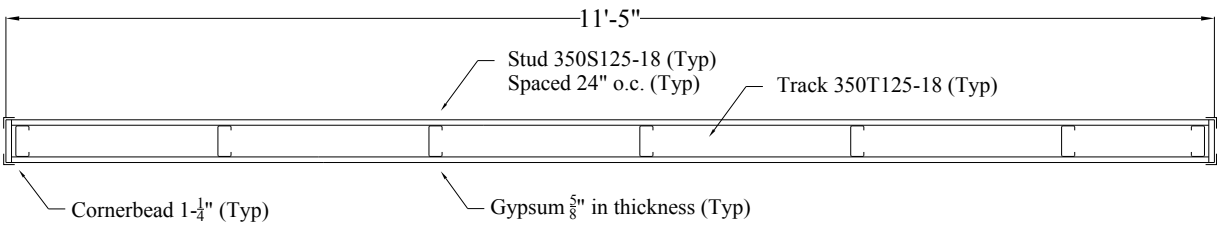

Figure 3.24 – Geometry of Specimens in Configuration 3

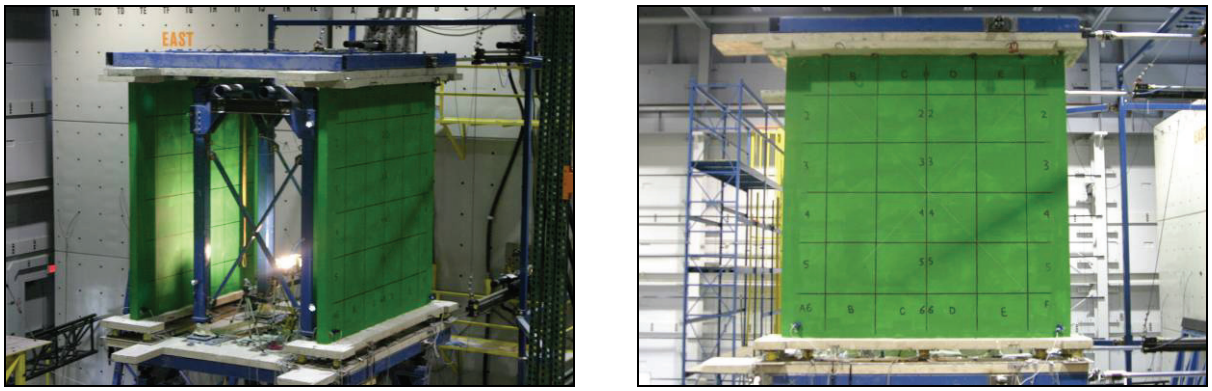

Figure 3.25 – Photos of Specimens in Configuration 3

Figure 3.26 – Damage to Boundary Stud and Finishing

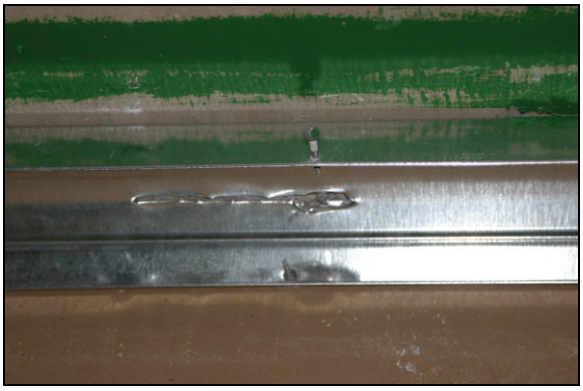

Figure 3.27 – Damage in Top Track at Pin Connectors

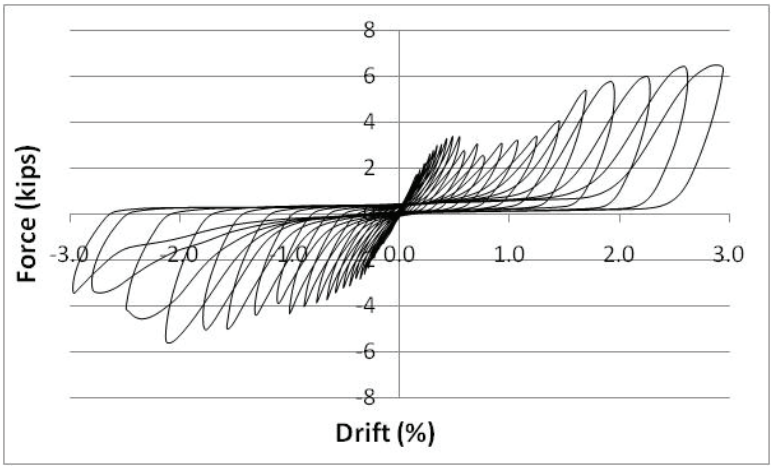

Figure 3.28 – Hysteretic Behavior of Specimen 5

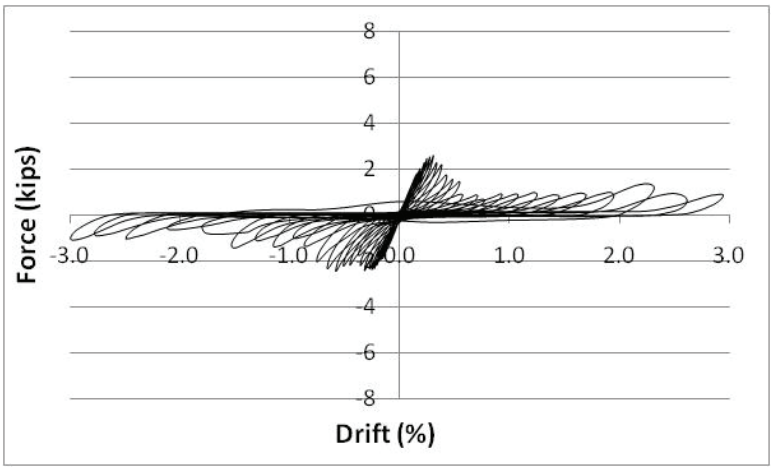

Figure 3.29 – Hysteretic Behavior of Specimen 10

3.6.1.4 Configuration 4

In order to develop the full shear capacity of the gypsum partition walls, specimens 7, 8 and 9 considered a full connection of studs and gypsum boards to the bottom and top tracks. During this test series, two failure mechanisms were observed. The first mechanism consisted of track slip, tracks tearing at the pin connections, similar to the damage just described for specimens 5, 6, and 10. The second failure mechanism consisted of a combination of crushing of the gypsum wallboards around the screws in the connection to the top tracks and inelastic flexural deformations occurring in the studs, as shown in Figure 3.30 and Figure 3.31. These “plastic hinges” always occurred at the height of the first row of gypsum board screw connectors, located approximately 12” from the top end of the studs. The capping force and

associated drift were respectively, 3.23 kips and 0.51% with standard deviations of 0.51 kips and 0.20%. In each of the specimens an increase in force due to racking was also observed; shown in Figure 3.32 is the force-displacement curve for Specimen 8 in which racking occurs in the positive drift direction.

Figure 3.30 – Damage in Studs Forming Plastic Hinges

Figure 3.31 – Detail of Hinge Forming in Studs

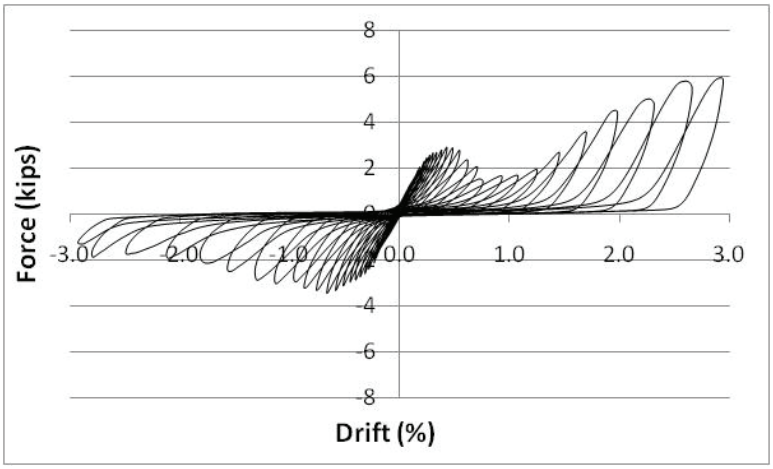

Figure 3.32 – Hysteretic Behavior of Specimen 8

3.6.1.5 Configurations 5 and 6

The next step in the testing program evaluated the effect of equivalent bookshelf and ceiling masses on the in-plane seismic performance of specimens 11 through 16. The bookshelf shown in Figure 3.33, was approximately 2'-6" tall by 9'-6" in length and was built out of pine material. The bottom of the bookshelves were placed 4'-6" from the floor level. Fully loaded, the bookshelf had a total weight of 510

pounds. Shown in Figure 3.34 is a photograph showing an example of a wall specimen with an attached bookshelf. The bookshelf was connected directly to the partition wall steel frame using 15 toggle bolts ¼" in diameter. The connectors were intentionally oversized to prevent their failure and to evaluate the effect of the attached mass on the partition walls. During testing, the books were protected from falling, to keep their mass attached to the wall during the whole test.

The attached ceiling weight was equivalent to the tributary weight of a rigid ceiling found in a 12'x12' room, approximately. The weight was simulated using a hollow steel section HSS5x3x1/4", attached at 8' from the floor, as shown in Figure 3.35, with a distributed weight of 12.2 plf. The equivalent ceiling was attached to partition walls using L2x2" steel moldings (20 gauge in thickness), which were connected directly to the gypsum wallboards using standard 1-1/4" fence staples spaced 24 inches on center. Details of the specimen geometry are shown in Figure 3.36. For these specimens, damage similar to specimens 5, 6 and 10, as shown in Figure 3.26 and Figure 3.27, was observed. No additional damage was observed in the studs around the bookshelves and negligible damage was observed around the bookshelves and ceiling connectors. The hysteretic behavior of specimen 13, a specimen that incorporated an attached bookshelf mass, is given in Figure 3.37. Figure 3.38 shows the hysteretic behavior for specimen 10, which considered the equivalent ceiling weight attached. The capping parameters for specimens 11 thru 16 were F_u = 1.44 kips and Δ_u = 0.54% with standard deviations of 0.60 kips and 0.22% respectively.

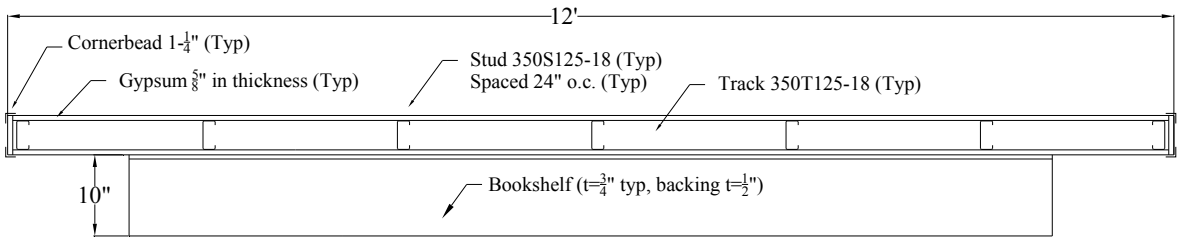

(a) Plan view specimen with attached bookshelf

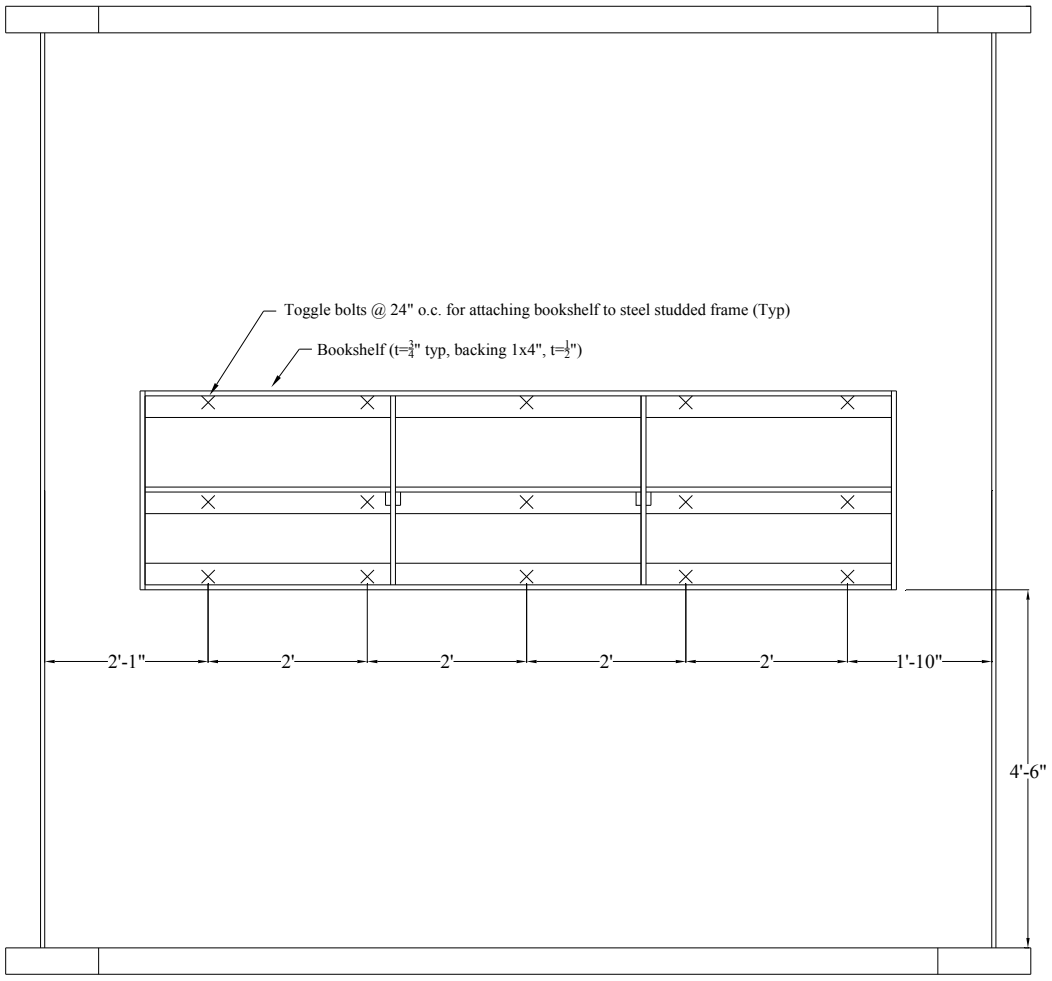

(b) Elevation view specimen with attached bookshelf

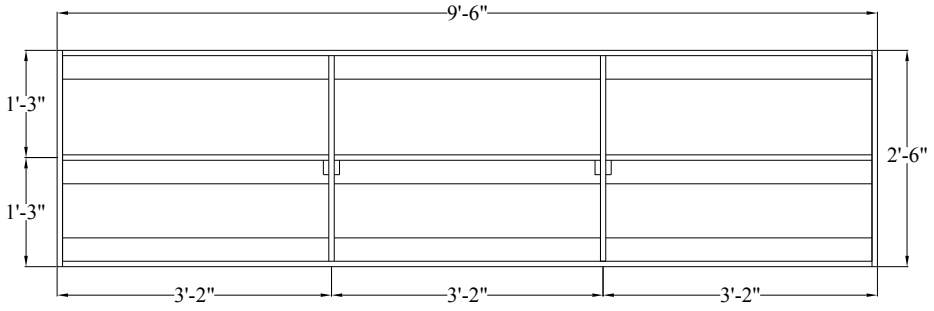

(c) Detail attached bookshelf

Figure 3.33 – Details of Specimens with Bookshelf Attached

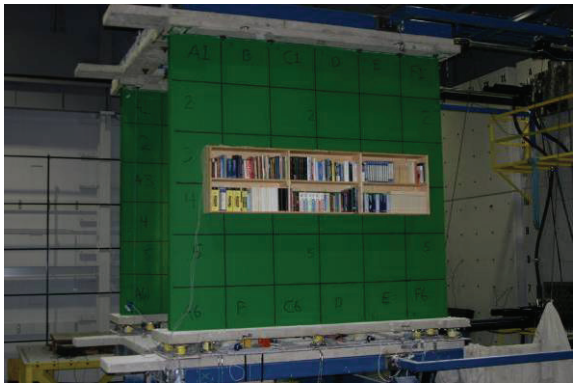

Figure 3.34 – Partition Wall Specimen with Attached Bookshelf

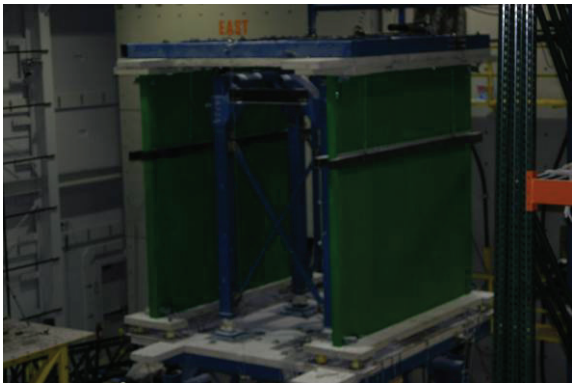

Figure 3.35 – Partition Wall Specimen with Attached Mass Simulating Ceiling Weight

3.6.1.6 Configuration 7

Specimens 17, 18 and 19 incorporated the partial-height seismically braced partition walls shown in Figure 3.39. These walls were also built using 25 gauge steel framing. Gypsum wallboards were fully attached at top and bottom tracks. These specimens had an in-plane wall with perpendicular walls attached at each end. The height of these walls was 8 ft. The walls were seismically braced following specifications of the Gypsum Association GA-50 standard: Seismic Bracing of Steel Stud Gypsum Board Partitions, using the same material used for the studs in the specimen, as shown in Figure 3.40. In these specimens, most of the damage was localized in the diagonal braces attaching the wall to the top concrete slab. Damage consisted of buckling of the braces and failure of the brace connection to the partition wall top tracks, as shown in Figure 3.41 and Figure 3.42, respectively. In one specimen, failure of the connectors between perpendicular wall top tracks was also observed, as shown in Figure 3.42. The mean capping force and drift for the partial height partition walls was 0.94 kips and 0.80% each with respective standard deviations of 0.18 kips and 0.19%.

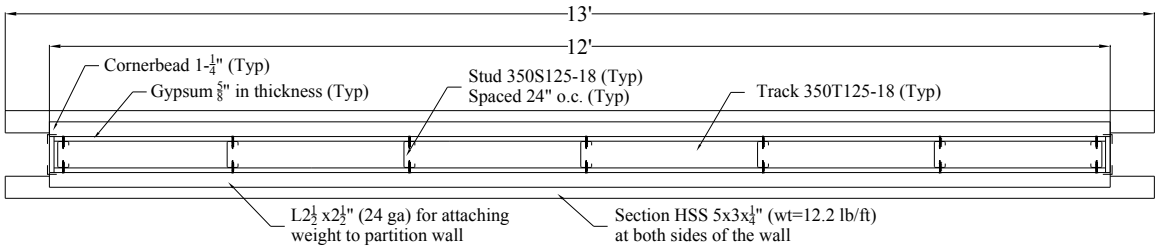

(a) Plan view specimen with attached equivalent ceiling weight

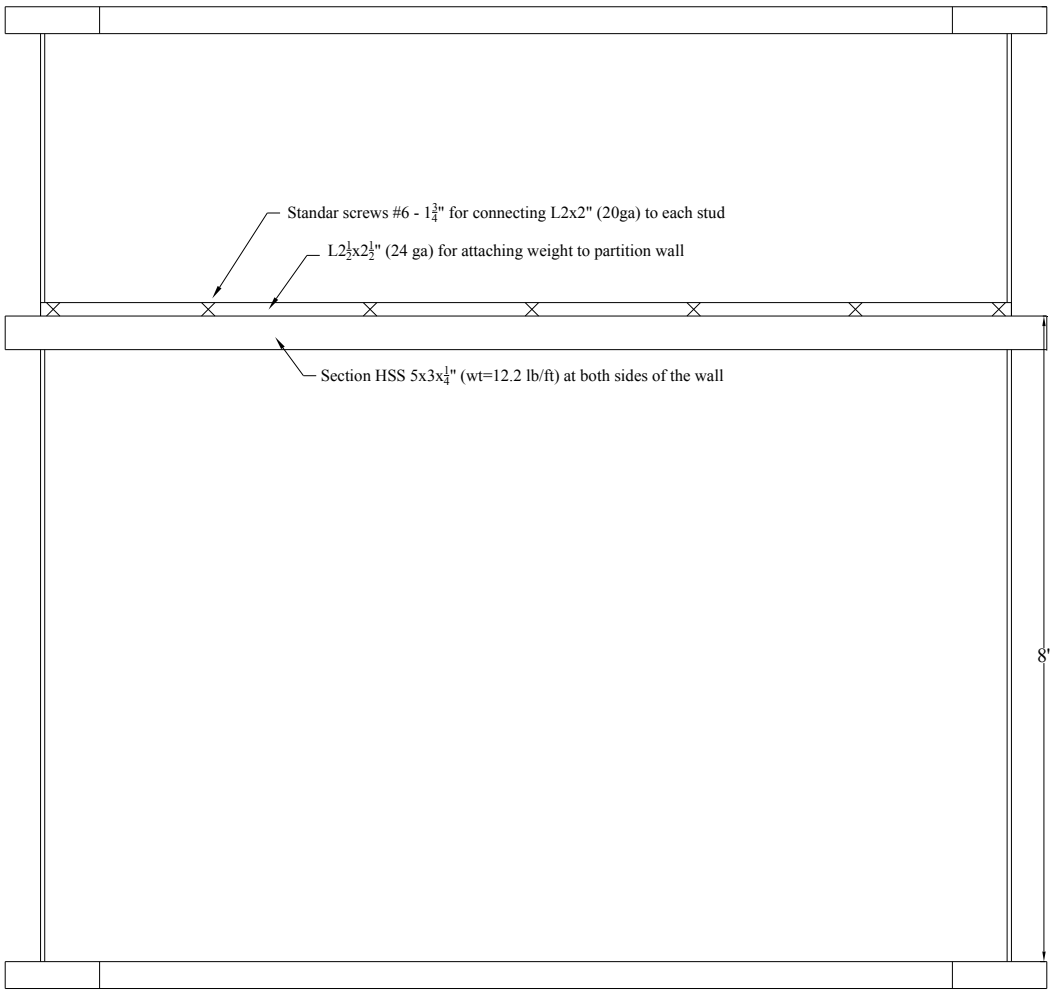

(b) Elevation view specimen with attached equivalent ceiling

Figure 3.36 – Details of Specimens with Equivalent Rigid Ceiling Attached

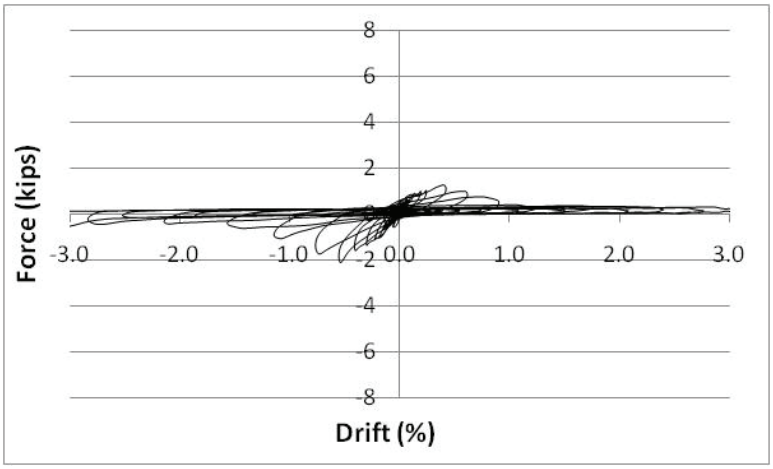

Figure 3.37 – Hysteretic Behavior of Specimen 13

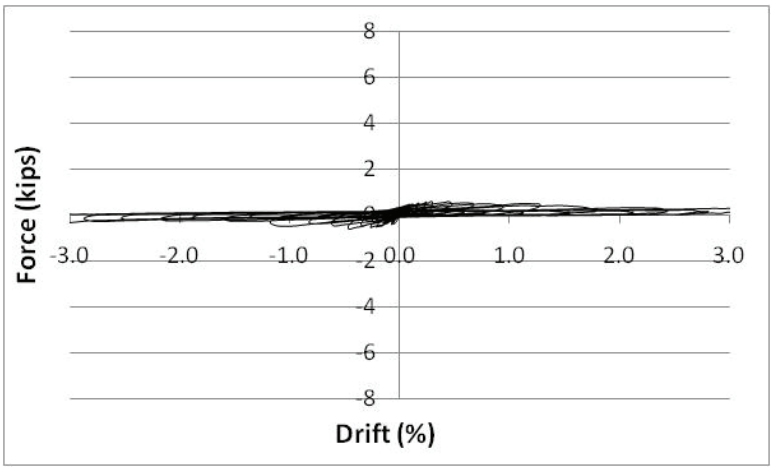

Figure 3.38 – Hysteretic Behavior of Specimen 15

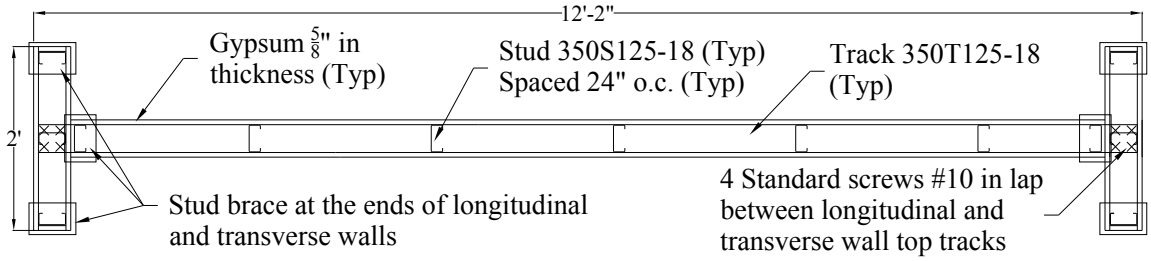

(a) Plan view partial height wall specimen

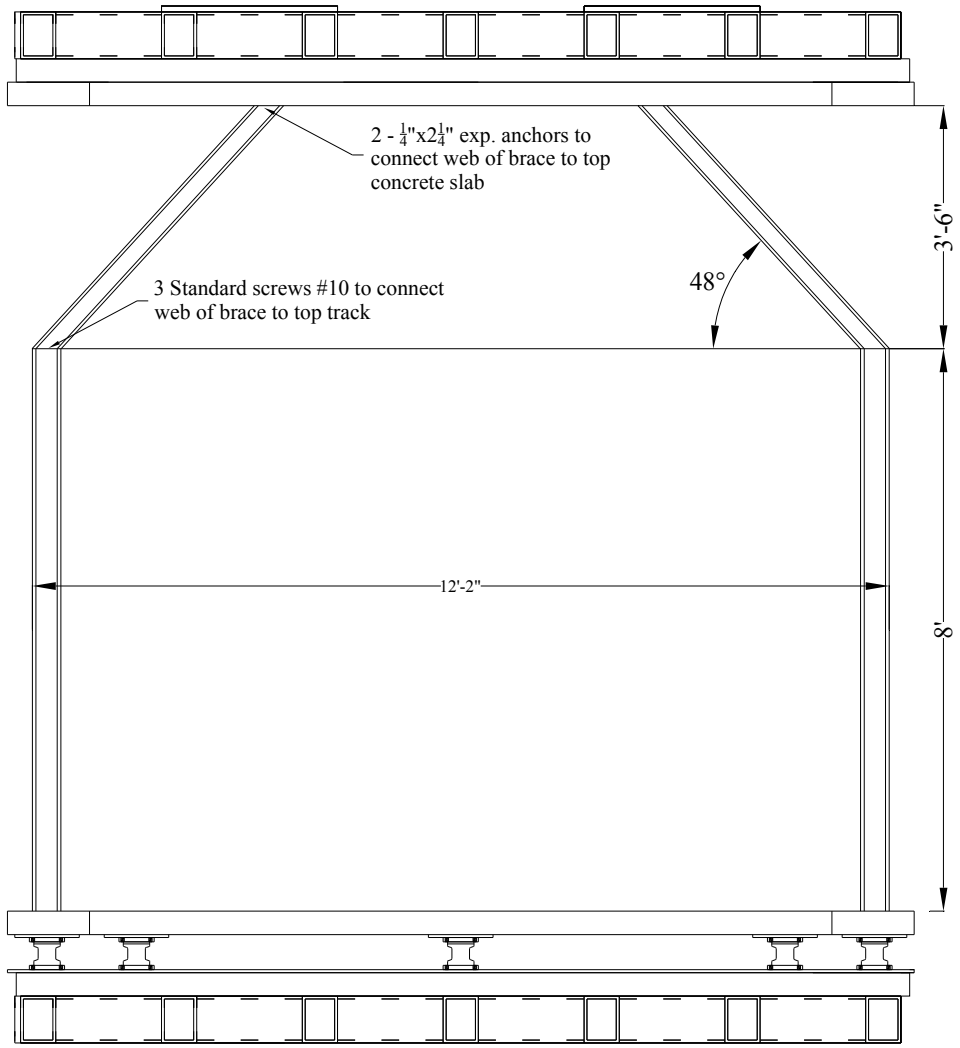

(b) Elevation view partial height wall specimen

Figure 3.39 –Partial Height Partition Wall

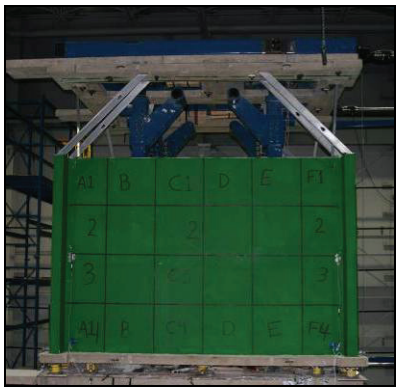

Figure 3.40 – View of Partial Height Partition Wall

Figure 3.41 – Damage in Seismic Diagonal Bracing, Buckling of Braces

Figure 3.42 – Damage in Seismic Diagonal Bracing Connection to Top Track and Damage of Connection between Perpendicular Walls

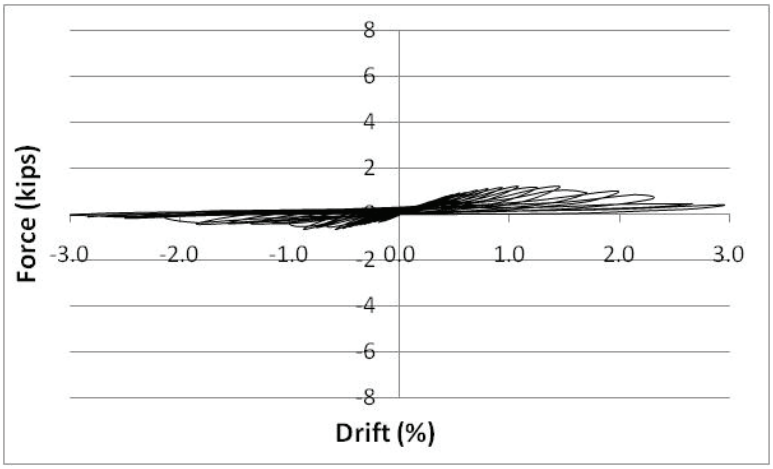

Figure 3.43 – Hysteretic Behavior of Specimen 19

3.6.1.7 Configuration 8

Specimens 20, 21 and 22 consisted of walls constructed using typical "institutional" construction details. The walls were constructed using 20 gauge steel tracks and studs. The studs were spaced 16" on center. Furthermore, the screw spacing was reduced to 8" in the perimeter of the walls. The 1" nails connecting the tracks to the concrete slabs were spaced at 24" o.c. The typical construction detail for the wall intersections is shown in Figure 3.8b. These specimens were built to allow the top track to slip horizontally (i.e., no screws attaching gypsum boards or studs to the track). Figure 3.44 shows the geometry of the tested specimens.

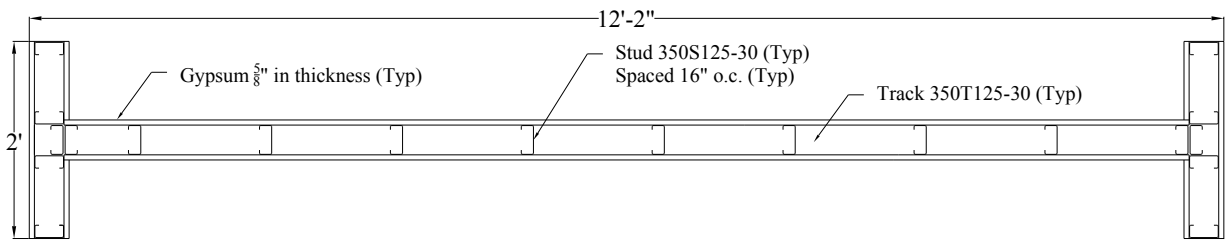

Figure 3.44 – Detail Geometry Institutional Gypsum Partition Wall

In these tests, severe vertical cracks were observed in the transverse walls' gypsum boards, on the side opposite the longitudinal wall, as shown in Figure 3.45 and Figure 3.46. Mean capping force for the partial height walls was F_u = 2.76 kips with a standard deviation of 0.39 kips and mean capping drift Δ_u = 0.75% having a standard deviation of 0.19%. Figure 3.47 shows the hysteresis loops observed for Specimen 22.

Figure 3.45 – Damage in Gypsum Board on Outside Face of Transverse Wall

Figure 3.46 – Damage in Transverse Wall

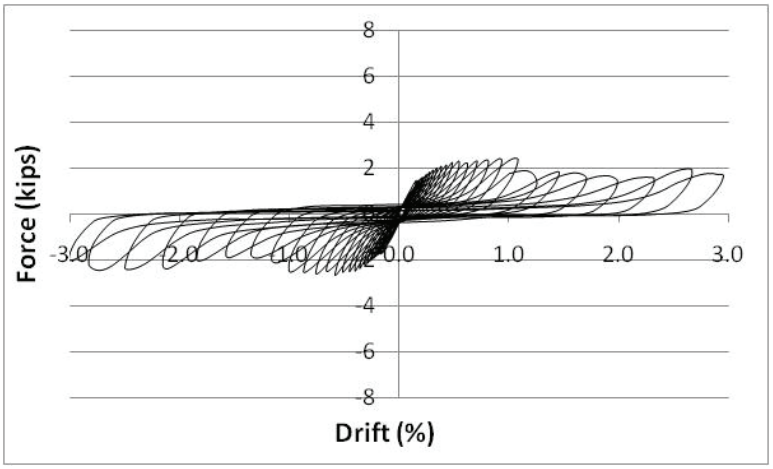

Figure 3.47 – Hysteretic Behavior of Specimen 22

3.6.1.8 Configuration 9

The following test Specimens 23, 24 and 26, were similar to the specimens in Configuration 8. However, they were fully connected to the top and bottom tracks as an attempt to develop the shear capacity of the institutional walls. Track to concrete slabs fasteners were also spaced at 24" o.c. The geometry of these specimens is the same shown in Figure 3.44. Three failure mechanisms were observed in these tests. The first two mechanisms were similar to the mechanisms observed in specimens 7, 8 and 9 (commercial construction). i.e. tearing around track at concrete fasteners and plastic hinges forming in the studs, these are shown in Figure 3.27 and Figure 3.48. The third failure mechanism consisted of failure of the joints between gypsum panels, as shown in Figure 3.49. Capping parameters for these specimens were F_u = 7.17 kips with a standard deviation of 1.11 kips and Δ_u = 0.54% with a standard deviation of 0.13%, the hysteretic behavior for specimen 23 is shown in Figure 3.50.

Figure 3.48 – Damage in Studs Forming Plastic Hinges (Stud Spacing 12” o.c.)

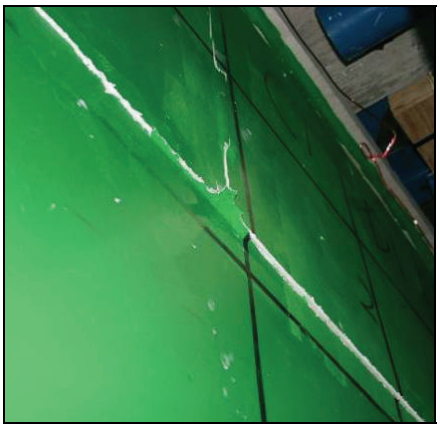

Figure 3.49 – Damage in Gypsum Panel Joints

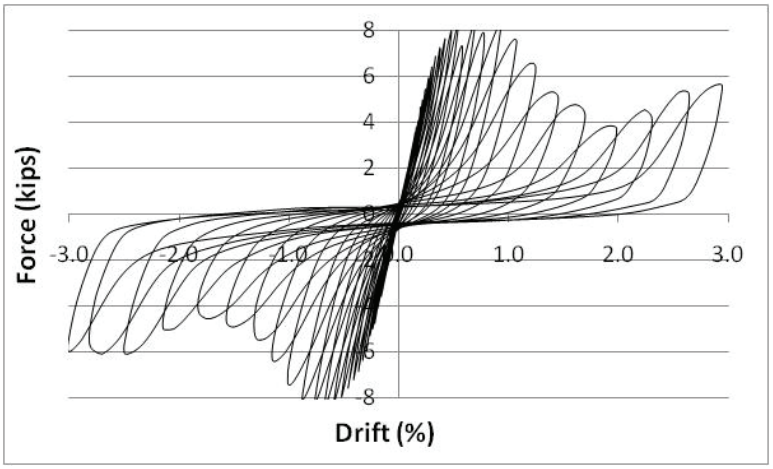

Figure 3.50 – Hysteretic Behavior of Specimen 23

3.6.1.9 Configuration 10

Based on the previous observations for Specimens 23, 24, and 26, Specimens 25, 27, and 28 were constructed with a reduction in the track to concrete slab nail spacing from 24 to 12 inches, as another attempt to induce shear failure in the walls (damage at gypsum panel adjoining edges). Nevertheless, in all tests the damage observed was formation of hinges by bending of the top portion (top 12”) of the studs after crushing of gypsum around the screws in the connections of the drywall to the top tracks, as shown in Figure 3.51 and Figure 3.52. Similar capping parameters for this configuration to the previous configuration using 24” o.c. concrete nail spacing was observed with F_u = 7.10 kips and Δ_u = 0.54%, the respective standard deviations were 0.65 kips and 0.04%.

Figure 3.51 – Hinges Forming in Steel Studs

Figure 3.52 – Crushing of Gypsum around Screws

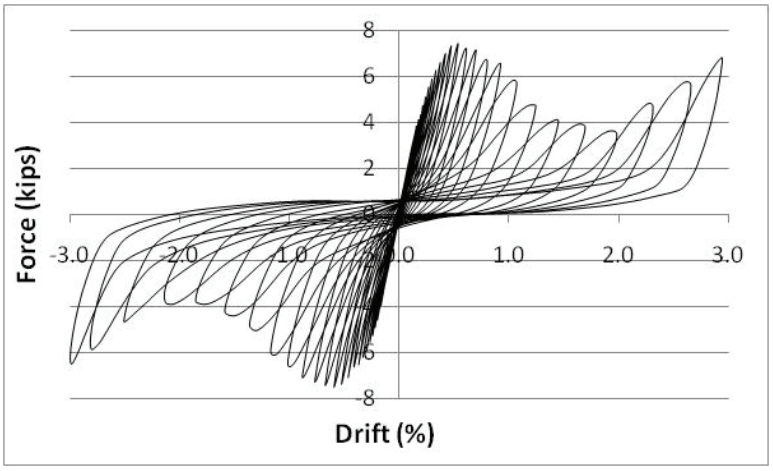

Figure 3.53 – Hysteretic Behavior of Specimen 27

3.6.1.10 Configuration 11

Test specimens 29 and 30, were built to be identical to Specimens 11-16 (Figure 3.25), but without attached masses. The dynamic fragility test protocol was used for these specimens. The purpose of these tests was to obtain a baseline used to determine the effect of the attached weights on the seismic performance of the configuration. However, no differences in damage were identified. Most of the damage concentrated in the flexural bending of boundary studs, and the superficial damage to gypsum boards attached to the end of the wall and the corner beads, as shown in Figure 3.26 and Figure 3.27. Figure 3.54 shows the hysteretic behavior for Specimen 30. Although there was no discernible difference in the damage states for these walls, the capping parameters for these walls decreased to F_u = 0.59 kips and Δ_u = 0.51%, respective standard deviations were 0.11 kips and 0.23%.

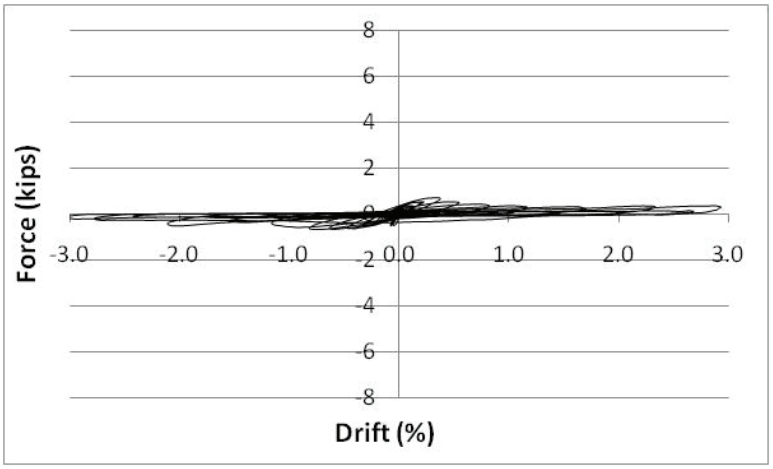

Figure 3.54 – Hysteretic Behavior of Specimen 30

3.6.1.11 Configuration 12

The configuration for Specimens 31 and 32 simulated typical wall corner conditions. The specimens were "C" shaped walls, as shown in Figure 3.55 and Figure 3.56. Figure 3.57 shows a photo of the C shaped wall specimens. This configuration used the slip track connection details, 25 gauge steel, and studs and gypsum not attached to the top track. In Figure 3.58, the observed damage at the wall intersection shows separation of the two walls and crushing of the gypsum board at the top corners. The hysteretic behavior for the two wall specimens returned a mean capping strength of 0.82 kips at a drift ratio of 0.59% with deviations of 0.12 kips and 0.13% respectively.

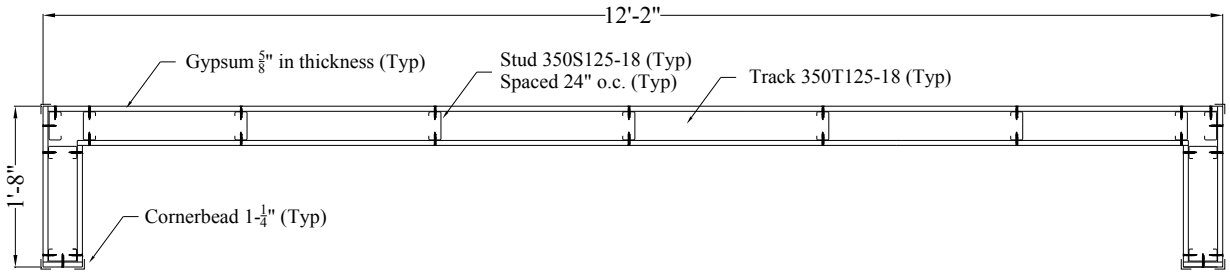

Figure 3.55 – Geometry of C shaped Partition Walls

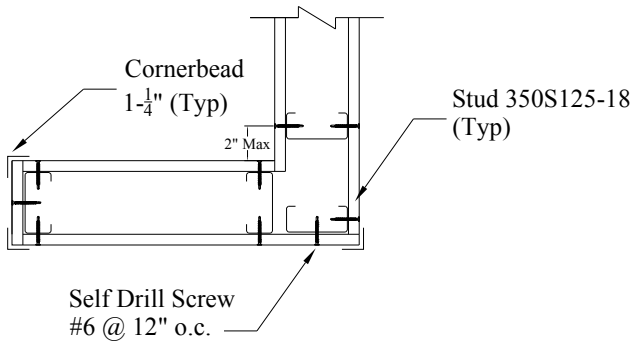

Figure 3.56 – Framing Detail for C shaped Wall Corner

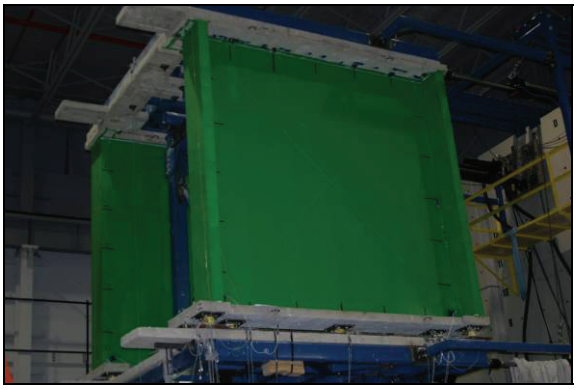

Figure 3.57 – Isometric View C shaped Wall Specimens

Figure 3.58 – Damage in Wall Corner

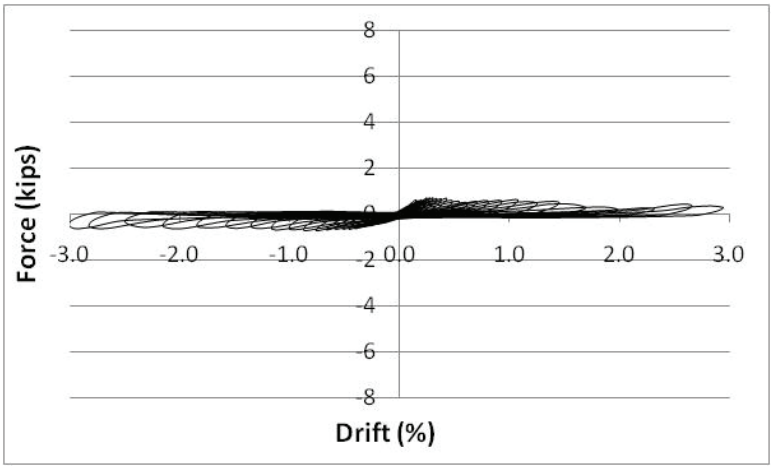

Figure 3.59 – Hysteretic Behavior of Specimen 32

3.6.1.12 Configurations 13 and 15

The final specimens tested in-plane consisted of two unique configurations developed to offset the damage states to higher drift ratios or completely prevent damage. Two walls were used to test one of the configurations, having "I" and "C" wall geometries. Figure 3.60 shows photos taken during the construction of Specimens 33 and 35. These configurations considered ½" gaps at the intersection of perpendicular walls, covered with sacrificial cornerbead attached to the walls using joint compound, as shown in Figure 3.61. These gaps allowed the in-plane partition wall to penetrate into the perpendicular walls and undergo high drift ratios with low forces being transferred through the wall. This configuration completely removed the damage state of gypsum crushing around screws and focused all damage in the sacrificial corner molding at the wall intersections, as shown in Figure 3.62 through Figure 3.64. Figure 3.65 shows the hysteretic behavior for specimen 33. The mean capping force for the two specimens was 0.48 kips at a drift ratio of 1.01%, the respective standard deviations were 0.24 kips and 0.44%.

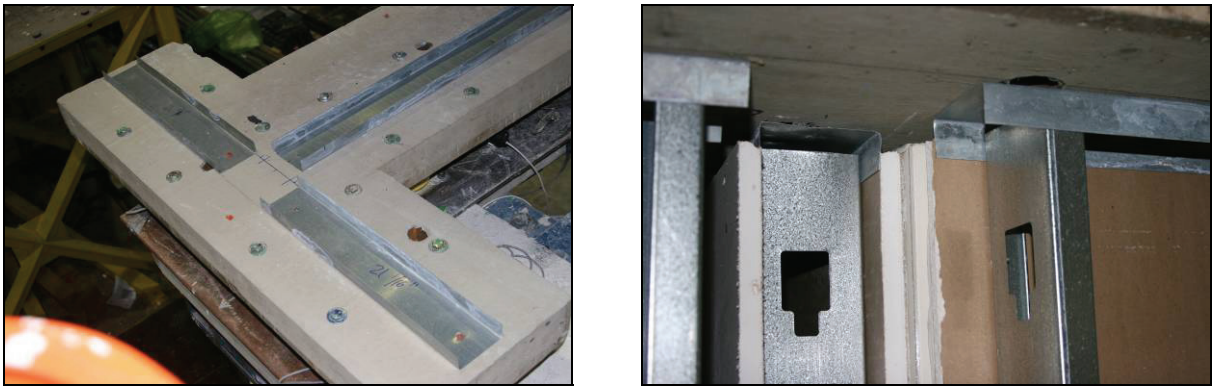

Figure 3.60 – Details of Construction of Protected Specimens

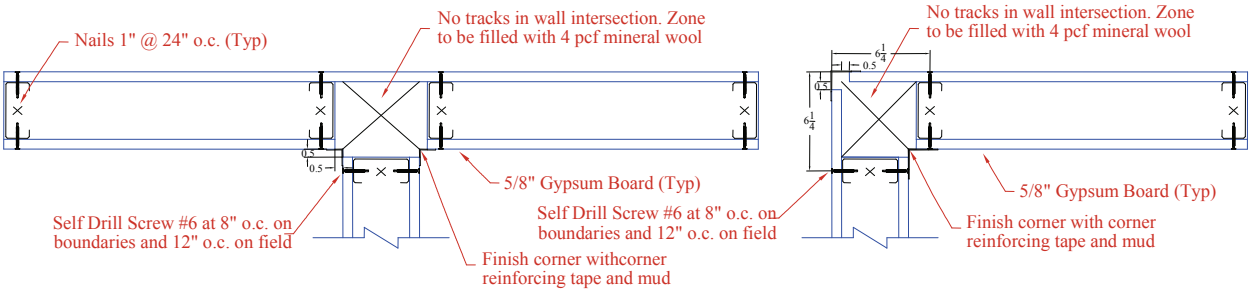

(a) Wall Intersections (left) and Wall Corners (Right)

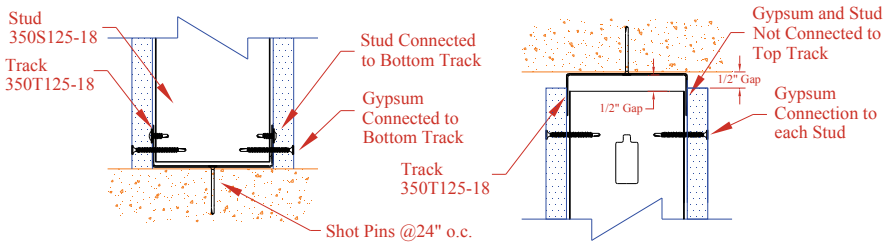

(b) Wallboard and Steel Framing Connectivity

Figure 3.61 – Details Proposed for Reducing Seismic Damage

Figure 3.62 – Damage of Sacrificial Cornerbead

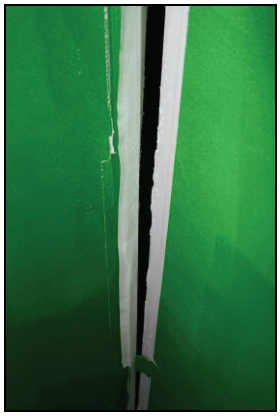

Figure 3.63 – Damage of Sacrificial Cornerbead

Figure 3.64 – Damage of Sacrificial Cornerbead

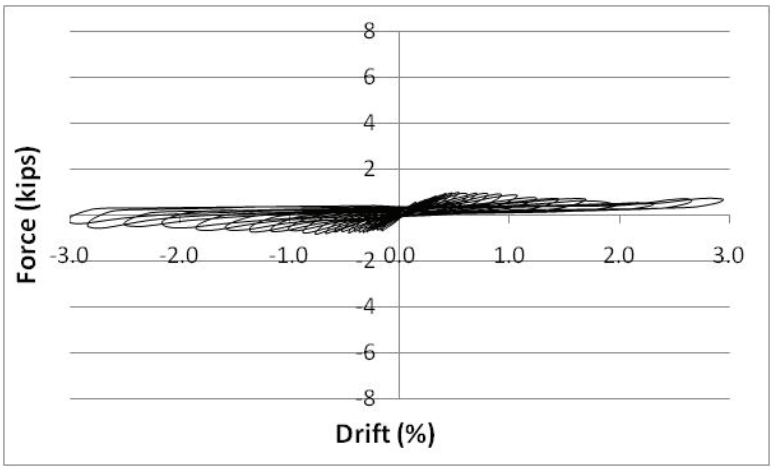

Figure 3.65 – Hysteretic Behavior of Specimen 31

3.6.1.13 Configurations 14 and 16

The second configuration oriented to reduce the damage in partition walls was proposed by William Holmes, a member of the practicing committee for the NEES Nonstructural Grand Challenge Project. This configuration uses the tracks in the perpendicular walls as a beam to absorb the lateral forces at increasing drifts. No track to concrete slab connectors are used within a distance of 2' from wall intersections. In this way, advantage is taken from the flexibility of the tracks. This configuration is shown in Figure 3.67a. In its original conception, only the flexibility of top tracks was considered (Figure 3.67b). In an effort to further improve this detail, the experimental team at UB decided to use what is called double slip track (or "Holmes Modified"), where advantage is taken from top and bottom tracks flexibility (Figure 3.67c). Damage similar to the "slip track" (the original, the one without unfastened tracks) type configurations was observed, however this damage was observed occurring at higher drift ratios. Damage similar to the "institutional slip track" (specimens 21, 22, and 23) was observed at large drift levels. Vertical cracking of gypsum board in the perpendicular wall opposite the longitudinal wall, as shown in Figure 3.67, was observed. Figure 3.67 also shows the failure of a transverse wall track connector. Figure 3.68 shows the flexibility of the top track for the double slip track case. Figure 3.69 shows the damage at wall intersection. Figure 3.70 shows the hysteretic behavior for specimen 34, average capping parameters F_u and Δ_u for specimens 34 and 36 are 0.66 kips and 0.79% with standard deviations of 0.38 kips and 0.19% respectively.

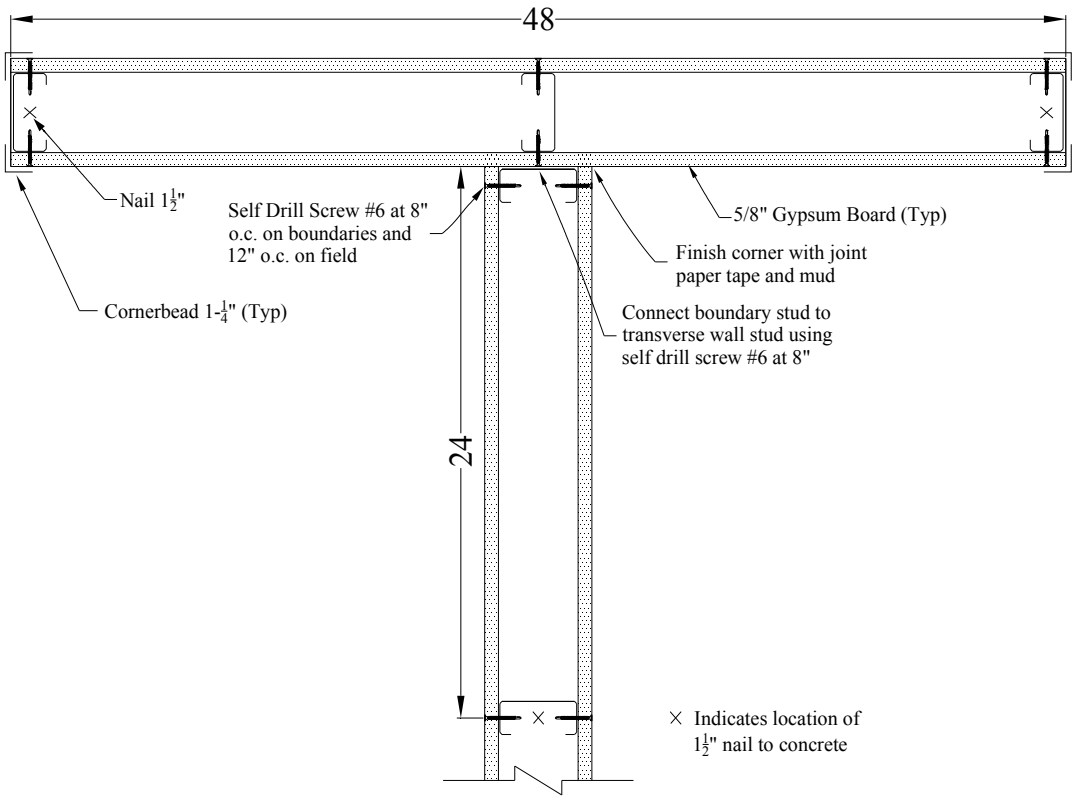

(a) Detail wall intersection

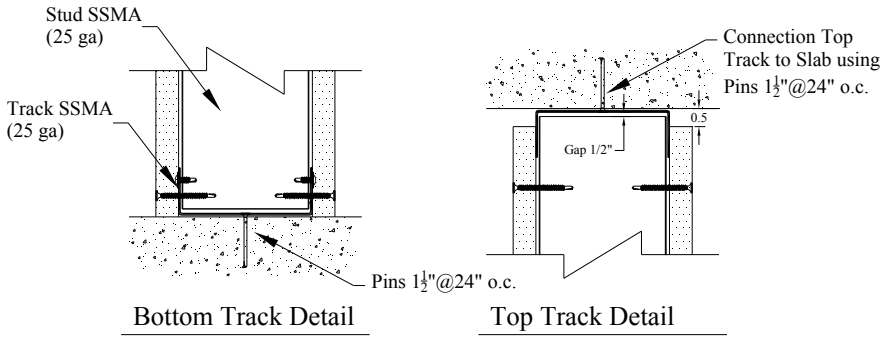

(b) Typical connection detail for slip track

Figure 3.66 – Framing Detail Proposed by W. Holmes and Modified Version (Cont'd)

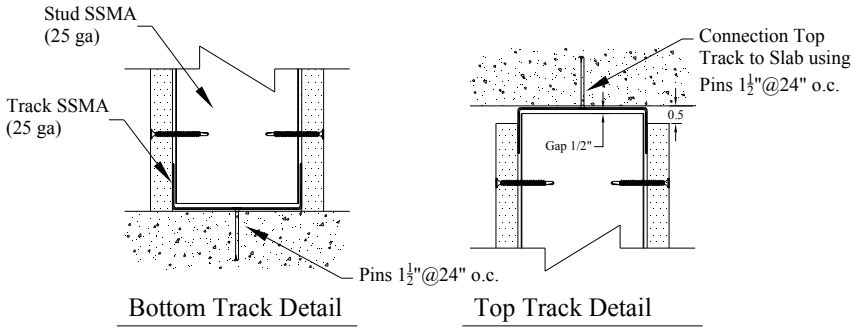

(c) Connection detail for double slip track

Figure 3.66 – Framing Detail Proposed by W. Holmes and Modified Version (Cont'd)

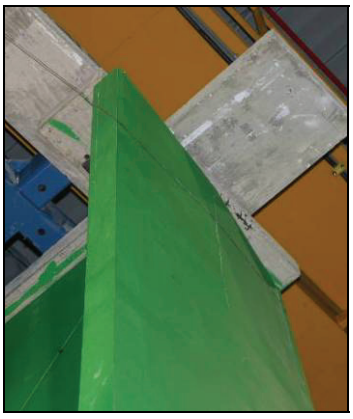

Figure 3.67 – Failure in Track Connector

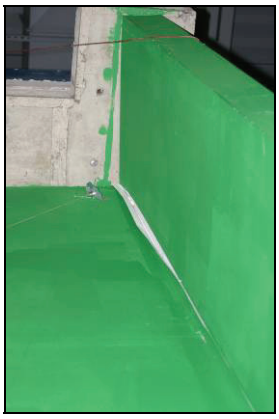

Figure 3.68 – Out-of-plane Bending of Top Track (Double Slip Track Case)

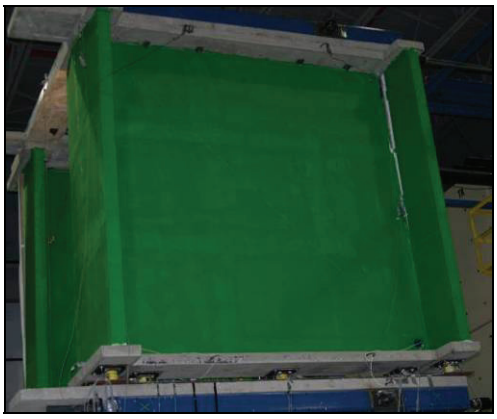

Figure 3.69 – Damage at Wall Intersection

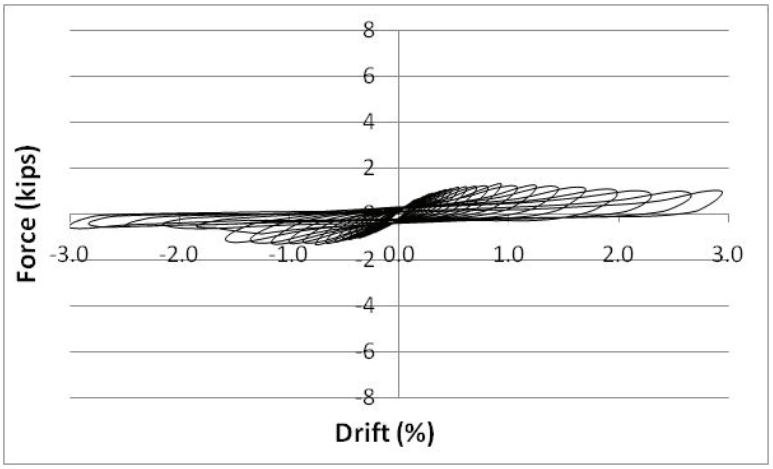

Figure 3.70 – Hysteretic Behavior of Specimen 34

3.6.2 Performance Observations during Out-of-plane Testing

This subsection summarizes the main observations for the fourteen additional specimens tested dynamically in the out-of-plane configuration.

3.6.2.1 Configurations 17 and 18

Configurations 17 and 18, associated to specimens 37 and 38, consisted of partition walls with and without return walls. These tests specimens, without additional mass attached, served as a baseline for comparing later the effect of attached weights such as suspended ceilings or bookshelves. Several screws connecting the gypsum boards to studs pulled out in these tests, as shown in Figure 3.71 and Figure 3.72. Figure 3.73 shows the damage observed at the top end of some of the steel studs.

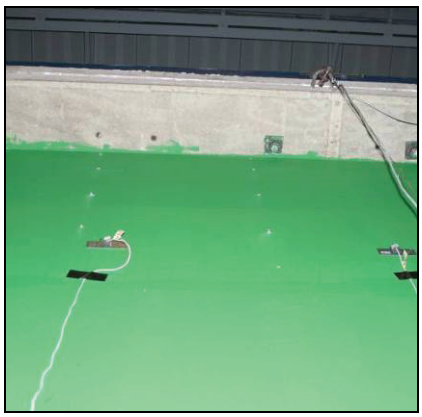

Figure 3.71 – Damage Observed in Screws in Specimens 37 and 38

Figure 3.72 – Damage Observed in Screws in Specimens 37 and 38

Figure 3.73 – Damage Observed in Top End of Studs

3.6.2.2 Configuration 19

Specimens 39, 45 and 47 consisted of partition walls with returns and an attached bookshelf (weighting 510 lb), similar to that described for Configuration 5. Figure 3.74 shows a couple photos for the test specimens. In two of the three specimens tested, the damage consisted of bending of the boundary studs and damage along the top portion of corner beads (return walls), as shown in Figure 3.75. All bookshelf connectors needed tightening after running each of these tests. The third specimen tested for this configuration, Specimen 47, collapsed as shown in Figure 3.76.

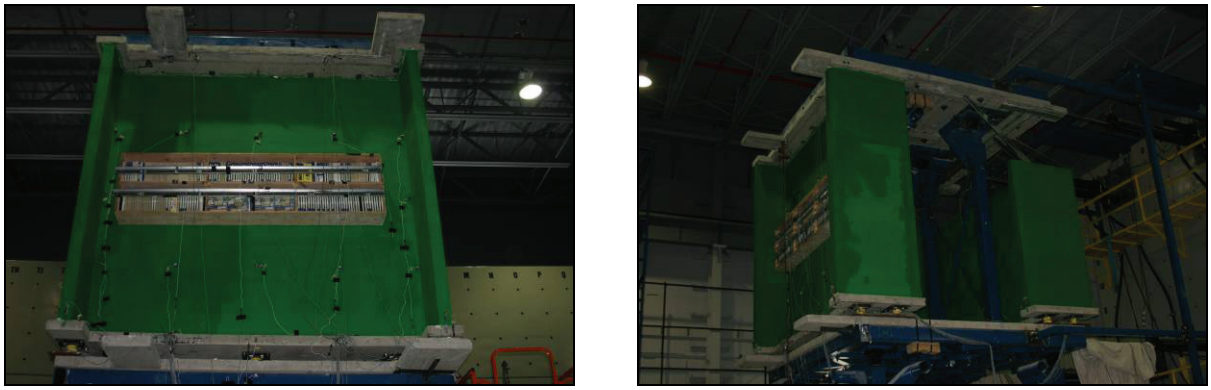

Figure 3.74 – Test Specimens with Attached Bookshelves

Figure 3.75 – Typical Damage in Transverse Walls

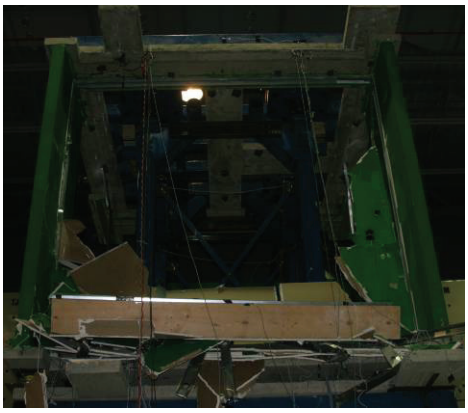

Figure 3.76 – Collapse of Partition Wall

3.6.2.3 Configuration 20

Specimens 40, 41 and 43 consisted of partition walls with attached bookshelves but without returns. In two of the three specimens tested, collapse of the wall was observed (Figure 3.77). In a third case, damage similar to the damage shown in Figure 3.71 was observed. Additionally, a horizontal crack was observed all along the width of the specimen, located approximately at 5 ft from the bottom end of the wall (Figure 3.78). Figure 3.79 shows the case of pulled out screws. It should be noted that all specimens with bookshelves that failed during testing were specimens previously used for other tests. After their first use, all visible damage was repaired (including replacement of nails in track-to-slab connections, replacement of damaged studs, replacement of pulled out screws, replacement of joint paper tape and mud, etc.) and the walls were tested again. These observations indicates that partition walls with attached masses located in zones of high seismicity, and that may experience more than one strong earthquake during their lifetime, may be highly vulnerable to collapse.

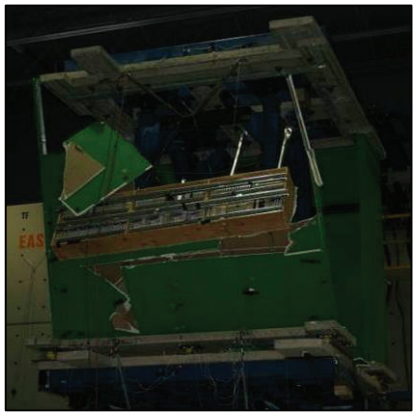

Figure 3.77 – Collapse of Wall Without Returns and With Attached Bookshelf

Figure 3.78 – Crack Along Partition Wall

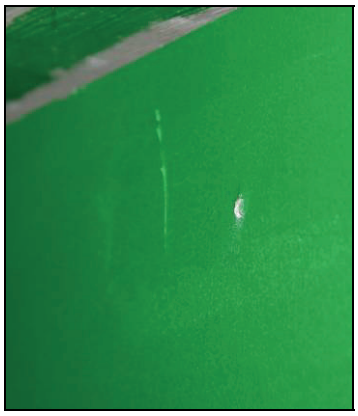

Figure 3.79 – Pulled Out Screw

3.6.2.4 Configuration 21

Specimens 42, 44 and 46, corresponded to partition walls with returns, to which the equivalent weight of a rigid ceiling was attached at 8' from the bottom of the walls. 1- ¼" galvanized fence staples, spaced 24 inches on center, were used to connect the molding angles to the gypsum boards. The configuration of these specimens is identical to the one shown in Figure 3.36. In two of three tests, severe crushing of the gypsum around the staple connectors was observed, as shown in Figure 3.80. In the third test, the equivalent ceiling disconnected completely from the partition walls. In all cases, the types of damage shown in Figure 3.75 and Figure 3.81 were observed. Figure 3.82 shows the complete detachment of the equivalent rigid ceiling from the gypsum wallboard.

Figure 3.80 – Damage Around Molding Connector

Figure 3.81 – Damage in Bottom Portion of Transverse Wall

Figure 3.82 – Damage of All Ceiling Connectors

3.6.2.5 Configuration 22

Finally, Specimens 48, 49 and 50 considered partial height seismically braced partition walls, whose geometry and characteristics are shown in Figure 3.39. Similarly to Specimens 17, 18 and 19, the damage consisted of buckling of the diagonal braces and failure of the connection of these braces to the partition wall top tracks, as shown in Figure 3.41 and Figure 3.42, respectively. Nevertheless, a new type of damage, consisting of bending of the top track around the connection of the diagonal brace was observed, as shown in Figure 3.83. When bending of the top tracks was observed, buckling of the diagonal braces was not observed, and vice versa. Figure 3.84 shows the damage of the connectors of top tracks for perpendicular walls. Figure 3.85 also shows damage of a top track around a detached diagonal brace.

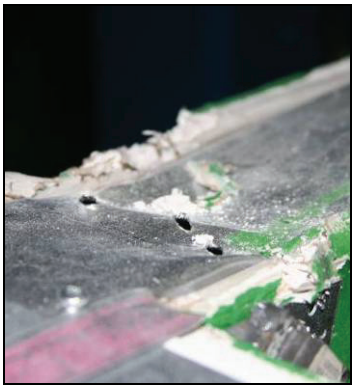

Figure 3.83 – Damage of Top Track

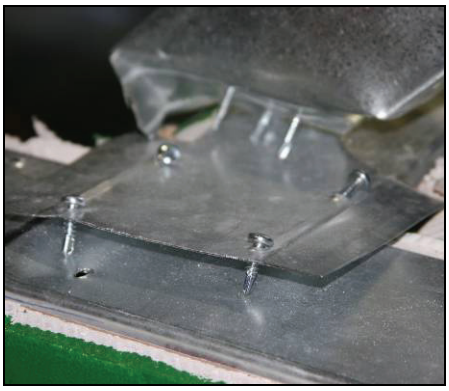

Figure 3.84 – Damage of Top Track Connectors between Perpendicular Walls

Figure 3.85 – Detached Brace and Damaged Top Track

3.6.3 Summary of Experimental Observations

Table 3-8 summarizes the main damage mechanisms observed for each configuration tested.

Table 3-8 Summary of Damage and Failure Mechanisms of Test Specimens

Config	Specimen ID	Main Damage/Failure Observed
1	1, 2 & 3	Damage concentrated in transverse walls top tracks: Tearing of track web, nails pulled out from concrete, and bending of track flanges. Damage was also observed in the transverse walls top gypsum panels. Longitudinal walls exhibited limited crushing at wall corners.
2	4	Crushing of gypsum boards around all screws connecting sheathing to top track, at a relatively low drift level (~0.4%). Then, a similar damage to specimens 1, 2 & 3 was observed.
3	5, 6 & 10	Damage along steel cornerbeads. Crushing of gypsum boards at wall corners. Nails in connections of tracks to concrete passing thru the track webs. In specimen 10, tearing of the top track was observed.
4	7, 8 & 9	Specimen 7 & 9: Top and bottom tracks slipped after track tearing around all nailed connections.
		Specimen 8: Moment hinges were observed in all studs, approximately 1 ft under top end connection.
5	11, 12 & 13	Damage concentrated in top 4 feet of wall end: Boundary stud bent after being pulled from gypsum boards and top track. Limited rocking of screws attaching gypsum board to bottom track. Books were protected against fallings in order to keep the mass attached to the walls during the test. However, for Specimen 12, the safety device was removed and books fell down from the bookshelf.
6	14, 15, & 16	Damage Similar to specimens 11, 12 &13 was observed. Limited popout of screws was observed in the steel angle connecting equivalent "ceiling" to walls (Specimen 16).
7	17, 18 & 19	Damage in seismic braces due to buckling. Failure in braces to top track connections. In specimen 18, the connection between the top tracks of longitudinal and transverse walls failed. Failure in some of the track to concrete connections were observed.
8	20, 21 & 22	Failure of bottom and top tracks of transverse walls. Severe damage of the studs in wall intersections. Severe damage of gypsum board in transverse wall due to out-of-plane bending. Bending of transverse wall top track flanges observed. Damage along vertical edges of sheathing of longitudinal wall.
9	23, 24 & 26	Specimen 23: Track fasteners passing thru the top track. Hinges formed 1' under top end of studs. Failure of top track in transverse wall. Slight crushing of wall corners.
		Specimen 24: Track fasteners passing thru the bottom track. Failure of bottom tracks of transverse walls. Damage in gypsum panel joints.
		Specimen 26: Tears along all bottom track connections and global wall slip.
10	25, 27 & 28	Crushing of gypsum around screws connecting to top track and plastic hinge forming on studs due to bending.
11	29 & 30	Damage in the upper 4' of the steel cornerbeads and wall boundary studs. Nails at the end of the tracks passing thru the track webs.
12	31 & 32	Wall corners totally opened. Damage along cornerbeads. Studs in transverse walls pulled out from transverse wall top track.
13	33	Joint cornerbead detached from walls at drifts levels as low as 0.2-0.4%. Damage does not progress in the specimen at larger drift levels.
14	34	Damage was observed for the first time at a drift level of 1.2%. Then joint paper tape detached from wall intersection (1.2-1.4% drift), vertical cracks in gypsum of transverse walls (1.6% drift), and failure of fasteners in transverse wall track connections (1.8% drift) were observed.
15	35	Exterior joint cornerbead detached from walls at drifts levels close to 0.6%. Damage does not progress in the specimen at larger drift levels.
16	36	Joint paper tape detached from wall intersection (0.4-0.6% drift), failure of fasteners in transverse wall track connections (0.6% drift), and vertical cracks in gypsum of transverse walls (1.4% drift), were observed.
17	37	Minor damage observed at top end of cornerbeads and crushing of corners of return walls. Screws pulled out from wallboards to stud connections.
18	38	Most of the screws in the connection of the top row of gypsum boards to studs completely pulled out.
19	39, 45 & 47	Screws pulled out from gypsum to stud connections. Bookshelf connectors needed to be tightened after the test. Damage along top end of cornerbeads. Specimen 47 collapsed.
20	40, 41 & 43	Screws pulled out from gypsum to stud connections. Bookshelf connectors needed to be tightened after the test. Horizontal cracks along gypsum board joints. Damage along top end of cornerbeads. Specimens 40 and 43b collapsed.
21	42, 44 & 46	Screws pulled out from gypsum to stud connections. Damage at the top and bottom ends of cornerbeads. In specimens 42 and 44, crushing of gypsum boards around fence staples connectors was observed. In specimens 44b and 46, the equivalent ceiling got completely detached from the partition wall.
22	48, 49 & 50	Screws in connections of braces to walls' top tracks pulled out. Buckling of seismic braces. Buckling of top tracks around seismic brace connections.

3.7 Summary

A total of 50 cold-formed steel stud partition wall subsystem experiments were conducted at the University at Buffalo as part of the NEES Nonstructural Grand Challenge project. Thirty-six of these walls were tested in-plane under quasi-static and dynamic loading protocols, the other 14 wall specimens were built and tested in the out-of-plane direction.

The test plan and construction details for the configurations were selected with close collaboration of the Practice Committee and Advisory Board for the NEES Nonstructural Grand Challenge Project. The results of the experiments are used to populate the seismic fragility database presented in Chapter 4, to provide input for the design and execution of the system-level experiments to be performed at the

University of Nevada, Reno, and to generate the data required for developing analysis tools. During the dynamic and quasi-static in-plane experiments, it has been observed that using slip tracks and incorporating ¼ to ½" gaps at the top end of the gypsum wallboards reduce the damage associated with drift of the longitudinal walls and concentrate the damage in the vertical joints between perpendicular walls. Although no significant difference in the seismic performance of specimens with institutional and commercial construction details was observed, significant differences were observed in the seismic performance of specimens constructed using identical construction techniques. Adding typical bookshelf masses to the partition walls may induce out-of-plane collapse due to cumulative damage effects. Severe damage was observed around the connectors of ceiling wall moldings to the gypsum wallboards and in the diagonal braces used in partial height partition walls. A series of construction details were proposed to reduce the seismic damage to partition walls. The effectiveness of these improved details was demonstrated through the testing program.

Chapter 4

SEISMIC FRAGILITY ANALYSIS FOR COLD-FORMED STEEL STUD GYPSUM PARTITION WALLS

The experimental results, described in Chapter 3 and Appendix A, were processed to populate a comprehensive seismic fragility database for light steel stud gypsum partition walls. This Chapter presents the techniques, procedures, and criteria considered to process the experimental data and generate the seismic fragility database. Three damage states are considered, defined in terms of the level of repair required, as recommended by the ATC-58 Project (Porter et al., 2007).

4.1 Definition of Damage States and Seismic Fragility Groups

A summary of damage observations for all partition wall configurations tested is given in Table 3-8. The basic data considered in this fragility analysis is presented in Appendix A. For fragility analysis purposes, observations of damage during testing were assigned to one of the three Damage States (DSs) defined in Table 4-1. These DSs were defined in terms of the nature of the damage observed and the characteristics of the required repair actions. The first damage state (DS_1) corresponds to superficial damage requiring only cosmetic repairs. The second damage state (DS_2), generally occurring at higher drift ratios, consists of damage requiring the replacement of portions of the partition wall assembly. The third damage state (DS_3) is associated to severe damage of the wall assembly that would require complete removal and replacement of the wall.

The damage state DS_2 for acceleration sensitive partitions (specimens with attached weights) consisted of failure of the 1-¼" fence staples used to connect the equivalent weight of the unbraced rigid ceiling to the partition walls, while the damage state DS_3, consisted of the collapse of walls with attached bookshelves. The damage state DS_1, although observed in most of the tests, could not be evaluated from the recorded time-stamped videos because the exact occurrence of the associated damage could not be identified. As mentioned earlier in Chapter 3, the partition walls that collapsed during out-of-plane dynamic fragility testing corresponded to refurbished specimens.

Table 4-1. Definition of Damage States

Damage State		Description of Damage Associated	Repair Actions
DS_1	Superficial damage to the walls	Cracks along corner beads, cracks along joint paper tape, screws pulled out from connections of gypsum boards to steel framing	Cosmetic repairs, including: replacement of corner beads, replacement of screws pulled out, replacement of joint paper tape, application of joint compound, sanding, and painting
DS_2	Local damage of gypsum wallboards and/or steel frame components	Crushing of wall corners, out-of-plane bending and cracking of gypsum wallboards at wall intersections, damage of screws connecting wallboards to boundary studs, bending of boundary studs, buckling of diagonal braces (partial height partition walls), damage of gypsum wallboards around ceiling connectors or damage induced by ceiling impact	Local repairs, including: repair or replacement of gypsum wallboards, replacement of boundary studs, replacement of seismic braces, replacement of ceiling connectors
DS_3	Severe damage to walls	Tears in steel tracks around connectors of track to concrete slab, track fasteners passing thru track webs, track flanges bent at wall intersections, hinges forming in studs, partition wall collapse	Replacement of partition wall (Steel framing and gypsum wallboards)

Additionally, the fragility data was grouped according to the taxonomy of the specimens tested, as shown in Table 4-2. The specimens assigned to each seismic fragility group are shown in Table 3-5.

Table 4-2. Definition of Seismic Fragility Groups

Group	Sub Group	Specimens	Description
0	0	1-36	All specimen data
1	1a	1-3, 11-16, and 29-32	Full-height specimens. Commercial construction practice and slip tracks
	1b	4-10	Full-height specimens. Commercial construction practice and partial/full connections
	1c	1-16, and 29-32	Full-height specimens. Commercial construction practice (slip tracks and full connection)
2	2a	20-22	Full-height specimens. Institutional construction practice and slip tracks
	2b	23-28	Full-height specimens. Institutional construction practice and partial/full connections
	2c	20-28	Full-height specimens. Institutional construction practice (slip tracks and full connection)
3	3	17-19	Partial-height specimens
4	4	33-36	Specimens including improved corner details

4.2 Seismic Fragility Analysis Procedure

Table 4-3 presents a summary of the drift levels at which each damage observation was triggered for all drift sensitive specimens. The damage observations in Table 4-3 were sorted in ascending order of the median drift level triggering each type of observed damage, and then grouped and assigned to one of the DS's defined in Table 4-1. As previously mentioned, these DS's were defined in terms of the nature of the damage observed and the characteristics of the required repair actions. In the fragility assessment, it is assumed that the drift level triggering a specific DS for a given specimen corresponds to the minimum drift level triggering one of the damage observations associated to that DS. Furthermore, the fragility data was grouped according to the taxonomy of the specimens tested, as defined in Table 4-2 and shown in Table 3-5.

In a similar fashion, the seismic fragility of the acceleration sensitive partition walls was assessed. Table 4-4 presents a summary of several Engineering Demand Parameters (EDP's) associated with the damage in acceleration sensitive partition walls. In particular, the damage state DS_2, consisting of failure of the connectors attaching the equivalent unbraced rigid ceiling to the partition walls, and the damage state DS_3, consisting of the collapse of walls with attached bookshelves, were evaluated. In Table 4-4, the values in bold correspond to either damaged or collapsed specimens. Table 4-4 demonstrates that all collapses of specimens with bookshelves occurred after imposing the peak floor accelerations and peak spectral demands. Moreover, all partition walls that collapsed during testing corresponded to refurbished specimens. Among the EDP's shown in Table 4-4, and for sake of simplicity, peak floor accelerations were selected for developing fragility curves.

Table 4-3 Drifts Levels (%) Triggering Several Damage States in Displacement Sensitive Walls

				Specimen ID																																			
				1	2	3	4	5	6	7	8	9	10	11	12	13	14	15	16	17	18	19	20	21	22	23	24	25	26	27	28	31	32	33	34	35	36	48	49	50
Damage State	DS_1	Damage Observation	Cracks along longitudinal wall corner beads	-	-	-	-	0.20	0.40	-	-	-	0.20	0.28	0.10	0.48	0.13	0.56	0.27	-	-	-	-	-	-	-	-	-	-	-	-	-	0.40	0.20	-	0.20	-	-	-	-
			Crack along tape/pulled tape/crushing wall vertical edges	0.20	0.20	0.40	0.62	-	-	0.20	0.40	0.20	-	-	-	-	-	-	-	1.00	1.16	2.66	0.20	0.40	1.00	0.40	0.62	0.40	0.62	0.40	0.40	0.20	0.62	0.20	1.00	-	0.40	-	-	-
			Gypsumboard screw popout/rocking (top track)	-	-	-	0.62	0.40	0.40	0.40	0.40	0.40	0.40	-	-	-	-	-	-	-	-	0.62	-	-	-	0.40	0.40	0.40	0.40	0.62	0.40	-	-	-	-	-	-	-	-	-
			Gypsumboard screw popout/rocking (bottom track)	0.62	0.62	-	0.40	0.62	0.81	0.40	0.62	0.40	1.84	-	-	-	-	-	-	-	-	-	-	-	-	0.62	1.00	0.40	0.40	0.40	0.40	-	-	-	1.16	-	-	-	-	-
			Minimum Drift Level Triggering DS_1	0.20	0.20	0.40	0.40	0.20	0.40	0.20	0.40	0.20	0.20	0.28	0.10	0.48	0.13	0.56	0.27	1.00	1.16	0.62	0.20	0.40	1.00	0.40	0.40	0.40	0.40	0.40	0.40	0.20	0.40	0.20	1.00	0.20	0.40	-	-	-
	DS_2	Damage Observation	Damage in gypsumboard transverse wall	0.62	0.62	0.62	1.16	-	-	1.99	1.99	-	-	-	-	-	-	-	-	-	-	-	1.35	0.81	0.62	-	1.16	1.00	1.00	1.35	1.16	1.84	1.84	-	1.57	-	1.35	-	-	-
			Crushing partition wall corners	2.82	3.00	0.62	0.62	0.40	0.62	0.62	2.32	0.40	1.00	-	-	-	-	-	-	-	-	-	1.16	-	-	0.81	1.35	0.40	-	0.62	0.81	-	-	-	-	-	-	-	-	-
			Boundary stud detached from gypsum/bending	0.62	0.62	1.00	1.16	1.00	1.00	1.99	1.00	0.81	1.84	2.23	1.73	1.66	1.30	2.45	1.04	-	-	-	2.15	1.00	2.15	1.35	2.15	1.99	2.15	1.00	1.35	1.99	1.99	-	1.99	-	1.00	-	-	-
			Damage along gypsumboads edges	-	-	-	-	-	-	-	2.32	-	-	-	-	-	-	-	-	-	-	-	1.35	-	-	1.16	0.40	0.40	1.57	1.00	-	1.99	-	-	-	-	-	-	-	-
			Brace buckling/top track bending (partial height walls)	-	-	-	-	-	-	-	-	-	-	-	-	-	-	-	-	0.81	0.81	1.00	-	-	-	-	-	-	-	-	-	-	-	-	-	-	-	1.26	0.93	1.34
			Failure of seismic braces connectors (partial height walls)	-	-	-	-	-	-	-	-	-	-	-	-	-	-	-	-	2.15	2.66	2.15	-	-	-	-	-	-	-	-	-	-	-	-	-	-	-	3.05	3.03	3.03
			Failure stud connectors at walls intersection (inst. const.)	-	-	-	-	-	-	-	-	-	-	-	-	-	-	-	-	-	-	-	1.00	1.16	-	-	0.81	-	-	1.35	1.99	-	-	-	1.35	-	1.99	-	-	-
			Minimum Drift Level Triggering DS_2	0.62	0.62	0.62	0.62	0.40	0.62	0.62	1.00	0.40	1.00	2.23	1.73	1.66	1.30	2.45	1.04	0.81	0.81	1.00	1.00	0.81	0.62	0.81	0.40	0.40	1.00	0.62	0.81	1.84	1.84	-	1.35	-	1.00	1.26	0.93	1.34
	DS_3	Damage Obs.	Damage transverse wall track fasteners/bending flanges	0.62	1.00	0.62	1.16	-	-	1.00	1.00	0.81	-	-	-	-	-	-	-	-	-	0.81	2.32	-	1.00	3.00	1.35	-	1.00	1.99	2.32	0.62	1.00	-	1.84	-	0.62	-	-	-
			Longitudinal wall track fastening failure	-	-	-	-	2.32	2.66	1.84	-	0.62	0.81	-	-	-	-	-	-	1.99	-	-	-	-	1.99	2.15	1.16	0.81	1.84	-	-	1.00	-	-	-	-	-	-	-	-
			Failure connection between walls (partial height)	-	-	-	-	-	-	-	-	-	-	-	-	-	-	-	-	-	1.84	1.57	-	-	-	-	-	-	-	-	-	-	-	-	-	-	-	-	-	-
			Field screw popout/rocking (hinge forming in field stud)	-	-	-	-	-	-	-	1.16	-	-	-	-	-	-	-	-	-	-	-	-	-	-	1.00	1.35	0.62	-	0.81	0.81	-	-	-	1.99	-	-	-	-	-
			Minimum Drift Level Triggering DS_3	0.62	1.00	0.62	1.16	2.32	2.66	1.00	1.00	0.62	0.81	-	-	-	-	-	-	1.99	1.84	0.81	2.32	-	1.00	1.00	1.16	0.62	1.00	0.81	0.81	0.62	1.00	-	1.84	-	0.62	-	-	-

Table 4-4 Engineering Demand Parameters Triggering Several Damage States in Acceleration Sensitive Walls

				Specimen ID											
				37	38	39	40	41	42	43	43b	44	44b	45	46	47
Damage State	DS_1	-	Damage associated to DS_1 could not be identified from the recorded videos and response histories	-	-	-	-	-	-	-	-	-	-	-	-	-
			EDP Triggering DS_1 (N/A)	-	-	-	-	-	-	-	-	-	-	-	-	-
	DS_2	Repairable	Peak Floor Acceleration (average bottom and top platform peak accelerations) (g)	-	-	-	-	-	0.80	-	-	0.81	**0.81**	-	**0.72**	-
			Peak Spectral Acceleration (g)	-	-	-	-	-	4.74	-	-	4.75	**4.73**	-	**4.60**	-
			Peak Specimen Acceleration (g)	-	-	-	-	-	2.06	-	-	1.44	**2.00**	-	**1.73**	-
			Peak Interstory Drift (%)	-	-	-	-	-	3.14	-	-	3.15	**3.15**	-	**0.24**	-
			EDP Triggering DS_2 (Peak Floor Acceleration)	-	-	-	-	-	0.80	-	-	0.81	**0.81**	-	**0.72**	-
	DS_3	Collapse	Peak Floor Acceleration (average bottom and top platform peak accelerations) (g)	0.82	0.81	0.81	**0.80**	0.81	-	0.81	**0.80**	-	-	0.79	-	**0.78**
			Peak Spectral Acceleration (g)	4.72	4.73	4.72	**4.76**	4.72	-	4.72	**4.70**	-	-	4.72	-	**4.71**
			Peak Specimen Acceleration (g)	2.50	2.86	4.11	**2.71**	2.60	-	2.04	**1.39**	-	-	1.72	-	**2.09**
			Peak Interstory Drift (%)	3.19	3.19	3.22	**0.43**	3.14	-	3.15	**0.36**	-	-	3.16	-	**0.39**
			EDP Triggering DS_3 (Peak Floor Acceleration)	0.82	0.81	0.81	**0.80**	0.81	-	0.81	**0.80**	-	-	0.79	-	**0.78**

Using the ATC-58 framework Porter et al. (2007), experimental fragility curves for displacement and acceleration sensitive partition walls (groups 0 thru 4) were determined. Table 4-5 summarizes the median (x_m) and logarithmic standard deviation (β) values for all specimen groups. For displacement sensitive partition walls, the x_m and β fragility curve parameters were calculated as:

$$x_m^j = e^{\frac{1}{M}\sum_{i=1}^{M} \ln r_i^j} \quad \textbf{(4-1)}$$

$$\beta^j = \sqrt{\left(\frac{1}{M-1}\sum_{i=1}^{M}\left(ln\left(r_i^j / x_m^j\right)\right)^2\right)^2 + \beta_u^2} \quad \textbf{(4-2)}$$

Table 4-5 Summary Parameters Fragility Curves

Fragility parameters in terms of inter-story drifts (%)

Group	Sub Group	Description	DS_1		DS_2		DS_3	
			x_m (%)	β	x_m (%)	β	x_m (%)	β
0	0	All speci en data	0.35	0.56	0.69	0.39	1.04	0.55
1	1a	Full-height specimens. Commercial construction practice and slip tracks	0.26	0.45	0.68	0.35	0.75	0.36
	1b	Full-height specimens. Commercial construction practice and partial/full connections	0.27	0.44	0.61	0.41	1.18	0.59
	1c	Full-height specimens. Commercial construction practice (slip tracks and full connection)	0.27	0.43	0.64	0.38	0.96	0.61
2	2a	Full-height specimens. Institutional construction practice and slip tracks	0.36	0.55	0.79	0.34	-	-
	2b	Full-height specimens. Institutional construction practice and partial/full connections	0.40	0.25	0.63	0.43	0.88	0.33
	2c	Full-height specimens. Institutional construction practice (slip tracks and full connection)	0.42	0.31	0.69	0.40	0.98	0.52
3	3	Partial-height specimens	0.74	0.29	1.00	0.33	1.79	0.28
4	4	Specimens including improved corner details	0.34	0.77	-	-	-	-

Fragility parameters in terms of imposed floor accelerations (g)

Group	Sub Group	Description	DS_1		DS_2		DS_3	
			x_m (%)	β	x_m (%	β	x_m (%)	β
0	0	All acceleration sensitive walls tested out-of-plane	-	-	0.70	0.25	0.80	0.25

where j = 1, 2 and 3, denotes the j^{th} damage state; r_i^j denotes the demand parameter triggering the j^{th} damage state in the i^{th} specimen of the seismic fragility group; and M denotes the number of specimens included in the seismic fragility group. In Equation 4-2, the factor β_u = 0.25 accounts for the fact that all specimens experienced the same loading history.

The performance data collected for acceleration sensitive partition walls consisted basically of survival/failure data. Imposed peak floor and specimen accelerations, and peak acceleration response spectra amplitudes are correlated to final specimen condition. For this reason, for acceleration sensitive specimens, the x_m and β fragility curve parameters were calculated as:

$$x_m = e^{\bar{x}-\bar{y}\beta_r} \tag{4-3}$$

$$\beta = \sqrt{\beta_r^2 + \beta_u^2} \tag{4-4}$$

where

$$\beta_r = \frac{\sum_{j=1}^{N}\left(x_j - \bar{x}\right)^2}{\sum_{j=1}^{N}\left(x_j - \bar{x}\right)\left(y_j - \bar{y}\right)} \tag{4-5}$$

$$\bar{x} = \frac{1}{N}\sum_{j=1}^{N} x_j \tag{4-6}$$

$$\bar{y} = \frac{1}{N}\sum_{j=1}^{N} y_j \tag{4-7}$$

$$x_j = \begin{cases} ln\left(\dfrac{1}{M_j}\displaystyle\sum_{i=1}^{M} r_i^j\left(H\left(r_i^j - a_j\right) - H\left(r_i^j - a_{j+1}\right)\right)\right) & j < N \\ ln\left(\dfrac{1}{M_j}\displaystyle\sum_{i=1}^{M} r_i^j H\left(r_i^j - a_j\right)\right) & j = N \end{cases} \tag{4-8}$$

$$H\left(z\right) = \begin{cases} 1 & z > 0 \\ 1/2 & z = 0 \\ 0 & z < 0 \end{cases} \tag{4-9}$$

$$y_j = \Phi^{-1}\left(\frac{m_j + 1}{M_j + 1}\right) \tag{4-10}$$

$$m_j = \begin{cases} \displaystyle\sum_{i=1}^{M} f_i\left(H\left(r_i^j - a_j\right) - H\left(r_i^j - a_{j+1}\right)\right) & j < N \\ \displaystyle\sum_{i=1}^{M} f_i H\left(r_i^j - a_j\right) & j = N \end{cases} \tag{4-11}$$

$$M_j = \begin{cases} \displaystyle\sum_{i=1}^{M} H\left(r_i^j - a_j\right) - H\left(r_i^j - a_{j+1}\right) & j < N \\ \displaystyle\sum_{i=1}^{M} H\left(r_i^j - a_j\right) & j = N \end{cases} \tag{4-12}$$

$$a_j = r^j_{N(j-1)+1} \qquad \textbf{(4-13)}$$

In the previous equations $N = \lfloor \sqrt{M} \rfloor$ is the number of elements in the analysis bin; the operator $\lfloor \ \rfloor$ denotes the floor function; $\sum_{j=1}^{N} M_j = M$, the number of specimens in the seismic fragility group; $\Phi^{-1}(\ )$ denotes the inverse cumulative lognormal function; and f_i = 1 or 0 depends on whether the specimen failed or not. The other parameters are as defined previously. Figure 4.1 shows the final fragility curves calculated from the experimental data, for which the Lilliefors goodness-of-fit test at the 5% significance level was assessed. When preparing the fragility curves, the Peirce's criterion for identification of outliers was considered.

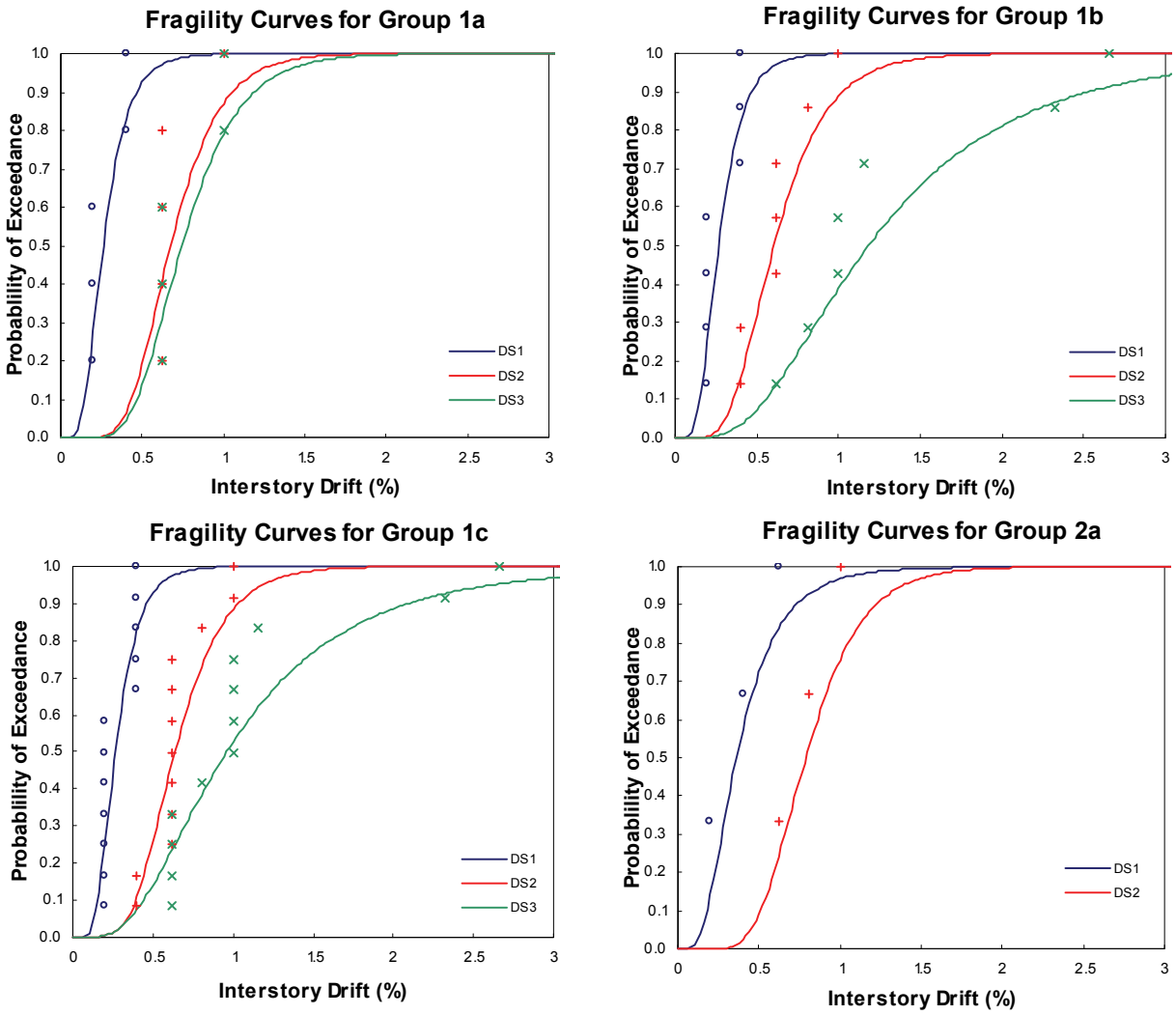

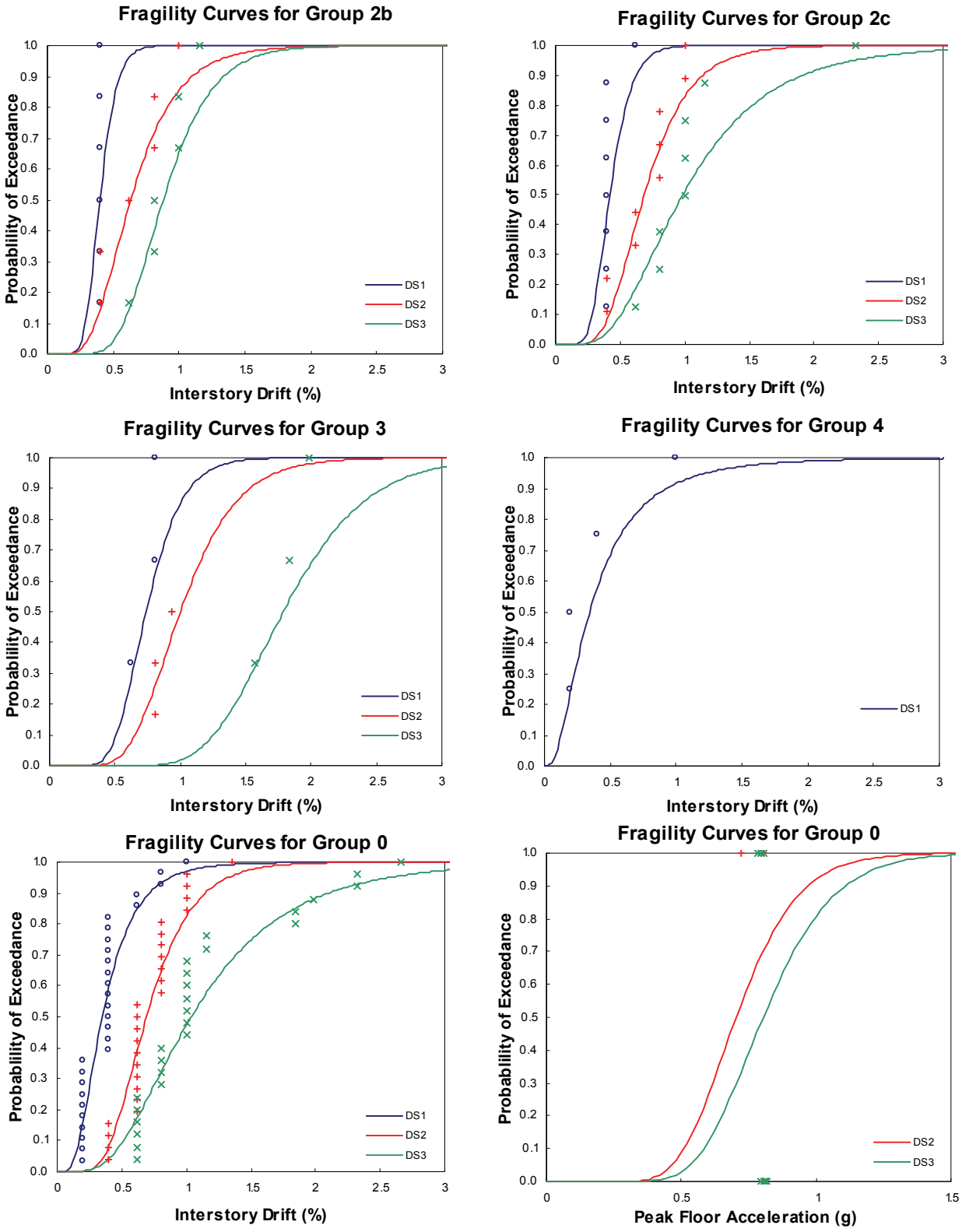

Figure 4.1 – Experimental Fragility Curves for Light Steel Stud Gypsum Partition Walls

Several considerations for deriving fragility curves from the experimental data shown in Table 4-3, Table 4-4, and Appendix C include:

1. Calculation of fragilities for displacement sensitive walls from observations made during in-plane dynamic tests was neglected due to their lack of accuracy.

2. For the seismic fragility Group 0, the fragility curves considering inter-story drifts as EDP do not satisfy the Lilliefors goodness-of-fit test. This situation can be graphically observed in Figure 4.1 when comparing the experimental data to the derived fragility curves. Two possible reasons arise to explain this situation. First, the factor β_u, introduced to take into account that only one loading history was used during the experimental fragility evaluation, deviates the best-fit curve from the experimentally obtained data; and second, the specimen's damage progression was assessed at discrete points. Both situations can be graphically observed in Figure 4.1. Nevertheless, the fragility analysis results are compatible with the experimental observations detailed in Appendix A and the data acquisition procedures considered.

3. For the seismic fragility group 1a, the fragility curve for DS_2 does not satisfy the Lilliefors goodness-of-fit test. This situation is also graphically observed in Figure 4.1. The reasoning for this noncompliance is basically identical to the previous explanation. Similar situations were observed for DS_1 in seismic fragility group 1b; DS_1 and DS_2 in seismic fragility group 1c; DS_1 in seismic fragility group 2b; and DS_1 in seismic fragility group 2c.

4. There is not enough data (only two data points) for generating a fragility curve for DS_3 in seismic fragility group 2a.

5. When generating the fragility curve for DS_1 in seismic fragility group 2c, the data corresponding to specimen 20 was discarded because it did not pass the Peirce's criterion for outliers.

6. When generating the fragility curve for DS_3 in seismic fragility group 3, the data corresponding to specimen 19 was changed from 0.81% to 1.57% because the original value did not pass the Peirce's criterion for outliers.

7. There is not enough data for generating seismic fragility curves for DS_2 and DS_3 for the seismic fragility group 4, the group including specimens provided with construction details aimed at mitigating the seismic damage. DS_2 and DS_3 were not observed in tests considering the solution details referred to as "corner gap".

8. The seismic fragility curves determined for acceleration sensitive partition walls are valid for walls with attached weights, comparable to the 510 lb bookshelves used in the test series, and partition walls interacting with rigid ceilings connected using methods similar to the ones used here. Nevertheless, extensive data useful for developing modeling tools, and that would allow for extrapolating the experimental results, has been made available through the NEES Repository.

From the use of the ATC-58 methodology, for generating the experimental seismic fragility curves, in combination with the testing procedures described in this document, the following additional conclusions are made:

1. It was observed that some data points that were considered outliers during the analysis of a subgroup, were not outliers when assessing the seismic fragility for the entire group,

2. As commented earlier in this chapter, the use of the factor β_u deviates the best-fit curve from the experimentally obtained data,

3. The inspection of the damage progression at relatively "coarse" discrete points, yielded fragility curves that did not fulfill the Lilliefors goodness-of-fit test at the 5% significance level, as indicated by ATC-58.

The seismic fragility curves were developed considering a single EDP as recommended by ATC-58. Inter-story drifts and peak floor accelerations were considered, independently, for displacement and acceleration sensitive partition walls.

Finally, and in regards to the results obtained from the seismic fragility assessment, the following conclusions can be made:

1. In general terms, the logarithmic standard deviations observed for the three damage states assessed are comparable, for all test configurations.

2. Logarithmic standard deviations, β, achieved values as high as 0.59 for specimens constructed using commercial construction details (e.g., for seismic fragility group 1b). This value is consistent with experimental observations that showed that identical specimens, constructed using the same techniques, identical details, and by the same team, exhibited failure mechanisms completely different.

3. For seismic fragility group 1c, the group considering all commercial construction specimens tested, a

logarithmic standard deviation $\beta = 0.61$ was calculated. This value is reasonable from the point of view that several different construction details, such as slip track and fully connected specimens, were included in this seismic fragility group.

4. Damage states for partition walls constructed using typical commercial construction details are triggered, in general, before the same damage states for partition walls constructed using institutional construction details. The logarithmic standard deviations β for commercial construction are, in general, greater than the standard deviations for institutional construction walls.

5. In the absence of details regarding the characteristics of the light steel stud gypsum partition walls found in a building, it is recommended to adopt as fragility parameters the median values 0.35, 0.69 and 1.04%, with logarithmic standard deviations 0.56, 0.39 and 0.55, for damage states DS_1, DS_2 and DS_3, respectively.

6. The use of innovative details to reduce the damage at wall intersections did not shift the mean seismic demand at which the damage state DS_1 is triggered. Nevertheless, when corner gaps were used, the damage states DS_2 and DS_3 were completely eliminated. When the solution proposed by Mr. W. Holmes and its modified version (double slip track) the damage states DS_2 and DS_3 were shifted from 0.64 and 0.96% to 0.98 and 1.23%, respectively. Nevertheless, the data obtained for these tests were not enough to generate a seismic fragility curve. Additional tests may be required to better evaluate the effectiveness of the proposed solutions.

7. The logarithmic standard deviation β, calculated for the acceleration sensitive specimens, is equal to $\beta_{//}$, the minimum value that could be considered in this case. The median value triggering DS_3 is equal to the median peak floor acceleration imposed on the specimens that collapsed. All collapses occurred after imposing the peak floor accelerations. In order to improve these results, it would be convenient to reevaluate the dynamic fragility testing procedure. Based on the experimental observations, it is recommended to apply the protocol using progressively increasing levels of peak floor accelerations. Although such a procedure could result in imposing an excessive number of small and medium cycles and induce failure due to fatigue, it would be representative of cumulative damage and aging effects.

4.3 Summary

A seismic fragility database for light-frame steel stud gypsum partition walls was developed following the recommendations of ATC-58 (Porter et al. (2007). The testing procedures and the obtained results have been discussed in detail. Alternative construction methods to shift and eliminate damage states have been developed. Additional experiments are required to better quantify the effects of using the alternative improved corner details. Efficiency of the database has been quantified. It is observed that the factor β_u, introduced to take into account one loading history, was used during the experimental fragility evaluation, and deviates the best-fit curve from the experimentally obtained data. Assessing the damage progression at discrete points complicates compliance to the Lilliefors test. Nevertheless, the fragility analysis results are compatible with the experimental observations. The results obtained from the dynamic tests demonstrate a need to reevaluate the procedures used for the current experimental seismic fragility analysis. It might be convenient to apply the dynamic fragility testing protocol in a sequence imposing increasing levels of peak floor accelerations, in order to better characterize the seismic demands triggering different damage states. Extensive experimental data useful for developing modeling tools, and that would allow for extrapolating the experimental fragility results, have been made available through the NEES Repository.

Chapter 5
PARAMETERIZATION OF HYSTERETIC RESPONSE OF PARTITION WALL SUBSYSTEM

To better understand the effect nonstructural partition walls have on the seismic performance of a steel moment resistant frame structure, it is necessary to have a method for modeling the walls that are to be considered as part of the building. The methodology proposed in this chapter uses regression analysis to fit the force-displacement (hysteresis) curves for 35 wall specimens designed and constructed according to 16 different construction techniques. These analyses yield the required parameters to be used along with a hysteretic model available in a nonlinear dynamic analysis program. Comparisons between some sample specimens and the corresponding numerical model hysteresis loops and dissipated energy are presented. Finally, recommended parameter values are made for the wall specimens based on six groups; commercial and institutional slip track walls, commercial and institutional full connection walls, partial height, and improved wall intersection detail.

5.1 Evaluation of Experimental Hysteresis Loops

The hysteretic data for each of the 36 specimens tested in-plane is evaluated in this chapter. There were two similarities immediately observed in the recorded data. The first was the tri-linear backbone curve consisting of an initial stiffness, post-yield stiffness, and post capping stiffness, see Figure 5.1. Initial stiffness is captured at low inter-story drifts and is often characterized as the range in which the system remains "elastic" or removal of imposed drift will return the forces in the system back to zero. The post-yield stiffness occurs after individual wall components (i.e., studs, tracks, fasteners, joints, etc.) begin to get damaged. In this range, the forces continue to increase at a slower rate than the initial stiffness until the highest maintainable force is reached in the system; this maximum allowable force is the capping strength. The third stiffness parameter is defined as the post capping stiffness in this report but can also be referred to as the rate of strength degradation. The slope of this line is negative and the forces should tend to zero or some inherent level of force that the system can maintain due to some minimal force resistance remaining in the system. In many of the specimen a ratcheting effect was observed from the gypsum binding in the corners, as shown in Figure 5.1. This occurred after the system degraded in strength. At

this point, the specimen's stiffness increased and sometimes surpassed the capping strength. This effect happened at drift levels generally greater than 2% and was explained in greater detail in chapter 3. Because this happened at higher drift levels and a significant amount of damage had already occurred, the increase in strength is ignored for modeling purposes. The post-capping stiffness therefore is the negative slope of the backbone curve after the capping strength is observed and before the strength degradation ceases.

The second observed similarity in the hysteresis loops for the 36 wall specimens was a pinching effect. Pinching occurs after members or connections in the system have begun to yield, and as the system undergoes cyclic displacements these failures delay the onset of an increasing stiffness. The pinching effect often is associated with a non-zero force at zero drift levels, see Figure 5.1.

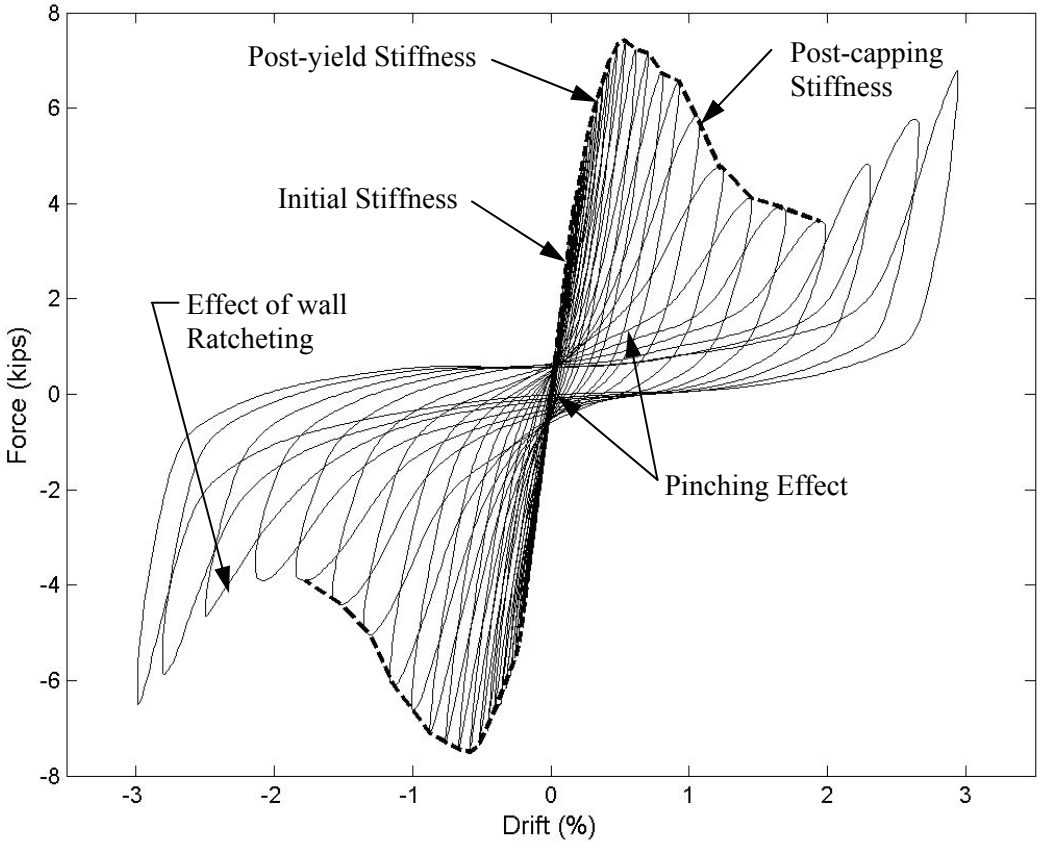

Figure 5.1 – Typical Hysteretic Behavior of a Cold-formed Steel-framed Gypsum Partition Wall

A total of 35 wall specimens were used in determining the required parameters, all but one of the tested in-plane partition walls. Specimen 1 was neglected in this analysis because the tri-linear backbone curve

was not evident, as shown in Figure 5.2. This figure shows that for both the positive and negative drift levels the forces and stiffnesses vary, but both continue to increase until the ratcheting effect began at a drift ratio of approximately 1%. The high ratcheting effects in this specimen were due to a very small gap between the top of the gypsum board and the top slab.

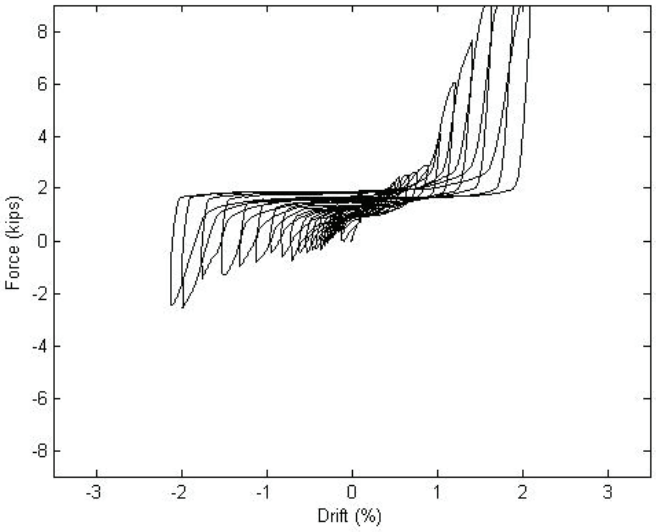

Figure 5.2 – Hysteresis Loop for Specimen 1

5.2 Parameterization of Experimental Data

The mechanical behavior observed in the partition wall specimens can be modeled using the Wayne Stewart degrading stiffness hysteresis model (see Figure 5.3) available in the software RUAUMOKO (Carr, 2005). The software suite RUAUMOKO was developed primarily for nonlinear response history analysis of structures and is capable of doing static analysis, frequency analysis, earthquake loading (acceleration or displacement input), and pushover analysis, both monotonic and cyclic. One of the unique capabilities of this program is the number of hysteretic models that are available, at the current date, 50 different models are available for use in the program. Of these fifty, the Wayne Stewart hysteretic model (Stewart, 1987) most resembles the data obtained from the specimens tested.

According to Carr, "This very general rule was initially developed by Wayne Stewart for the representation of timber framed structural walls sheathed in plywood nailed to the framework. The model allows for initial slackness as well as subsequent degradation of the stiffness as the nails enlarged the holes and withdrew themselves from the framework." Shown in Figure 5.3 is an example of the Wayne

Stewart hysteretic model and parameter notation, and Figure 5.4 is an example of the same model with strength degradation included. The model is applicable to these walls because of the similarities in damage at the connections of the panels to the framing members (i.e., screws attaching the gypsum boards to the steel tracks, and nails attaching plywood to wood framework). As the drift levels increased the screws began to rock until the gypsum was completely damaged around the screws or the screws completely pulled through the gypsum. The effects of this damage in the hysteretic model are captured in the pinching and softening parameters. This hysteretic model also has the capability to model a tri-linear curve.

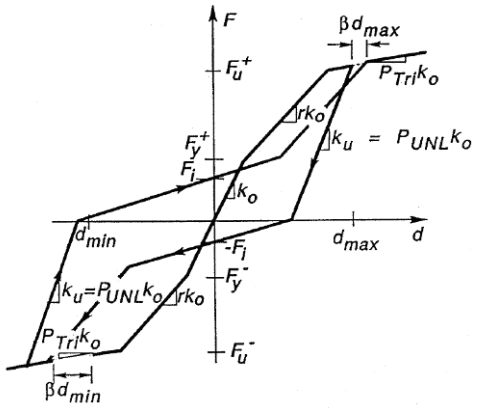

Figure 5.3 – Wayne Stewart Hysteretic Model (from Carr, 2005)

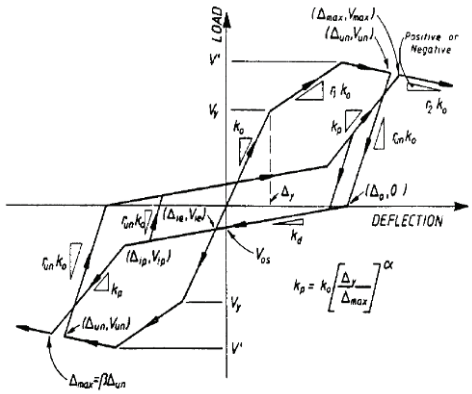

Figure 5.4 – Wayne Stewart Model with Degradation (from Carr, 2005)

Nine input parameters are required for this hysteretic rule. These parameters along with their ranges are listed in Table 5-1 and shown in Figure 5.3. One parameter used in the model but not requiring calculation is the binary flag that tells the program to run the model as a defined loop or a modified loop. The modified loop option was used because under this rule the factor determining the post-yielding stiffness can be given a negative value.

Table 5-1 Range Limits for Wayne Stewart Hysteretic Model

Parameter	Range	Comments
k_0	> 0	Initial stiffness
r	0 ≤ r < 1	Post yield stiffness factor
P_{tri}	≤ 0	Post capping stiffnes factor, strength degradation considered
P_{UNL}	> 1	Unloading stiffness factor
F_y	> 0	Yield strength
F_u	> 0	Capping strength
F_i	> 0	Intercept stregth
α	≤ 1	Reloading or pinch power factor
β	≥ 1	Beta or softening factor

Each of the stiffness parameters are a factor of the initial stiffness k_0. The Wayne Stewart model also allows for gaps in the element, but because a gap is not observed in the experimental data, these values were set to zero to have no effect in the modeling.

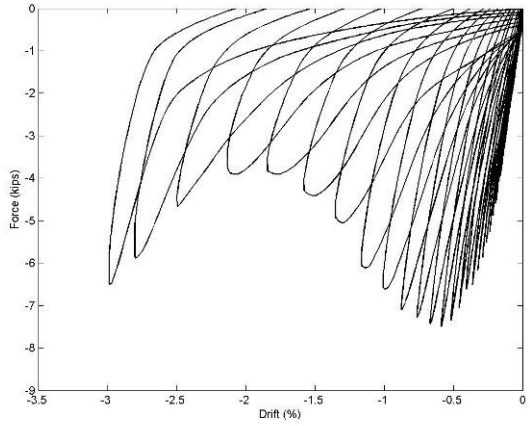

Figure 5.5 - Negative Drift Force-Displacement Curve

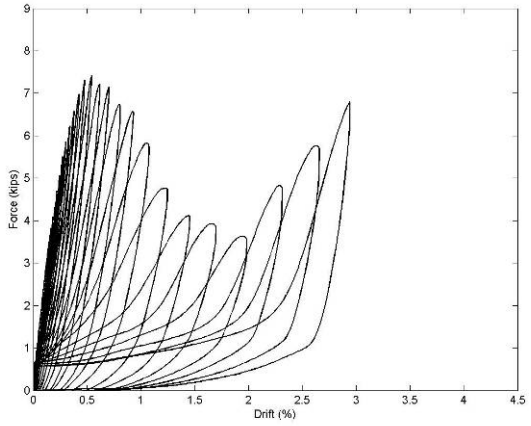

Figure 5.6 - Positive Drift Force-Displacement Curve

Recommended parameters for modeling in RUAUMOKO of steel stud gypsum partition walls were obtained by analyzing the hysteresis data recorded for specimens 2 to 36. The negative and positive branches of the hysteresis loops, such as the one shown in Figure 5.1, were decoupled from each other to examine the force-displacement curves individually, as shown in Figure 5.5 and Figure 5.6. This method of examining both branches of the drift levels returned values for calibrating each required parameter. The

following sections explain the method used to obtain each of the parameters used in the Wayne Stewart model.

5.2.1 Initial Stiffness (k_0)

The initial stiffness is the rate of change of the force transferred through the wall with an increased displacement at low drift levels before damage is observed in the specimen. The initial stiffness remains fairly constant within low drift levels (0-0.3 % drift approximately) and begins to decrease as larger drifts are imposed and damage is induced in the partition wall.

In order to determine the parameter k_0, the method of least squares was used. Least square regression is a method to fit both linear and nonlinear types of data points. The Wayne Stewart hysteretic model is nonlinear, but for simplification in the analysis, the required parameters are calculated individually. Because this approach is used, a linear least square regression is accomplished using the following:

$$S = \sqrt{\sum_{i=n}^{1}\sum_{j=1}^{n}\left(F_j - k_i D_j\right)^2} = \sqrt{\sum_{i=n}^{1}\sum_{j=1}^{n}\left(F_j - \frac{F_i}{D_i}D_j\right)^2} \quad \text{where, } k_i D_j \le F_n \qquad \textbf{(5-1)}$$

where D_j is the recorded relative displacement between the top and bottom platforms of the UB-NCS, F_j is the sum of the recorded shear forces in the load cells located at the base of the partition wall, and k_i is the slope of displacement D_i and F_i. In the given equation the variable n is the number of the data point at the peak force in the backbone curve. Because a least square regression is used to minimize the deviations from an assumed linear equation the best fit occurs when the variable S is minimized. The imposed limit is to account for the nonlinearity observed in this range of data. Associated with the variable S is a constant for stiffness, displacement, and force. The stiffness is equal to the initial stiffness parameter (k_0), as shown in Figure 5.7. Figure 5.8 presents a histogram plotting different ranges of k_0 for the 35 specimens (70 analyses). There is a wide distribution of this parameter with peaks occurring in the ranges of 0-3 kips/inch and 15-17 kips/inch. The distribution of the initial stiffness parameter, preliminarily, indicates the walls can be separated into two groups based on the wall configurations, but upon further inspection there is a slight plateau in the range of 5.0 to 9.0 kips/inch. This plateau could represent another key group in determining parameters for the hysteretic model; later in this chapter this notion will be explored more in depth.

The histograms that will be presented throughout this chapter plot the analyzed parameter on the horizontal axis, and on the vertical axis is the frequency of occurrence or number of specimens that

exhibited values in the defined ranges. Porter et al. (2007) uses a bin size of:

$$M = \lfloor \sqrt{N} \rfloor \quad \textbf{(5-2)}$$

where M is the size of the bin and N is the number of data points (in this analysis 70 data points are used), therefore the bin size is eight. The size of the ranges used on plotting the histograms was solely based on the range of parameter values divided by the bin size M.

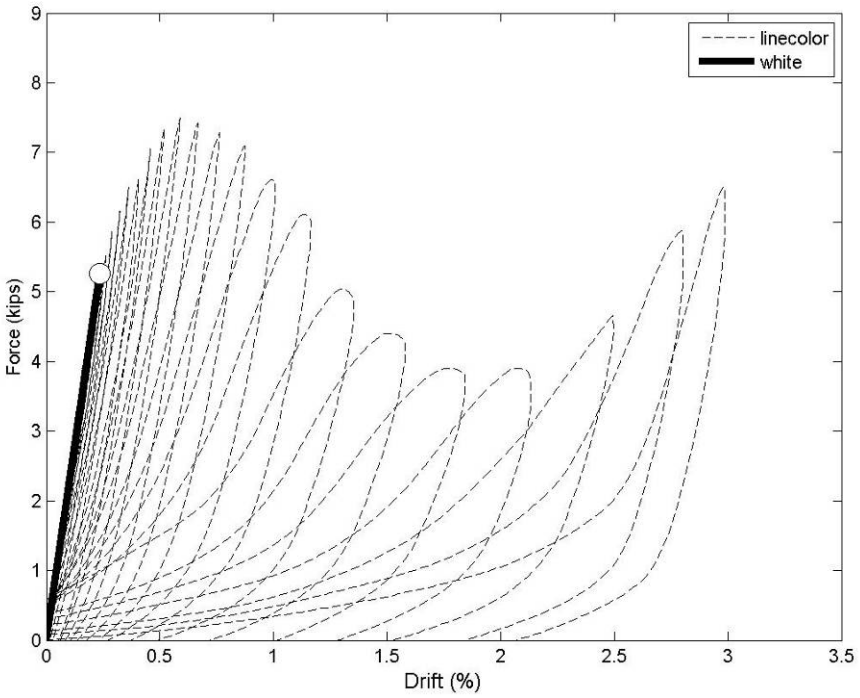

Figure 5.7 – Plot of Initial Stiffness and Yield Force

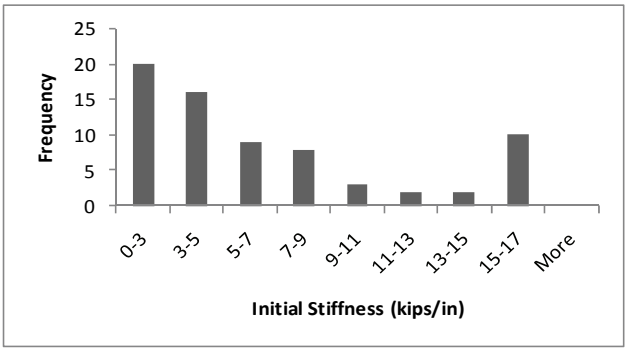

Figure 5.8 – Histogram for Initial Stiffness Parameter (k_0)

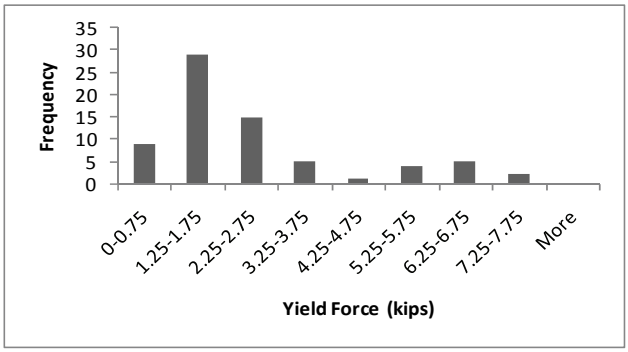

Figure 5.9 – Histogram for Yield Force Parameter (*Fy*)

5.2.2 Yield Force (F_y)

As drift levels increase from zero, yielding begins to occur in the system until at an inherent drift ratio the stiffness reduces at a faster rate. The force associated with this drift is defined as the yield force or yield strength (F_y). At low drift levels this yielding is minimal and mostly evident as small cracks in the corners or slight rocking around screws located in the top and/or bottom tracks. The point of yield is generally not evident by visual examinations, but can be obtained through analyzing the backbone curve of the recorded data. The yield force was obtained through the same least square regression that was used to determine the initial stiffness, see Equation 3-2. The force at which the regression is minimized is defined as the yield force. Because the stiffness used in the regression was calculated from recorded forces and displacements, the yield force marked in the figure lies at one of these points on the backbone curve. In the histogram plotted in Figure 5.9, the frequency of yield forces in the defined ranges obtained in the analysis of the 35 wall specimens, similar distributions are observed for the parameter F_y. The highest frequencies occur in the ranges of 1.25-1.75 kips and 6.25-6.75 kips. These yield forces again represent two very different wall strengths based on the configurations used in detailing, but most often occurred at drift ratios of 0.2% to 0.6%.

5.2.3 Post-Yield Stiffness Factor (*r*)

Once yielding begins to occur the stiffness begins to decrease, this decreased level of stiffness is defined as the post-yielding stiffness and is a percentage of the initial stiffness represented by rk_0, see Figure 5.10. The required input parameter for the Wayne Stewart hysteretic model is the factor *r*. This factor is the ratio of the calculated stiffness observed in the backbone curve at force levels between the yield and

maximum forces over the initial stiffness, and ranges for this parameter are presented in Table 5-1. To calculate the post-yield stiffness, the same method of least square regression, previously used to calculate the initial stiffness and yield force is used. Although for this parameter the initial displacement and force are set to occur at the yield displacement (D_y) and corresponding force. The limitation of $k_i * D_j \leq F_n$ in Equation 3.2 is not applied in this analysis and therefore a variance in the maximum force in the numerical model can occur. An imposed limit of ±15% was placed on this force. The level of 15% is based solely on trial and error and an effort to maintain similarity between the recorded data and the numerical model. A plot representing the post-yield stiffness can be seen in Figure 5.10. In this figure it is noticed that the calculated stiffness did cause a maximum force higher than the recorded maximum force. Also the forces at the peak drift levels at each cycle are located both above and below the calculated post-yield stiffness thus showing the best fit line for the recorded data. Figure 5.11 shows the range of values obtained for this parameter. In Figure 5.11 a peak frequency occurs in the range of 0.33 to 0.46 with a lognormal distribution. Based on the results of the analyses, wall type and construction details appear to have little effect on the post-yield stiffness factor, but could be considered as a function of the steel stud partition wall subsystem. In an effort to simplify modeling of the partition walls using the Wayne Stewart hysteretic model, post-yield stiffness factors within the peak frequency range could be used for any wall configuration to numerically simulate a full scale specimen.

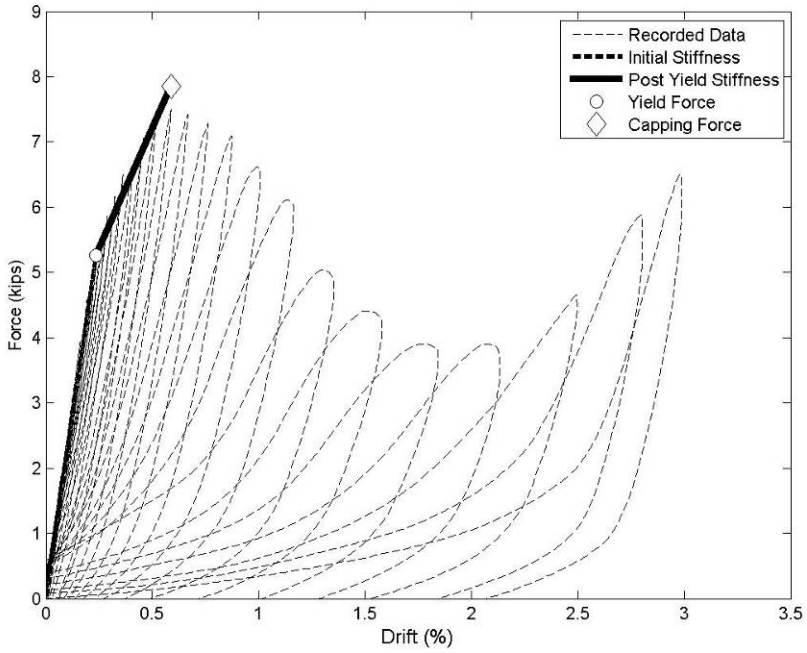

Figure 5.10 – Plot of Post-yield Stiffness and Capping Force

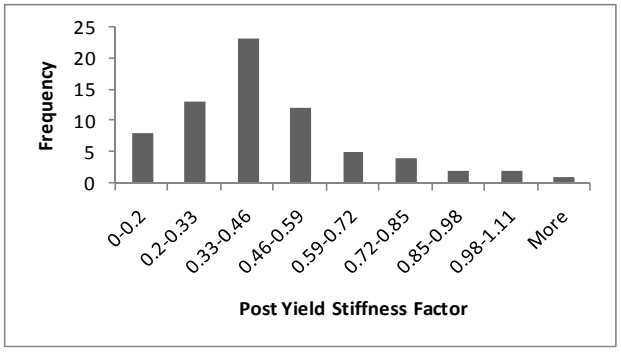

Figure 5.11 – Histogram for Post-yield Stiffness Parameter (*r*)

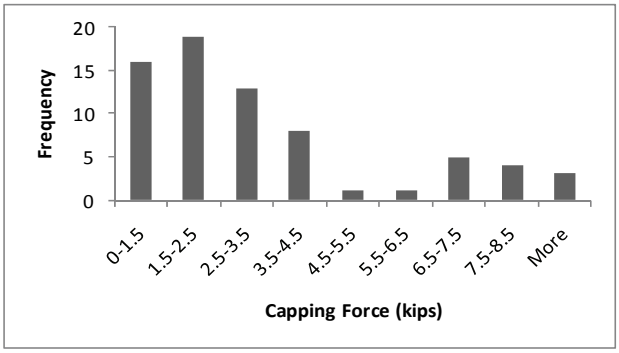

Figure 5.12 – Histogram for Capping Force Parameter (F_u)

5.2.4 Capping Force (F_u)

The maximum force calculated in the previous section, in the Wayne Stewart model, is defined as the Capping Force and represented by (F_u). The capping force is located at the drift level where the stiffness at lower drift is positive and the slope of the curve at higher drift level is negative. Failure of the system to resist force has begun and the system goes into higher damage states. This force is determined through the

regression analysis used to obtain the post-yield stiffness parameter. Figure 5.10 illustrates the location of the capping force parameter versus the recorded data, and it is again noted that the capping force can be lesser (no less than 85%), greater (no greater than 115%), or equal to the maximum force observed in the test specimen. Figure 5.12 shows the range of values obtained and their frequency of occurrence in the 35 wall specimens. The distribution of capping forces in the 2nd and 7th bins 1.5 – 2.5 kips and 6.5 – 7.5 kips respectively, is similar to the distributions of k_0 and F_y, demonstrating that within the 16 configurations there is a high number of walls that are weaker and a much lower percent that would be considered stronger. As was noted in the previous section, because there are nine required parameters for the hysteretic model, it is desirable to determine if a simplification can be made in determining some of these values. Figure 5.13 show a histogram of the ratio of the yield force to the capping force. In this chart it is evident by the distribution of the 35 specimens that the capping and yield force do correlate, with the yield force being in the range of 0.75 to 0.85 of the capping force. Therefore, if the ultimate or yield force is known for a nonstructural partition wall, built to any of the configurations previously described, it is possible to use this ratio to estimate the other required force and thus minimize the total number of required parameters.

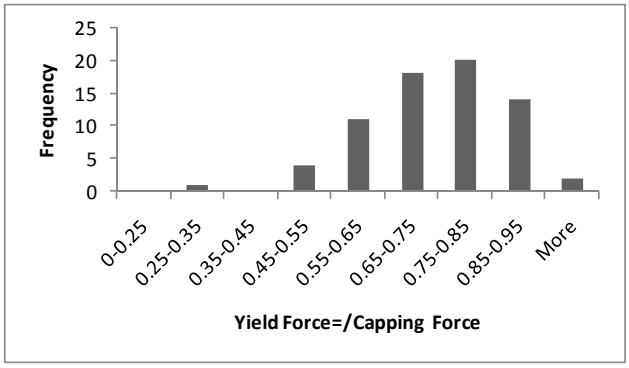

Figure 5.13 Ratio of Yield Force to Capping Force (F_y/F_u)

5.2.5 Post Capping Stiffness Factor (P_{Tri})

As previously mentioned, after the capping force is reached, the drift ratio will continue to increase without an increase in forces. When strength degradation is considered the drift will increase with a decrease in forces and the system loses the ability to resist lateral forces. This rate of change results in the first occurrence of a negative slope in the backbone curve and is defined as $P_{Tri}*k_0$. See Figure 5.14 for a visual representation and Figure 5.15 for the range limits. The coefficient P_{Tri} is calculated through

dividing the calculated post capping stiffness by the initial stiffness. This parameter can be defined as the slope of the third segment of the tri-linear backbone curve that accounts for strength degradation. To determine the value of this parameter, a least square regression was performed on the remaining section of the backbone curve using Equation 5-1. The minimum drift and force levels considered in the computation of P_{Tri} are set equal to the drift (D_u) and force at which the capping strength occurs in the curve. Figure 5.14 gives a representation of this stiffness. As shown in Figure 5.14, the portion of the time history data recorded during the wall ratcheting process previously described has been neglected. Figure 5.15 shows the range of values obtained for the post capping stiffness factor to have a mode in the range of -0.18 to -0.06. The high frequency of this parameter in a specific range suggests that the post-capping stiffness factor is not necessarily a function of the wall configurations and could be considered a factor of steel stud gypsum partition walls in general. This high frequency also leads to the assumption that the post capping factor could be eliminated as a required parameter or fixed for the Wayne Stewart model. This assumption will be verified later in this chapter.

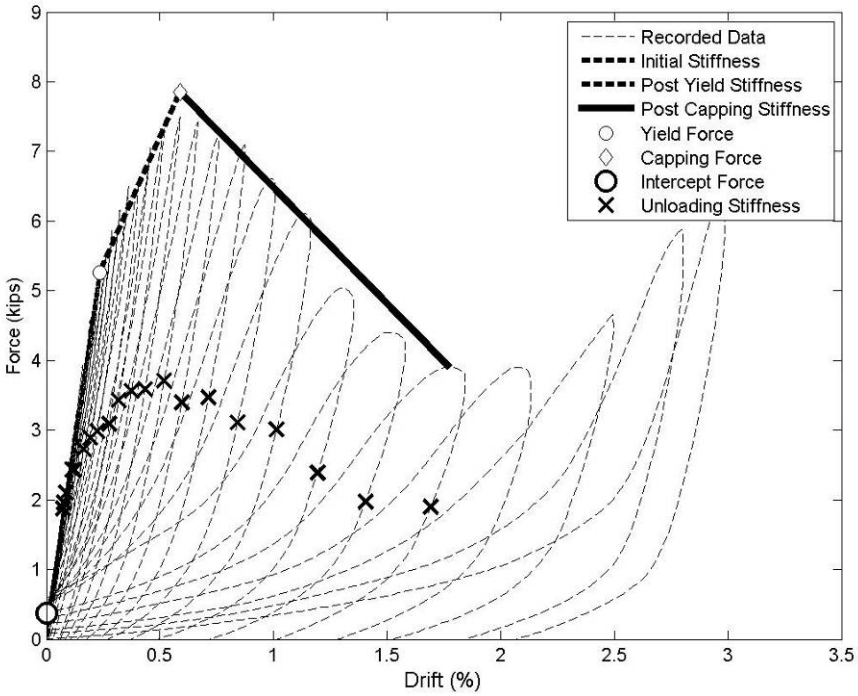

Figure 5.14 – Post Capping Stiffness, Unloading Stiffness, and Intercept Force

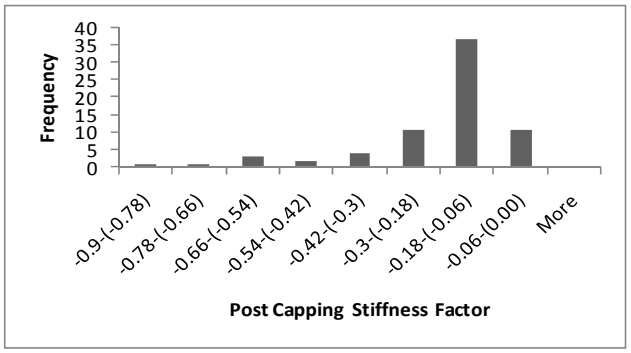

Figure 5.15 – Histogram for Post Capping Stiffness Parameter (P_{Tri})

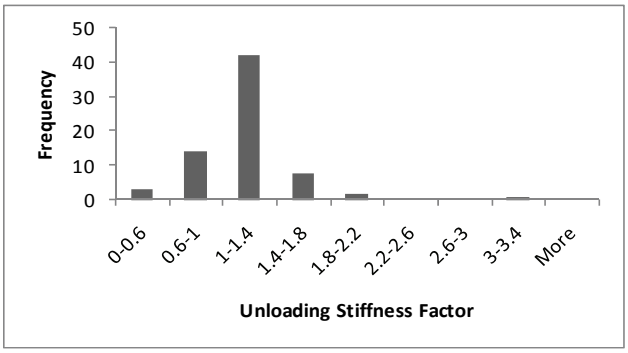

Figure 5.16 – Histogram for Unloading Stiffness Parameter (P_{UNL})

5.2.6 Unloading Stiffness Factor (P_{UNL})

The one remaining stiffness to be determined in parameterizing the Wayne Stewart model is the unloading stiffness. This stiffness is defined as the rate of change in forces as imposed drift is reversed, or when drift levels decrease. This parameter is defined in terms of the initial stiffness as $P_{UNL}*k_0$. The factor P_{UNL} required for the numerical model is the ratio of the calculated unloading stiffness to the initial stiffness.

After a close examination of the unloading phase of the recorded data, it was observed that the unloading stiffness varied through the cycles. While the unloading stiffness varied over the unloading process, it was observed that within drift levels less than 1%, the unloading stiffness remained constant. Therefore, the tangent slope at 0.5 times the force at each maximum excursion was computed, as illustrated in Figure 5.14. The median value of the calculated unloading stiffness was used to define this parameter. From Figure 5.16 the mode for this factor occurred in the range of 1.00 to 1.40. From Figure 5.16 the unloading factor has a high frequency in the range below 1.00, but based on the limit for the unloading stiffness of the Wayne Stewart model defined in Table 5-1 this range does not meet the requirements, and the parameter defaults to the minimum factor of 1.00 in the program RUAUMOKO.

5.2.7 Intercept Force (F_i)

As mentioned previously, one of the determining factors for using the Wayne Stewart hysteretic model was the ability of this model to simulate the pinching effect observed in the test specimens. Although the pinching effect is associated with damage in the system, and consequently a delay in increased stiffness

occurs, often times when this effect is observed some level of force is observed at low drift levels and is defined as the intercept force (F_i). These forces are an inherent behavior in this type of system and can be caused by binding, friction, damage, etc. To determine this parameter the forces measured within a displacement of ±0.01 inches are used from the experimental data. This tolerance yields two continuous force recordings because of the frequency of data acquisition. Another limit imposed on these data points, to determine when the system has become relatively stable at the 0% drift ratio, is a stiffness under 20% of the initial stiffness. The median of the filtered forces is taken as the intercept force. Figure 5.17 shows the histogram of the calculated intercept force and shows that these forces are all well under 1 kip for the specimens tested. A high frequency of occurrence is in the defined range of 0.1 to 0.2 kip. To further simplify the number of required parameters for the Wayne Stewart model, the relationship between F_i to F_y was also investigated and the results are presented in the histogram in Figure 5.18. The mode of the intercept force to yield force is in the range from 0% to 9% of the yield force.

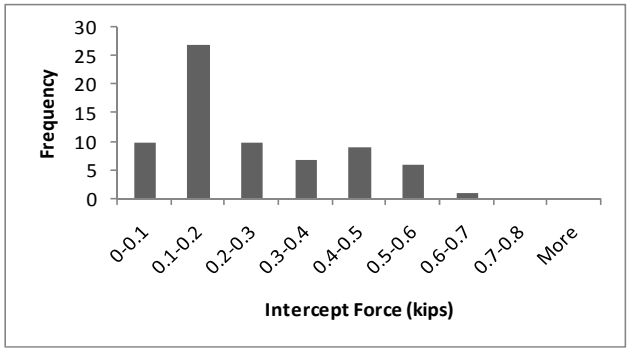

Figure 5.17 – Histogram for Intercept Force Parameter (F_i)

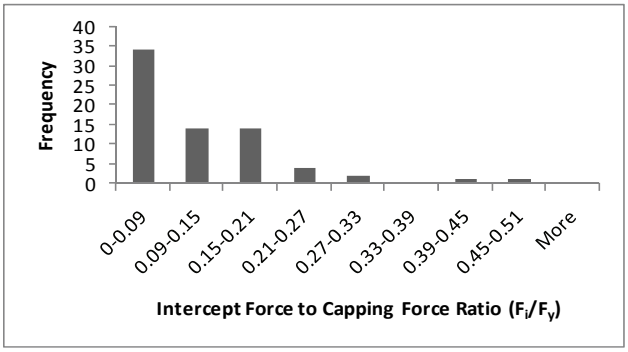

Figure 5.18 – Histogram for Intercept Force to Yield Force Ratio (F_i/F_y)

5.2.8 Softening Factor (β) and Reloading or Pinching Factor (α)

The two remaining parameters of the Wayne Stewart hysteretic model to determine are the factors β and α. The first of these, β or softening factor, is a percentage of the force reached at the point of maximum displacement in the previous cycle in the same direction (i.e., if $\beta = 1$, then during reloading the first force reached on the backbone curve will be the same force reached at the last peak drift), as illustrated in Figure 5.19. The limits for β are defined in Table 5-1. In Figure 5.19, α is arbitrarily fixed at 0.5, and β varies from 1.00 to 1.10 with an intermediate step of 1.05. The β factor begins to take effect only after the yield force has been reached and surpassed in the system.

The reloading or pinching factor α affects the rate at which the stiffness degrades per cycle, and is

calculated in the Wayne Stewart model using:

$$k_p = k_0 * \left[\frac{\Delta_y}{\Delta_{\max}} \right]^{\alpha} \qquad \textbf{(5-3)}$$

where k_0 has been previously defined as the initial stiffness, Δ_y is the drift at yield, and Δ_{max} is the maximum observed drift in the previous cycle. In Figure 5.20 three plots are shown each having the same value β=1.05 for the softening factor but varying levels of α. In Figure 6.20 (a), α = 0, or in other words, there is no stiffness degradation. In Figure 6.20 (b), a value α=0.5 is considered, exhibiting a constant decay of stiffness. Figure 6.20 (c) considers a value α = 1.0, which corresponds to the upper limit for this factor. In each of these figures the parameters for the Wayne Stewart model are clearly shown, including the initial, post-yield, post capping, and unloading stiffness values. The yield, capping, and intercept forces, and lastly the effect of α and β factors are also presented in this figure.

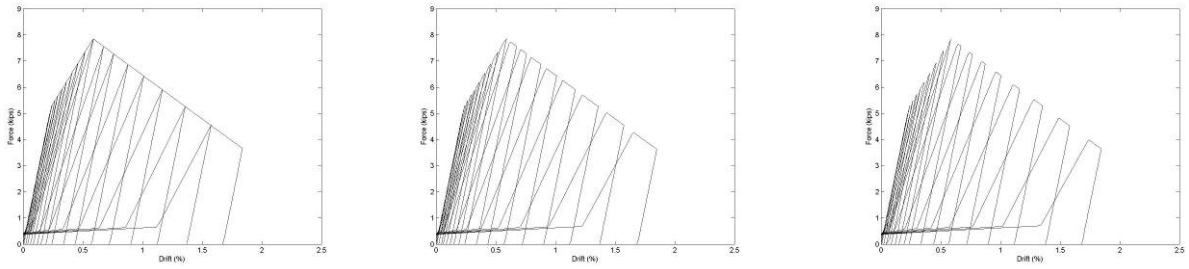

(a) **(b)** **(c)**

Figure 5.19 – Numerical Model Hysteresis Loop (α = 0.5, β = (a) 1.00, (b) 1.05, (c) 1.1)

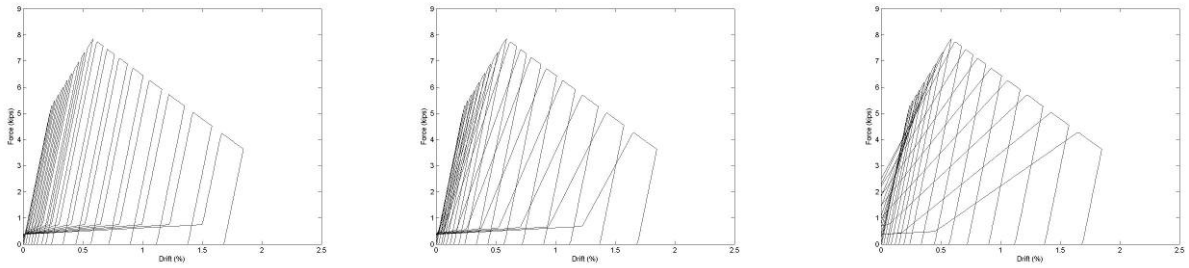

(a) **(b)** **(c)**

Figure 5.20 – Numerical Model Hysteresis Loop (β = 1.05, α = (a) 0.0, (b) 0.5, (c) 1.0)

The range of possible values for α is also observed in the histogram in Figure 5.22. The softening and reloading factors were determined simultaneously through a least square regression on the dissipated

energy for both the observed and numerical models. The difference between the observed dissipated energy at the excursions is the variable to minimize in the best fit process. This was checked numerically for all 35 specimens. Figure 5.21 and Figure 5.22 show histograms for the values of the optimal softening and reloading factors. The range for β was limited from 1.05 to 1.13 and increased by intervals of 0.02, while for α the range was set as 0.3 to 0.9 and also increased by intervals of 0.2. Outside these ranges, the hysteresis for the numerical model did not simulate the hysteresis data from the specimens. From the histogram for the softening factor, at $\beta = 1.03$ the frequency content peaks. For the factor α, the frequency is consistent for all assigned values.

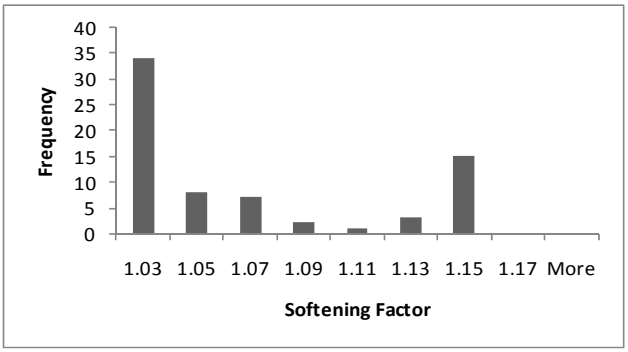

Figure 5.21 – Histogram for Softening Factor Parameter (β)

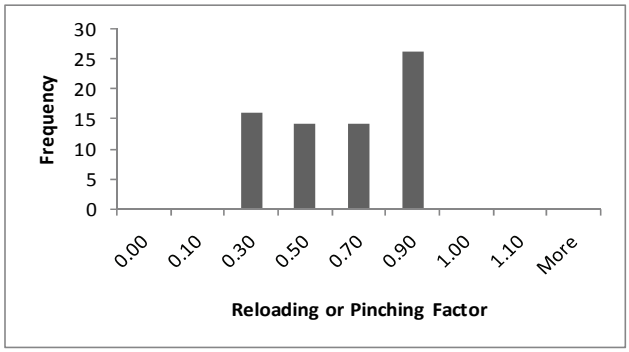

Figure 5.22 – Histogram for Reloading or Pinching Factor (α)

5.2.8.1 Example of Specimen Data vs. Numerical Data

As an example, Specimen 27 was parameterized for the strengths and stiffnesses, see Chapter 3 and Appendix A for construction configuration details. The method described in Section 6.2.8 was used for obtaining α and β parameters for this specimen. The factor α is assigned the minimum value of 0.3 and the maximum value of 0.9. β is assigned the values of 1.05 and 1.11. In Figure 5.23 and Figure 5.24 the hysteresis loop and energy dissipation time history for both the experimental data and numerical model are compared. For this specimen, and when $\beta = 1.05$ and $\alpha = 0.3$, the energy difference is minimized, so the parameters would be assigned the respective values.

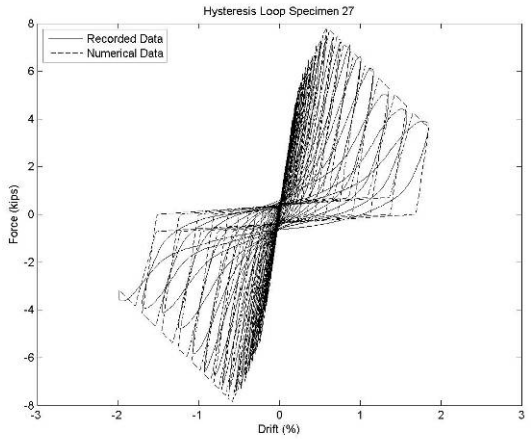

Figure 5.23 – Hysteresis Loops (β=1.05, α=0.3)

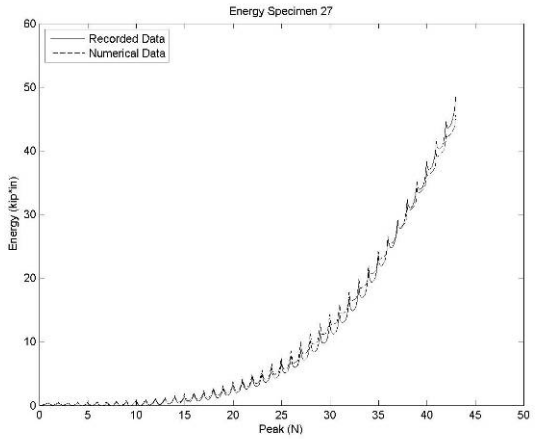

Figure 5.24 – Dissipated Energy (β=1.05, α=0.3)

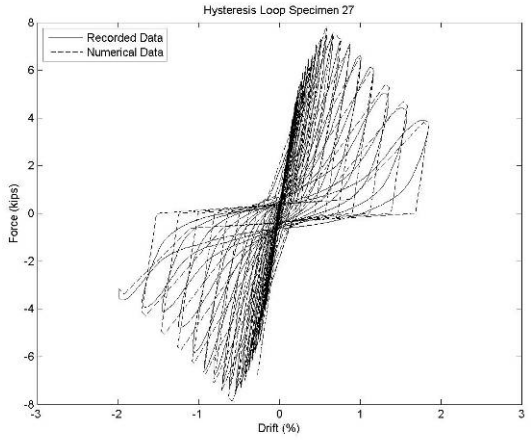

Figure 5.25 – Hysteresis Loops (β=1.11, α=0.9)

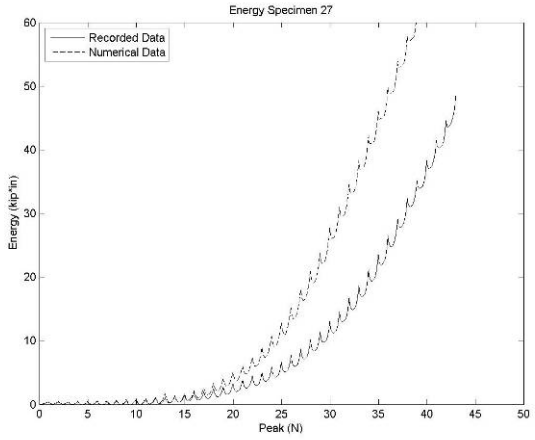

Figure 5.26 – Dissipated Energy (β=1.11, α=0.9)

An interesting phenomenon occurs as β and α are increased. Figure 5.25 and Figure 5.26 show that the mechanical behavior visually improves between the two models, but the dissipated energy plots begin to diverge at low peak drifts. The variances between the experimental data and the numerical model are explained by the combined effect of the reloading factor at very low drifts and the unloading factor considered.

5.3 Development of Model for Steel stud Gypsum Partition Walls

In this section a model is proposed to simulate the mechanical behavior of the several types of gypsum partition walls tested. The model, shown in Figure 5.27, consists of three different elements, two frame type members and one nonlinear shear spring. Frame elements were used for the columns and beam. The beam was set to be infinitely rigid through the use of rigid links on each end of the beam extending to the center of the member and the columns were set to remain elastic. Actual material properties for these members are arbitrary because the test is displacement controlled. By assigning these parameters to the model, a single degree of freedom system with free translation in the x-axis is obtained. The spring element in the model is placed vertically to resemble partition walls, see Figure 5.27. The Wayne Stewart Hysteretic Model is assigned to the spring element in the transverse axis of the spring which coincides with the horizontal or global x-axis. The node at the center of the beam is assigned a displacement time history that has the same amplitudes as the quasi-static protocol used to test the individual partition wall specimens, see Figure 3.3. Because the beam is rigid, the horizontal displacement of the beam is the same displacement in the transverse shear spring. The imposed displacement causes forces in the spring based on the parameters entered for the Wayne Stewart model. These displacements and forces are compared to the recorded data for the individual specimens and then used to calculate the dissipated energy.

5.4 Wall Group Parameters

A total of 16 configurations were used in the construction of the 36 specimens tested. Based on the performance of each of the test specimens, the walls were separated into six groups with similar mechanical behavior and construction specifications. These six groups have been previously defined for preliminary seismic fragility analysis in Chapter 4 as Groups 1a, 1b, 2a, 2b, 3, and 4 and are respectively commercial slip track, commercial full connection, institutional slip track, institutional full connection, partial height, and improved detail construction. Group 1a considers specimens 2-3, 11-16, 29-32; 1b consists of specimens 4-6, 10, 20-21; 2a takes into account specimens 7-9; 2b accounts for specimens 23-28; group 3 specimens are 17-19; and group 4 considers specimens 33-36. An explanation of the individual group configurations can be found in Chapter 3.

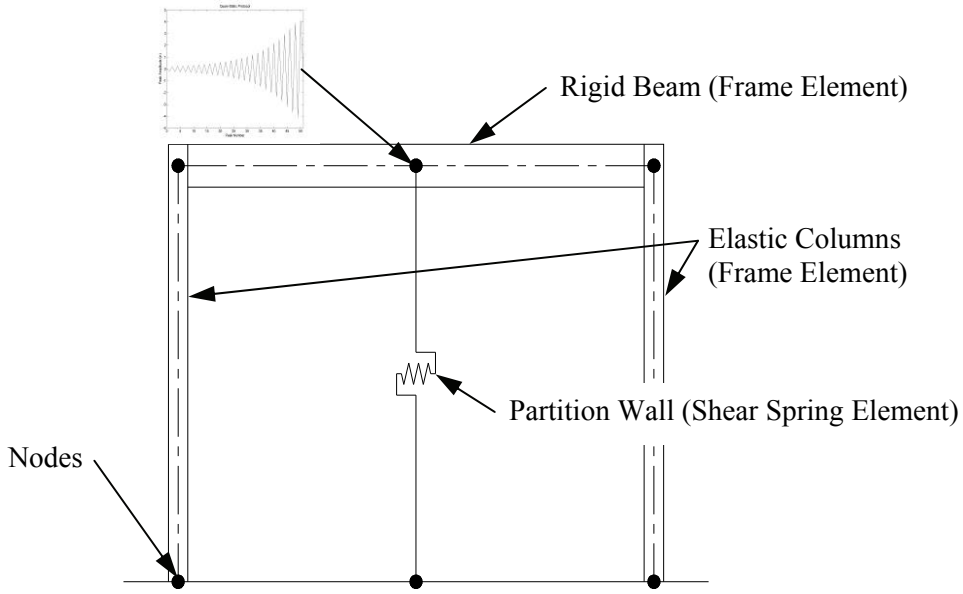

Figure 5.27 - RUAUMOKO Single Degree of Freedom Model

The histograms plotted in Section 5.2 show ranges obtained for the needed parameters for all 70 regression analyses (2 x 35 specimens) considered. To better understand the hysteretic response of the partition walls in each of the defined groups, the data are separated by group and presented in the following tables and figures. Data and histograms are given for each of the six groups.

5.4.1 Initial Stiffness Parameter by Wall Groups

In Figure 5.21 the frequency of occurrence for a range of initial stiffness are given for the six groups. From the histogram it is evident that the groups 1a, 3, and 4 all have similar ranges for the initial stiffness. The stiffness of these wall configurations is in the lower ranges of the total spectrum of specimens tested. The specimens within 1a have an initial stiffness in the range of >0 and ≤9 kips/inch, and have a lognormal distribution. The mean initial stiffness for this group is 3.45 kips/inch. All walls in group 3 and 75% of the decoupled loops in group 4 have a stiffness within the range of 0-3 kips/inch, these walls have a mean initial stiffness of 1.35 and 1.37 kips/inch respectively, at low drifts the groups 3 and 4 are performing similarly. The specimens with stiffness ranges greater than 1a are those that are considered part of 1b and 2a. Distribution of group2b is close to lognormal, the mean initial stiffness for this group is 6.62 kips/inch. For institutional walls, the initial stiffness mode was 5-7 kips/inch and the mean stiffness

for group 2a is 6.68 kips/inch. The walls with the highest stiffness are those specimens that are considered part of group 2b or institutional full connection wall configurations and have initial stiffness values in the range of 15-17 kips/inch. The mean initial stiffness for group 2b is 15.06 kips/inch. The mean values for the individual groups have been plotted in Figure 5.39.

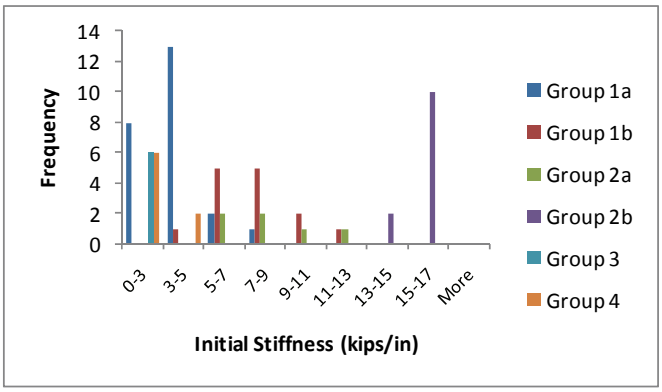

Figure 5.28 – Grouping Histogram of Initial Stiffness Parameter (k_0)

5.4.2 Yield Force Parameter for Wall Groups

The histogram presented for the yield force is similar in shape to k_0. Basically walls of groups 1a, 3, and 4 all have yield forces in the lower end of all the ranges considered. Mean values for these groups are plotted in

Figure 5.29 and values can be found in Table 5-2. Group 1a has a mean yield strength of 1.11 kips, group 3 and group 4 are similar to one another with respective mean yield forces of 0.65 and 0.58 kips, groups 1b and 2a have similar yield levels of 2.17 and 2.64 kips, respectively, and the group with the highest level of yield forces is group 2b, institutional full connection wall configurations. Close to normal distribution of this wall type is observed in the histogram plotted in the following figure. Mean yield force for this group is 5.53 kips.

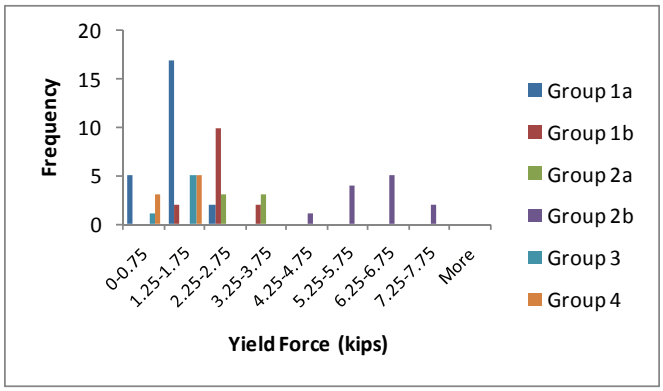

Figure 5.29 – Grouping Histogram of Yield Force Parameter (*Fy*)

5.4.3 Post-Yield Stiffness Factor Parameter for Wall Groups

In section 5.2.3 the assertion is made that this factor is not based on the individual wall configurations, but is based on the inherent properties of cold-formed steel-framed gypsum partition walls. Figure 5.30 shows the distribution of this factor for the individual wall groups over the ranges provided. For groups 1a, 1b, 2a, 2b, and 4 the frequencies peak in the range of 0.33-0.46 for this parameter. Group 3 has an identical mode in the ranges of 0.46-0.59 and 0.59-0.72. The group which considers all of the partial height walls have a high distribution, with walls having a post-yield stiffness factor in both of the lower two ranges. One post-yield stiffness factor will be considered for all the wall specimens regardless of wall configuration. This value is the mean of the total test specimens calculated, and is $r = 0.37$ with a standard deviation of 0.23, see Table 5-2. This value will be used in conjunction with the other determined parameters at the end of this section to understand model effectiveness.

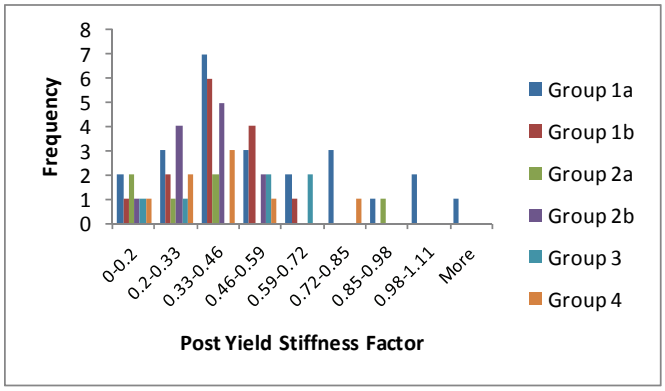

Figure 5.30 – Grouping Histogram of Post-yield Stiffness Parameter (*r*)

5.4.4 Post Capping Stiffness Parameter for Wall Groups

There is a high distribution for the post capping stiffness parameter, as shown in Figure 5.31. While the distribution is high, the highest occurrence is in the range of -0.06 to -0.18 with substantial occurrences also in the range of 0.0 to -0.06 and -0.18 to -0.30. The mean post capping stiffness factor is -0.24 which is outside of the range with highest probability of occurrence, therefore, the median value of -0.18 is chosen to use for P_{Tri}.

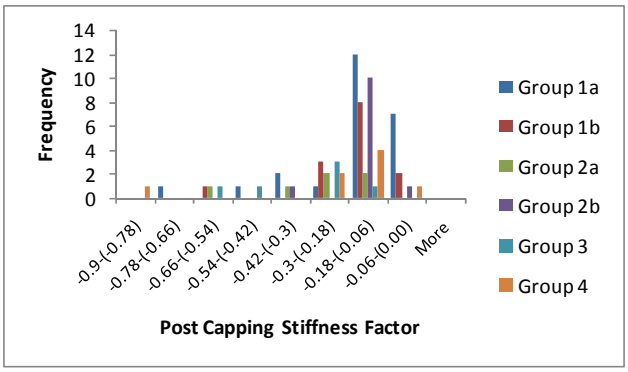

Figure 5.31 – Grouping Histogram of Post Capping Stiffness Parameter (P_{Tri})

5.4.5 Unloading Stiffness Parameter for Wall Groups

Figure 5.32 shows that the unloading stiffness has the highest frequency of occurrence in the range of 1.0 to 1.4. Although the highest frequency was observed in this range, the mean value for this parameter is 0.97, and has a median of 0.91. As mentioned previously the imposed limitation by RUAUMOKO is, $P_{UNL} > 1$. Therefore this factor is rounded and set equal to 1.0 in order to more closely simulate the mean behavior of all the models. Not only will this value be close to the mean, it also is in the range of highest occurrence.

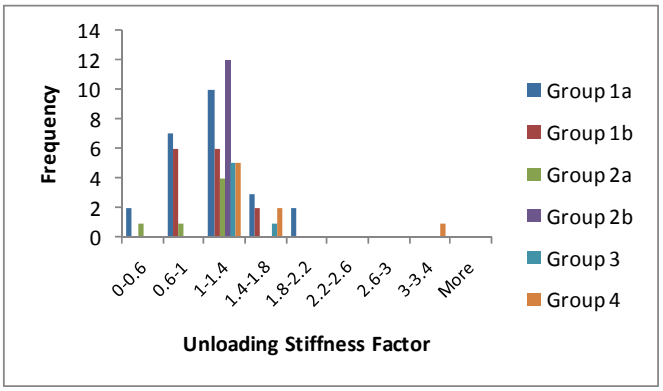

Figure 5.32 – Grouping Histogram of Unloading Stiffness Parameter (P_{UNL})

5.4.6 Ultimate Force Parameter for Wall Groups

The histogram presented in Figure 5.33 shows the ranges and frequencies of capping forces observed in all 35 walls. As mentioned previously, the commercial slip track, partial height, and improved detail wall configurations had similar levels of observed forces. Groups 1b and 2a also had the same level of capping forces. Lastly, the institutional full connection had the highest capping forces of all the specimens tested.

To simplify modeling of the partition walls, the ratio of yield force to capping force can be used to calculate either F_y or F_u. The histogram presented in Figure 5.34 shows that the peak occurrence for individual groups occurs over four different ranges. In this figure a histogram for all specimens is considered and a close to normal distribution is observed. Also, both the median and mean values are within one one-hundreth of each other. Therefore, the factor of $F_y/F_u = 0.7$ (mean value) is recommended for use at this point, this factor has a standard deviation of 0.13. This factor will be verified at the end of this section, when comparison plots will be made between the recorded data and the simulated mechanical behavior.

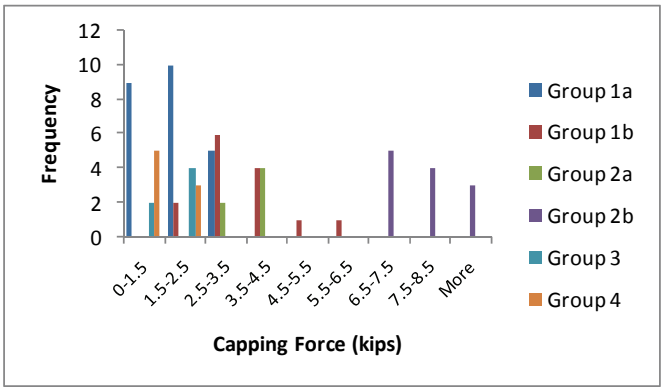

Figure 5.33 – Grouping Histogram of Capping Force Parameter (F_u)

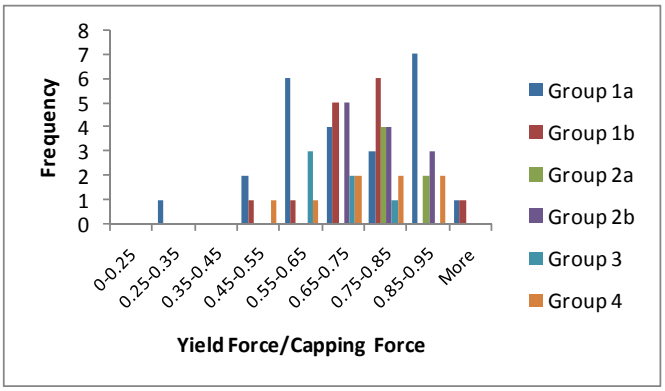

Figure 5.34 – Grouping Histogram of Ratio of Yield Force to Capping Force (F_y/F_u)

5.4.7 Intercept Force Parameter for Wall Groups

As the drift levels return to zero, some level of forces are observed in the system. This force is the intercept force and values for the 35 different walls are presented in Figure 5.35. The first observation of this histogram is that the majority of forces are well under 1 kip, which at first seems like they could be considered negligible, but upon reviewing the yield forces this assumption is incorrect. Because even with small values for this parameter, for the weaker type systems, the energy could begin to diverge from the recorded data at very low drift levels. The second observation of the histogram is the distribution is very wide with the mean being 0.09 and a standard deviation of 0.08, and the different wall groups have peaks in different ranges. For simplification in parameterizing the hysteretic model, the mean value of 0.09 will be used to compare simulations.

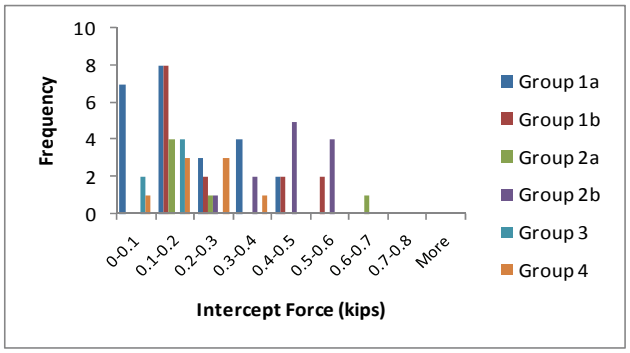

Figure 5.35 – Grouping Histogram of Intercept Force Parameter (F_i)

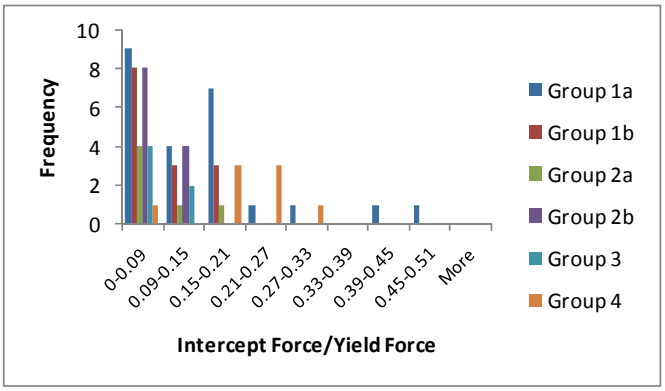

Figure 5.36 – Grouping Histogram of Ratio of Intercept Force to Yield Force (F_i/F_y)

5.4.8 Softening and Reloading Factor Parameters for Wall Groups

As was mentioned previously, the parameters α and β were determined through a least square regression on the observed energy at the peak displacement for each excursion. The two parameters are extracted when the regression is minimized. Figure 5.37 and Figure 5.38 shows histograms plotting the reloading and softening factors. In Figure 5.37 it is observed that there is a wide distribution of the results and that the error in fitting the dissipated energy has the highest frequency when α=0.9 and β=1.03. Also by this figure it appears that the variance of frequency is more affected by a change in α than a change in β. Figure 5.38 is given to better understand this phenomenon. In this figure, groupings for similar β but varying α values are given. This plot better illustrates the frequency of occurrence for the individual parameters. As previously stated, the highest frequencies occur for α=0.9 and β=1.03, but this frequency only accounts for 21% of the total loops analyzed. Upon further analysis of these parameters it was found

that the energy difference was minimized when β=1.03 for almost 50% of the analyses. And when α=0.9 minimization occurred in over a third of the total analyses. For simplification of required parameters a mean value of 1.07 is recommended for β, and the mean of 0.64 for the reloading factor α. These values will be used in the following section for the comparison of the numerical simulations versus the recorded data.

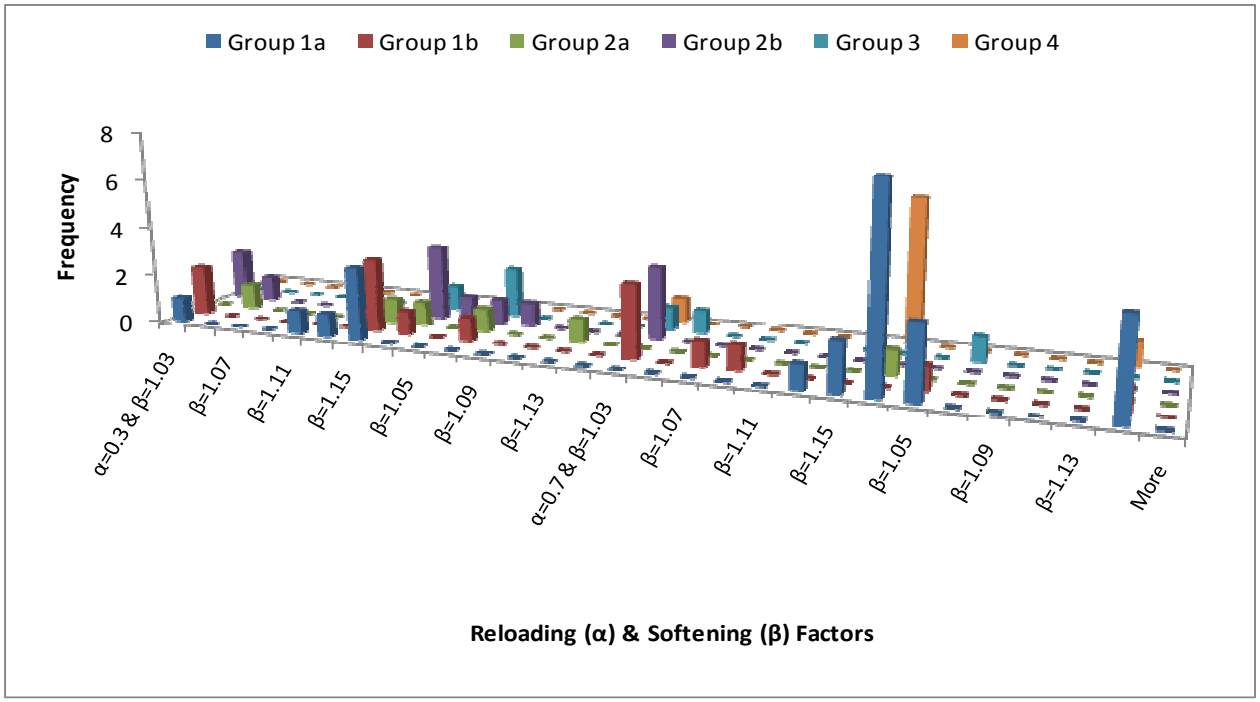

Figure 5.37 – Grouping Histogram of Softening Factor (β) and Reloading or Pinching Factor (α)

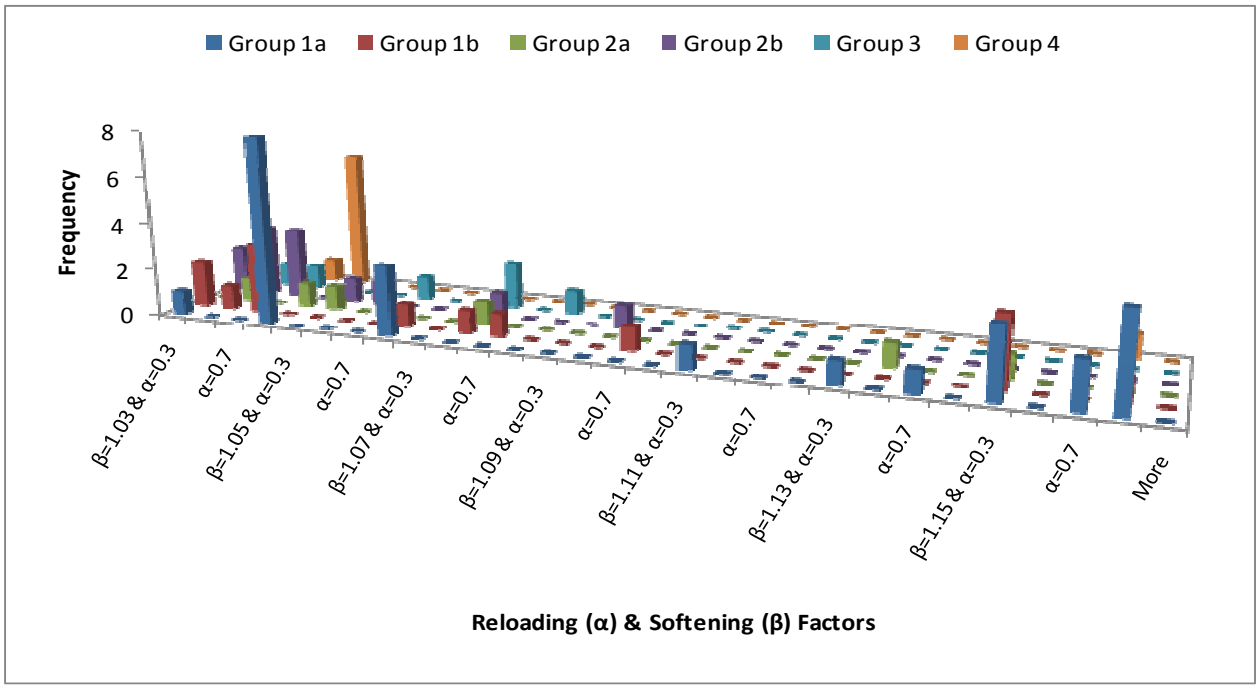

Figure 5.38 – Grouping Histogram of Reloading or Pinching Factor (α) and Softening Factor (β)

5.4.9 Comparison of Mean Parameters

To better understand the relationship of the stiffness and force parameters, the following figures, Figure 5.39 and Figure 5.40 provide the mean initial, post-yield, post capping, and unloading stiffness for each of the wall groups. Through this analysis the fully connected institutional construction group had the highest initial stiffness while the improved detail and partial height walls had the lowest initial stiffness. In Figure 5.40 the same trends observed in Figure 5.39 exist for mean strength capacities. The Groups 3 and 4 had the lowest strength capacities, followed by the commercial slip track, commercial full connection and institutional slip track. The group with the highest capacity was group 2b, corresponding to institutional full connection. The strength ratios were examined and found to have similar characteristics independent of the configurations. This can also be observed in Figure 5.40, where the groups have similar changes in the strength capacities.

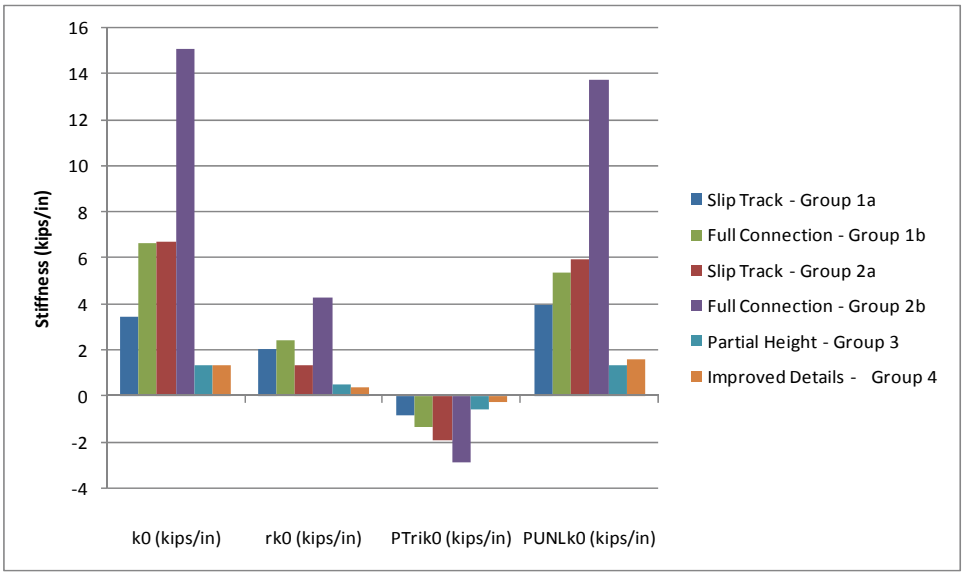

Figure 5.39 – Wall Grouping Mean Stiffness Parameters

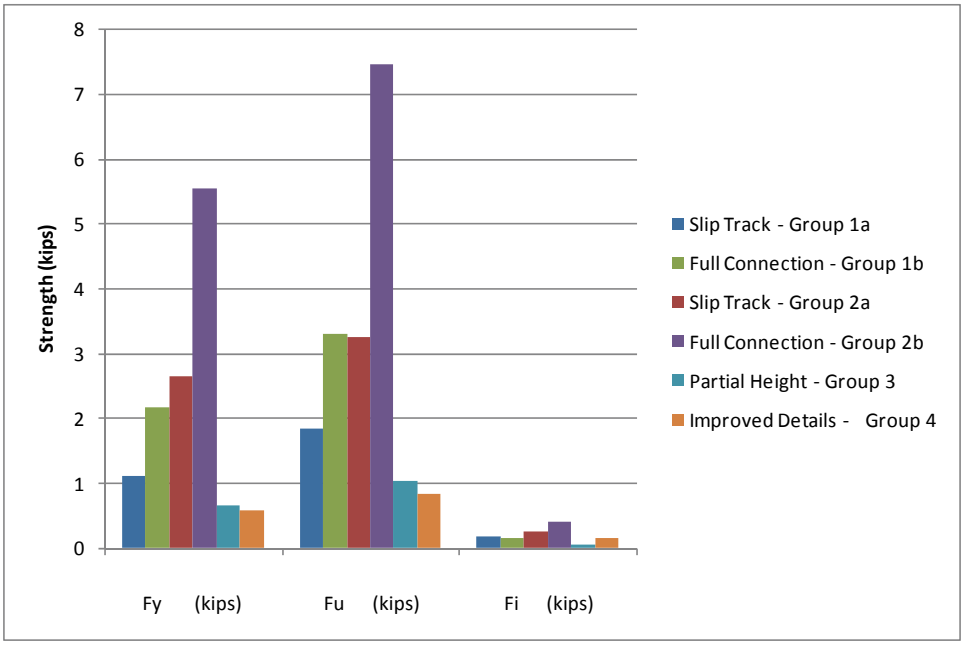

Figure 5.40 – Wall Grouping Mean Strength Parameters

In Table 5-2 the mean parameters for each group are given along with the standard deviations and parameter per unit length of wall. Through the analyses on the 35 specimen, it was observed that the response of the fully connected institutional partition walls were most consistent. This consistency is shown by examining the standard deviations for the individual groups. Group 2b had only a maximum of 5% variance for the initial stiffness parameter and 14% variance for the yield force parameter. The

variance from the mean increased for other parameters. The fully connected institutional walls in general had the lowest distribution. In terms of consistency the partial height wall group was the next most consistent; followed by the institutional slip track; then the commercial slip track; the commercial full connection and improved detail wall groups had the greatest variance.

Table 5-2 Wall Grouping Mean Parameters and Standard Deviations

Group Description	k_0 (kips/in)	r	rk_0 (kips/in)	P_{Tri}	$P_{Tri}k_0$ (kips/in)	P_{UNL}	$P_{UNL}k_0$ (kips/in)	F_y (kips)	F_u (kips)	F_i (kips)	β	α	F_y/F_u	F_i/F_y
	Mean Parameters													
All Configurations - Group 0	5.67	0.37	2.57	-0.24	-1.62	0.97	6.70	2.00	2.81	0.20	1.07	0.64	0.70	0.09
Slip Track - Group 1a	2.63	0.48	1.30	-0.21	-0.54	0.93	2.65	0.84	1.33	0.14	1.09	0.73	0.67	0.17
Full Connection - Group 1b	7.23	0.33	2.43	-0.26	-1.86	0.79	5.39	2.38	3.21	0.18	1.07	0.51	0.75	0.07
Slip Track - Group 2a	5.46	0.29	1.59	-0.19	-1.01	1.04	5.63	1.94	2.98	0.28	1.08	0.60	0.66	0.14
Full Connection - Group 2b	15.06	0.28	4.29	-0.19	-2.87	0.91	13.68	5.53	7.44	0.40	1.04	0.50	0.74	0.07
Partial Height - Group 3	1.37	0.38	0.50	-0.39	-0.55	1.00	1.36	0.65	1.02	0.06	1.05	0.63	0.64	0.09
Improved Details - Group 4	1.35	0.32	0.43	-0.27	-0.25	1.38	1.61	0.58	0.84	0.14	1.05	0.88	0.68	0.24
	Standard Deviations													
All Configurations - Group 0	4.94	0.23	1.52	0.17	1.16	0.39	2.70	1.82	2.41	0.16	0.05	0.24	0.13	0.08
Slip Track - Group 1a	1.29	0.28	1.01	0.17	0.45	0.40	2.45	0.46	0.70	0.13	0.06	0.26	0.18	0.15
Full Connection - Group 1b	2.14	0.22	2.14	0.18	1.31	0.27	1.41	0.69	1.11	0.15	0.05	0.23	0.10	0.05
Slip Track - Group 2a	0.82	0.07	0.41	0.07	0.32	0.15	0.56	0.33	0.40	0.15	0.05	0.21	0.10	0.06
Full Connection - Group 2b	0.74	0.12	1.77	0.07	1.06	0.07	0.84	0.76	0.91	0.09	0.02	0.15	0.06	0.02
Partial Height - Group 3	0.21	0.20	0.22	0.20	0.30	0.12	0.19	0.15	0.22	0.04	0.02	0.16	0.06	0.06
Improved Details - Group 4	0.72	0.19	0.28	0.26	0.11	0.74	0.84	0.34	0.47	0.08	0.04	0.07	0.11	0.11
	Parameters per Linear Foot for 11'-5" Wall Height													
All Configurations - Group 0	0.473		0.214		-0.135		0.558	0.167	0.234	0.017				
Slip Track - Group 1a	0.219		0.108		-0.045		0.221	0.070	0.111	0.012				
Full Connection - Group 1b	0.603		0.203		-0.155		0.449	0.198	0.267	0.015				
Slip Track - Group 2a	0.455	N/A	0.132	N/A	-0.084	N/A	0.469	0.162	0.248	0.023	N/A			
Full Connection - Group 2b	1.255		0.358		-0.239		1.140	0.461	0.620	0.033				
Partial Height - Group 3	0.114		0.041		-0.046		0.113	0.054	0.085	0.005				
Improved Details - Group 4	0.113		0.035		-0.021		0.134	0.048	0.070	0.012				

5.5 Mean Parameters vs. Test Data Comparison

In this section two hysteretic models for each wall group are compared to the recorded force-displacement test data. The first group uses the nine specific parameters obtained for each partition wall group obtained in Section 5.4 and summarized in Table 5-2. The second model uses a set of ratios obtained by statistical analysis on each of the individual wall group parameters. The purpose of these comparisons is to determine the quality of the two hysteretic fitting methods. For the simplified recommended values, recall that of the nine required parameters, only two are required for the individual wall groups, and are:

- Initial Stiffness (k_0)

- Yield Force (F_y)

Mean values for these two parameters can be found in Table 5-2 and are given based on wall group. The remaining seven parameters, are either calculated based on these two parameters or have been assigned a set value through the analyses explained previously, and are:

- Post-Yield Stiffness Ratio (r = 0.37)
- Post-Capping Stiffness Ratio (P_{Tri} = -0.24)
- Capping Force ($F_u = F_y/0.70$)
- Intercept Force($F_i = F_y$ * 0.09)
- Unloading Stiffness (P_{UNL} =1.00)
- Softening Factor (β = 1.07)
- Reloading or Pinching Factor (α = 0.64)

In the following plots one or two wall specimen from each wall group is examined to help determine whether the recommended values are sufficient. The comparison plots for each specimen is included in Appendix D.

5.5.1 Comparisons for Commercial Slip Track (Group 1a)

This group is one of the largest, with 12 specimens considered to have similar detailing or response. Therefore two specimens are examined for this wall grouping. Specimen 13 was tested under the dynamic protocol and specimen 31 was subjected to the quasi-static protocol. Figure 5.41 and Figure 5.42 are plots for specimen 13. For the specimen subjected to the dynamic protocol drifts less than 0.20% are filtered out, as well as the data obtained after the maximum excursion was reached. A difference is observed in the hysteretic behavior of both the data considering recommended and mean group parameters. In the positive drift, the strength levels are overestimated; but in the negative drift, strength levels are closely simulated. In the negative drift levels, a closer correlation to the recorded data is observed. This difference between stiffness and forces is further supported upon examination of the dissipated energy. Both models closely match the energy dissipation of the specimen. In Figure 5.41 a problem with simulating the Wayne Stewart hysteretic model in RUAUMOKO is observed. At large displacements

when the strength capacity should be approximately zero, the model continues on the same post capping slope across the zero force level. This phenomenon will create unreal forces in the system and had to be resolved, the method for doing so is explained in the following chapter.

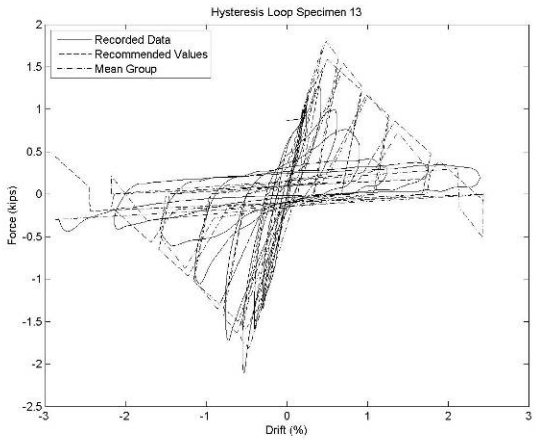

Figure 5.41 – Specimen 13 Hysteretic Behavior

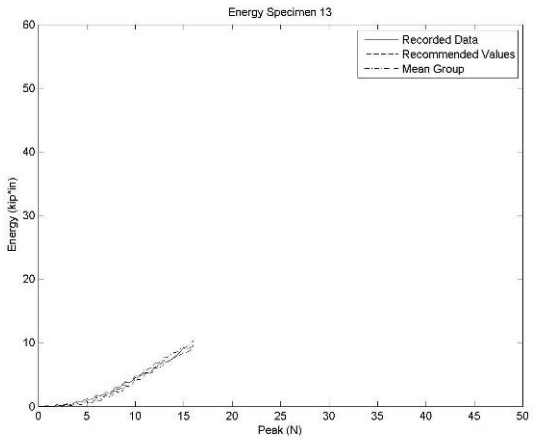

Figure 5.42 - Specimen 13 Dissipated Energy

Figure 5.43 and Figure 5.44 are a comparison of the data for specimen 31. Similar observations are made for the recommended and mean group parameter models stiffnesses and forces. Again to determine how well the models correlate, an evaluation of the dissipated energy for each model is required. The plot of dissipated energy shows that the group parameters model better simulates the dissipated energy of the recorded data for specimen 31. It is noted however that energy level differences between models are very small for the first 20 peaks. Also, when the system is in the elastic range, and only when the system becomes highly inelastic is dispersion observed. The difference between the numerical models and the recorded data for this group is better understood when an evaluation of the standard deviations for the individual parameters is considered. This group overall had one of the highest deviation levels for stiffness and forces. This distribution can be attributed to the difference in detail configurations and testing protocols. Although there were differences, the groups integrity was maintained based on the levels of forces observed, the maximum capping force was 2.86 kips in any one specimen. With this low level of capping force, the dissipated energy levels are also smaller, most having a total dissipated energy of 10 kip-inches. For a comparison of all the specimens considered in this group see Appendix D.

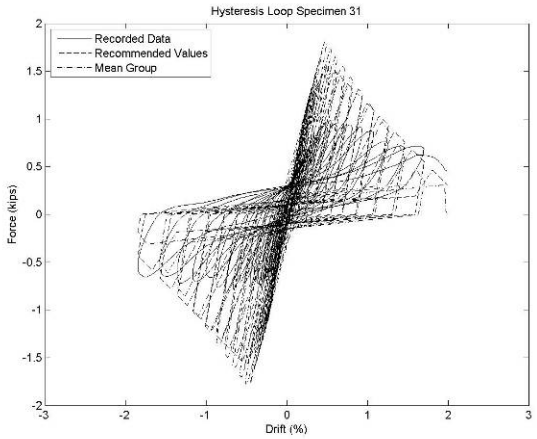

Figure 5.43 – Specimen 31 Hysteretic Behavior

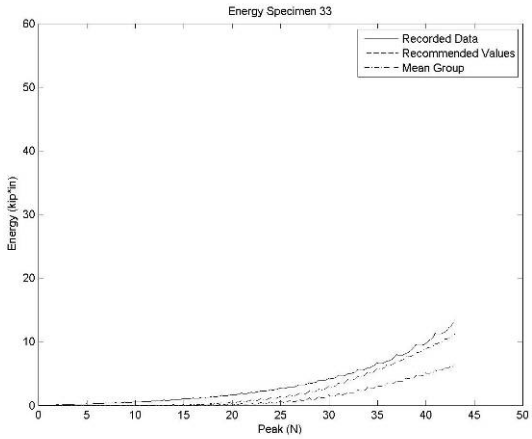

Figure 5.44 - Specimen 31 Dissipated Energy

5.5.2 Comparisons for Commercial Full Connection (Group 1b)

This group of wall specimens considers data for 7 of the total 35 walls considered in the analysis. Figure 5.45 and Figure 5.46 are the comparison plots for specimen 22 (see Chapter 3 for configuration). In both figures it is observed that for both models (mean group and recommended parameters) a good fit is obtained. While both models have a resemblance to the recorded data, the recommended values models dissipated energy levels approaches the dissipated energy for the recorded data at higher drift levels.

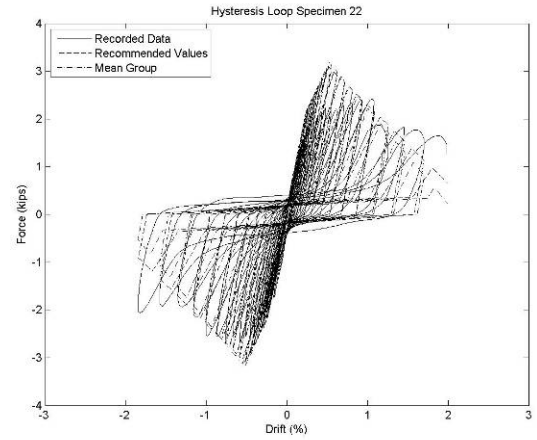

Figure 5.45 – Specimen 22 Hysteretic Behavior

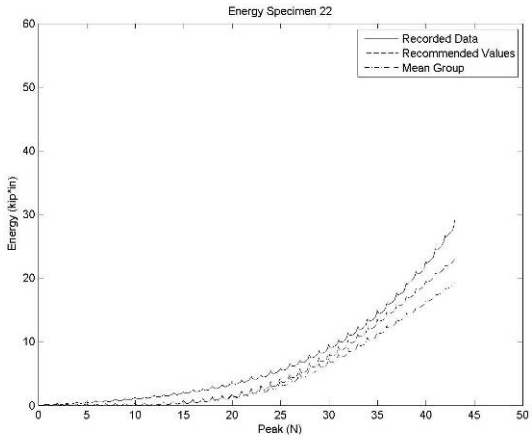

Figure 5.46 - Specimen 22 Dissipated Energy

5.5.3 Comparisons for Institutional Slip Track (Group 2a)

Only three specimens comprise the institutional slip track partition wall group. For comparison, the plots for specimen 7 are given in Figure 5.47 and Figure 5.48. Initial observation of the hysteretic behavior shows evidence of wall racking occurring in the positive drift levels. While this effect is observed in the positive drift levels, in the negative drift the mean group parameter model closely simulates the observed forces in the specimen. For the recommended value numerical model, there are few similarities observed in the hysteresis loops. The dissipated energy plot however has an interesting characteristic: as the system goes inelastic, the energy of the numerical model approaches the recorded data. Through these observations it is evident that at lower drift levels, the numerical models dissipate much lower amounts of energy than the actual specimen, but as the drift amplitudes increase, the numerical model can dissipate higher levels of energy.

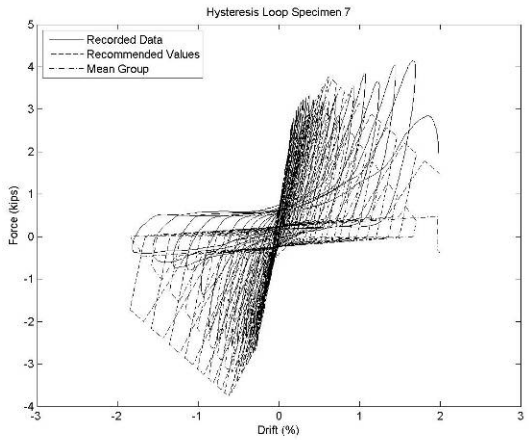

Figure 5.47 – Specimen 7 Hysteretic Behavior

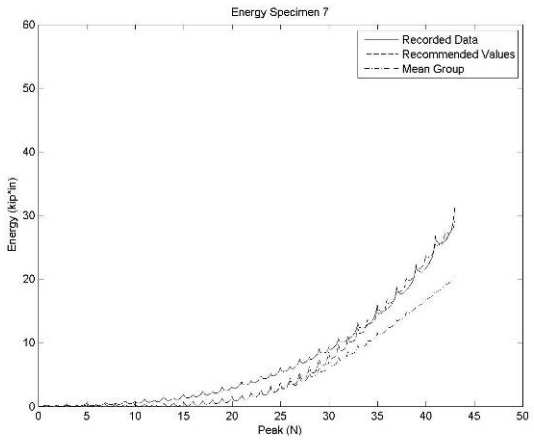

Figure 5.48 - Specimen 7 Dissipated Energy

5.5.4 Comparisons for Institutional Full Connection (Group 2b)

This group of walls considers six of the total 35 (configurations 23-28) specimens. In the following figures specimen 23 and 27 are examined. Plots of the other specimens are included in Appendix D. While only two of the six specimens are examined here, it should be understood that the results found here represent well the other four specimens because this group had on average the lowest standard deviations. In Figure 5.49 and Figure 5.50 comparison plots for specimen 23 are demonstrated. The hysteretic behavior of both models compares well with the recorded data with the largest variances occurring in the mean group parameters model. An observation in the dissipated energy plot is the

resemblance of both numerical models to the specimen results at drift levels in the elastic range. In the previous models, this resemblance only occurs in specimen 13. As the energy levels begin to diverge, the mean group parameter model continues to most closely resemble the recorded data, while the dissipated energy for the recommended values model gives an overestimate (conservative) for dissipated energy. Figure 5.51 and Figure 5.52 are comparison plots for specimen 27 and are given as support of the assertion that one average group 2b had the lowest standard deviations. The same observations made for specimen 23 can be made for specimen 27 (i.e., close resemblance in hysteretic behavior, dissipated energy at inelastic drift levels, and mean group parameter model dissipated energy at increased drift amplitudes).

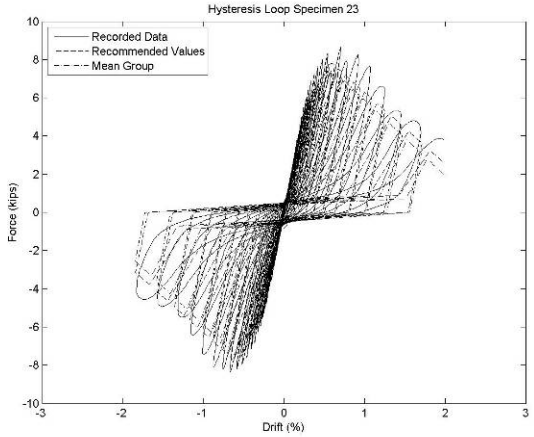

Figure 5.49 – Specimen 23 Hysteretic Behavior

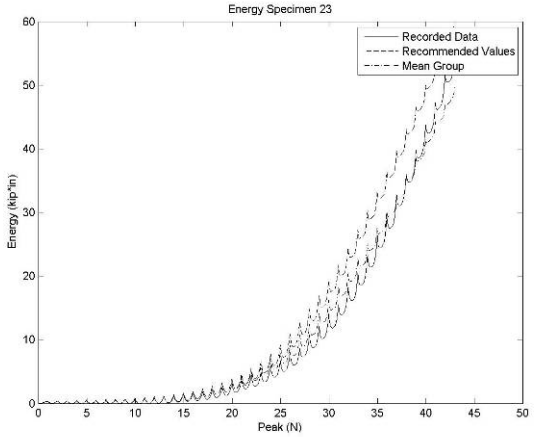

Figure 5.50 - Specimen 23 Dissipated Energy

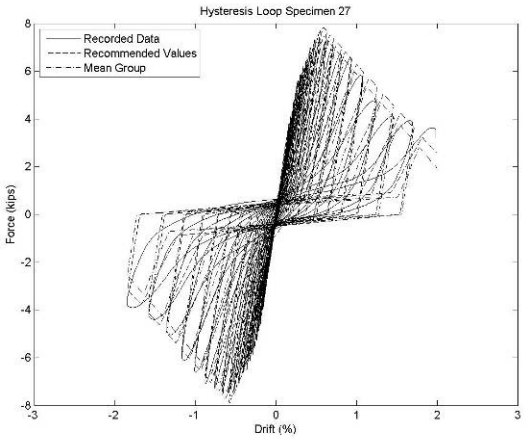

Figure 5.51 – Specimen 27 Hysteretic Behavior

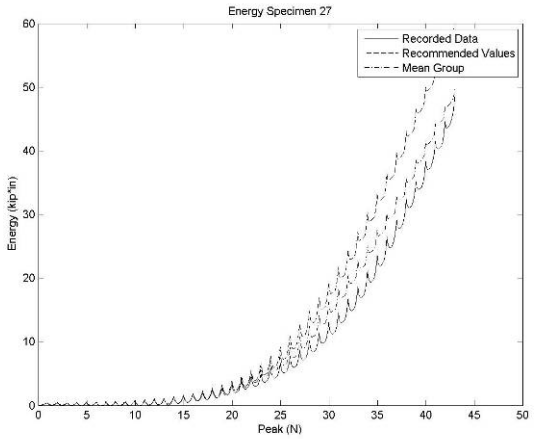

Figure 5.52 - Specimen 27 Dissipated Energy

5.5.5 Comparisons for Partial Height (Group 3)

Group three considers only three of the total 35 specimen considered in the analysis, specimens 17-19. For comparison the data for the two models is plotted along with the recorded specimen data. The greatest variance between the models and specimen is the positive intercept force, other variances in capping strength and post capping stiffness are also observed. The variances between the models and the recorded data appear to be almost negligible when evaluating the dissipated energy for the models. The energy for the two numerical models are virtually identical into the 35th excursion, at which level they diverge through a few peaks until they again converge upon levels nearly equal. Although the two models closely match the recorded data, it is apparent that they are an underestimate of the levels of dissipated energy that would be observed in specimen.

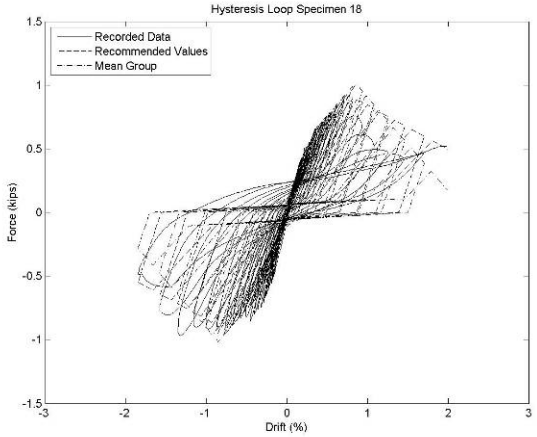

Figure 5.53 – Specimen 18 Hysteretic Behavior

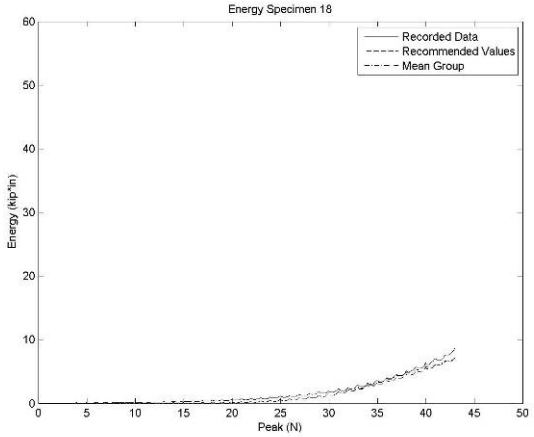

Figure 5.54 - Specimen 18 Dissipated Energy

5.5.6 Comparisons for Improved Details (Group 4)

Figure 5.55 and Figure 5.56 are comparison plots for specimen 33, one of the four specimens considered in this group. The hysteretic behaviors for the numerical models appear to have little correlation to the recorded data. This claim is substantiated as an evaluation of the dissipated energy is made. At drift levels in the elastic range, first 20 – 25 peaks, the numerical models dramatically underestimate dissipated energy. Only after the system goes inelastic does the dissipated energy level for the model considering the mean group parameters begin to simulate the energy levels dissipated by the specimen. The model considering the recommended values has little correlation to the recorded data.

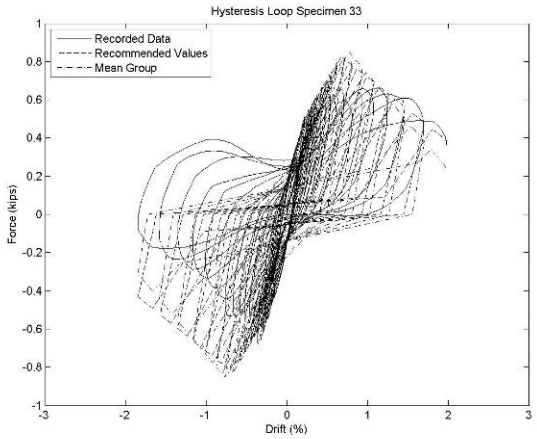

Figure 5.55 – Specimen 33 Hysteretic Behavior

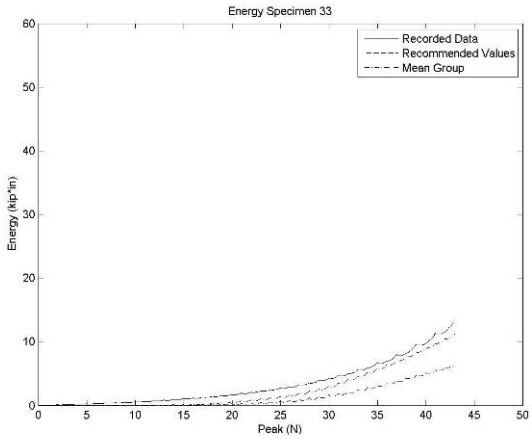

Figure 5.56 - Specimen 33 Dissipated Energy

5.6 Conclusion

The recorded force-displacement data from 35 cold-formed steel-framed gypsum partition walls was analyzed. The data was found to have mechanical behavior that can be described as having a tri-linear backbone, pinching effects, and stiffness and strength degradation. It was determined to fit the data to the Wayne Stewart hysteretic model available in the non-linear dynamic analysis program RUAUMOKO. A total of nine parameters are required for the Wayne Stewart model. Each parameter was obtained from the recorded data through least square regressions, filters, and trial and error.

Two groups of parameters were determined through the analysis. One set of parameters is based on the mean values for the individual groups defined for development of the seismic fragility database in chapter 4. The second set requires only the mean initial stiffness and the capping strength for the individual group. With these parameters determined, the remaining seven parameters required for the Wayne Stewart model can be assigned based on ratios and statistical observations.

A numerical model with a spring element assigned the hysteretic behavior of the Wayne Stewart model was developed in RUAUMOKO to test the two groups of parameters. The hysteretic behavior and dissipated energy for the numerical models are plotted versus the recorded data for select specimens in each wall group. Comparing the results indicates that modeling a cold-formed steel-framed gypsum partition wall using a tri-linear hysteretic model with pinching and strength and stiffness degradation, can simulate well the mechanical behavior and dissipated energy of the nonstructural partition wall system.

Chapter 6

EFFECT OF NONSTRUCTURAL PARTITION WALLS ON THE SEISMIC RESPONSE OF A MEDICAL FACILITY BUILDING MODEL

Current structural design codes for steel moment-resisting frames and other structural systems do not include the nonstructural partition wall systems as part of the lateral force-resisting system. This chapter provides some insights as to whether this method of design should be reevaluated. While the lateral stiffness and strength of an individual steel stud gypsum partition wall is small in relation to a steel moment-resisting frame, if there are many such walls in a building structure, collectively the walls will increase the lateral stiffness and strength of the structure. This combined effect contributes to the dynamic properties of the structure and its seismic response. In this chapter, each of the nonstructural partition wall groups described in Chapters 3, 4 and 5 are incorporated into an existing numerical model of a four story steel moment frame medical facility building and subjected to three random historical earthquakes. The effect of several types of steel stud gypsum partition walls on the seismic response are analyzed and compared to each other and the response of the original structure (structure not considering the nonstructural partition walls).

The analysis considered in this chapter considers an existing building model developed at the University at Buffalo (UB) for MCEER, formerly the Multidisciplinary Center for Earthquake Engineering Research. The building model considered was developed for the nonlinear dynamic analysis software platform RUAUMOKO. Nonlinear shear spring elements with hysteretic behavior according to the Wayne Stewart hysteresis model were added to the building model at each floor level. The properties of the springs are based on the average values determined in the previous chapter for the different wall groupings. The actual parameters used for the spring model are then scaled according to the length and height of the partition walls as defined in the original building plans.

6.1 MCEER WC70 Building Model

6.1.1 Background

Studies conducted for MCEER at the University at Buffalo, State University of New York (UB) developed a nonlinear building model. Yuan et al. (2002) developed a model for a four story steel moment frame medical facility for SAP2000; further analysis conducted by Wanitkorkul et al. (2005) developed a nonlinear building model for RUAUMOKO. This building model known as WC70 was based on a hospital building designed and constructed in the early 1970's. The building was designed to meet the seismic requirements of the 1970 Uniform Building Code (UBC). In the N-S direction there are three bays, the two exterior bays are 16'-0" in length and the middle bay is 24'-6" with a total length of 56'-6". In the E-W direction there are ten bays with varying lengths, although symmetric about the center of the building, with a total dimension of 275'-0", as shown in Figure 6.1. The lateral force resistance of the structure in the N-S direction is obtained through four moment-resisting steel frames located symmetrically in the building. Two moment frames at each end of the structure with two frames located near the center, frames at lines B, N, F and J in Figure 6.1. Lateral resistance in the E-W direction of the structure is also obtained through steel moment-resisting frames.

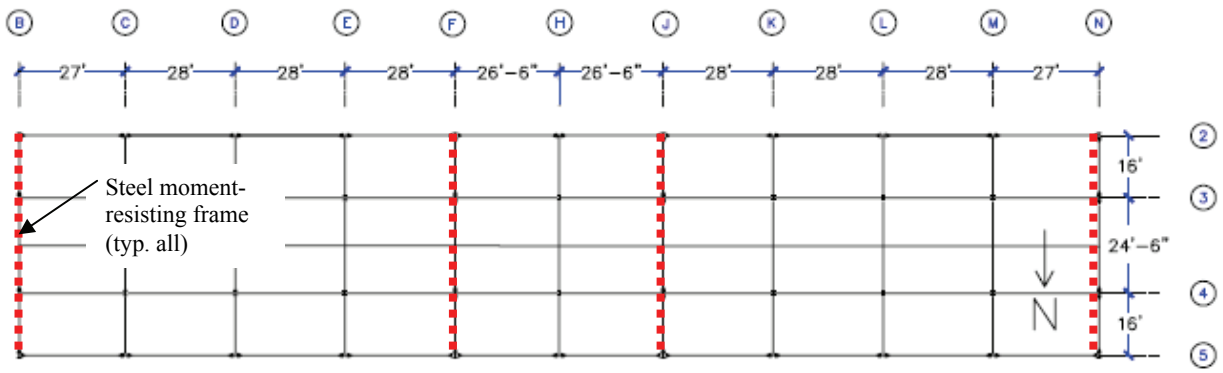

Figure 6.1 – Second Floor Plan of WC70 Building Model taken from Yuan et al (2002)

The dynamic properties and response of the building will only be considered in the N-S direction (strong axis of columns). To simplify the modeling and analysis of the hospital building a 2-D model was developed by Wanitkorkul & Filiatrault (2005), as shown in Figure 6.2. The model consists of two three-bay frames, which represent one half of the building, and a set of four gravity load columns. Properties assigned to the columns and beams of the steel moment frame are based on individual member section properties, frame member designations are given in Table 6-1. The gravity load columns are modeled as

spring elements with a high axial stiffness and are pin connected at each end to account for P-Δ effects. All the frame members in the considered building model are assigned bi-linear properties and the springs (gravity columns) remain elastic. Inter-story heights are 13 feet 6 inches for the first floor level and 12 feet 6 inches for the three upper levels. Horizontal diaphragms are considered at each level to make compatible the lateral displacements of earthquake and gravity load resisting frames.

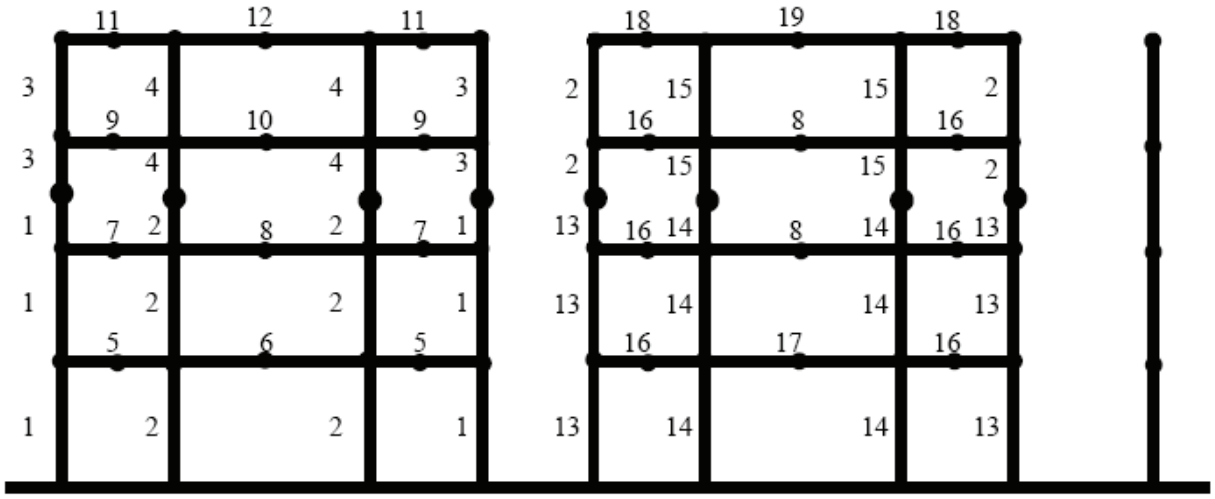

Figure 6.2 – North South Steel Moment Frame Elevation and Element Numbers (see Table 6-1) taken from Wanitkorkul et al. (2005)

Table 6-1 Moment-resisting Frame Member Designations taken from Wanitkorkul et al. (2005)

Section No.	Designation	Section No.	Designation
1	W 14x193	11	W 24x68
2	W 14x342	12	W 24x104
3	W 14x159	13	W 14x398
4	W 14x257	14	W 14x455
5	W 24x146	15	W 14x370
6	W 33x221	16	W 24x162
7	W 24x131	17	W 33x241
8	W 30x211	18	W 24x94
9	W 24x103	19	W 30x173
10	W 30x211		

Loads acting on the structure are Dead Loads (D), Live Loads (L), and Earthquake Loads (E). The applied loads were determined based on the materials used in construction and from code analysis. The seismic weight at each floor is a sum of the dead load and 65% of the live load at the considered floor elevation and is given in Table 6-2 (Wanitkorkul et al. 2005).

Table 6-2 Individual Floor Level Seismic Weights

	Seismic Weights (kN)		
Floor	**Exterior MRF**	**Interior MRF**	**Gravity Column**
Roof	546	1012	3415
4	622	1083	3562
3	635	1095	3562
2	659	1128	3562

6.1.2 Building Model Modifications

The structural elements in the RUAUMOKO building model were originally assigned a bilinear mechanical behavior with no strength degradation considered. With this material behavior, forces will continue to increase with increased lateral displacements during a pushover analysis (i.e., no ultimate force will be achieved). Figure 6.3 shows a plot of the drift ratio $\Delta_R/h_{Building}$, where Δ_R is roof displacement and $h_{Building}$ is the total height of the building, versus the ratio of total base shear V_B to seismic weight W. Load is applied according to the lateral load distribution of ASCE 7-05 Section 12.8.3, where w is the seismic weight at each floor level defined in Table 6-2. In this pushover curve no strength degradation occurs after the building system has yielded. This demonstrates the limitation of the current building model to simulate the decrease of lateral load resistance at increasing drift ratios.

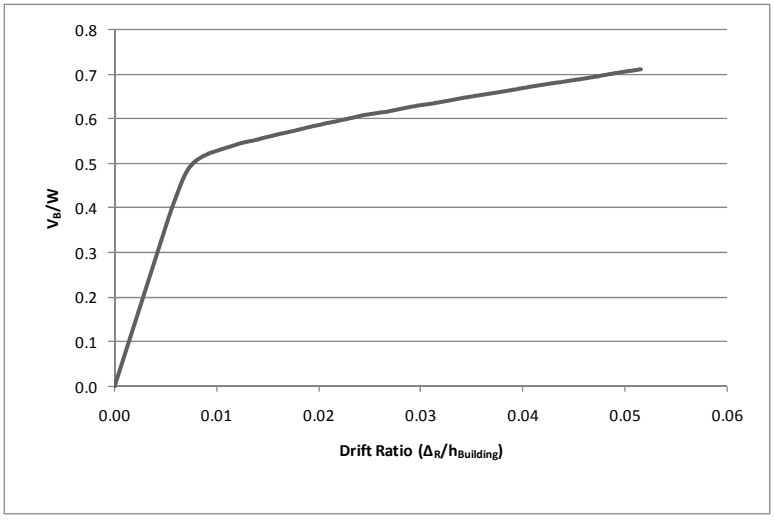

Figure 6.3 – WC70 Pushover Curve

The method proposed to simulate local failure mechanisms within the structure is from research obtained after the 1994 Northridge earthquake, when a common failure mode in steel moment-resisting frames was observed Wanitkorkul et al. (2005) after Bonowitz et al. (1995). A statistical review of 53 full scale bolted web-welded beam-columns joints was conducted by Filiatrault et al. (2001) in order to quantify their strength degradation. In this review, onset of strength degradation occurred at a mean plastic rotation of 0.0103 radians and was determined to be related to the weld fracture and beam depth, with a standard deviation of 0.0077 rad. A plot of the strength degradation versus the curvature ductility is given in Figure 6.4.

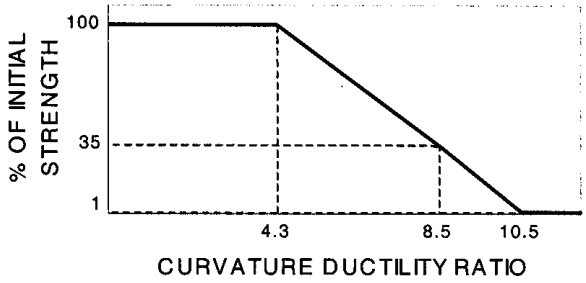

Figure 6.4 – Flexural Strength Degradation Model taken from Filiatrault et al. (2001)

The curvature ductility (μ_c) is then related to the plastic rotation through the following calculations:

$$\mu_c = \frac{\varphi_{ult}}{\varphi_y} \qquad \textbf{6-1}$$

where φ_y and φ_{ult} are respectively the yield and ultimate curvature ductility's and given by:

$$\varphi_y = \frac{M_y}{EI} \qquad \textbf{6-2}$$

and

$$\varphi_{ult} = \varphi_y + \varphi_p \qquad \textbf{6-3}$$

where M_y is the yield moment of the member, EI are section properties, and φ_p is related to the plastic rotation (θ_p) by:

$$\varphi_p = \frac{\theta_p}{L_p} \qquad \textbf{6-4}$$

where φ_p is plastic curvature ductility, and L_p is the plastic hinge length given by:

$$L_p = 0.9 * d_{member} \qquad \textbf{6-5}$$

where d_{member} is the depth of the frame member.

Strength degradation was added to each end of the beam and column members in the building model based on plastic rotations, but are applied in RUAUMOKO through the curvature ductility. Prior to the 1994 Northridge earthquake it was believed that steel moment connections were capable of developing large plastic rotations of 0.02 radians or larger (FEMA 350, 2000). The building models in this research use the observations by Filiatrault et al. and FEMA 350 to develop models with failures (strength degradation) at curvatures associated to plastic rotations of 0.01, 0.02 and 0.03 radians through Equations 6-1 thru 6-5. RUAUMOKO simulates strength degradation based on ductility of the member and/or the number of cycles. Table 6-3 gives the ductility ratio at which strength degradation begins and the ductility at which the member loses its ability to withstand forces or becomes perfectly plastic (i.e., stiffness equal to zero). The plot Figure 6.5 is a visual representation Table 6-3 where curvature ductility is on the x-axis and percent of Initial Strength is on the y-axis. While the numerical model uses curvature ductility to define strength degradation, further discussions will use the plastic rotations to differentiate between the unique building models.

Table 6-3 Strength Degradation Parameters Assigned to Beam and Column Ends

Plastic Rotation (rad)	Curvature Ductility	
	100% Initial Strength (ϕ_y)	0% Initial Strength (ϕ_P)
0.01	4.22	10.68
0.02	7.44	13.91
0.03	10.67	17.13

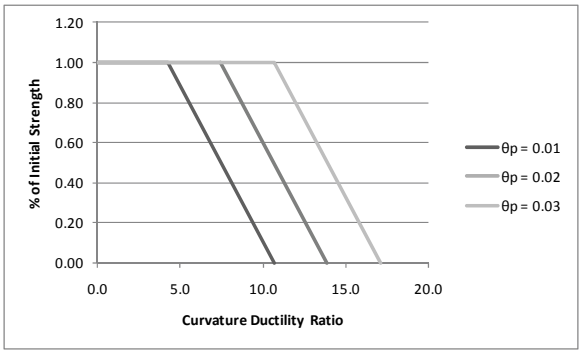

Figure 6.5 – Plot of Strength Degradation for Maximum Plastic Rotation Failure Mechanism

The pushover curve for the three building models with strength degradation and without considering partition walls is given in Figure 6.6. The pushover curve for the original unmodified building is also plotted in the same figure with a dashed line for reference. The building model with the onset of strength degradation set to occur at plastic rotations of 0.01 radians begins to degrade in lateral force resistance at a drift ratio of 1.2% while the models with onset of degradation at 0.02 and 0.03 radians, respectively, begin degrading at drift ratios of 1.8% and 2.5%. Failure in the structure occurs at the base level as 'soft-story' effects are observed. Because the failure is due to the ductility of the members, the onset of yielding for each model occurs at the same drift ratio.

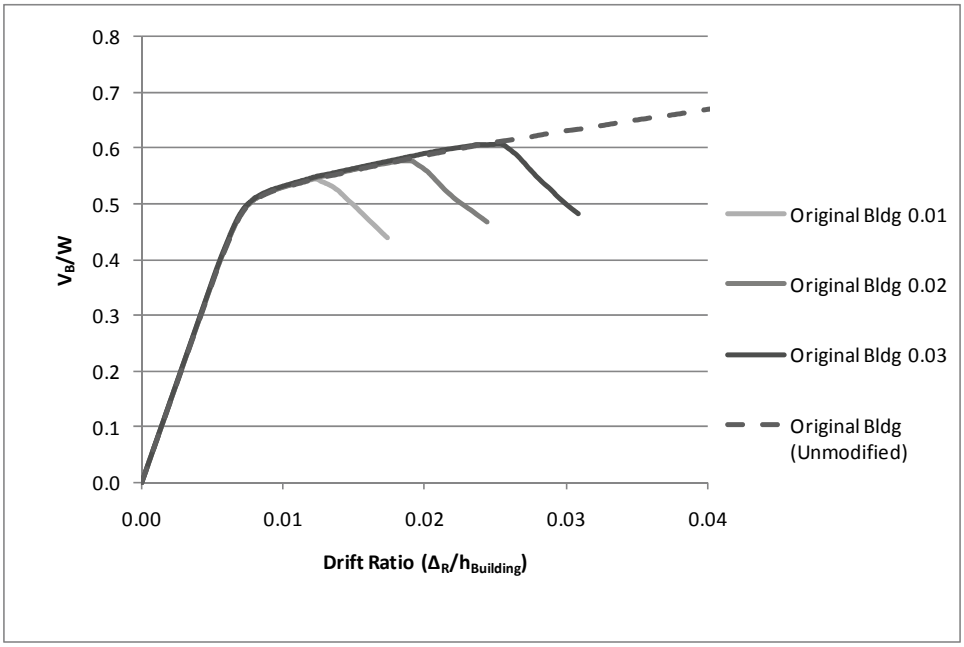

Figure 6.6 – Modified WC70 Pushover Curve

6.2 Effect of Added Nonstructural Partition Walls to WC70 Building Model

In order to understand the effect of nonstructural partition wall subsystems on the dynamic properties of the structure, the walls need to be incorporated into the building model. Nonlinear shear spring elements, with hysteretic behavior defined in the transverse axis of a vertical spring element, are applied to the building model and are attached to the midpoint of the beams in the center bay of the exterior frames. Because axial deformations are neglected, the locations of the shear springs in each floor level are negligible. Originally, four shear spring elements, one per level, were used to simulate the partition wall mechanical behavior, as shown in Figure 6.7, but it was later found that an additional spring was required at each level to accurately capture the pushover response. The shear springs are to account for the total linear feet of in-plane partition walls at each floor level. The additional spring was needed to account for instability in the Wayne Stewart hysteretic model, as illustrated in Figure 6.8. The tri-linear backbone curve of shear spring #1 would approach zero strength as expected, but as displacements continued to increase, the force in the element would cross the x-axis and begin to produce negative forces. Therefore, to correct this unrealistic behavior, another spring, shear spring #2, was included at each floor level that would activate at the drift at which zero force was achieved. The parameters for these spring elements are essentially zero until the maximum ductility ratio is reached, at which point the tri-linear slope is assigned a positive stiffness equal to $k_0 P_{Tri}$. The values for shear springs 1 and 2 are summed and the total is plotted in the Figure 6.8as the combined effect.

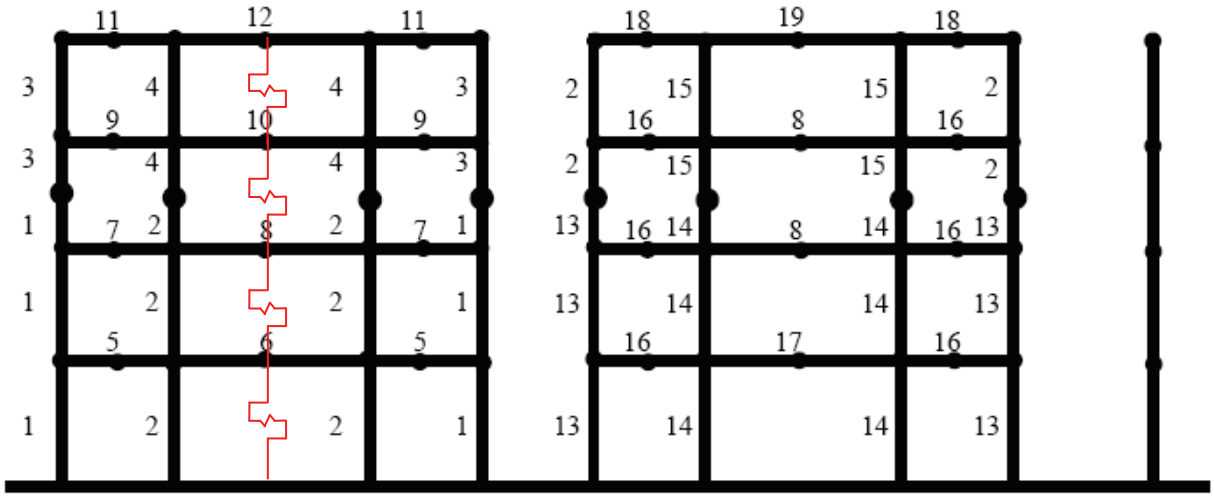

Figure 6.7 – Location of Shear Springs in the North South Steel Moment Frame modified from Wanitkorkul et al. (2005)

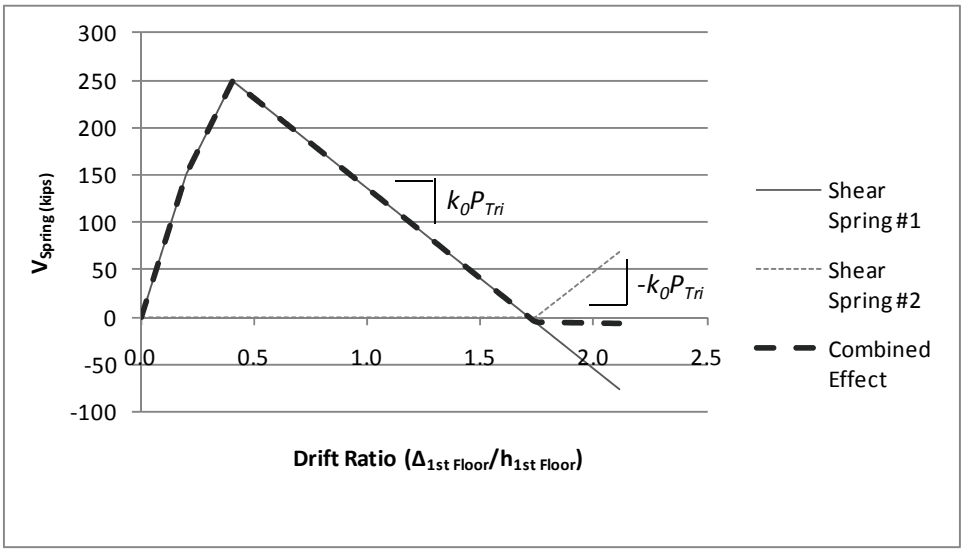

Figure 6.8 – Forces in First Floor Shear Springs

6.3 Determining Spring Parameters for Wall Groups

Recalling that the parameters for the Wayne Stewart model were calibrated following full scale gypsum wall experimental tests of twelve feet in length and eleven feet five inches tall, scaling the parameters is required. Refer to Section 5.2 for a list of the required parameters for the Wayne Stewart hysteretic model. The total length of partition walls oriented in the direction of analysis, for each floor level, was measured from the original building architectural drawings. Table 6-4 includes the total length of walls measured at each floor level. Given that the structural model considers only one half of the building, one half of the total partition wall length was used to calculate the stiffness and force parameters applied to each shear spring hysteretic model. It is recognized that an assumption is made at this step in the analysis; this assumption is that the length of partition walls in each half of the building are equal. While this is an assumption and may not be the case, it must be remembered that the purpose of this analysis is to determine, if any, the effect of the nonstructural partition walls on the dynamic response of the building. Further analysis would be required to determine the increase in floor rotations (e.g., torsion) due to unsymmetrical placed partition walls.

Table 6-4 Estimated Partition Wall Lengths in the North-South Direction of the WC70 Building

Floor	Total Length (ft)	Length for 1/2 of Building (ft)
1	736	368
2	672	336
3	814	407
4	628	314

Scaling of hysteretic parameters is based on the estimated length of the partition walls at each floor level. Table 6-5 shows the parameters assigned to the spring elements in the model for each floor, the parameters α=0.64 and β=1.07 are constant for each of the wall groups.

Table 6-5 Wayne Stewart Hysteretic Parameters for WC70 Building Model

Partition Wall System	Building Level	k_0 (klf)	r	P_{tri}	P_{UNL}	F_y (kips)	F_u (kips)	F_i (kips)
Commercial Slip Track	1	18.44	0.63	-0.25	1.08	150.60	248.88	24.37
	2	16.93				138.25	228.48	22.37
	3	20.51				167.47	276.75	27.10
	4	15.82				129.20	213.52	20.91
Commercial Full Connection	1	35.36	0.39	-0.22	0.86	295.05	446.10	22.18
	2	32.46				270.86	409.54	20.36
	3	39.32				328.10	496.08	24.66
	4	30.33				253.13	382.72	19.03
Institutional Slip Track	1	35.66	0.20	-0.28	0.91	358.24	439.07	35.56
	2	32.74				328.87	403.08	32.64
	3	39.66				398.37	488.26	39.54
	4	30.59				307.34	376.69	30.51
Institutional Full Connection	1	80.47	0.28	-0.19	0.91	750.63	1009.60	54.09
	2	73.87				689.10	926.85	49.65
	3	89.48				834.71	1122.70	60.14
	4	69.04				643.98	866.16	46.40
Partial Height	1	7.32	0.38	-0.39	1.00	88.10	139.00	8.36
	2	6.72				80.88	127.60	7.68
	3	8.14				97.97	154.57	9.30
	4	6.28				75.59	119.25	7.17
Improved Detail	1	7.22	0.32	-0.27	1.38	78.73	114.08	19.55
	2	6.63				72.28	104.73	17.95
	3	8.03				87.55	126.86	21.74
	4	6.19				67.55	97.87	16.78

6.4 Comparison of Dynamic Response for Individual Wall Groups

Now that the shear springs are inserted into the model and assigned the individual scaled parameters for the model being used, an analysis of the effects of the partition walls on the dynamic response of the structure can be evaluated. In the following sections, the dynamic responses considered are: (1) Elastic natural period of vibration; (2) equivalent damping ratio; (3) maximum observed story drift ratio; and (4) maximum floor absolute acceleration. The two latest parameters are evaluated by subjecting the structures to three different earthquake time histories.

6.4.1 Elastic Periods of Vibration

The first dynamic characteristic to consider is the elastic period for the first two modes of vibration of the structure, since 96% of the seismic mass is participating in the first and second mode of vibration. Table 6-6 shows the elastic natural vibration periods estimated through eigenvalue analysis. Upon review of the periods for the different structures, it is observed that the period drops 1% with even a small addition of stiffness. The most noticeable difference is observed in the institutional full connection building model. In this case, a drop in the period of 11.4% in the first mode and 10.5% in the second mode are observed. The reduction in structural period is associated with an increase of approximately 30% in overall lateral stiffness. While this can be considered good for the structure because drift levels will most likely decrease, an increase in stiffness in general is associated with an increase in absolute floor accelerations. While the floor accelerations are often neglected in structural design, for important structures (e.g., medical facilities) with highly sensitive equipment, the damage caused by accelerations can often be costly and potentially dangerous.

Table 6-6 Period Comparison of the First and Second Mode of Vibration

	Period of Vibration			
	1st Mode	% Reduction	2nd Mode	% Reduction
Original Building	0.762	-	0.257	-
Commercial Slip Track	0.739	**3.0**	0.25	**2.7**
Commercial Full Connection	0.722	**5.2**	0.245	**4.7**
Institutional Slip Track	0.719	**5.6**	0.244	**5.1**
Institutional Full Connection	0.675	**11.4**	0.23	**10.5**
Partial Height	0.752	**1.3**	0.254	**1.2**
Improved Detail	0.753	**1.2**	0.254	**1.2**

6.4.2 Equivalent Damping Ratio

Each of the building models are assigned 2% Rayleigh damping to the first and third modes of vibration. With the added partition walls the damping ratio increases to approximately 2.4%. To determine the increase in the equivalent damping ratio, the building model was subjected to an impulse acceleration to initiate vibration but to maintain elastic response, and the top level displacements were recorded. Figure 6.9 is the measured free vibration displacement for the original structure, and is a classical representation of an under-damped system.

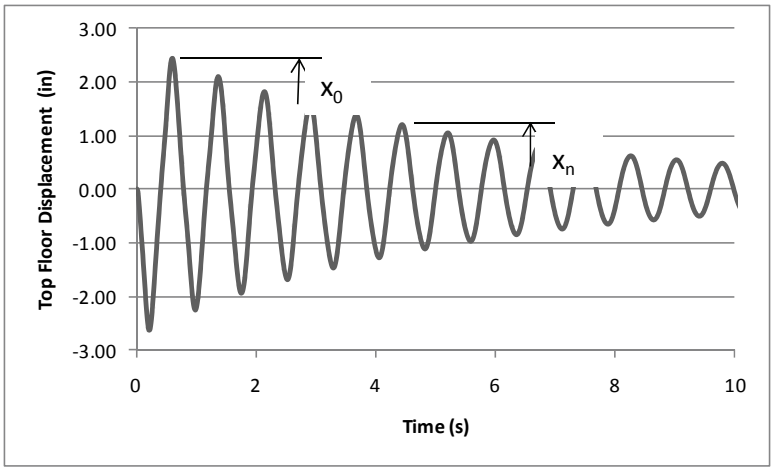

Figure 6.9 – Top Floor Free Vibration Displacement

Through the use of the logarithmic decrement:

$$\delta = \frac{1}{n} \ln \frac{x_0}{x_n} \qquad \textbf{6-6}$$

where x_n is the peak displacement n cycle away and x_0 is the maximum amplitude. The damping ratio can be determined by:

$$\zeta = \frac{1}{\sqrt{1 + \left(\frac{2\pi}{\delta}\right)^2}} \qquad \textbf{6-7}$$

Table 6-7 gives the equivalent damping ratio for each of the building models without any member yielding. Although only 2% Rayleigh damping is assigned to the building models, the original structure with no added stiffness from nonstructural partition walls, using the logarithmic decrement returned an equivalent damping ratio of 2.26%. The equivalent damping ratio increases with increased stiffness due to the added partition walls.

Also given in Table 6-7 is the base shear coefficient for each of the models. This coefficient is a ratio of the peak shear force in the ground level columns and partition walls over the total seismic weight of the structure. Values are given for three structures, and show that for the building model under consideration, independent of the added partition wall stiffness, the base shear coefficient is only a function of the definition of failure at plastic rotation in the steel frame members.

Table 6-7 Equivalent Damping and Base Shear for Building Models

	Equivalent Damping (%)	Plastic Rotation		
		0.01 rad	0.02 rad	0.03 rad
Original Building	2.26	0.55	0.58	0.61
Commercial Slip Track	2.79	0.55	0.58	0.61
Commercial Full Connection	2.75	–	–	–
Institutional Slip Track	2.94	–	–	–
Institutional Full Connection	3.22	0.55	0.58	0.61
Partial Height	2.38	–	–	–
Improved Detail	2.53	–	–	–

6.4.3 Earthquake Time History Details

In order to understand the effect of the partition walls on the seismic response of the structure, the various building models are subjected to three recorded earthquake time histories. The randomly chosen earthquakes considered in the analysis are: the El Centro North-South (NS) component, and LA14 and LA16 from the LA suite provided by the SAC Joint Venture Project (SAC 1997). The El Centro ground motion was chosen based on its historical value. The El Centro ground motion time history has been the most commonly used time history in earthquake engineering and was the first major ground motion ever recorded (Chopra, 2000). The non-scaled NS component of the El Centro acceleration time history is shown in Figure 6.10a. This ground motion has a Peak Ground Acceleration (PGA) of 0.35g. The other two ground motions were picked randomly from the LA Suite. Figure 6.10b is a plot of the LA 14 ground motion with a PGA of 0.66g. Figure 6.10c is a plot of the time history for the LA 16 ground motion and has a PGA of 0.58g.

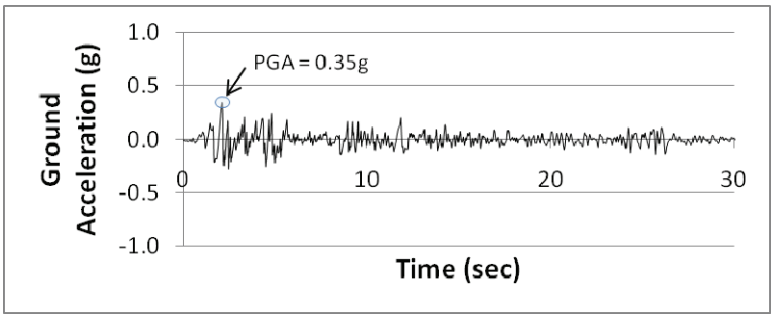

(a)

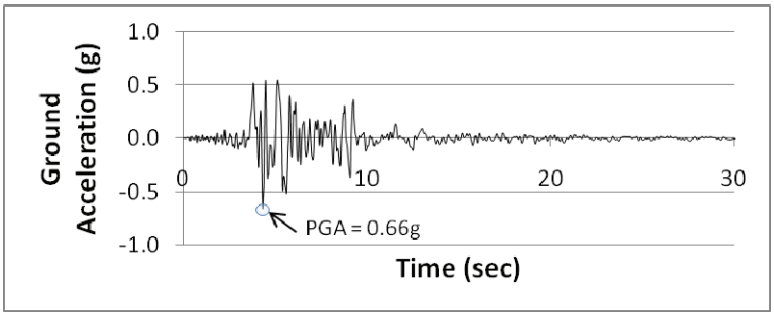

(b)

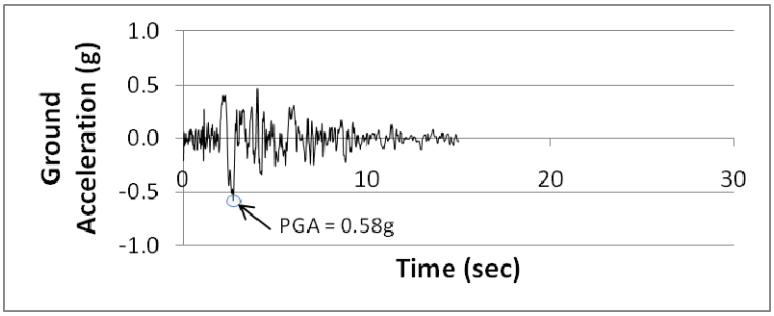

(c)

Figure 6.10 – Earthquake Ground Motions: (a) El Centro North-South Component; (b) LA 14; and (c) LA 16

The three earthquakes will be used as input for the dynamic responses of the building models. All three ground motions will be run at the Design Earthquake (DE) level of 10% in 50 years probability of exceedance; the two LA ground motions will be scaled by 1.5 to the maximum considered earthquake (MCE) intensity which corresponds to a probability of exceedance of 2% in 50 years and used to determine dynamic responses.

6.4.4 Maximum Drifts Ratios

Inter-story drift is the most common measurement to determine the performance of a structure during and after a seismic event. FEMA 356 (2000) considers a structure to have the performance levels of 'immediate occupancy' if the transient drift ratio remains below 0.7%, 'life safety' if the ratio remains below 2.5%, and in 'collapse prevention' performance level if it remains under 5%. Likewise ASCE 7-05 (ASCE, 2005) also gives limiting drift ratios in Table 12.12.1 that are based on the type of structure considered and the occupancy category. Figure 6.11 contains plots of the envelope maximum drift ratios for each floor for the DEs. The inter-story drift ratios for the structures with added stiffness due to the partition walls decreased 11% from 1% to 0.88% under the El Centro ground motion and increased by 0.8% to 21% for the LA16 and LA14 ground motions respectively. Under the LA14 ground motion a soft story effect is observed in the building response which coincides with a reduced stiffness at the second floor due to the reduced amount length of partition walls on this level. Drift ratios for LA14 do remain well under the FEMA recommended life safety drift ratio of 2.5%; however, no building model maintains immediate occupancy drift levels for the respective ground motion. Interestingly, the drift ratios for each of the building models subjected to LA16 ground motion well exceed the 2.5% life safety drift ratio. Table 6-8 gives the maximum observed drift ratios for each of the structures under the given ground motions, although a reduction of inter-story drifts are observed at most floor elevations for the stiffer structures in each ground motion, the maximum drift ratio does not follow this trend. Figure 6.12 has plots of the maximum drift ratio for each floor for the MCE levels. The inter-story drift ratios for the different structures under the LA14 MCE ground motion are similar at each of the floor levels. The maximum drift ratio in the models under the LA14 MCE do increase for the partition wall models from 4.0% for the partial height wall model to 21.0% for the institutional full connection partition wall model. As the building models were subjected to the LA16 ground motion the models collapsed numerically, for those models, the maximum inter-story drift was set to 5.0%, correlating to the collapse prevention drift ratios as defined in FEMA 356.

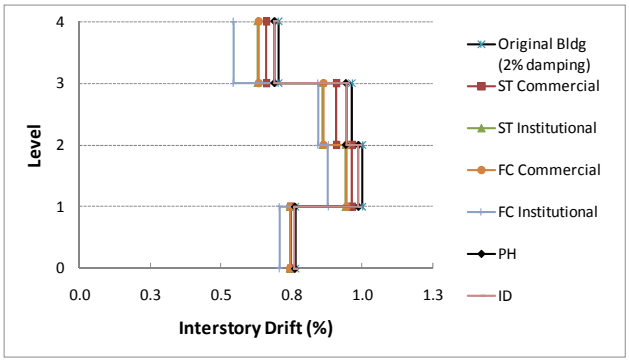

(a)

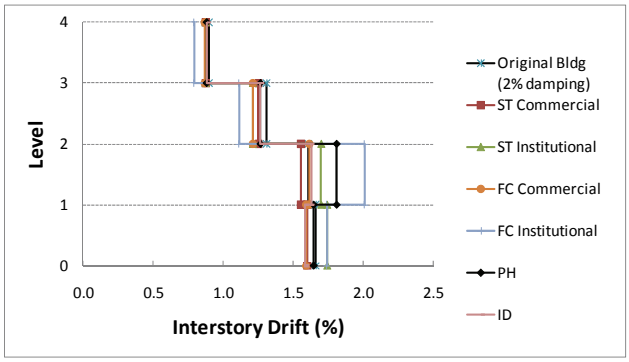

(b)

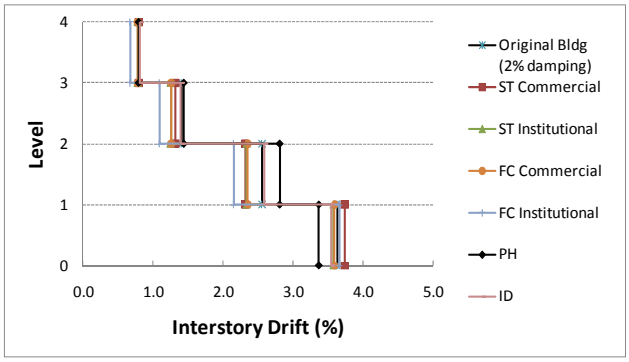

(c)

Figure 6.11 – Maximum Drift Ratio for DE (a) El Centro, (b) LA 14, and (c) LA 16

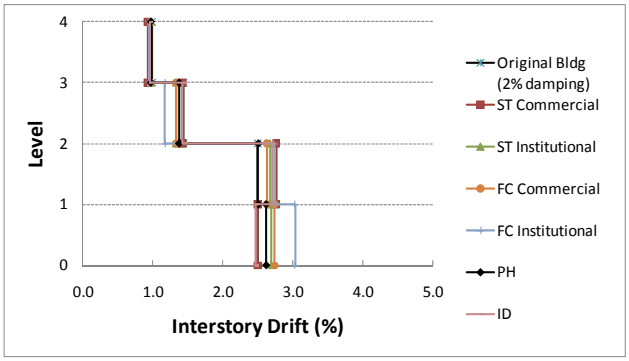

(a)

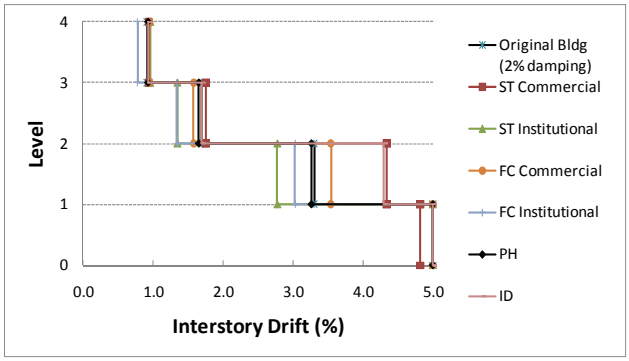

(b)

Figure 6.12 – Maximum Drift Ratio for MCE (a) LA 14 and (b) LA 16

Table 6-8 Comparison of Maximum Inter-story Drift Ratios

	DE (10% in 50 yrs)			MCE (2% in 50 yrs)	
	El Centro	LA 14	LA 16	LA 14	LA 16
Original Building	1.00	1.66	3.63	2.50	5.00
Commercial Slip Track	0.96	1.60	3.74	2.76	4.82
Commercial Full Connection	0.95	1.62	3.60	2.75	5.00
Institutional Slip Track	0.94	1.74	3.58	2.70	5.00
Institutional Full Connection	0.88	2.01	3.66	3.03	5.00
Partial Height	0.99	1.81	3.37	2.62	5.00
Improved Detail	0.99	1.63	3.55	2.70	5.00

After the earthquake has occurred, depending on the ground motion intensity the building may not return to original position. This-post earthquake deformation can be considered permanent and have a considerable effect on future use of the structure. If displacements (residual drift) are large enough, the building is considered unstable because *P-Δ* effects along with small lateral loads could cause the structure to collapse. According to FEMA 356 for steel moment frames, residual drifts must be negligible for immediate occupancy and ≤1% for life safety. The residual drift for each of the buildings subjected to the different ground motions is presented in Figure 6.13 and Figure 6.14. These figures show that an overall decrease is observed in the residual inter-story drift levels. The most dramatic representation is in Figure 6.13(a), residual drift for the El Centro ground motion, drift ratios during this earthquake reached nearly 1.0% in almost all of the buildings, however residual drifts were very low (<0.1%) with drift levels for the stiffest structure reducing to below 0.04%. A similar trend is observed for the building models under the LA14 10% in 50 years ground motion intensity. Under LA16, recall that maximum drift ratios were nearly identical for each of the building models and while the trend for residual drift is observed in upper floor levels, in the first floor level where drift ratios exceeded 3.5%, residual drift well exceeds the 1.0% life safety requirement and buildings with partition walls exceeded the original building. Residual drift for MCE ground motions showed that for LA14 overall a reduction is observed from the DE ground motion; and because collapse was observed during LA16, residual drift ratios would also show collapse. Table 6-9 gives the values for maximum residual drift for each of the building models under each of the earthquakes.

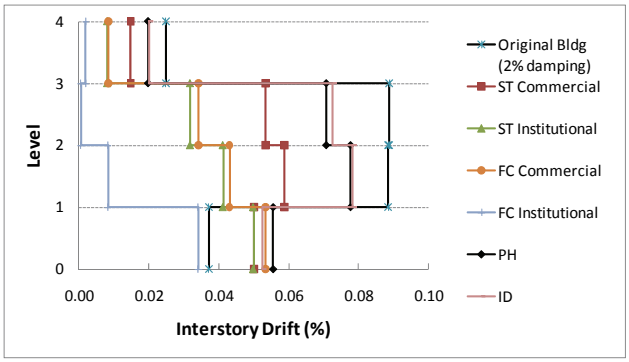

(a)

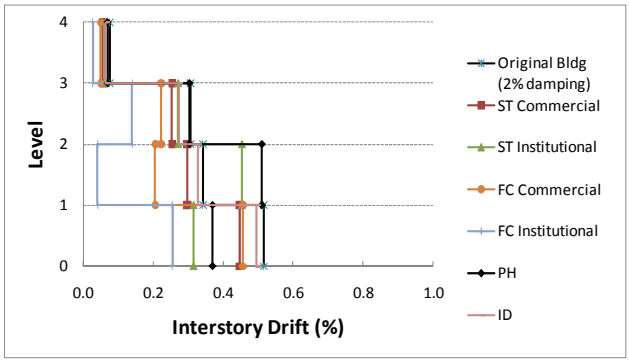

(b)

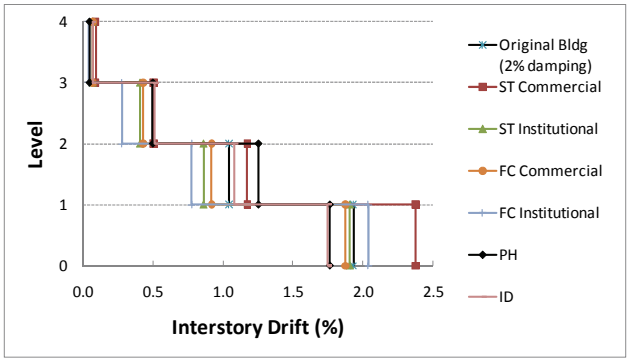

(c)

Figure 6.13 – Residual Drift Ratios for DE (a) El Centro, (b) LA 14, and (c) LA 16

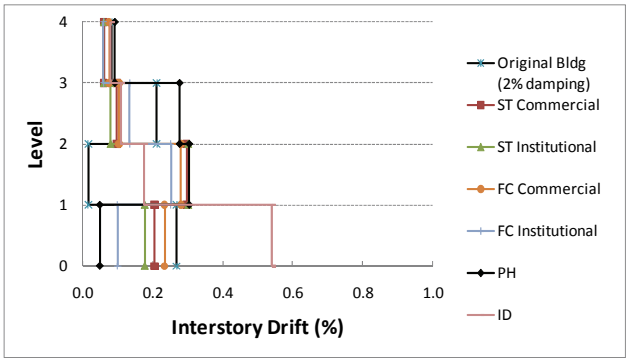

(a)

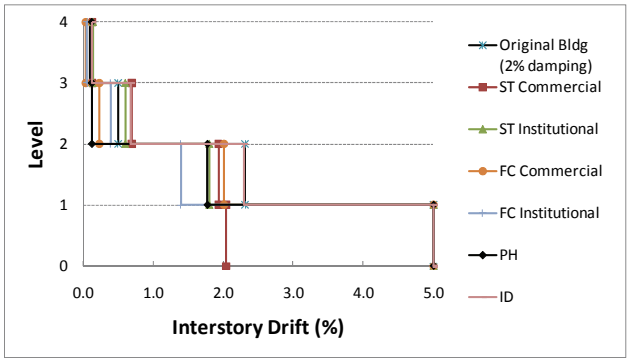

(b)

Figure 6.14 – Residual Drift Ratios for MCE (a) LA 14 and (b) LA 16

Table 6-9 Comparison of Residual Inter-story Drift Ratios (%)

	DE (10% in 50 yrs)			MCE (2% in 50 yrs)	
	El Centro	LA 14	LA 16	LA 14	LA 16
Original Building	0.09	0.52	1.93	0.27	5.00
Commercial Slip Track	0.06	0.45	2.38	0.30	2.04
Commercial Full Connection	0.05	0.46	1.88	0.28	5.00
Institutional Slip Track	0.05	0.45	1.91	0.30	5.00
Institutional Full Connection	0.03	0.26	2.04	0.25	5.00
Partial Height	0.08	0.51	1.76	0.30	5.00
Improved Detail	0.08	0.50	1.75	0.54	5.00

To understand the simulated mechanical response of the gypsum partition walls, a plot of the hysteretic behavior of the four shear springs in the building with the full connection institutional wall parameters are plotted in Figure 6.15. This hysteretic behavior is for the building subjected to the LA 14 DE ground motion. To further understand the effect of the partition walls on the building a plot of the kinetic plus the strain energy is given in Figure 6.16 for three models (original, commercial slip track, and institutional full connection). This figure shows that under the LA 14 DE ground motion higher levels of energy are dissipated through hysteretic response in the models with partition walls included.

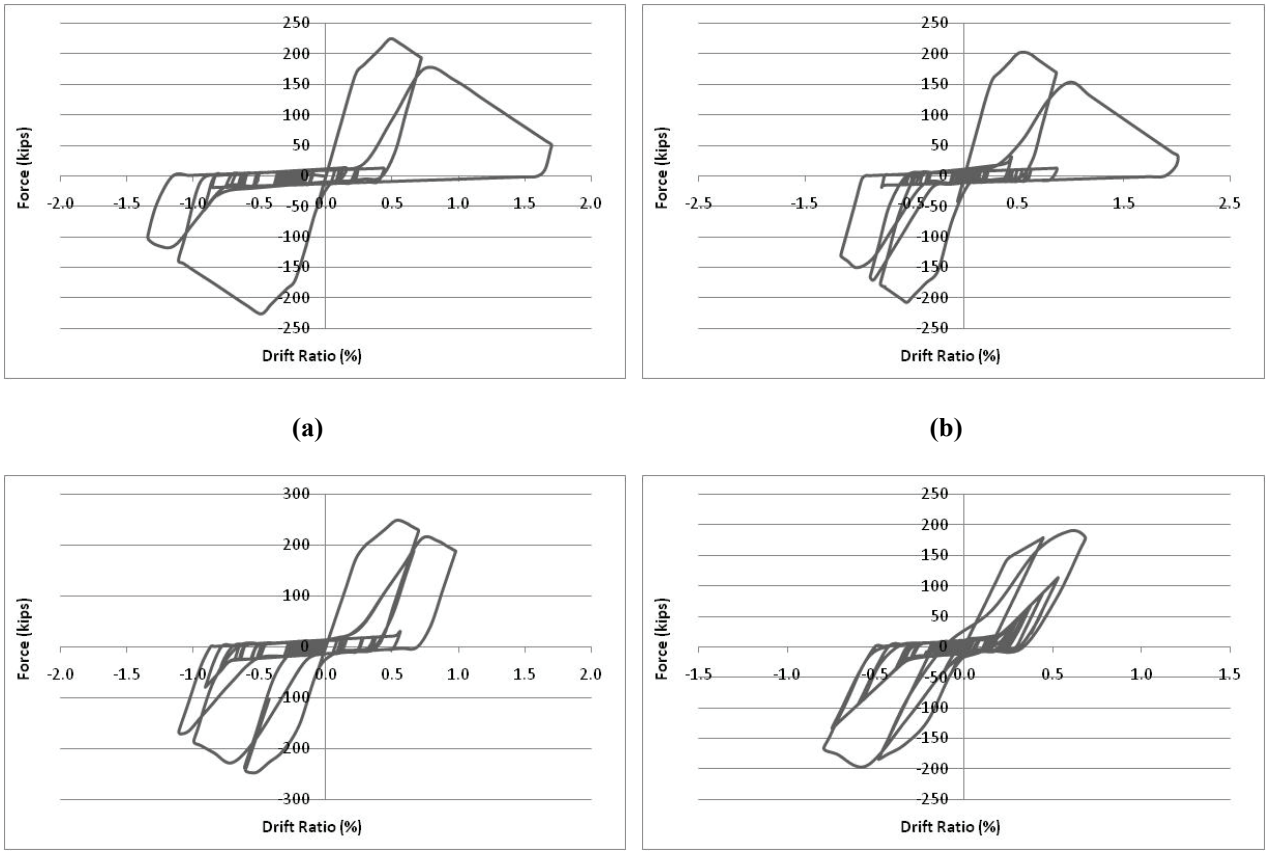

Figure 6.15 –Shear Spring Force-Displacement Curve for LA 14 DE Floors (a) 1, (b) 2, (c) 3, and (d) 4

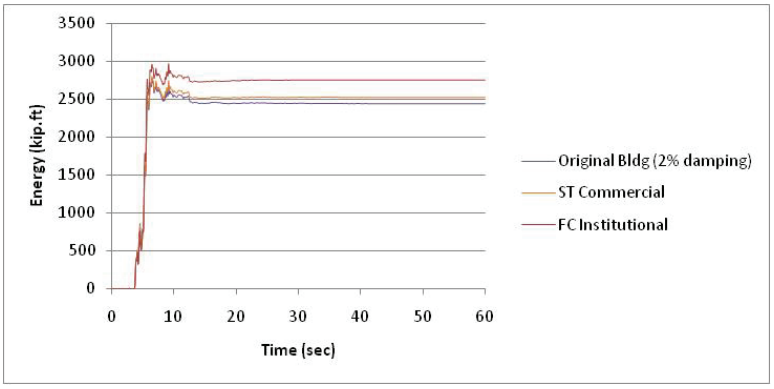

Figure 6.16 – LA14 DE Kinetic+Strain Energy Comparison

6.4.5 Maximum Absolute Floor Acceleration Results

The last dynamic response to consider for each of the building models is the individual story floor absolute accelerations. In Figure 6.17 and Figure 6.18, the envelopes of maximum floor accelerations are plotted for each story level for the ground motions at DE and MCE levels. In general the building models implementing the nonstructural partition walls experience a decrease in maximum observed floor accelerations for design earthquakes. The building model considering full connection institutional walls experiences a decrease in maximum top floor accelerations by 2.8% in LA 14 and 4.9% in LA 16 to 9.0% in El Centro. Top floor LA14 MCE accelerations are approximately equal while absolute floor accelerations in lower floor levels are reduced up to 16.0% at the second floor. Absolute floor accelerations for the buildings subjected to the LA16 MCE ground motions have large variations, but because this building model experienced collapse (numerically) the accelerations are not reliable. Change in building model accelerations is caused by the amount of ductility and time of yielding in the partition walls.

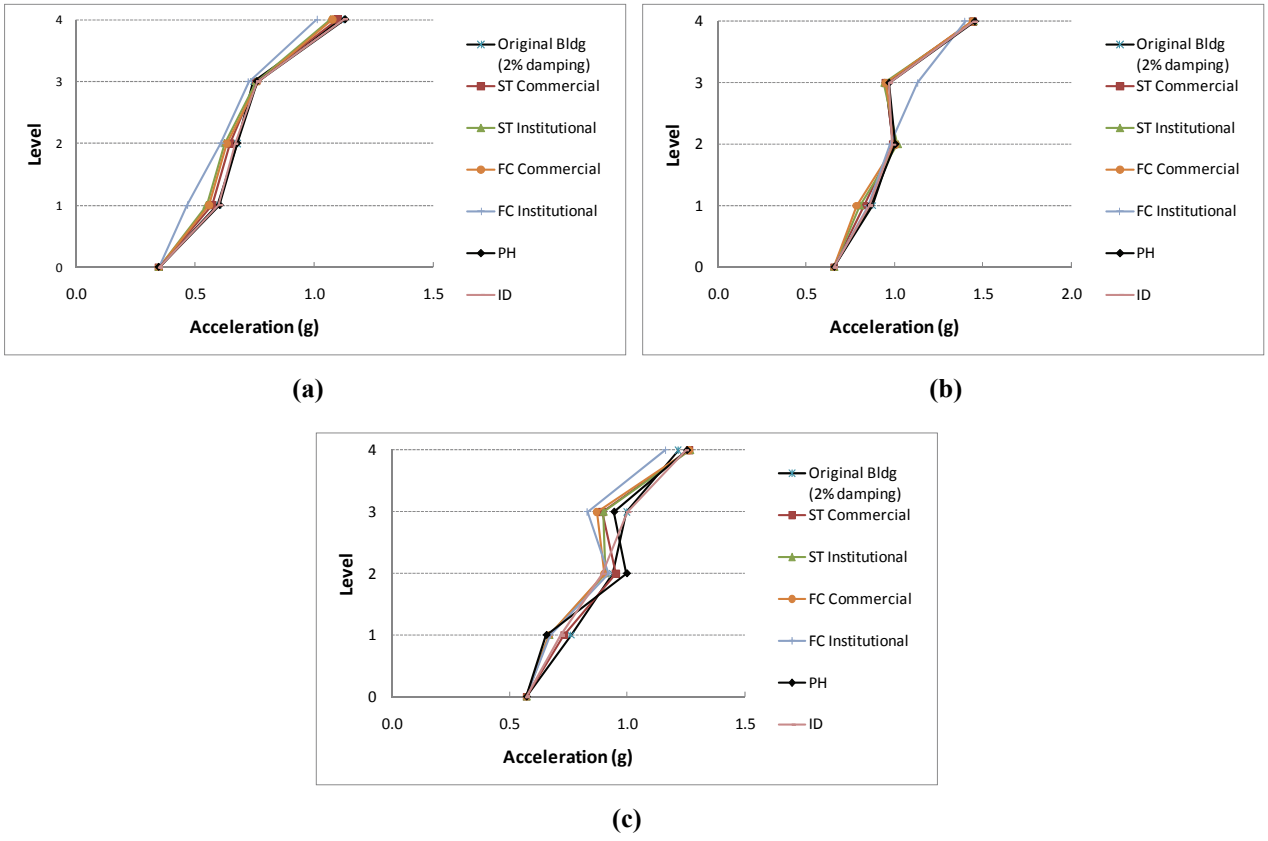

Figure 6.17 – Maximum Floor Absolute Acceleration for DE (a) El Centro, (b) LA 14, and LA 16

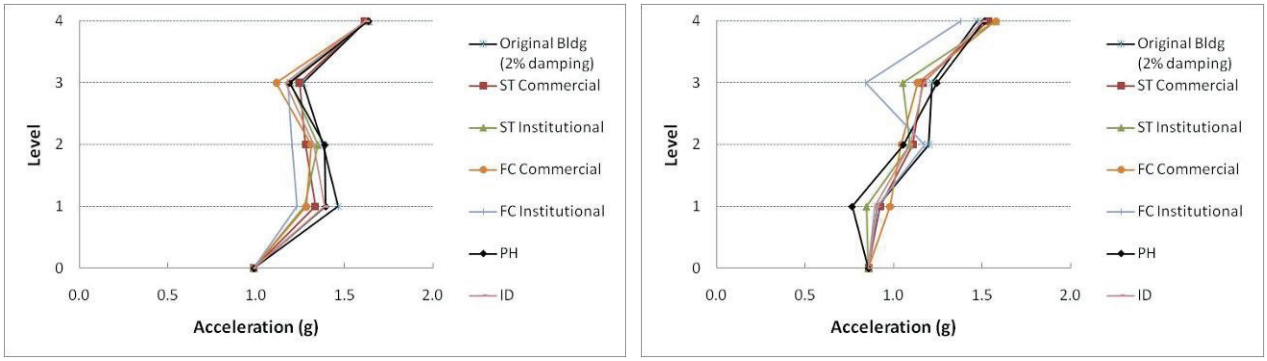

Figure 6.18 – Maximum Floor Absolute Acceleration for MCE LA 14

Table 6-10 Comparison of Maximum Absolute Floor Accelerations (g)

	DE (10% in 50 yrs)			MCE (2% in 50 yrs)	
	El Centro	LA 14	LA 16	LA 14	LA 16
Original Building	1.11	1.44	1.22	1.63	1.47
Commercial Slip Track	1.10	1.44	1.27	1.61	1.53
Commercial Full Connection	1.08	1.44	1.26	1.63	1.58
Institutional Slip Track	1.07	1.45	1.27	1.64	1.58
Institutional Full Connection	1.01	1.40	1.16	1.64	1.38
Partial Height	1.13	1.45	1.25	1.63	1.51
Improved Detail	1.12	1.45	1.25	1.62	1.51

6.5 Conclusion

A dynamic analysis of a numerical model known as WC70, elaborated from the plans for an existing medical facility structure built in the early 1970's, was conducted in this chapter. This building was chosen because of the extensive research that has been conducted by MCEER. Modifications to the

structure were required to introduce strength degradation in the structural elements and to include the effect of nonstructural partition walls. The strength degradation for the structural beams and columns was based on curvature ductility following the conclusions from previous research. Shear spring elements with the Wayne Stewart hysteretic model, calibrated to experimental results, were used to simulate the partition wall elements. The parameters for the individual wall groups were applied to the Wayne Stewart hysteretic model scaled linearly for the total length of partition walls at each floor level.

The first two periods of vibration, equivalent damping, inter-story drifts (maximum and residual), and floor accelerations were compared for the individual building models. The periods of vibration were obtained through the use of modal analysis; the damping, drift, and accelerations are determined by analyzing the models to five different earthquake excitations; the equivalent damping was determined by subjecting the building to a high impulse acceleration and determining the logarithmic decrement on the top floor displacement time history.

In general, as the stiffness of the structure is increased by the addition of shear springs, the period decreases because there is no change to the building mass. In the building models considered, no changes were made to the seismic mass of the structures to account for the partition walls, because dead loads should already account for these forces. A change in maximum inter-story drift showed no significant trend between the low and high intensity ground motions; however, including partition walls reduced drifts in the other floor levels. Also, residual drifts tended to reduce for structures that included the partition wall behavior (up to 60% in El Centro and 50% in LA14). The maximum absolute floor accelerations were reduced in each of the DE ground motions, up to 9.0%. Because the dynamic responses were found to be highly dependent on the ground motions used to analyze the structure, the following chapter will subject three of the building models to a suite of 44 scaled ground motions to understand the effect of including partition walls on the collapse probability of a structure.

Chapter 7

APPLICATION OF A FEMA P695 METHODOLOGY ANALYSIS TO A STEEL MOMENT-RESISTING FRAME STRUCTURE CONSIDERING NONSTRUCTURAL PARTITION WALLS

The seismic design of structures employs the use of factors to account for yielding in structural members. This design philosophy allows a reduction in seismic forces the structure will need to resist, by adjusting forces through the implementation of seismic performance factors (SPFs). This method of design ensures a more economical lateral force-resisting system for resisting seismic loads. ASCE 7-05 (ASCE, 2006) has tabulated values for the SPFs; response modification factor (R), overstrength factor (Ω_0), and deflection amplification factor (C_d). Because these factors are based on historical performance and engineering judgment, a recent effort was undertaken to quantify the SPFs for new systems and existing systems. The FEMA P695 methodology is found in the document "Quantification of Building Seismic Performance Factors" (FEMA, 2009), and was developed by the Applied Technology Council for the Federal Emergency Management Agency. While the primary objective of this methodology is to determine the SPFs for new structural systems and qualify the factors for structural systems already assigned in ASCE 7-05, the methodology is used in this chapter to determine the effect on the collapse performance of a steel moment-resisting frame when the interaction of nonstructural partition walls are considered. It is shown herein that inclusion of the nonstructural partition walls as part of the lateral force-resisting system provides an improvement in the lateral response (i.e., collapse performance).

7.1 Overview of the FEMA P695 Methodology

The FEMA P695 methodology uses a combination of design requirements, test data, a suite of recorded ground motions, and incremental dynamic analysis methods to determine the collapse probability of a seismic force-resisting system. One important aspect of this methodology is the requirement that each of these phases be reviewed and approved by a peer review panel. Assuming these steps are completed correctly, and the system meets the collapse probability criteria, the assumed (e.g., new system) or established (e.g., existing system) SPFs are qualified under this methodology.

The first phase of the methodology, after the seismic force-resisting system has been determined, requires the development of an archetype design space. This design space encapsulates possible configurations under current code requirements, which include but are not limited to seismic design category, gravity loads, story elevations, etc. The design space is subdivided into performance groups based on index archetype configurations. The index archetype configurations are used to develop index archetype designs, which along with performance groups, are used in the analysis phase of the methodology.

After archetype designs have been determined, and lateral force-resisting components designed to resist the factored lateral forces, a numerical nonlinear model of each archetype is developed in a program capable of conducting nonlinear time history analyses. Mechanical properties of the members, connections, and/or complete systems are attributed to the building model to accurately simulate the dynamic response. The mechanical responses or hysteretic behaviors involved in the lateral force-resisting system are determined from full-scale test data. The chosen hysteretic behavior depends on the acquired test data for the member, connection, or system tested and must include strength degradation.

With the index archetype designs determined, system performance characterized, and nonlinear models developed, the analysis phase can be initiated. The archetype models are subjected to a quasi-static pushover and dynamic analyses. The pushover analysis requires lateral loading equivalent to the methods described in Chapter 12 of ASCE 7-05. The dynamic analysis is accomplished by subjecting the index archetype building models to forty-four ground motions from the Pacific Earthquake for Engineering Research (PEER) Next Generation Attenuation (NGA) database. The earthquakes are scaled to incremental intensities to determine at what level of intensity collapse occurs. This analysis is a modification of regular Incremental Dynamic Analysis (IDA), where the scale intensity is increased until collapse occurs in 22 of the 44 ground motions (median value). The median spectral acceleration associated to this scale is compared to the spectral acceleration for the maximum considered earthquake at the period of the structure. The system overstrength, ductility, and response factors are determined through the structural analysis phase. The SPFs for the lateral force-resisting system are qualified if the collapse probability of the index archetype design and performance group are less than 10% and 20%, respectively, under the maximum considered earthquake intensity level.

7.2 Application of the FEMA P695 Analysis

An abbreviated summary of the FEMA P695 methodology has been given for familiarization. Application of the methodology in this chapter, however, varies in some aspects from the intended purpose of qualifying SPFs for a seismic resisting system and is only for representational purposes. This variation in

using the methodology is considered in Section 11.4.2 of FEMA P695, under "Consideration of Gravity and Nonstructural System Components." In this section, the effect of nonstructural components on the collapse performance and possible increase or decrease in seismic design requirements is a recommended evaluation. Therefore, the collapse response of building models developed in the previous chapter, with and without partition walls, will be examined and the results compared.

Another variation on the application of the methodology is in regards to the requirement of a peer review panel. This panel is to actively participate in decisions regarding the input parameters for each of the stages and help in determining system uncertainties. Because SPFs for a seismic resisting system are not being evaluated and no effort is made to adjust code requirements, the use of a peer review panel is beyond the scope of this project.

7.2.1 Design Requirements

A total of nine building models were analyzed under the methodology. The building models were developed for analyzing the dynamic responses in the previous chapter. The structures used are the original building model, the model including commercial slip track partition walls, and the model including institutional full connection walls. From each of these building models three models are developed based on the onset of strength degradation in the structural members; θ_p = 0.01, 0.02, and 0.03 radians, see Section 6.1.2. Table 7-1 shows the index archetypes and the associated variables. It is assumed that analyzing these models will sufficiently describe the effect on collapse performance of including nonstructural partition walls in the lateral force-resisting system. The other wall groups of improved detail, partial height, commercial full connection, and institutional slip track are not considered in this analysis.

Table 7-1 Index Archetype Building Models

Archetype	Model	Failure Plastic Rotation
1	Original Building	0.01
2		0.02
3		0.03
4	Commercial Slip Track	0.01
5		0.02
6		0.03
7	Institutional Full Connection	0.01
8		0.02
9		0.03

The design requirement for the development of the index archetype configurations is determined in Chapter 4 of FEMA P695. Table 4-1 of FEMA P695 presents many of the factors or variables that could be considered in this process. Because the building models analyzed in this section are identical with changes only to member properties and the addition of shear springs, configurations outside this range are neglected.

Uncertainty for the design requirements is based on the following grading system: (A) Superior; (B) Good; (C) Fair; and (D) Poor. These rankings are based on the level of understanding of dynamic response of the seismic resisting system and the extent of design configurations. For the current analysis the number of design configurations is limited, also the code to which the building was designed is outdated. However, the level of understanding of steel moment-resisting frames, due to testing and historical observations is high; hence, an uncertainty of C-Fair is recommended.

7.2.2 Test Data

In order to develop an archetype model that will sufficiently simulate the proposed structures, an understanding of the mechanical behavior of different components of the structure must be well understood. It is recommended to have test data that simulates the mechanical behavior of individual members, connections, and/or the complete system. FEMA P695 requires that test data comes from a certified laboratory. The analyzed test data for the nonstructural partition walls considered in these models can be found in Chapters 3 and 4 of this report. Research regarding other structural members in the building model can be found in Yuan et al. (2002).

36cold-formed steel-framed gypsum partition walls were tested in-plane using the University at Buffalo

Nonstructural Components Simulator (UB-NCS) through the summer and fall of 2008. Quasi-static and dynamic cyclic protocols that were developed at UB by Retamales et al. (2008) specifically for the UB-NCS were used to develop force-displacement curves for nonstructural partition wall systems using steel studs and gypsum wall boards. The mechanical behavior of these systems is represented by a tri-linear backbone curve with strength and stiffness degradation. Pinching effects are also considered part of the mechanical behavior of steel stud gypsum partition walls. The test data considered for the current analysis develops a phenomenological model and does not include the mechanical behavior of the individual members or connections.

The other required test data for the building models accounts for the beam and column strength degradation at the location of plastic hinges. The hysteretic behavior (i.e., moment-curvature relationship) of AISC steel members is well understood, research from Filiatrault et al. (2001) of steel, beam to column connections, related strength degradation to the curvature ductility (Section 6.1.2) and is used in the building models.

The uncertainty assigned to the test data are categorized as C-Fair. Although an extensive number of walls were tested, and under many of these configurations a consistent response was observed, the more conservative ranking was given.

7.2.3 Model

The last phase in the development process of the methodology is the development of a numerical model representative of the design requirements and test data. The model must be developed in a program that is capable of running dynamic nonlinear analysis. Table 5-2 in FEMA P695 is an outline of some of the general considerations for developing the index archetype models. Key components consist of the plan and elevation configurations, mathematical idealization, and 2-D versus 3-D component and system behaviors.

The WC70 hospital building model has undergone extensive research by Yuan et al. (2002) and Wanitkorkul & Filiatrault (2005). The building models used in this analysis were developed by Wanitkorkul and modified to include shear springs and strength degradation in steel member connections. Because of the extensive research on this structure and the available hysteresis loops which can simulate the test data in RUAUMOKO, uncertainty for the models used in this analysis is assigned to category B-Good.

7.2.4 Time Histories

A total of 44 recorded earthquakes are used to determine the collapse performance of archetype models. These ground motions are obtained from the Pacific Earthquake Engineering Research Center (PEER) database, and scaled to have the same maximum ground velocity, factors for scaling the ground motions are found in Table A-4D in FEMA P695. The spectral accelerations for the 44 ground motions are determined and then median spectral acceleration at the period of the structure is determined, as shown in Figure 7.1.

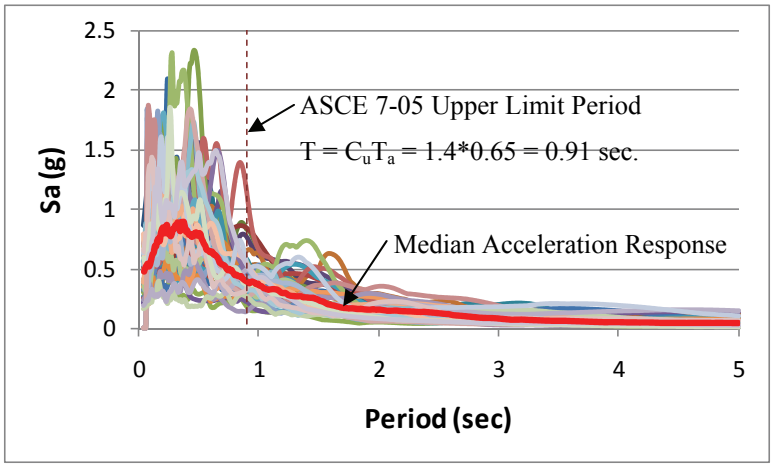

Figure 7.1 – Acceleration Response Spectra for the 44 Far Field Ground Motions

7.2.5 Nonlinear Structural Analysis

7.2.5.1 Quasi-static Pushover

The methodology requires a quasi-static pushover analysis to determine response characteristics of the seismic force-resisting system. The pushover analysis is accomplished by applying lateral loads obtained from the equivalent lateral force procedure in ASCE 7-05 Chapter 12. These forces are slowly incremented until the system fails. The top floor displacement and base shear are recorded and plotted. The resulting base shear versus top floor displacement will have an appearance similar to the plot shown in Figure 7.2.

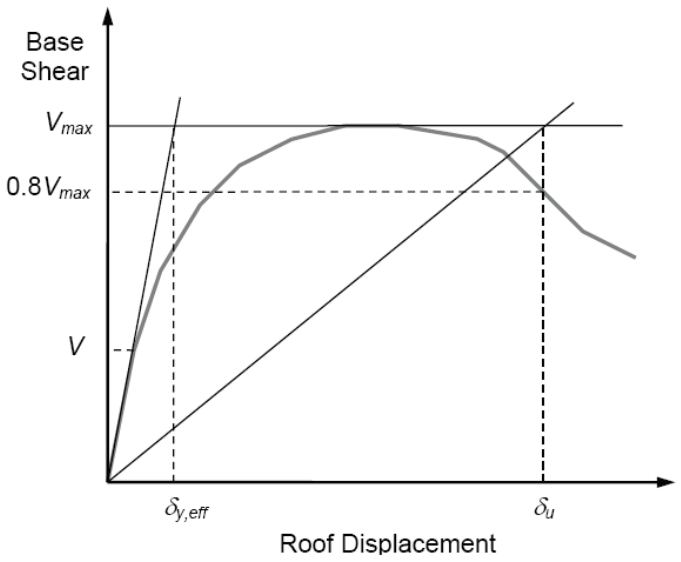

Figure 7.2 – Pushover Curve and Important Parameters, after FEMA P695 (FEMA, 2009)

The response parameters obtained from the pushover analysis are overstrength (Ω) and the period based ductility (μ_T), are given in Table 7-2, and compared to the SPFs for the seismic force-resisting system from ASCE 7-05 Ω_0 and C_d respectively. The system overstrength is determined from Equation 6-5 of FEMA P695:

$$\Omega = \frac{V_{\max}}{V} \qquad \textbf{7-1}$$

where V_{max} is the maximum base shear and V is the design base shear from Equation 12.8.1 of ASCE 7-05. The period based ductility (μ_T) is determined from the pushover curve by Equation 6-6 of FEMA P695:

$$\mu_T = \frac{\delta_u}{\delta_{y,eff}} \qquad \textbf{7-2}$$

where δ_u is the displacement at 80% of the peak force in the degrading branch of the pushover curve, as shown in Figure 7.2 and $\delta_{y,eff}$ is given by equation 6-7 and 6-8 of FEMA P695.

Table 7-2 System Overstrength and Period Based Ductility for Building Models

Plastic Rotation (rad)	System Overstrength (Ω)			Period Based Ductility (μ_T)		
	Original Building	Slip Track	Full Connection	Original Building	Slip Track	Full Connection
0.01	3.93	3.96	4.11	1.90	1.90	1.68
0.02	4.17	4.18	4.21	2.52	2.58	2.51
0.03	4.38	4.37	4.39	3.05	3.03	3.10

Reviewing the system overstrength in Table 7-2, it is shown that overstrength increases as the strength degradation based on plastic rotation increases. However, an interesting phenomenon occurs as the system overstrength for the various models are compared. The system overstrength Ω for the building models including nonstructural partition walls increases from the original building model. However the amount of increase depends on the plastic rotation used for modeling strength degradation. For example, the institutional full connection partition wall model is 4.5% stronger than the original building using a plastic rotation of 0.01 radians, meanwhile the same models using 0.03 radians for plastic rotation reduces to just 0.3% stronger. The reason for this reduction in strength is due to the partition walls resisting part of the lateral forces in the models with the lesser plastic rotations at maximum shear force. The models with higher allowable plastic rotations reach failure rotations only after the partition walls have lost all strength capacity. The reduction in maximum base shear for the models considering partition walls is evident in the plots in Figure 7.3. In the region of yielding, independent of steel strength degradation, the slip track and full connection models have a moderate to higher strength resistance respectively, but in the region of strength degradation in steel members, the strength capacity of the models is dependant of the column and beam allowable plastic rotations.

Ductility of the seismic force-resisting frame is affected by the strength degradation in the steel frame members and the type of nonstructural partition walls included. The increase in plastic rotation capacity from 0.01 radians to 0.02 radians causes an increase in ductility of more than 40%; increasing from 0.02 radians to 0.03 radians an increase of approximately 30% in ductility is observed. Meanwhile, the addition of commercial slip track partition walls causes an increase in building ductility of 45% from the original building; however the additional stiffness in the system by including institutional full connection partition walls increases system ductility from the slip track models by only 14%. The addition of nonstructural partition walls will cause an increase in system ductility because of the change in the initial stiffness of the structure, which reduces the yield displacement.

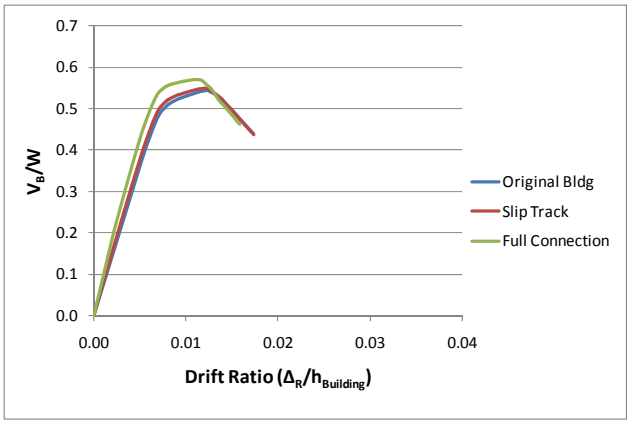

(a) Onset of Strength Degradation at $\theta_P = 0.01$ radians

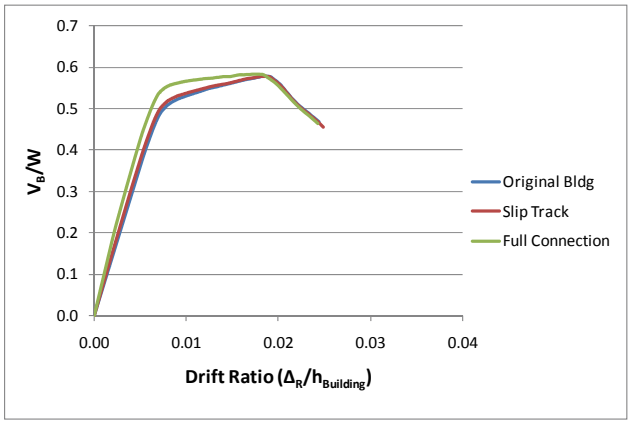

(b) Onset of Strength Degradation at $\theta_P = 0.02$ radians

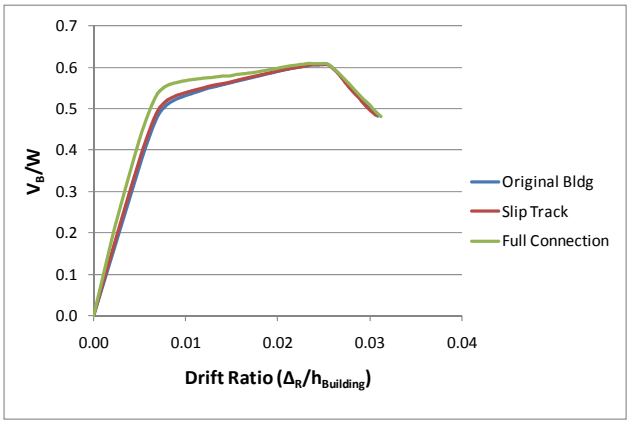

(c) Onset of Strength Degradation at $\theta_P = 0.03$ radians

Figure 7.3 – Pushover Curves for Index Archetype Models with Strength Degradation at Various Plastic Rotations

7.2.5.2 Dynamic Analysis

The purpose of the dynamic analysis is to measure responses that are associated with collapse of the structure. FEMA 356 associates structural collapse with inter-story drift ratios (i.e., peak transient and residual), but collapse could also be determined based on ductility demands on individual members. For the current analysis, collapse probability will be based on a peak transient inter-story drift ratio of 5%. To obtain the inter-story drift ratios, the index archetype building models were individually subjected to the 44 recorded and scaled far field ground motions previously mentioned.

The methodology requires that each of the archetypes be subjected to each of the 44 earthquake time histories at increasing levels of intensity. The maximum observed inter-story drift in the structure is

determined for each level of intensity and plotted vs. the maximum considered earthquake median spectral acceleration of the 44 scaled earthquakes. The FEMA P695 methodology however does not require a complete IDA in determining collapse performance. The methodology requires an IDA carried out until an intensity that will cause collapse (i.e., inter-story drift ≥ 5% for this analysis) in 50% of the time histories. Figure 7.4 thru Figure 7.6 are plots of the complete IDA for each of the index archetype building models. The phenomenon known as "structural resurrection" (i.e. local reduction of maximum inter-story drift with increased spectral acceleration) is observed in each of the IDA plots.

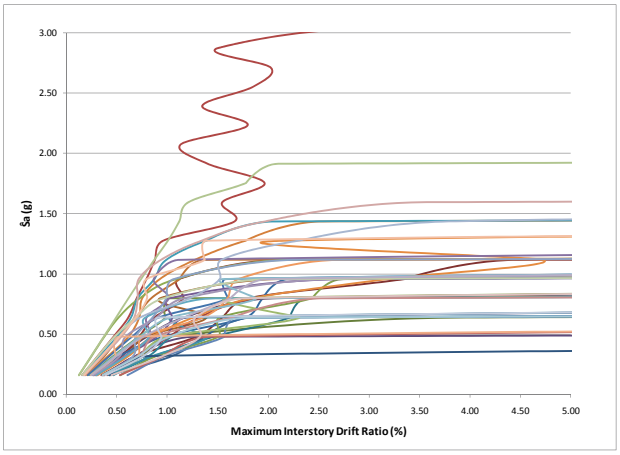

(a) Onset of Strength Degradation at θ_P = 0.01 radians

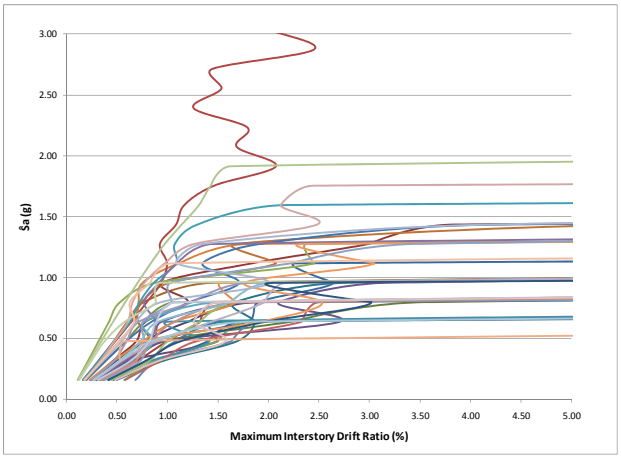

(b) Onset of Strength Degradation at θ_P = 0.02 radians

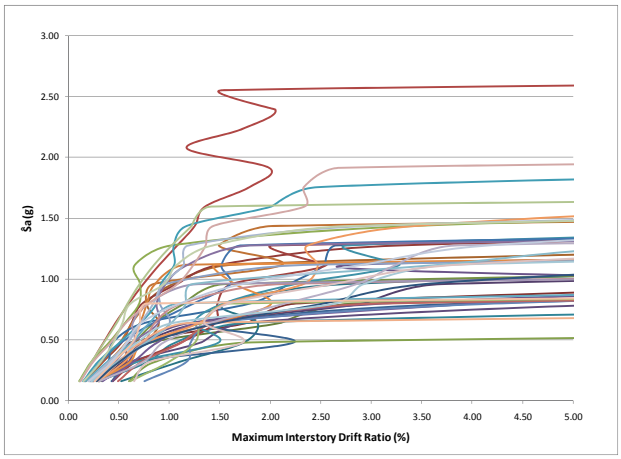

(c) Onset of Strength Degradation at θ_P = 0.03 radians

Figure 7.4 – Original Building IDA Curves with Various Plastic Rotations

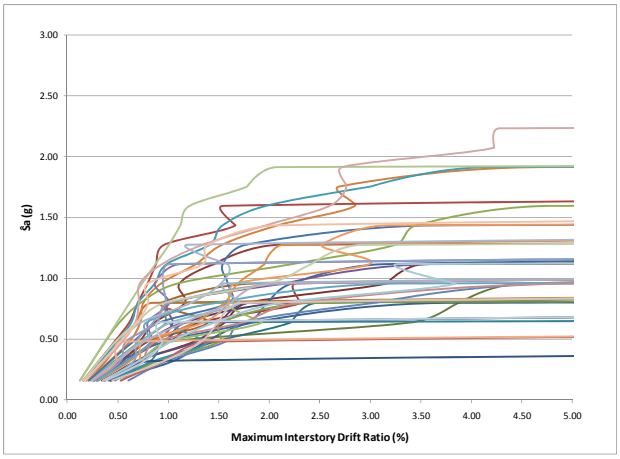

(a) Onset of Strength Degradation at $\theta_P = 0.01$ radians

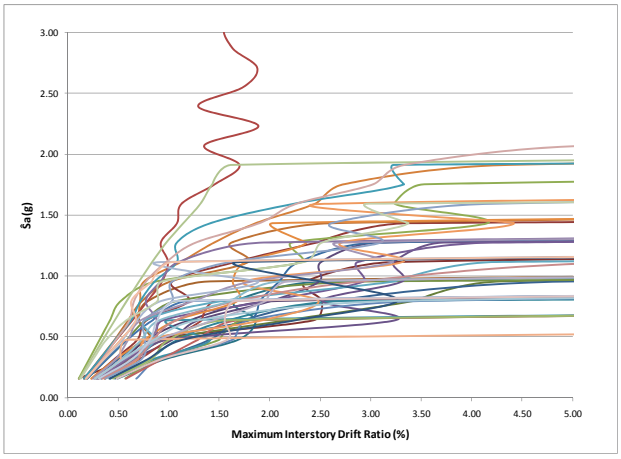

(b) Onset of Strength Degradation at $\theta_P = 0.02$ radians

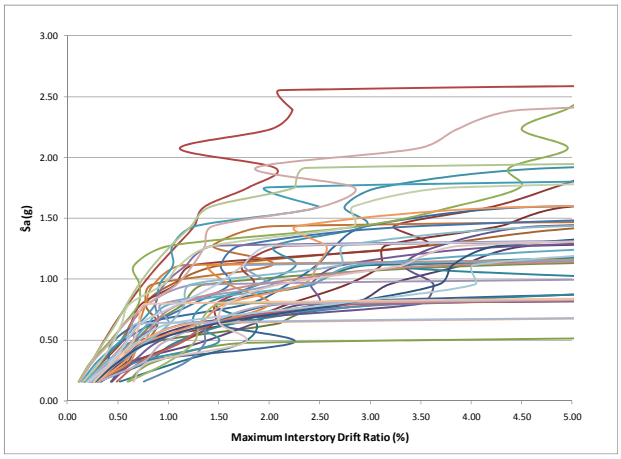

(c) Onset of Strength Degradation at $\theta_P = 0.03$ radians

Figure 7.5 – Commercial Slip Track IDA Curves with Various Plastic Rotations

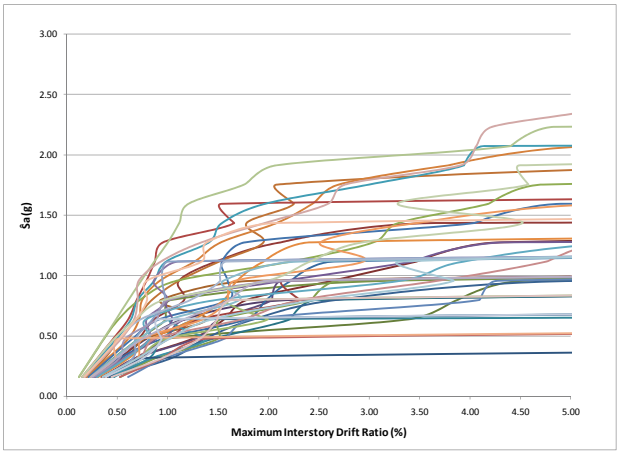

(a) Onset of Strength Degradation at $\theta_P = 0.01$ radians

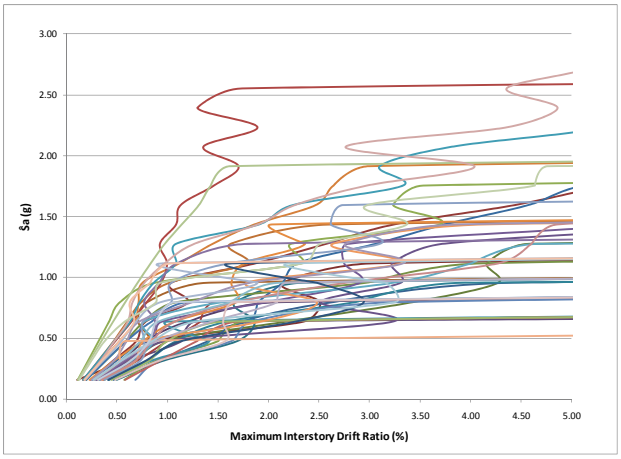

(b) Onset of Strength Degradation at $\theta_P = 0.02$ radians

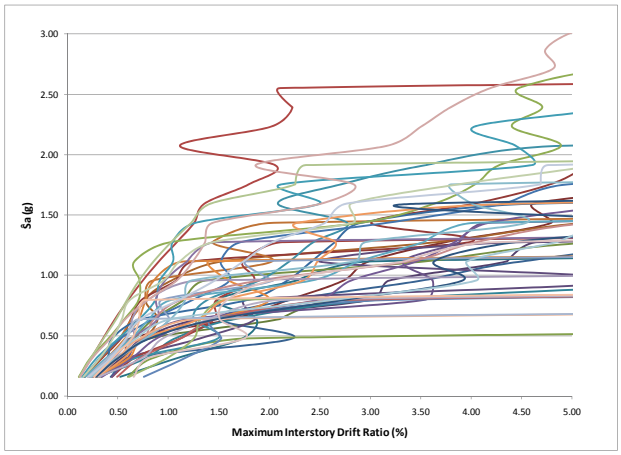

(c) Onset of Strength Degradation at $\theta_P = 0.03$ radians

Figure 7.6 – Institutional Full Connection IDA Curves with Various Plastic Rotations

The median spectral acceleration of the intensity at which the building collapses in 50% of the time histories is defined as the collapse spectral acceleration ($\hat{S}_{CT}$). $\hat{S}_{CT}$ for the archetypes is given in Table 7-3 and this spectral acceleration is compared to the MCE spectral acceleration (S_{MT}) by the formula:

$$CMR = \frac{\hat{S}_{CT}}{S_{MT}} \qquad \textbf{7-3}$$

where CMR is defined by the FEMA P695 methodology as the collapse margin ratio and given for the index archetypes in Table 7-3 and S_{MT} is determined by:

$$S_{MT} = \begin{cases} 1.5 * S_{DS} \rightarrow T_U \leq T_s \\ \dfrac{1.5 * S_{D1}}{T_U} \rightarrow T_U > T_s \end{cases} \qquad \textbf{7-4}$$

where T_s is the transition period (0.6 seconds for Seismic Design Category SDC D_{max}; 0.4 seconds for all other SDC) and S_{DS} and S_{D1} are the short and one-second respective design spectral response accelerations for the SDC and determined in accordance with methods of ASCE 7-05 Chapter 11. The period for which S_{MT} is calculated is the upper limit period T_U as specified in Section 12.8.2 of ASCE 7-05 and given by:

$$T_U = T_a C_u$$

where T_a is the approximate period of the structure given by ASCE 7-05 Equation 12.8-7 and C_u is the upper limit coefficient given in ASCE 7-05 Table 12.8-1. The current analysis determines the collapse probability for the archetypes in a the seismic design category D_{min} (S_{DS} = 0.5 and S_{D1} = 0.2). The upper limit period for the structure is 0.9 seconds which exceeds T_s = 0.4 seconds, therefore S_{MT} = 0.2/0.9*1.5 = 0.33.

Table 7-3 Collapse Spectral Acceleration and Collapse Margin Ratio for Index Archetypes

Plastic Rotation (rad)	Collapse Spectral Acceleration ($\hat{S}_{CT}$)			Collapse Margin Ratio (CMR)		
	Original Building	Slip Track	Full Connection	Original Building	Slip Track	Full Connection
0.01	0.92	0.96	1.02	2.76	2.88	3.07
0.02	0.92	1.08	1.20	2.76	3.24	3.59
0.03	1.00	1.20	1.32	3.00	3.59	3.95

The CMR is then multiplied by the Spectral Shape Factor (SSF) to determine the adjusted Collapse Margin Ratio (ACMR). The SSF is determined from Table 7-4 and is based on the SDC and μ_T and period T. The ACMR for the index archetypes considered in this analysis are given in Table 7-5.

Table 7-4 Spectral Shape Factor (SSF) for Buildings in Seismic Design Category D_{min}, (after FEMA, 2009)

T (sec.)	Period Elongation Ratio, $\Delta_u/\Delta_{y,eff}$							
	1.0	1.1	1.5	2	3	4	6	≥ 8
≤ 0.5	1	1.05	1.1	1.13	1.18	1.22	1.28	1.33
0.6	1	1.05	1.11	1.14	1.2	1.24	1.3	1.36
0.7	1	1.06	1.11	1.15	1.21	1.25	1.32	1.38
0.8	1	1.06	1.12	1.16	1.22	1.27	1.35	1.41
0.9	1	1.06	1.13	1.17	1.24	1.29	1.37	1.44
1.0	1	1.07	1.13	1.18	1.25	1.31	1.39	1.46
1.1	1	1.07	1.14	1.19	1.27	1.32	1.41	1.49
1.2	1	1.07	1.15	1.2	1.28	1.34	1.44	1.52
1.3	1	1.08	1.16	1.21	1.29	1.36	1.46	1.55
1.4	1	1.08	1.16	1.22	1.31	1.38	1.49	1.58
≥ 1.5	1	1.08	1.17	1.23	1.32	1.4	1.51	1.61

Table 7-5 Spectral Shape Factors and Adjusted Collapse Margin Ratios (ACMR) for Index Archetypes

Plastic Rotation (rad)	Spectral Shape Factor (SSF)			Adjusted Collapse Margin Ratio (ACMR)		
	Original Building	Slip Track	Full Connection	Original Building	Slip Track	Full Connection
0.01	1.07	1.09	1.13	2.92	3.36	3.59
0.02	1.09	1.13	1.15	3.11	3.79	4.39
0.03	1.13	1.15	1.15	3.50	4.46	5.10

7.2.6 FEMA P695 Methodology Performance Evaluation

The FEMA P695 methodology requires index archetype designs and performance groups to attain a collapse performance of 10% and 20% respectively under the maximum considered earthquake intensity for the seismic force-resisting system to be qualified. To determine the collapse probability for the index archetype models, the ACMR must exceed the acceptable levels given in Table 7-6. The acceptable ACMR is based on the total system collapse uncertainty (β_{TOT}), which is given in Tables 7-2 thru 7-4 in FEMA P695. β_{TOT} is determined based on the uncertainties for design requirements (β_{DR}), test data (β_{TD}), model quality (β_{MDL}), and μ_T. In review, the archetype designs were assigned the following uncertainties:

- Design Requirements = C-Fair
- Test Data = C-Fair
- Model = B-Good

Table 7-6 Acceptable Adjusted Collapse Margin Ratios

Total System Collapse Uncertainty	Collapse Probability				
	5%	10% (*ACMR10%*)	15%	20% (*ACMR20%*)	25%
0.25	1.51	1.38	1.30	1.23	1.18
0.30	1.64	1.47	1.36	1.29	1.22
0.35	1.78	1.57	1.44	1.34	1.27
0.40	1.93	1.67	1.51	1.40	1.31
0.45	2.10	1.78	1.59	1.46	1.35
0.50	2.28	1.90	1.68	1.52	1.40
0.55	2.47	2.02	1.77	1.59	1.45
0.60	2.68	2.16	1.86	1.66	1.50
0.65	2.91	2.30	1.96	1.73	1.55
0.70	3.16	2.45	2.07	1.80	1.60
0.75	3.43	2.61	2.18	1.88	1.66
0.80	3.73	2.79	2.29	1.96	1.72
0.85	4.05	2.97	2.41	2.04	1.77
0.90	4.39	3.17	2.54	2.13	1.83
0.95	4.77	3.38	2.68	2.22	1.90

β_{TOT} for the index archetypes from the FEMA P695 Tables 7-2 thru 7-4 require the assignment of β_{TOT} for the models with system ductility less than one, 0.55, for models with system ductility less than 2, 0.6, and for all others, 0.65. Linear interpolation between the tables is permissible, but in the current analysis conservative uncertainty values are used in determining the collapse performance. Using the total system uncertainties and the ACMR, an evaluation is made on the collapse performance of the index archetypes as pass (i.e., $\leq$ 10% collapse probability) or fail, as shown in Table 7-7. Collapse performance for all index archetype models meets the performance criteria defined in the FEMA P695 methodology. Considering the archetypes as a performance group also shows that the response modification factor for the steel moment-resisting frame system is qualified because the average collapse performance level meets the 10% limitation.

Table 7-7 ACMR Comparison and Collapse Performance Evaluation

Plastic Rotation (rad)	$ACMR_{Model}/ACMR_{10\%}$			Collapse Performance (Pass/Fail)		
	Original Building	Slip Track	Full Connection	Original Building	Slip Track	Full Connection
0.01	2.92/1.67	3.36/1.73	3.59/1.73	Pass	Pass	Pass
0.02	3.11/1.73	3.79/1.73	4.39/1.73	Pass	Pass	Pass
0.03	3.50/1.73	4.46/1.73	5.10/1.73	Pass	Pass	Pass

7.3 Discussions

Nine structures have been analyzed according to a FEMA P695 type analysis. The methodology is primarily used for qualifying new and existing systems, but a recommendation on further use of the methodology is to determine the impact of nonstructural components on the collapse performance of a lateral force-resisting system. This was the emphasis of the analysis considered here. The methodology was used to determine the impact of nonstructural partition walls on the collapse performance of a steel moment-resisting frame building in seismic design category D_{min} (S_{DS} = 0.5, S_{D1} = 0.2). Nine index archetypes considering different partition wall types (i.e., commercial slip track and institutional full connection) and steel member plastic rotations (θp = 0.01, 0.02, and 0.03 rad) in the columns and beams were analyzed.

It was found that including the partition walls in the lateral force-resisting frame structural performance, according to a FEMA P695 analysis improved collapse performance. Fragility curves demonstrating each of the models performance specified in Table 7-3 is given in Figure 7.7. From this figure it can be seen that a shift to the right, corresponding to an increased median collapse spectral acceleration, is observed. The original building models failed at much lower spectral accelerations ($\hat{S}_{CT}$ = 1.00g for the original building model with θ_P = 0.03 radians) than the models including nonstructural partition walls ($\hat{S}_{CT}$ = 1.20g for the commercial slip track model with θ_P = 0.03 radians and $\hat{S}_{CT}$ = 1.32g for the institutional full connection model with θ_P = 0.03 radians). An increase of 32% in median collapse spectral acceleration was not expected. However, two observations are made in relation to the change in building performance when including partition wall behavior: (1) equivalent viscous damping was increased by over 23% and 42% for the models including commercial slip track and institutional full connection partition walls, respectively, and (2) a shift in soft story behavior is observed in the models with and without partition walls. Based on the performance criteria and analysis procedure of FEMA P695, it is shown that including nonstructural partition walls in the lateral force resistance of a structure will increase the seismic collapse performance.

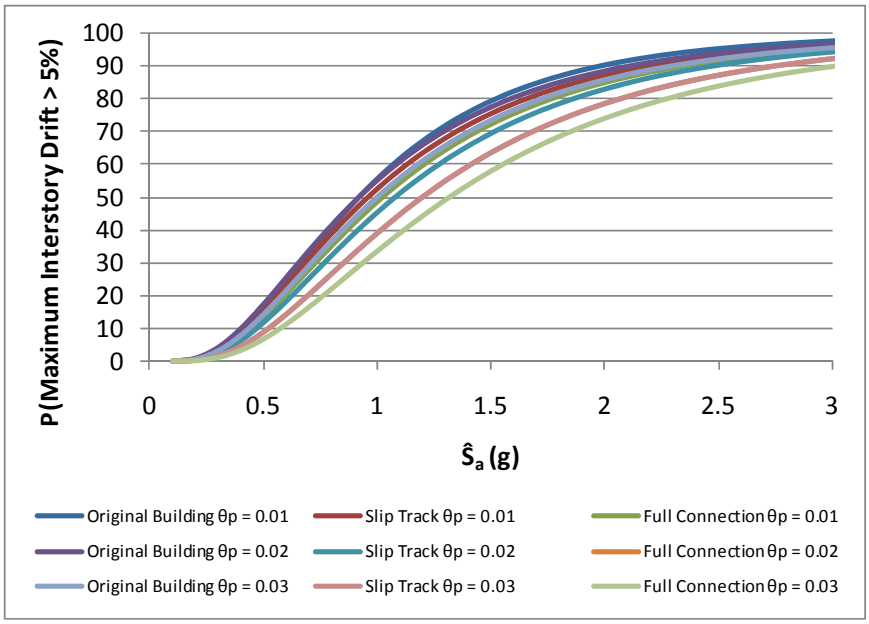

Figure 7.7 – Fragility Curve for Index Archetype Models

Because of the change in collapse performance for the models considering the response of nonstructural partition walls, it is recommended that further analyses that include each of the partition wall types considered in previous chapters be performed. Also, it is recommended that shear behavior of the partition walls be considered in buildings with different characteristics. Some of these could include taller buildings, buildings using reinforced concrete as the lateral force-resisting system, and building models that consider in-plane and perpendicular partition wall behavior. Lastly, further analysis describing the impact of equivalent viscous damping on collapse performance would be beneficial.

Chapter 8
CONCLUSIONS AND RECOMMENDATIONS FOR FUTURE RESEARCH

The work contained in this report focused on developing analysis tools for modeling the mechanical behavior of nonstructural partition walls common to commercial and institutional construction. As part of the experimental phase of this research program, innovative designs to improve seismic fragility were also designed and tested. From the testing of full-scale partition wall specimens, an experimental seismic fragility database was developed for several wall configurations.

The purpose of the partition walls is architectural in nature. Partition walls are located during the planning process of the structure; they separate large open areas into smaller more useable spaces. Partition walls in general are nonstructural, and are not used to resist lateral or gravitational forces. Inter-story drifts and absolute floor accelerations are expected to be introduced into the partition wall system; however the structural frame is designed to resist these loads. The nonstructural partition walls analyzed in this report are constructed from cold-formed steel framing members and gypsum wallboard panels. Although this wall system is not considered a structural member, analysis has shown that a building's dynamic properties can be significantly affected when the force-displacement behavior of the wall is included as a component in the lateral force resistant system.

8.1 Summary of Experimental Study

The mechanical behavior of 50 partition walls was obtained from experiments conducted as part of the NEES Nonstructural Grand Challenge Project. The NEES-NGC project is a multi-year project funded by the National Science Foundation. This project will serve to enhance the seismic behavior of building systems through gaining a better understanding of the seismic fragility of nonstructural components and systems. The data for ceiling, piping, and partition wall subsystems, together, will be used to further the area of performance based earthquake engineering. The partition wall systems considered in this report were designed in cooperation with the NEES-NGC Practice Committee and Advisory Board, and members of the University at Buffalo's experimental team. The walls were constructed on the University at Buffalo's Nonstructural Components Simulator (UB-NCS). The walls were built using 22 different

configurations with designs ranging from practical commonplace construction techniques to new innovative walls systems. A minimum of three specimens were tested per configuration unless data for two different configurations showed similar behavior.

Sixteen of the 22 configurations, coinciding with 36 of the 50 specimens, were constructed so lateral forces run parallel to the long direction of the wall. Because in-plane wall systems are primarily displacement sensitive, only four of the configurations were tested using a dynamic test protocol developed by Retamales et al. (2008) specifically for testing distributed acceleration/displacement sensitive nonstructural components and systems. The remaining specimens were tested using a quasi-static test protocol compatible with the dynamic one.

The 14 test specimens that were tested out-of-plane make up the remaining six configurations. Each of these configurations was tested using the dynamic protocol. This protocol is used when a system is sensitive to both absolute floor accelerations and inter-story drifts. Displacements and accelerations are applied in this case perpendicular to the wall system.

Wall configurations included in the partition wall test plan included: framing material thickness, connection methods, attached masses for dynamic tests, end of wall construction methods, and partial height walls. The different framing thicknesses used in this study are representative of commercial and institutional constructions. The connection details used in the testing encompass the most common techniques currently in practice; other details were developed to improve the seismic fragility of partition walls constructed using methods described herein. The key difference in connections of different configurations are lack of connection of studs or gypsum panels to the top track, or shorter walls stabilized by diagonal braces attached to the top of the wall and floor slab above. Tests were conducted using a dynamic protocol developed for the NCS to capture the effect of high floor accelerations after damage is caused by high inter-story drifts. For wall systems that were not acceleration sensitive, a quasi-static protocol was used for testing.

Damage observations that were conducted throughout the test protocol were used to continuously determine damage progression in the specimens and were done visually and through time stamped high definition video cameras. The walls that were subjected to the quasi-static loading protocol were inspected at increasing levels of drift. Photographs and notes were taken at these intervals. The dynamic tests were more difficult to monitor damage progression because of high accelerations, distance of the camera to the specimen, and the quickness at which damage occurred; for those damage states that were obvious, the time was calculated from the time stamp on the film and an approximate drift level of occurrence was determined.

8.2 Seismic Fragility Database

The partition wall configurations developed during the experimental testing phase are separated into four unique groups for fragility analysis. The observed damage in the partition walls is graded based on the level of required repairing; these damage states (DS_1, DS_2, and DS_3), are, respectively, associated with cosmetic repairs, partial component replacement, and complete wall removal.

Overall observations on the seismic fragility demonstrate comparable standard deviations for all partition wall configurations. For groups with high deviations, this result corresponds to the experimental observations for the same wall systems. Damage in commercial construction partition walls was observed to occur at lower drift ratios when directly compared to institutional construction walls. Whereas the innovative design configurations experienced DS_1 at similar drifts as common partition walls, the higher damage states were either shifted to higher drifts or completely eliminated.

8.3 Experimentally Calibrated Hysteretic Model

The force-displacement curves for the thirty-six in-plane specimens were fitted using best fit regression techniques. The nonlinear Wayne Stewart hysteretic model available in the nonlinear time history software RUAUMOKO was parameterized to each of the wall specimen hysteresis curves. This model was originally developed to model wood framed shear walls with structural sheathing; the key elements of the model include tri-linear backbone behavior, stiffness and strength degradation, and pinching. Because the partition walls are constructed in a similar manner to the wood framed shear walls, similar behaviors were observed. Hence, by utilizing the Wayne Stewart hysteretic model to simulate the wall response, good fits were obtained.

In order to have a larger bin of fit parameters, the positive and negative drift hysteretic behaviors were analyzed independently. Required parameters for the Wayne Stewart model include: stiffness (pre-yield, post-yield, post capping, and unloading), strength (yield, capping, and intercept), and pinching and softening factors. The tri-linear backbone of the model was fit to the backbone of the cyclic behavior using least squares regression. Unloading stiffness and intercept force were fit by filtering the data and determining the median value. The pinching and softening factors were determined through a parametric analysis.

The parameters for similar wall configurations, divided according to the six in-plane wall groups also used for the seismic fragility assessment, were statistically analyzed. A total of six values for each of the

hysteretic parameters were determined for the partition walls. These groups were commercial slip track, commercial full connection, institutional slip track, institutional full connection, partial height, and improved details. The mechanical behavior of the partial height and improved details partition wall configurations were similar and experienced very low energy dissipation due primarily to the low lateral strength capacity of the wall systems. The configuration with the next higher strength capacity included commercial slip track partition walls. This group includes all wall configurations that have no connection from the stud or gypsum panel to the top track and use 25 gauge steel framing material. The behavior of the commercial full connection (i.e., gypsum and/or 25 gauge steel stud attached to the top track) and institutional slip track (same as commercial construction details with steel framing material of 20 gauge thickness) walls were similar but analyzed individually. The partition wall system with the highest strength capacity and energy dissipation was the institutional full connection. This group considered wall systems constructed using 20 gauge steel framing and included a connection of each of the stud flanges to the top and bottom tracks and a connection of the gypsum to both top and bottom tracks.

8.4 Summary of Dynamic Analyses

The parameterized hysteretic models obtained from the results of the partition walls tested for the NEES-NGC were applied to a test model. This test model was developed from the design of an existing four story medical facility in southern California. The building design incorporates four wide flange steel moment frames to resist lateral force. The nonlinear hysteretic model simulating the nonstructural partition walls was applied to the structure using shear spring elements. The strength and stiffness parameters of the shear spring were linearly scaled from experimental data.

The models were subjected to three earthquake ground motions in order to analyze the effect of the nonstructural partition walls on the dynamic properties and the seismic response of the building. The three earthquake ground motions were chosen arbitrarily. Each of the building models were subjected to the Design Earthquake (DE) ground motion and to the Maximum Considered Earthquake (MCE).

The structural models showed a decrease in the natural period of vibration and an increase in the damping ratio when the partition walls are included. An eigenvalue analysis on the models returned a reduction in the natural period of 1% (approximately) for the models including the partial height and improved details partition walls, and varied depending on the stiffness of the wall systems, to over 11% for the institutional full connection partition walls. The equivalent damping ratios obtained from the logarithmic decrement increased from 2.26 for the original building model to 3.22 for the building model that included the behavior of the institutional full connection walls.

The addition of the nonstructural partition walls to the test structure showed significant effects to the lateral building drift and acceleration responses. Including partition walls generally reduced the inter-story drift levels, but this did not always correspond to a reduction in the maximum inter-story drifts. The most significant effect on the lateral response of the structure is in the maximum absolute top floor and individual floor accelerations, which were shown to decrease in each of the ground motions considered.

8.5 Summary of FEMA P695 Based Collapse Probability Analysis

Current earthquake design provisions use Seismic Performance Factors (SPFs) to reduce design forces in order to achieve economical structures provided with adequate ductility. SPFs are chosen from observations on different systems after seismic events, material behavior, and research. The values chosen for these factors have direct correlation to the cost of a building system and can therefore potentially affect individual building industries. In an effort to simplify this procedure and determine a "closed form solution" to the problem of selecting these highly contentious factors, the FEMA P695 document has proposed a methodology. The proposed methodology can be used to assess current SPFs and to assign SPFs for new structural systems. Design requirements, test data, modeling tools, and a suite of ground motions are used to make SPFs assignments.

The application of this SPF methodology, as it relates the study of this report, has no direct relation to the methodology's primary goals. A non-direct use of the methodology, however, can be found in the following quote taken from FEMA P695, p.11-12:

> "The methodology could be used to investigate the importance of … certain nonstructural components to collapse performance, and investigate the feasibility of enhancing current seismic design requirements to more appropriately incorporate these systems in the seismic design process. This would include accounting for both the possible beneficial and detrimental effect of these systems on collapse performance. Comparisons of collapse results for archetypical models both with and without selected … [nonstructural] components could be made to quantify the results."

To clarify, it is possible to determine the effect of nonstructural components on the collapse performance of a structure by studying building models that are similar but that do and do not include nonstructural component interaction. Utilizing this idea, three models were chosen for analysis. These models include the original unmodified building (i.e., partition wall shear springs not included), commercial slip track, and institutional full connection. It is expected that these models generated an accurate spectrum of

collapse performance of the test structure with and without partition walls.

Because steel frame members in the original building model were assigned bilinear properties, it was necessary to incorporate a failure mechanism into the existing elements in the model. Three individual models from each of the models already mentioned, making nine in total, were developed. Variations in these models were based on strength reduction at plastic rotations of 0.01, 0.02, and 0.03 radians and associated to ductility ratios through plastic hinge lengths of the individual elements.

Results were determined through conducting an incremental dynamic analysis and assigning collapse to occur at a drift ratio of 5% (prevention against collapse drift level according to FEMA 356 performance based design standards). The results from the FEMA P695 based analysis showed that including the partition wall behavior as an element in the lateral force-resisting system does improve collapse performance in some cases by increasing the median collapse spectral acceleration up to 32%.

8.6 Further Research Needs and Summary

The research discussed in this report has improved the understanding of nonstructural partition walls, namely the mechanical behavior and the effect of the walls on the lateral response of a structural model, and for each of these topics further research is needed. Following is a list of possible areas for further study:

Study: Test individual configurations of shorter and longer lengths

Reason: Develop parameters for configurations based on wall lengths. In this study stiffnesses and strengths were assumed linear; this assumption, although helping to demonstrate general response trends, is an oversimplification on the combined length of wall systems. Knowing the change in behavior for longer wall systems will return more accurate behavior.

Study: Develop a test plan to study the response of partition walls with and without openings.

Reason: Common to commercial buildings, independent of use, are long passageways. These passageways include openings to allow for access to individual spaces. Determining the effect of openings on the hysteretic behavior of partition walls is the key to ensure accuracy in modeling.

Study: Test the same wall configurations using different protocols.

Reason: Research has shown that the response of a system can be affected significantly depending on the protocol used for testing (i.e., CUREE vs. Sequential Phased Displacement).

Study: Analyze the lateral behavior of a wider sample of test model structures.

Reason: Lateral response and collapse performance are dependent on the construction material, failure mechanisms, and building plans. Adjusting any one of these parameters could potentially demonstrate different behaviors and responses.

Study: Develop modeling tools to simulate the mechanical behavior of out-of-plane nonstructural partition walls.

Reason: Although the experimental program analyzed the seismic fragility of out-of-plane walls only in-plane partition walls were parameterized for modeling. These walls are acceleration sensitive; being able to re-simulate their dynamic behavior will help aid in understanding the effects on absolute floor accelerations and drift ratios.

Study: Determine correct equivalent damping ratio when including partition wall behavior in structural model and effect of equivalent damping on collapse performance according to the FEMA P695 methodology procedures.

Reason: Rayleigh damping was 2% for each of the building models used in the analyses, this value may be conservative when including partition walls. The increase in collapse performance of 32% was surprising, preliminary analyses using increased damping in the original building model were conducted and showed an increase in collapse performance; clarification on correct damping assignment could be critical in correctly characterizing later system behavior.

The work included in this report significantly enhances the understanding of the seismic behavior of nonstructural steel cold-formed gypsum partition walls. The comprehensive test plan that included 50 full scale partition walls, constructed and tested to both quasi-static and dynamic protocols developed for the UB-NCS, generated data regarding partition wall in-plane and out-of-plane seismic behavior and seismic fragility. Dynamic analyses that included the mechanical behavior of steel stud gypsum partition walls in the structural frame of a four-story steel moment resistant test model demonstrated a decrease in

maximum absolute floor accelerations. In one of the first applications of the FEMA P695 methodology procedure on nonstructural components, the inclusion of nonstructural components was shown to significantly improve the collapse performance the test model. These findings reiterate the need for the valuable research that is being conducted as part of the NEES-NGC project, and the need for reevaluating the influence of common nonstructural steel stud gypsum partition wall configurations on the seismic response of commercial and institutional structures.

Finally, despite the improved collapsed performance provided by cold-formed gypsum partition walls, designers of lateral force-resisting systems should remain cautious about relying on nonstructural components for system performance. This is because during the life of a structure, it is likely that these nonstructural components and elements of the building will be altered without further structural analysis.

Chapter 9
REFERENCES

ASCE 7-05. (2006). *Minimum Design Loads for Buildings and Other Structures.* Reston: Amercian Society of Civil Engineers.

ASTM. (2003). *ASTM A370 2003 Standar Test Methods and Definitions for Mechanical Testing of Steel Products.* American Society of Testing Materials.

ASTM. (2007). *ASTM C754-07 Standard specification for installation of steel framing members to receive screw-attached gypsum panel products.* American Society of Testing Materials.

ASTM. (1997). *ASTM E1049-85 (R1997) Standard practices for cycle counting in fatique analysis.* American Society of Testing Materials.

Bersofsky, A. M. (2004). *A Seismic Performance Evaluation of Gypsum Wallboard Partitions.* San Diego: University of California San Deigo.

Bonowitz, D., Durkin, M., Gates, W., Morden, M., & Youssef, N. (1995). *Surveys and Assessment of Damage to Buildings Affected by the Northridge Earthquake of January 17, 1994, Technical Report SAC95-06.* Sacramento, CA: SAC Joint Venture.

Bracci, J. M., Reinhorn, A. M., & Mander, J. B. (1992). *Seismic Resistance of Reinforced Concrete Frame Structures Designed Only for Gravity Loads: Part I/Design and Properties of a One/Third Scale Model Structure. Technical Report NCEER-92-0027.* Buffalo, NY: National Center for Earthquake Engineering Research, Universtiy at Buffalo, State University of New York.

Carr, A. J. (2005). *Computer Program RUAUMOKO.* Canterbury: Dept. of Civil Engineering, University of Canterbury.

FEMA. (2000). *FEMA 350: Recommended Seismic Design Criteria for New Steel Moment-Frame Buildings.* Washington D.C.: Federal Emergency Management Agency (FEMA).

FEMA. (2000). *FEMA 356: Prestandard and Commentary for the Seismic Rehabilitation of Buildings.* Washington D.C.: Federal Emergency Management Agency (FEMA).

FEMA. (2006). *FEMA 461: Interim Protocols for Determining Seismic Performance Characteristics of Structural and Nonstructural Components through Laboratory Testing.* Washington D.C.: Federal Emergency Management Agency (FEMA).

FEMA. (2009). *FEMA P695: Quantification of Building Seismic Performance Factors,* prepared by the Applied Technology Council *(ATC).* Washington, D.C.: Federal Emergency Management Council (FEMA).

Gad, E. F., Chandler, A. M., & Duffield, C. F. (2001). Modal Analysis of Steel-Framed Residential Structures for Application to Seismic Design. *Journal of Vibration and Control, 7*, 91-111.

Gad, E. F., Duffield, C. F., Stark, G., & Pham, L. (1995). Contribution of Non-structural Components to the Dynamic Performance of Domestic Steel Framed Structures. *Proceedings Pacific Conference on Earthquake Engineering*, (pp. 177-186). Melbourne.

ICC-ES. (2007). *AC156: Acceptance criteria for seismic qualification by shake-table testing of nonstructural components and systems.* International Code Council Evaluation Service.

Krawinkler, H., Parisi, F., Ibarra, L., Ayoub, A., & Medina, R. (2001). *Development of a Testing Protocol for Woodframe Structures, CUREE-Caltech Woodframe Project, CUREE Publication No. W-02.* Richmond: Constortium of Universities for Reasearch in Earthquake Engineering.

Lang, A. F., & Restrepo, J. I. (2005). *Performance Evaluation of Gypsum Wallboard Partitions.* Berkeley: Pacific Earthquake Engineering Research Center (PEER).

Lee-Hyung, L., Kato, M., Matsumiya, T., Suita, K., & Nakashima, M. (2007). Seismic Performance Evaluation of Non-structural Components. *Earthquake Engineering and Structural Dynamics , 36*, 367-382.

Li, B., Hutchinson, G. L., & Duffield, C. F. (2009). The Influence of Non-structural Components on Tall Building Stiffness. *The Structural Design of Tall and Special Buildings*, online; in print Vol. 20, Issue 7, pages 853–870, November 2011.

Memari, A. M., Kasal, B., Manbeck, H. B., & Adams, A. R. (2008). *Experimental Cyclic Racking Evaluation of Light-frame Wood Stud and Steel Stud WAll Systems.* University Park: The Pennsylvania Housing Research Center.

Mosqueda, G., Retamales, R., Filiatrault, A., & Reinhorn, A. (2008). Testing Facility for Experimental Evaluation of Nonstructural Components under Full-Scall Floor Motions. *Journal of Structural Design of Tall and Special Buildings*, online; in print:Volume 18, Issue 4, pages 387–404, June 2009.

Porter, K., Kennedy, R., & Bachman, R. (2007). Creating Fragility Functions for Performance-Based Earthquake Engineering. *Earthquake Spectra , 23* (2), 471-489.

Retamales, R., Mosqueda, G., Filiatrault, A., & Reinhorn, A. (2008). *New Experimental Capabilities and Loading Protocols for Seismic Qualification and Fragility Assessment of Nonstructural Components.* Buffalo: Technical Report MCEER-08-0026, MCEER, University at Buffalo, State University of New York.

Serrette, R. L., Encalada, J., Juadines, M., & Nguyen, H. (1997). Static Racking Behavior of Plywood, OSB, Gypsum, and Fiberbond Walls with Metal Framing. *Journal of Structural Engineering, 123* (8), 1079-1086.

SSMA. (2001). *Product technical information. ICBO ER-4943P.* Steel Stud Manufacturers Association.

Stewart, W. G. (1987). *The Seismic Design of Plywood Sheathed Shearwalls, Ph.D. Thesis.* Christchurch: Department of Civil Engineering, University of Canterbury.

Su, R. K., & Chandler, A. M. (2005). Influence of Non-structural Components on Lateral Stiffness of Tall Buildings. *The Structural Design of Tall and Special Buildings , 14*, 143-164.

Taghavi, S., & Miranda, E. (2003). *Response Assessment of Nonstructural Building Elements.* Berkeley: Pacific Earthquake Engineering Research Center (PEER).

Wanitkorkul, A., & Filiatrault, A. (2005). *Simulation of Strong Ground Motions for Seismic Fragility Evaluation of Nonstructural Components in Hospitals, Technical Report MCEER-05-0005.* Buffal: Multidisciplinary Center for Earthquake Engineering Research, University at Buffalo, State University of New York.

Whittaker, A. S., & Soong, T. T. (n.d.). *Applied Technology Council.* Retrieved December 9, 2009, from Applied Technology Council: http://www.atcouncil.org/pdfs/Whittaker.pdf

Wilcoski, J., & Gambil, J. B. (1997). *The CERL Equipment Fragility and Protection Procedure (CEFAPP), USACERL technical report 97/58.* Chanmpaign, IL: U.S. Army Corps of Engineers.

Yuan, Y. T., Whittaker, A. S., & Bruneau, M. (2002). *MCEER Publications*. Retrieved September 2009, from University at Buffalo, State University of New York: http://mceer.buffalo.edu/publications/resaccom/02-sp09/pdfs_screen/15_yang2.pdf.

MCEER Technical Reports

MCEER publishes technical reports on a variety of subjects written by authors funded through MCEER. These reports are available from both MCEER Publications and the National Technical Information Service (NTIS). Requests for reports should be directed to MCEER Publications, MCEER, University at Buffalo, State University of New York, 133A Ketter Hall, Buffalo, New York 14260. Reports can also be requested through NTIS, P.O. Box 1425, Springfield, Virginia 22151. NTIS accession numbers are shown in parenthesis, if available.

NCEER-87-0001 "First-Year Program in Research, Education and Technology Transfer," 3/5/87, (PB88-134275, A04, MF-A01).

NCEER-87-0002 "Experimental Evaluation of Instantaneous Optimal Algorithms for Structural Control," by R.C. Lin, T.T. Soong and A.M. Reinhorn, 4/20/87, (PB88-134341, A04, MF-A01).

NCEER-87-0003 "Experimentation Using the Earthquake Simulation Facilities at University at Buffalo," by A.M. Reinhorn and R.L. Ketter, to be published.

NCEER-87-0004 "The System Characteristics and Performance of a Shaking Table," by J.S. Hwang, K.C. Chang and G.C. Lee, 6/1/87, (PB88-134259, A03, MF-A01). This report is available only through NTIS (see address given above).

NCEER-87-0005 "A Finite Element Formulation for Nonlinear Viscoplastic Material Using a Q Model," by O. Gyebi and G. Dasgupta, 11/2/87, (PB88-213764, A08, MF-A01).

NCEER-87-0006 "Symbolic Manipulation Program (SMP) - Algebraic Codes for Two and Three Dimensional Finite Element Formulations," by X. Lee and G. Dasgupta, 11/9/87, (PB88-218522, A05, MF-A01).

NCEER-87-0007 "Instantaneous Optimal Control Laws for Tall Buildings Under Seismic Excitations," by J.N. Yang, A. Akbarpour and P. Ghaemmaghami, 6/10/87, (PB88-134333, A06, MF-A01). This report is only available through NTIS (see address given above).

NCEER-87-0008 "IDARC: Inelastic Damage Analysis of Reinforced Concrete Frame - Shear-Wall Structures," by Y.J. Park, A.M. Reinhorn and S.K. Kunnath, 7/20/87, (PB88-134325, A09, MF-A01). This report is only available through NTIS (see address given above).

NCEER-87-0009 "Liquefaction Potential for New York State: A Preliminary Report on Sites in Manhattan and Buffalo," by M. Budhu, V. Vijayakumar, R.F. Giese and L. Baumgras, 8/31/87, (PB88-163704, A03, MF-A01). This report is available only through NTIS (see address given above).

NCEER-87-0010 "Vertical and Torsional Vibration of Foundations in Inhomogeneous Media," by A.S. Veletsos and K.W. Dotson, 6/1/87, (PB88-134291, A03, MF-A01). This report is only available through NTIS (see address given above).

NCEER-87-0011 "Seismic Probabilistic Risk Assessment and Seismic Margins Studies for Nuclear Power Plants," by Howard H.M. Hwang, 6/15/87, (PB88-134267, A03, MF-A01). This report is only available through NTIS (see address given above).

NCEER-87-0012 "Parametric Studies of Frequency Response of Secondary Systems Under Ground-Acceleration Excitations," by Y. Yong and Y.K. Lin, 6/10/87, (PB88-134309, A03, MF-A01). This report is only available through NTIS (see address given above).

NCEER-87-0013 "Frequency Response of Secondary Systems Under Seismic Excitation," by J.A. HoLung, J. Cai and Y.K. Lin, 7/31/87, (PB88-134317, A05, MF-A01). This report is only available through NTIS (see address given above).

NCEER-87-0014 "Modelling Earthquake Ground Motions in Seismically Active Regions Using Parametric Time Series Methods," by G.W. Ellis and A.S. Cakmak, 8/25/87, (PB88-134283, A08, MF-A01). This report is only available through NTIS (see address given above).

NCEER-87-0015 "Detection and Assessment of Seismic Structural Damage," by E. DiPasquale and A.S. Cakmak, 8/25/87, (PB88-163712, A05, MF-A01). This report is only available through NTIS (see address given above).

NCEER-87-0016 "Pipeline Experiment at Parkfield, California," by J. Isenberg and E. Richardson, 9/15/87, (PB88-163720, A03, MF-A01). This report is available only through NTIS (see address given above).

NCEER-87-0017 "Digital Simulation of Seismic Ground Motion," by M. Shinozuka, G. Deodatis and T. Harada, 8/31/87, (PB88-155197, A04, MF-A01). This report is available only through NTIS (see address given above).

NCEER-87-0018 "Practical Considerations for Structural Control: System Uncertainty, System Time Delay and Truncation of Small Control Forces," J.N. Yang and A. Akbarpour, 8/10/87, (PB88-163738, A08, MF-A01). This report is only available through NTIS (see address given above).

NCEER-87-0019 "Modal Analysis of Nonclassically Damped Structural Systems Using Canonical Transformation," by J.N. Yang, S. Sarkani and F.X. Long, 9/27/87, (PB88-187851, A04, MF-A01).

NCEER-87-0020 "A Nonstationary Solution in Random Vibration Theory," by J.R. Red-Horse and P.D. Spanos, 11/3/87, (PB88-163746, A03, MF-A01).

NCEER-87-0021 "Horizontal Impedances for Radially Inhomogeneous Viscoelastic Soil Layers," by A.S. Veletsos and K.W. Dotson, 10/15/87, (PB88-150859, A04, MF-A01).

NCEER-87-0022 "Seismic Damage Assessment of Reinforced Concrete Members," by Y.S. Chung, C. Meyer and M. Shinozuka, 10/9/87, (PB88-150867, A05, MF-A01). This report is available only through NTIS (see address given above).

NCEER-87-0023 "Active Structural Control in Civil Engineering," by T.T. Soong, 11/11/87, (PB88-187778, A03, MF-A01).

NCEER-87-0024 "Vertical and Torsional Impedances for Radially Inhomogeneous Viscoelastic Soil Layers," by K.W. Dotson and A.S. Veletsos, 12/87, (PB88-187786, A03, MF-A01).

NCEER-87-0025 "Proceedings from the Symposium on Seismic Hazards, Ground Motions, Soil-Liquefaction and Engineering Practice in Eastern North America," October 20-22, 1987, edited by K.H. Jacob, 12/87, (PB88-188115, A23, MF-A01). This report is available only through NTIS (see address given above).

NCEER-87-0026 "Report on the Whittier-Narrows, California, Earthquake of October 1, 1987," by J. Pantelic and A. Reinhorn, 11/87, (PB88-187752, A03, MF-A01). This report is available only through NTIS (see address given above).

NCEER-87-0027 "Design of a Modular Program for Transient Nonlinear Analysis of Large 3-D Building Structures," by S. Srivastav and J.F. Abel, 12/30/87, (PB88-187950, A05, MF-A01). This report is only available through NTIS (see address given above).

NCEER-87-0028 "Second-Year Program in Research, Education and Technology Transfer," 3/8/88, (PB88-219480, A04, MF-A01).

NCEER-88-0001 "Workshop on Seismic Computer Analysis and Design of Buildings With Interactive Graphics," by W. McGuire, J.F. Abel and C.H. Conley, 1/18/88, (PB88-187760, A03, MF-A01). This report is only available through NTIS (see address given above).

NCEER-88-0002 "Optimal Control of Nonlinear Flexible Structures," by J.N. Yang, F.X. Long and D. Wong, 1/22/88, (PB88-213772, A06, MF-A01).

NCEER-88-0003 "Substructuring Techniques in the Time Domain for Primary-Secondary Structural Systems," by G.D. Manolis and G. Juhn, 2/10/88, (PB88-213780, A04, MF-A01).

NCEER-88-0004 "Iterative Seismic Analysis of Primary-Secondary Systems," by A. Singhal, L.D. Lutes and P.D. Spanos, 2/23/88, (PB88-213798, A04, MF-A01).

NCEER-88-0005 "Stochastic Finite Element Expansion for Random Media," by P.D. Spanos and R. Ghanem, 3/14/88, (PB88-213806, A03, MF-A01).

NCEER-88-0006 "Combining Structural Optimization and Structural Control," by F.Y. Cheng and C.P. Pantelides, 1/10/88, (PB88-213814, A05, MF-A01).

NCEER-88-0007 "Seismic Performance Assessment of Code-Designed Structures," by H.H-M. Hwang, J-W. Jaw and H-J. Shau, 3/20/88, (PB88-219423, A04, MF-A01). This report is only available through NTIS (see address given above).

NCEER-88-0008 "Reliability Analysis of Code-Designed Structures Under Natural Hazards," by H.H-M. Hwang, H. Ushiba and M. Shinozuka, 2/29/88, (PB88-229471, A07, MF-A01). This report is only available through NTIS (see address given above).

NCEER-88-0009 "Seismic Fragility Analysis of Shear Wall Structures," by J-W Jaw and H.H-M. Hwang, 4/30/88, (PB89-102867, A04, MF-A01).

NCEER-88-0010 "Base Isolation of a Multi-Story Building Under a Harmonic Ground Motion - A Comparison of Performances of Various Systems," by F-G Fan, G. Ahmadi and I.G. Tadjbakhsh, 5/18/88, (PB89-122238, A06, MF-A01). This report is only available through NTIS (see address given above).

NCEER-88-0011 "Seismic Floor Response Spectra for a Combined System by Green's Functions," by F.M. Lavelle, L.A. Bergman and P.D. Spanos, 5/1/88, (PB89-102875, A03, MF-A01).

NCEER-88-0012 "A New Solution Technique for Randomly Excited Hysteretic Structures," by G.Q. Cai and Y.K. Lin, 5/16/88, (PB89-102883, A03, MF-A01).

NCEER-88-0013 "A Study of Radiation Damping and Soil-Structure Interaction Effects in the Centrifuge," by K. Weissman, supervised by J.H. Prevost, 5/24/88, (PB89-144703, A06, MF-A01).

NCEER-88-0014 "Parameter Identification and Implementation of a Kinematic Plasticity Model for Frictional Soils," by J.H. Prevost and D.V. Griffiths, to be published.

NCEER-88-0015 "Two- and Three- Dimensional Dynamic Finite Element Analyses of the Long Valley Dam," by D.V. Griffiths and J.H. Prevost, 6/17/88, (PB89-144711, A04, MF-A01).

NCEER-88-0016 "Damage Assessment of Reinforced Concrete Structures in Eastern United States," by A.M. Reinhorn, M.J. Seidel, S.K. Kunnath and Y.J. Park, 6/15/88, (PB89-122220, A04, MF-A01). This report is only available through NTIS (see address given above).

NCEER-88-0017 "Dynamic Compliance of Vertically Loaded Strip Foundations in Multilayered Viscoelastic Soils," by S. Ahmad and A.S.M. Israil, 6/17/88, (PB89-102891, A04, MF-A01).

NCEER-88-0018 "An Experimental Study of Seismic Structural Response With Added Viscoelastic Dampers," by R.C. Lin, Z. Liang, T.T. Soong and R.H. Zhang, 6/30/88, (PB89-122212, A05, MF-A01). This report is available only through NTIS (see address given above).

NCEER-88-0019 "Experimental Investigation of Primary - Secondary System Interaction," by G.D. Manolis, G. Juhn and A.M. Reinhorn, 5/27/88, (PB89-122204, A04, MF-A01).

NCEER-88-0020 "A Response Spectrum Approach For Analysis of Nonclassically Damped Structures," by J.N. Yang, S. Sarkani and F.X. Long, 4/22/88, (PB89-102909, A04, MF-A01).

NCEER-88-0021 "Seismic Interaction of Structures and Soils: Stochastic Approach," by A.S. Veletsos and A.M. Prasad, 7/21/88, (PB89-122196, A04, MF-A01). This report is only available through NTIS (see address given above).

NCEER-88-0022 "Identification of the Serviceability Limit State and Detection of Seismic Structural Damage," by E. DiPasquale and A.S. Cakmak, 6/15/88, (PB89-122188, A05, MF-A01). This report is available only through NTIS (see address given above).

NCEER-88-0023 "Multi-Hazard Risk Analysis: Case of a Simple Offshore Structure," by B.K. Bhartia and E.H. Vanmarcke, 7/21/88, (PB89-145213, A05, MF-A01).

NCEER-88-0024 "Automated Seismic Design of Reinforced Concrete Buildings," by Y.S. Chung, C. Meyer and M. Shinozuka, 7/5/88, (PB89-122170, A06, MF-A01). This report is available only through NTIS (see address given above).

NCEER-88-0025 "Experimental Study of Active Control of MDOF Structures Under Seismic Excitations," by L.L. Chung, R.C. Lin, T.T. Soong and A.M. Reinhorn, 7/10/88, (PB89-122600, A04, MF-A01).

NCEER-88-0026 "Earthquake Simulation Tests of a Low-Rise Metal Structure," by J.S. Hwang, K.C. Chang, G.C. Lee and R.L. Ketter, 8/1/88, (PB89-102917, A04, MF-A01).

NCEER-88-0027 "Systems Study of Urban Response and Reconstruction Due to Catastrophic Earthquakes," by F. Kozin and H.K. Zhou, 9/22/88, (PB90-162348, A04, MF-A01).

NCEER-88-0028 "Seismic Fragility Analysis of Plane Frame Structures," by H.H-M. Hwang and Y.K. Low, 7/31/88, (PB89-131445, A06, MF-A01).

NCEER-88-0029 "Response Analysis of Stochastic Structures," by A. Kardara, C. Bucher and M. Shinozuka, 9/22/88, (PB89-174429, A04, MF-A01).

NCEER-88-0030 "Nonnormal Accelerations Due to Yielding in a Primary Structure," by D.C.K. Chen and L.D. Lutes, 9/19/88, (PB89-131437, A04, MF-A01).

NCEER-88-0031 "Design Approaches for Soil-Structure Interaction," by A.S. Veletsos, A.M. Prasad and Y. Tang, 12/30/88, (PB89-174437, A03, MF-A01). This report is available only through NTIS (see address given above).

NCEER-88-0032 "A Re-evaluation of Design Spectra for Seismic Damage Control," by C.J. Turkstra and A.G. Tallin, 11/7/88, (PB89-145221, A05, MF-A01).

NCEER-88-0033 "The Behavior and Design of Noncontact Lap Splices Subjected to Repeated Inelastic Tensile Loading," by V.E. Sagan, P. Gergely and R.N. White, 12/8/88, (PB89-163737, A08, MF-A01).

NCEER-88-0034 "Seismic Response of Pile Foundations," by S.M. Mamoon, P.K. Banerjee and S. Ahmad, 11/1/88, (PB89-145239, A04, MF-A01).

NCEER-88-0035 "Modeling of R/C Building Structures With Flexible Floor Diaphragms (IDARC2)," by A.M. Reinhorn, S.K. Kunnath and N. Panahshahi, 9/7/88, (PB89-207153, A07, MF-A01).

NCEER-88-0036 "Solution of the Dam-Reservoir Interaction Problem Using a Combination of FEM, BEM with Particular Integrals, Modal Analysis, and Substructuring," by C-S. Tsai, G.C. Lee and R.L. Ketter, 12/31/88, (PB89-207146, A04, MF-A01).

NCEER-88-0037 "Optimal Placement of Actuators for Structural Control," by F.Y. Cheng and C.P. Pantelides, 8/15/88, (PB89-162846, A05, MF-A01).

NCEER-88-0038 "Teflon Bearings in Aseismic Base Isolation: Experimental Studies and Mathematical Modeling," by A. Mokha, M.C. Constantinou and A.M. Reinhorn, 12/5/88, (PB89-218457, A10, MF-A01). This report is available only through NTIS (see address given above).

NCEER-88-0039 "Seismic Behavior of Flat Slab High-Rise Buildings in the New York City Area," by P. Weidlinger and M. Ettouney, 10/15/88, (PB90-145681, A04, MF-A01).

NCEER-88-0040 "Evaluation of the Earthquake Resistance of Existing Buildings in New York City," by P. Weidlinger and M. Ettouney, 10/15/88, to be published.

NCEER-88-0041 "Small-Scale Modeling Techniques for Reinforced Concrete Structures Subjected to Seismic Loads," by W. Kim, A. El-Attar and R.N. White, 11/22/88, (PB89-189625, A05, MF-A01).

NCEER-88-0042 "Modeling Strong Ground Motion from Multiple Event Earthquakes," by G.W. Ellis and A.S. Cakmak, 10/15/88, (PB89-174445, A03, MF-A01).

NCEER-88-0043 "Nonstationary Models of Seismic Ground Acceleration," by M. Grigoriu, S.E. Ruiz and E. Rosenblueth, 7/15/88, (PB89-189617, A04, MF-A01).

NCEER-88-0044 "SARCF User's Guide: Seismic Analysis of Reinforced Concrete Frames," by Y.S. Chung, C. Meyer and M. Shinozuka, 11/9/88, (PB89-174452, A08, MF-A01).

NCEER-88-0045 "First Expert Panel Meeting on Disaster Research and Planning," edited by J. Pantelic and J. Stoyle, 9/15/88, (PB89-174460, A05, MF-A01).

NCEER-88-0046 "Preliminary Studies of the Effect of Degrading Infill Walls on the Nonlinear Seismic Response of Steel Frames," by C.Z. Chrysostomou, P. Gergely and J.F. Abel, 12/19/88, (PB89-208383, A05, MF-A01).

NCEER-88-0047 "Reinforced Concrete Frame Component Testing Facility - Design, Construction, Instrumentation and Operation," by S.P. Pessiki, C. Conley, T. Bond, P. Gergely and R.N. White, 12/16/88, (PB89-174478, A04, MF-A01).

NCEER-89-0001 "Effects of Protective Cushion and Soil Compliancy on the Response of Equipment Within a Seismically Excited Building," by J.A. HoLung, 2/16/89, (PB89-207179, A04, MF-A01).

NCEER-89-0002 "Statistical Evaluation of Response Modification Factors for Reinforced Concrete Structures," by H.H-M. Hwang and J-W. Jaw, 2/17/89, (PB89-207187, A05, MF-A01).

NCEER-89-0003 "Hysteretic Columns Under Random Excitation," by G-Q. Cai and Y.K. Lin, 1/9/89, (PB89-196513, A03, MF-A01).

NCEER-89-0004 "Experimental Study of `Elephant Foot Bulge' Instability of Thin-Walled Metal Tanks," by Z-H. Jia and R.L. Ketter, 2/22/89, (PB89-207195, A03, MF-A01).

NCEER-89-0005 "Experiment on Performance of Buried Pipelines Across San Andreas Fault," by J. Isenberg, E. Richardson and T.D. O'Rourke, 3/10/89, (PB89-218440, A04, MF-A01). This report is available only through NTIS (see address given above).

NCEER-89-0006 "A Knowledge-Based Approach to Structural Design of Earthquake-Resistant Buildings," by M. Subramani, P. Gergely, C.H. Conley, J.F. Abel and A.H. Zaghw, 1/15/89, (PB89-218465, A06, MF-A01).

NCEER-89-0007 "Liquefaction Hazards and Their Effects on Buried Pipelines," by T.D. O'Rourke and P.A. Lane, 2/1/89, (PB89-218481, A09, MF-A01).

NCEER-89-0008 "Fundamentals of System Identification in Structural Dynamics," by H. Imai, C-B. Yun, O. Maruyama and M. Shinozuka, 1/26/89, (PB89-207211, A04, MF-A01).

NCEER-89-0009 "Effects of the 1985 Michoacan Earthquake on Water Systems and Other Buried Lifelines in Mexico," by A.G. Ayala and M.J. O'Rourke, 3/8/89, (PB89-207229, A06, MF-A01).

NCEER-89-R010 "NCEER Bibliography of Earthquake Education Materials," by K.E.K. Ross, Second Revision, 9/1/89, (PB90-125352, A05, MF-A01). This report is replaced by NCEER-92-0018.

NCEER-89-0011 "Inelastic Three-Dimensional Response Analysis of Reinforced Concrete Building Structures (IDARC-3D), Part I - Modeling," by S.K. Kunnath and A.M. Reinhorn, 4/17/89, (PB90-114612, A07, MF-A01). This report is available only through NTIS (see address given above).

NCEER-89-0012 "Recommended Modifications to ATC-14," by C.D. Poland and J.O. Malley, 4/12/89, (PB90-108648, A15, MF-A01).

NCEER-89-0013 "Repair and Strengthening of Beam-to-Column Connections Subjected to Earthquake Loading," by M. Corazao and A.J. Durrani, 2/28/89, (PB90-109885, A06, MF-A01).

NCEER-89-0014 "Program EXKAL2 for Identification of Structural Dynamic Systems," by O. Maruyama, C-B. Yun, M. Hoshiya and M. Shinozuka, 5/19/89, (PB90-109877, A09, MF-A01).

NCEER-89-0015 "Response of Frames With Bolted Semi-Rigid Connections, Part I - Experimental Study and Analytical Predictions," by P.J. DiCorso, A.M. Reinhorn, J.R. Dickerson, J.B. Radziminski and W.L. Harper, 6/1/89, to be published.

NCEER-89-0016 "ARMA Monte Carlo Simulation in Probabilistic Structural Analysis," by P.D. Spanos and M.P. Mignolet, 7/10/89, (PB90-109893, A03, MF-A01).

NCEER-89-P017 "Preliminary Proceedings from the Conference on Disaster Preparedness - The Place of Earthquake Education in Our Schools," Edited by K.E.K. Ross, 6/23/89, (PB90-108606, A03, MF-A01).

NCEER-89-0017 "Proceedings from the Conference on Disaster Preparedness - The Place of Earthquake Education in Our Schools," Edited by K.E.K. Ross, 12/31/89, (PB90-207895, A012, MF-A02). This report is available only through NTIS (see address given above).

NCEER-89-0018 "Multidimensional Models of Hysteretic Material Behavior for Vibration Analysis of Shape Memory Energy Absorbing Devices, by E.J. Graesser and F.A. Cozzarelli, 6/7/89, (PB90-164146, A04, MF-A01).

NCEER-89-0019 "Nonlinear Dynamic Analysis of Three-Dimensional Base Isolated Structures (3D-BASIS)," by S. Nagarajaiah, A.M. Reinhorn and M.C. Constantinou, 8/3/89, (PB90-161936, A06, MF-A01). This report has been replaced by NCEER-93-0011.

NCEER-89-0020 "Structural Control Considering Time-Rate of Control Forces and Control Rate Constraints," by F.Y. Cheng and C.P. Pantelides, 8/3/89, (PB90-120445, A04, MF-A01).

NCEER-89-0021 "Subsurface Conditions of Memphis and Shelby County," by K.W. Ng, T-S. Chang and H-H.M. Hwang, 7/26/89, (PB90-120437, A03, MF-A01).

NCEER-89-0022 "Seismic Wave Propagation Effects on Straight Jointed Buried Pipelines," by K. Elhmadi and M.J. O'Rourke, 8/24/89, (PB90-162322, A10, MF-A02).

NCEER-89-0023 "Workshop on Serviceability Analysis of Water Delivery Systems," edited by M. Grigoriu, 3/6/89, (PB90-127424, A03, MF-A01).

NCEER-89-0024 "Shaking Table Study of a 1/5 Scale Steel Frame Composed of Tapered Members," by K.C. Chang, J.S. Hwang and G.C. Lee, 9/18/89, (PB90-160169, A04, MF-A01).

NCEER-89-0025 "DYNA1D: A Computer Program for Nonlinear Seismic Site Response Analysis - Technical Documentation," by Jean H. Prevost, 9/14/89, (PB90-161944, A07, MF-A01). This report is available only through NTIS (see address given above).

NCEER-89-0026 "1:4 Scale Model Studies of Active Tendon Systems and Active Mass Dampers for Aseismic Protection," by A.M. Reinhorn, T.T. Soong, R.C. Lin, Y.P. Yang, Y. Fukao, H. Abe and M. Nakai, 9/15/89, (PB90-173246, A10, MF-A02). This report is available only through NTIS (see address given above).

NCEER-89-0027 "Scattering of Waves by Inclusions in a Nonhomogeneous Elastic Half Space Solved by Boundary Element Methods," by P.K. Hadley, A. Askar and A.S. Cakmak, 6/15/89, (PB90-145699, A07, MF-A01).

NCEER-89-0028 "Statistical Evaluation of Deflection Amplification Factors for Reinforced Concrete Structures," by H.H.M. Hwang, J-W. Jaw and A.L. Ch'ng, 8/31/89, (PB90-164633, A05, MF-A01).

NCEER-89-0029 "Bedrock Accelerations in Memphis Area Due to Large New Madrid Earthquakes," by H.H.M. Hwang, C.H.S. Chen and G. Yu, 11/7/89, (PB90-162330, A04, MF-A01).

NCEER-89-0030 "Seismic Behavior and Response Sensitivity of Secondary Structural Systems," by Y.Q. Chen and T.T. Soong, 10/23/89, (PB90-164658, A08, MF-A01).

NCEER-89-0031 "Random Vibration and Reliability Analysis of Primary-Secondary Structural Systems," by Y. Ibrahim, M. Grigoriu and T.T. Soong, 11/10/89, (PB90-161951, A04, MF-A01).

NCEER-89-0032 "Proceedings from the Second U.S. - Japan Workshop on Liquefaction, Large Ground Deformation and Their Effects on Lifelines, September 26-29, 1989," Edited by T.D. O'Rourke and M. Hamada, 12/1/89, (PB90-209388, A22, MF-A03).

NCEER-89-0033 "Deterministic Model for Seismic Damage Evaluation of Reinforced Concrete Structures," by J.M. Bracci, A.M. Reinhorn, J.B. Mander and S.K. Kunnath, 9/27/89, (PB91-108803, A06, MF-A01).

NCEER-89-0034 "On the Relation Between Local and Global Damage Indices," by E. DiPasquale and A.S. Cakmak, 8/15/89, (PB90-173865, A05, MF-A01).

NCEER-89-0035 "Cyclic Undrained Behavior of Nonplastic and Low Plasticity Silts," by A.J. Walker and H.E. Stewart, 7/26/89, (PB90-183518, A10, MF-A01).

NCEER-89-0036 "Liquefaction Potential of Surficial Deposits in the City of Buffalo, New York," by M. Budhu, R. Giese and L. Baumgrass, 1/17/89, (PB90-208455, A04, MF-A01).

NCEER-89-0037 "A Deterministic Assessment of Effects of Ground Motion Incoherence," by A.S. Veletsos and Y. Tang, 7/15/89, (PB90-164294, A03, MF-A01).

NCEER-89-0038 "Workshop on Ground Motion Parameters for Seismic Hazard Mapping," July 17-18, 1989, edited by R.V. Whitman, 12/1/89, (PB90-173923, A04, MF-A01).

NCEER-89-0039 "Seismic Effects on Elevated Transit Lines of the New York City Transit Authority," by C.J. Costantino, C.A. Miller and E. Heymsfield, 12/26/89, (PB90-207887, A06, MF-A01).

NCEER-89-0040 "Centrifugal Modeling of Dynamic Soil-Structure Interaction," by K. Weissman, Supervised by J.H. Prevost, 5/10/89, (PB90-207879, A07, MF-A01).

NCEER-89-0041 "Linearized Identification of Buildings With Cores for Seismic Vulnerability Assessment," by I-K. Ho and A.E. Aktan, 11/1/89, (PB90-251943, A07, MF-A01).

NCEER-90-0001 "Geotechnical and Lifeline Aspects of the October 17, 1989 Loma Prieta Earthquake in San Francisco," by T.D. O'Rourke, H.E. Stewart, F.T. Blackburn and T.S. Dickerman, 1/90, (PB90-208596, A05, MF-A01).

NCEER-90-0002 "Nonnormal Secondary Response Due to Yielding in a Primary Structure," by D.C.K. Chen and L.D. Lutes, 2/28/90, (PB90-251976, A07, MF-A01).

NCEER-90-0003 "Earthquake Education Materials for Grades K-12," by K.E.K. Ross, 4/16/90, (PB91-251984, A05, MF-A05). This report has been replaced by NCEER-92-0018.

NCEER-90-0004 "Catalog of Strong Motion Stations in Eastern North America," by R.W. Busby, 4/3/90, (PB90-251984, A05, MF-A01).

NCEER-90-0005 "NCEER Strong-Motion Data Base: A User Manual for the GeoBase Release (Version 1.0 for the Sun3)," by P. Friberg and K. Jacob, 3/31/90 (PB90-258062, A04, MF-A01).

NCEER-90-0006 "Seismic Hazard Along a Crude Oil Pipeline in the Event of an 1811-1812 Type New Madrid Earthquake," by H.H.M. Hwang and C-H.S. Chen, 4/16/90, (PB90-258054, A04, MF-A01).

NCEER-90-0007 "Site-Specific Response Spectra for Memphis Sheahan Pumping Station," by H.H.M. Hwang and C.S. Lee, 5/15/90, (PB91-108811, A05, MF-A01).

NCEER-90-0008 "Pilot Study on Seismic Vulnerability of Crude Oil Transmission Systems," by T. Ariman, R. Dobry, M. Grigoriu, F. Kozin, M. O'Rourke, T. O'Rourke and M. Shinozuka, 5/25/90, (PB91-108837, A06, MF-A01).

NCEER-90-0009 "A Program to Generate Site Dependent Time Histories: EQGEN," by G.W. Ellis, M. Srinivasan and A.S. Cakmak, 1/30/90, (PB91-108829, A04, MF-A01).

NCEER-90-0010 "Active Isolation for Seismic Protection of Operating Rooms," by M.E. Talbott, Supervised by M. Shinozuka, 6/8/9, (PB91-110205, A05, MF-A01).

NCEER-90-0011 "Program LINEARID for Identification of Linear Structural Dynamic Systems," by C-B. Yun and M. Shinozuka, 6/25/90, (PB91-110312, A08, MF-A01).

NCEER-90-0012 "Two-Dimensional Two-Phase Elasto-Plastic Seismic Response of Earth Dams," by A.N. Yiagos, Supervised by J.H. Prevost, 6/20/90, (PB91-110197, A13, MF-A02).

NCEER-90-0013 "Secondary Systems in Base-Isolated Structures: Experimental Investigation, Stochastic Response and Stochastic Sensitivity," by G.D. Manolis, G. Juhn, M.C. Constantinou and A.M. Reinhorn, 7/1/90, (PB91-110320, A08, MF-A01).

NCEER-90-0014 "Seismic Behavior of Lightly-Reinforced Concrete Column and Beam-Column Joint Details," by S.P. Pessiki, C.H. Conley, P. Gergely and R.N. White, 8/22/90, (PB91-108795, A11, MF-A02).

NCEER-90-0015 "Two Hybrid Control Systems for Building Structures Under Strong Earthquakes," by J.N. Yang and A. Danielians, 6/29/90, (PB91-125393, A04, MF-A01).

NCEER-90-0016 "Instantaneous Optimal Control with Acceleration and Velocity Feedback," by J.N. Yang and Z. Li, 6/29/90, (PB91-125401, A03, MF-A01).

NCEER-90-0017 "Reconnaissance Report on the Northern Iran Earthquake of June 21, 1990," by M. Mehrain, 10/4/90, (PB91-125377, A03, MF-A01).

NCEER-90-0018 "Evaluation of Liquefaction Potential in Memphis and Shelby County," by T.S. Chang, P.S. Tang, C.S. Lee and H. Hwang, 8/10/90, (PB91-125427, A09, MF-A01).

NCEER-90-0019 "Experimental and Analytical Study of a Combined Sliding Disc Bearing and Helical Steel Spring Isolation System," by M.C. Constantinou, A.S. Mokha and A.M. Reinhorn, 10/4/90, (PB91-125385, A06, MF-A01). This report is available only through NTIS (see address given above).

NCEER-90-0020 "Experimental Study and Analytical Prediction of Earthquake Response of a Sliding Isolation System with a Spherical Surface," by A.S. Mokha, M.C. Constantinou and A.M. Reinhorn, 10/11/90, (PB91-125419, A05, MF-A01).

NCEER-90-0021 "Dynamic Interaction Factors for Floating Pile Groups," by G. Gazetas, K. Fan, A. Kaynia and E. Kausel, 9/10/90, (PB91-170381, A05, MF-A01).

NCEER-90-0022 "Evaluation of Seismic Damage Indices for Reinforced Concrete Structures," by S. Rodriguez-Gomez and A.S. Cakmak, 9/30/90, PB91-171322, A06, MF-A01).

NCEER-90-0023 "Study of Site Response at a Selected Memphis Site," by H. Desai, S. Ahmad, E.S. Gazetas and M.R. Oh, 10/11/90, (PB91-196857, A03, MF-A01).

NCEER-90-0024 "A User's Guide to Strongmo: Version 1.0 of NCEER's Strong-Motion Data Access Tool for PCs and Terminals," by P.A. Friberg and C.A.T. Susch, 11/15/90, (PB91-171272, A03, MF-A01).

NCEER-90-0025 "A Three-Dimensional Analytical Study of Spatial Variability of Seismic Ground Motions," by L-L. Hong and A.H.-S. Ang, 10/30/90, (PB91-170399, A09, MF-A01).

NCEER-90-0026 "MUMOID User's Guide - A Program for the Identification of Modal Parameters," by S. Rodriguez-Gomez and E. DiPasquale, 9/30/90, (PB91-171298, A04, MF-A01).

NCEER-90-0027 "SARCF-II User's Guide - Seismic Analysis of Reinforced Concrete Frames," by S. Rodriguez-Gomez, Y.S. Chung and C. Meyer, 9/30/90, (PB91-171280, A05, MF-A01).

NCEER-90-0028 "Viscous Dampers: Testing, Modeling and Application in Vibration and Seismic Isolation," by N. Makris and M.C. Constantinou, 12/20/90 (PB91-190561, A06, MF-A01).

NCEER-90-0029 "Soil Effects on Earthquake Ground Motions in the Memphis Area," by H. Hwang, C.S. Lee, K.W. Ng and T.S. Chang, 8/2/90, (PB91-190751, A05, MF-A01).

NCEER-91-0001 "Proceedings from the Third Japan-U.S. Workshop on Earthquake Resistant Design of Lifeline Facilities and Countermeasures for Soil Liquefaction, December 17-19, 1990," edited by T.D. O'Rourke and M. Hamada, 2/1/91, (PB91-179259, A99, MF-A04).

NCEER-91-0002 "Physical Space Solutions of Non-Proportionally Damped Systems," by M. Tong, Z. Liang and G.C. Lee, 1/15/91, (PB91-179242, A04, MF-A01).

NCEER-91-0003 "Seismic Response of Single Piles and Pile Groups," by K. Fan and G. Gazetas, 1/10/91, (PB92-174994, A04, MF-A01).

NCEER-91-0004 "Damping of Structures: Part 1 - Theory of Complex Damping," by Z. Liang and G. Lee, 10/10/91, (PB92-197235, A12, MF-A03).

NCEER-91-0005 "3D-BASIS - Nonlinear Dynamic Analysis of Three Dimensional Base Isolated Structures: Part II," by S. Nagarajaiah, A.M. Reinhorn and M.C. Constantinou, 2/28/91, (PB91-190553, A07, MF-A01). This report has been replaced by NCEER-93-0011.

NCEER-91-0006 "A Multidimensional Hysteretic Model for Plasticity Deforming Metals in Energy Absorbing Devices," by E.J. Graesser and F.A. Cozzarelli, 4/9/91, (PB92-108364, A04, MF-A01).

NCEER-91-0007 "A Framework for Customizable Knowledge-Based Expert Systems with an Application to a KBES for Evaluating the Seismic Resistance of Existing Buildings," by E.G. Ibarra-Anaya and S.J. Fenves, 4/9/91, (PB91-210930, A08, MF-A01).

NCEER-91-0008 "Nonlinear Analysis of Steel Frames with Semi-Rigid Connections Using the Capacity Spectrum Method," by G.G. Deierlein, S-H. Hsieh, Y-J. Shen and J.F. Abel, 7/2/91, (PB92-113828, A05, MF-A01).

NCEER-91-0009 "Earthquake Education Materials for Grades K-12," by K.E.K. Ross, 4/30/91, (PB91-212142, A06, MF-A01). This report has been replaced by NCEER-92-0018.

NCEER-91-0010 "Phase Wave Velocities and Displacement Phase Differences in a Harmonically Oscillating Pile," by N. Makris and G. Gazetas, 7/8/91, (PB92-108356, A04, MF-A01).

NCEER-91-0011 "Dynamic Characteristics of a Full-Size Five-Story Steel Structure and a 2/5 Scale Model," by K.C. Chang, G.C. Yao, G.C. Lee, D.S. Hao and Y.C. Yeh," 7/2/91, (PB93-116648, A06, MF-A02).

NCEER-91-0012 "Seismic Response of a 2/5 Scale Steel Structure with Added Viscoelastic Dampers," by K.C. Chang, T.T. Soong, S-T. Oh and M.L. Lai, 5/17/91, (PB92-110816, A05, MF-A01).

NCEER-91-0013 "Earthquake Response of Retaining Walls; Full-Scale Testing and Computational Modeling," by S. Alampalli and A-W.M. Elgamal, 6/20/91, to be published.

NCEER-91-0014 "3D-BASIS-M: Nonlinear Dynamic Analysis of Multiple Building Base Isolated Structures," by P.C. Tsopelas, S. Nagarajaiah, M.C. Constantinou and A.M. Reinhorn, 5/28/91, (PB92-113885, A09, MF-A02).

NCEER-91-0015 "Evaluation of SEAOC Design Requirements for Sliding Isolated Structures," by D. Theodossiou and M.C. Constantinou, 6/10/91, (PB92-114602, A11, MF-A03).

NCEER-91-0016 "Closed-Loop Modal Testing of a 27-Story Reinforced Concrete Flat Plate-Core Building," by H.R. Somaprasad, T. Toksoy, H. Yoshiyuki and A.E. Aktan, 7/15/91, (PB92-129980, A07, MF-A02).

NCEER-91-0017 "Shake Table Test of a 1/6 Scale Two-Story Lightly Reinforced Concrete Building," by A.G. El-Attar, R.N. White and P. Gergely, 2/28/91, (PB92-222447, A06, MF-A02).

NCEER-91-0018 "Shake Table Test of a 1/8 Scale Three-Story Lightly Reinforced Concrete Building," by A.G. El-Attar, R.N. White and P. Gergely, 2/28/91, (PB93-116630, A08, MF-A02).

NCEER-91-0019 "Transfer Functions for Rigid Rectangular Foundations," by A.S. Veletsos, A.M. Prasad and W.H. Wu, 7/31/91, to be published.

NCEER-91-0020 "Hybrid Control of Seismic-Excited Nonlinear and Inelastic Structural Systems," by J.N. Yang, Z. Li and A. Danielians, 8/1/91, (PB92-143171, A06, MF-A02).

NCEER-91-0021 "The NCEER-91 Earthquake Catalog: Improved Intensity-Based Magnitudes and Recurrence Relations for U.S. Earthquakes East of New Madrid," by L. Seeber and J.G. Armbruster, 8/28/91, (PB92-176742, A06, MF-A02).

NCEER-91-0022 "Proceedings from the Implementation of Earthquake Planning and Education in Schools: The Need for Change - The Roles of the Changemakers," by K.E.K. Ross and F. Winslow, 7/23/91, (PB92-129998, A12, MF-A03).

NCEER-91-0023 "A Study of Reliability-Based Criteria for Seismic Design of Reinforced Concrete Frame Buildings," by H.H.M. Hwang and H-M. Hsu, 8/10/91, (PB92-140235, A09, MF-A02).

NCEER-91-0024 "Experimental Verification of a Number of Structural System Identification Algorithms," by R.G. Ghanem, H. Gavin and M. Shinozuka, 9/18/91, (PB92-176577, A18, MF-A04).

NCEER-91-0025 "Probabilistic Evaluation of Liquefaction Potential," by H.H.M. Hwang and C.S. Lee," 11/25/91, (PB92-143429, A05, MF-A01).

NCEER-91-0026 "Instantaneous Optimal Control for Linear, Nonlinear and Hysteretic Structures - Stable Controllers," by J.N. Yang and Z. Li, 11/15/91, (PB92-163807, A04, MF-A01).

NCEER-91-0027 "Experimental and Theoretical Study of a Sliding Isolation System for Bridges," by M.C. Constantinou, A. Kartoum, A.M. Reinhorn and P. Bradford, 11/15/91, (PB92-176973, A10, MF-A03).

NCEER-92-0001 "Case Studies of Liquefaction and Lifeline Performance During Past Earthquakes, Volume 1: Japanese Case Studies," Edited by M. Hamada and T. O'Rourke, 2/17/92, (PB92-197243, A18, MF-A04).

NCEER-92-0002 "Case Studies of Liquefaction and Lifeline Performance During Past Earthquakes, Volume 2: United States Case Studies," Edited by T. O'Rourke and M. Hamada, 2/17/92, (PB92-197250, A20, MF-A04).

NCEER-92-0003 "Issues in Earthquake Education," Edited by K. Ross, 2/3/92, (PB92-222389, A07, MF-A02).

NCEER-92-0004 "Proceedings from the First U.S. - Japan Workshop on Earthquake Protective Systems for Bridges," Edited by I.G. Buckle, 2/4/92, (PB94-142239, A99, MF-A06).

NCEER-92-0005 "Seismic Ground Motion from a Haskell-Type Source in a Multiple-Layered Half-Space," A.P. Theoharis, G. Deodatis and M. Shinozuka, 1/2/92, to be published.

NCEER-92-0006 "Proceedings from the Site Effects Workshop," Edited by R. Whitman, 2/29/92, (PB92-197201, A04, MF-A01).

NCEER-92-0007 "Engineering Evaluation of Permanent Ground Deformations Due to Seismically-Induced Liquefaction," by M.H. Baziar, R. Dobry and A-W.M. Elgamal, 3/24/92, (PB92-222421, A13, MF-A03).

NCEER-92-0008 "A Procedure for the Seismic Evaluation of Buildings in the Central and Eastern United States," by C.D. Poland and J.O. Malley, 4/2/92, (PB92-222439, A20, MF-A04).

NCEER-92-0009 "Experimental and Analytical Study of a Hybrid Isolation System Using Friction Controllable Sliding Bearings," by M.Q. Feng, S. Fujii and M. Shinozuka, 5/15/92, (PB93-150282, A06, MF-A02).

NCEER-92-0010 "Seismic Resistance of Slab-Column Connections in Existing Non-Ductile Flat-Plate Buildings," by A.J. Durrani and Y. Du, 5/18/92, (PB93-116812, A06, MF-A02).

NCEER-92-0011 "The Hysteretic and Dynamic Behavior of Brick Masonry Walls Upgraded by Ferrocement Coatings Under Cyclic Loading and Strong Simulated Ground Motion," by H. Lee and S.P. Prawel, 5/11/92, to be published.

NCEER-92-0012 "Study of Wire Rope Systems for Seismic Protection of Equipment in Buildings," by G.F. Demetriades, M.C. Constantinou and A.M. Reinhorn, 5/20/92, (PB93-116655, A08, MF-A02).

NCEER-92-0013 "Shape Memory Structural Dampers: Material Properties, Design and Seismic Testing," by P.R. Witting and F.A. Cozzarelli, 5/26/92, (PB93-116663, A05, MF-A01).

NCEER-92-0014 "Longitudinal Permanent Ground Deformation Effects on Buried Continuous Pipelines," by M.J. O'Rourke, and C. Nordberg, 6/15/92, (PB93-116671, A08, MF-A02).

NCEER-92-0015 "A Simulation Method for Stationary Gaussian Random Functions Based on the Sampling Theorem," by M. Grigoriu and S. Balopoulou, 6/11/92, (PB93-127496, A05, MF-A01).

NCEER-92-0016 "Gravity-Load-Designed Reinforced Concrete Buildings: Seismic Evaluation of Existing Construction and Detailing Strategies for Improved Seismic Resistance," by G.W. Hoffmann, S.K. Kunnath, A.M. Reinhorn and J.B. Mander, 7/15/92, (PB94-142007, A08, MF-A02).

NCEER-92-0017 "Observations on Water System and Pipeline Performance in the Limón Area of Costa Rica Due to the April 22, 1991 Earthquake," by M. O'Rourke and D. Ballantyne, 6/30/92, (PB93-126811, A06, MF-A02).

NCEER-92-0018 "Fourth Edition of Earthquake Education Materials for Grades K-12," Edited by K.E.K. Ross, 8/10/92, (PB93-114023, A07, MF-A02).

NCEER-92-0019 "Proceedings from the Fourth Japan-U.S. Workshop on Earthquake Resistant Design of Lifeline Facilities and Countermeasures for Soil Liquefaction," Edited by M. Hamada and T.D. O'Rourke, 8/12/92, (PB93-163939, A99, MF-E11).

NCEER-92-0020 "Active Bracing System: A Full Scale Implementation of Active Control," by A.M. Reinhorn, T.T. Soong, R.C. Lin, M.A. Riley, Y.P. Wang, S. Aizawa and M. Higashino, 8/14/92, (PB93-127512, A06, MF-A02).

NCEER-92-0021 "Empirical Analysis of Horizontal Ground Displacement Generated by Liquefaction-Induced Lateral Spreads," by S.F. Bartlett and T.L. Youd, 8/17/92, (PB93-188241, A06, MF-A02).

NCEER-92-0022 "IDARC Version 3.0: Inelastic Damage Analysis of Reinforced Concrete Structures," by S.K. Kunnath, A.M. Reinhorn and R.F. Lobo, 8/31/92, (PB93-227502, A07, MF-A02).

NCEER-92-0023 "A Semi-Empirical Analysis of Strong-Motion Peaks in Terms of Seismic Source, Propagation Path and Local Site Conditions, by M. Kamiyama, M.J. O'Rourke and R. Flores-Berrones, 9/9/92, (PB93-150266, A08, MF-A02).

NCEER-92-0024 "Seismic Behavior of Reinforced Concrete Frame Structures with Nonductile Details, Part I: Summary of Experimental Findings of Full Scale Beam-Column Joint Tests," by A. Beres, R.N. White and P. Gergely, 9/30/92, (PB93-227783, A05, MF-A01).

NCEER-92-0025 "Experimental Results of Repaired and Retrofitted Beam-Column Joint Tests in Lightly Reinforced Concrete Frame Buildings," by A. Beres, S. El-Borgi, R.N. White and P. Gergely, 10/29/92, (PB93-227791, A05, MF-A01).

NCEER-92-0026 "A Generalization of Optimal Control Theory: Linear and Nonlinear Structures," by J.N. Yang, Z. Li and S. Vongchavalitkul, 11/2/92, (PB93-188621, A05, MF-A01).

NCEER-92-0027 "Seismic Resistance of Reinforced Concrete Frame Structures Designed Only for Gravity Loads: Part I - Design and Properties of a One-Third Scale Model Structure," by J.M. Bracci, A.M. Reinhorn and J.B. Mander, 12/1/92, (PB94-104502, A08, MF-A02).

NCEER-92-0028 "Seismic Resistance of Reinforced Concrete Frame Structures Designed Only for Gravity Loads: Part II - Experimental Performance of Subassemblages," by L.E. Aycardi, J.B. Mander and A.M. Reinhorn, 12/1/92, (PB94-104510, A08, MF-A02).

NCEER-92-0029 "Seismic Resistance of Reinforced Concrete Frame Structures Designed Only for Gravity Loads: Part III - Experimental Performance and Analytical Study of a Structural Model," by J.M. Bracci, A.M. Reinhorn and J.B. Mander, 12/1/92, (PB93-227528, A09, MF-A01).

NCEER-92-0030 "Evaluation of Seismic Retrofit of Reinforced Concrete Frame Structures: Part I - Experimental Performance of Retrofitted Subassemblages," by D. Choudhuri, J.B. Mander and A.M. Reinhorn, 12/8/92, (PB93-198307, A07, MF-A02).

NCEER-92-0031 "Evaluation of Seismic Retrofit of Reinforced Concrete Frame Structures: Part II - Experimental Performance and Analytical Study of a Retrofitted Structural Model," by J.M. Bracci, A.M. Reinhorn and J.B. Mander, 12/8/92, (PB93-198315, A09, MF-A03).

NCEER-92-0032 "Experimental and Analytical Investigation of Seismic Response of Structures with Supplemental Fluid Viscous Dampers," by M.C. Constantinou and M.D. Symans, 12/21/92, (PB93-191435, A10, MF-A03). This report is available only through NTIS (see address given above).

NCEER-92-0033 "Reconnaissance Report on the Cairo, Egypt Earthquake of October 12, 1992," by M. Khater, 12/23/92, (PB93-188621, A03, MF-A01).

NCEER-92-0034 "Low-Level Dynamic Characteristics of Four Tall Flat-Plate Buildings in New York City," by H. Gavin, S. Yuan, J. Grossman, E. Pekelis and K. Jacob, 12/28/92, (PB93-188217, A07, MF-A02).

NCEER-93-0001 "An Experimental Study on the Seismic Performance of Brick-Infilled Steel Frames With and Without Retrofit," by J.B. Mander, B. Nair, K. Wojtkowski and J. Ma, 1/29/93, (PB93-227510, A07, MF-A02).

NCEER-93-0002 "Social Accounting for Disaster Preparedness and Recovery Planning," by S. Cole, E. Pantoja and V. Razak, 2/22/93, (PB94-142114, A12, MF-A03).

NCEER-93-0003 "Assessment of 1991 NEHRP Provisions for Nonstructural Components and Recommended Revisions," by T.T. Soong, G. Chen, Z. Wu, R-H. Zhang and M. Grigoriu, 3/1/93, (PB93-188639, A06, MF-A02).

NCEER-93-0004 "Evaluation of Static and Response Spectrum Analysis Procedures of SEAOC/UBC for Seismic Isolated Structures," by C.W. Winters and M.C. Constantinou, 3/23/93, (PB93-198299, A10, MF-A03).

NCEER-93-0005 "Earthquakes in the Northeast - Are We Ignoring the Hazard? A Workshop on Earthquake Science and Safety for Educators," edited by K.E.K. Ross, 4/2/93, (PB94-103066, A09, MF-A02).

NCEER-93-0006 "Inelastic Response of Reinforced Concrete Structures with Viscoelastic Braces," by R.F. Lobo, J.M. Bracci, K.L. Shen, A.M. Reinhorn and T.T. Soong, 4/5/93, (PB93-227486, A05, MF-A02).

NCEER-93-0007 "Seismic Testing of Installation Methods for Computers and Data Processing Equipment," by K. Kosar, T.T. Soong, K.L. Shen, J.A. HoLung and Y.K. Lin, 4/12/93, (PB93-198299, A07, MF-A02).

NCEER-93-0008 "Retrofit of Reinforced Concrete Frames Using Added Dampers," by A. Reinhorn, M. Constantinou and C. Li, to be published.

NCEER-93-0009 "Seismic Behavior and Design Guidelines for Steel Frame Structures with Added Viscoelastic Dampers," by K.C. Chang, M.L. Lai, T.T. Soong, D.S. Hao and Y.C. Yeh, 5/1/93, (PB94-141959, A07, MF-A02).

NCEER-93-0010 "Seismic Performance of Shear-Critical Reinforced Concrete Bridge Piers," by J.B. Mander, S.M. Waheed, M.T.A. Chaudhary and S.S. Chen, 5/12/93, (PB93-227494, A08, MF-A02).

NCEER-93-0011 "3D-BASIS-TABS: Computer Program for Nonlinear Dynamic Analysis of Three Dimensional Base Isolated Structures," by S. Nagarajaiah, C. Li, A.M. Reinhorn and M.C. Constantinou, 8/2/93, (PB94-141819, A09, MF-A02).

NCEER-93-0012 "Effects of Hydrocarbon Spills from an Oil Pipeline Break on Ground Water," by O.J. Helweg and H.H.M. Hwang, 8/3/93, (PB94-141942, A06, MF-A02).

NCEER-93-0013 "Simplified Procedures for Seismic Design of Nonstructural Components and Assessment of Current Code Provisions," by M.P. Singh, L.E. Suarez, E.E. Matheu and G.O. Maldonado, 8/4/93, (PB94-141827, A09, MF-A02).

NCEER-93-0014 "An Energy Approach to Seismic Analysis and Design of Secondary Systems," by G. Chen and T.T. Soong, 8/6/93, (PB94-142767, A11, MF-A03).

NCEER-93-0015 "Proceedings from School Sites: Becoming Prepared for Earthquakes - Commemorating the Third Anniversary of the Loma Prieta Earthquake," Edited by F.E. Winslow and K.E.K. Ross, 8/16/93, (PB94-154275, A16, MF-A02).

NCEER-93-0016 "Reconnaissance Report of Damage to Historic Monuments in Cairo, Egypt Following the October 12, 1992 Dahshur Earthquake," by D. Sykora, D. Look, G. Croci, E. Karaesmen and E. Karaesmen, 8/19/93, (PB94-142221, A08, MF-A02).

NCEER-93-0017 "The Island of Guam Earthquake of August 8, 1993," by S.W. Swan and S.K. Harris, 9/30/93, (PB94-141843, A04, MF-A01).

NCEER-93-0018 "Engineering Aspects of the October 12, 1992 Egyptian Earthquake," by A.W. Elgamal, M. Amer, K. Adalier and A. Abul-Fadl, 10/7/93, (PB94-141983, A05, MF-A01).

NCEER-93-0019 "Development of an Earthquake Motion Simulator and its Application in Dynamic Centrifuge Testing," by I. Krstelj, Supervised by J.H. Prevost, 10/23/93, (PB94-181773, A-10, MF-A03).

NCEER-93-0020 "NCEER-Taisei Corporation Research Program on Sliding Seismic Isolation Systems for Bridges: Experimental and Analytical Study of a Friction Pendulum System (FPS)," by M.C. Constantinou, P. Tsopelas, Y-S. Kim and S. Okamoto, 11/1/93, (PB94-142775, A08, MF-A02).

NCEER-93-0021 "Finite Element Modeling of Elastomeric Seismic Isolation Bearings," by L.J. Billings, Supervised by R. Shepherd, 11/8/93, to be published.

NCEER-93-0022 "Seismic Vulnerability of Equipment in Critical Facilities: Life-Safety and Operational Consequences," by K. Porter, G.S. Johnson, M.M. Zadeh, C. Scawthorn and S. Eder, 11/24/93, (PB94-181765, A16, MF-A03).

NCEER-93-0023 "Hokkaido Nansei-oki, Japan Earthquake of July 12, 1993, by P.I. Yanev and C.R. Scawthorn, 12/23/93, (PB94-181500, A07, MF-A01).

NCEER-94-0001 "An Evaluation of Seismic Serviceability of Water Supply Networks with Application to the San Francisco Auxiliary Water Supply System," by I. Markov, Supervised by M. Grigoriu and T. O'Rourke, 1/21/94, (PB94-204013, A07, MF-A02).

NCEER-94-0002 "NCEER-Taisei Corporation Research Program on Sliding Seismic Isolation Systems for Bridges: Experimental and Analytical Study of Systems Consisting of Sliding Bearings, Rubber Restoring Force Devices and Fluid Dampers," Volumes I and II, by P. Tsopelas, S. Okamoto, M.C. Constantinou, D. Ozaki and S. Fujii, 2/4/94, (PB94-181740, A09, MF-A02 and PB94-181757, A12, MF-A03).

NCEER-94-0003 "A Markov Model for Local and Global Damage Indices in Seismic Analysis," by S. Rahman and M. Grigoriu, 2/18/94, (PB94-206000, A12, MF-A03).

NCEER-94-0004 "Proceedings from the NCEER Workshop on Seismic Response of Masonry Infills," edited by D.P. Abrams, 3/1/94, (PB94-180783, A07, MF-A02).

NCEER-94-0005 "The Northridge, California Earthquake of January 17, 1994: General Reconnaissance Report," edited by J.D. Goltz, 3/11/94, (PB94-193943, A10, MF-A03).

NCEER-94-0006 "Seismic Energy Based Fatigue Damage Analysis of Bridge Columns: Part I - Evaluation of Seismic Capacity," by G.A. Chang and J.B. Mander, 3/14/94, (PB94-219185, A11, MF-A03).

NCEER-94-0007 "Seismic Isolation of Multi-Story Frame Structures Using Spherical Sliding Isolation Systems," by T.M. Al-Hussaini, V.A. Zayas and M.C. Constantinou, 3/17/94, (PB94-193745, A09, MF-A02).

NCEER-94-0008 "The Northridge, California Earthquake of January 17, 1994: Performance of Highway Bridges," edited by I.G. Buckle, 3/24/94, (PB94-193851, A06, MF-A02).

NCEER-94-0009 "Proceedings of the Third U.S.-Japan Workshop on Earthquake Protective Systems for Bridges," edited by I.G. Buckle and I. Friedland, 3/31/94, (PB94-195815, A99, MF-A06).

NCEER-94-0010 "3D-BASIS-ME: Computer Program for Nonlinear Dynamic Analysis of Seismically Isolated Single and Multiple Structures and Liquid Storage Tanks," by P.C. Tsopelas, M.C. Constantinou and A.M. Reinhorn, 4/12/94, (PB94-204922, A09, MF-A02).

NCEER-94-0011 "The Northridge, California Earthquake of January 17, 1994: Performance of Gas Transmission Pipelines," by T.D. O'Rourke and M.C. Palmer, 5/16/94, (PB94-204989, A05, MF-A01).

NCEER-94-0012 "Feasibility Study of Replacement Procedures and Earthquake Performance Related to Gas Transmission Pipelines," by T.D. O'Rourke and M.C. Palmer, 5/25/94, (PB94-206638, A09, MF-A02).

NCEER-94-0013 "Seismic Energy Based Fatigue Damage Analysis of Bridge Columns: Part II - Evaluation of Seismic Demand," by G.A. Chang and J.B. Mander, 6/1/94, (PB95-18106, A08, MF-A02).

NCEER-94-0014 "NCEER-Taisei Corporation Research Program on Sliding Seismic Isolation Systems for Bridges: Experimental and Analytical Study of a System Consisting of Sliding Bearings and Fluid Restoring Force/Damping Devices," by P. Tsopelas and M.C. Constantinou, 6/13/94, (PB94-219144, A10, MF-A03).

NCEER-94-0015 "Generation of Hazard-Consistent Fragility Curves for Seismic Loss Estimation Studies," by H. Hwang and J-R. Huo, 6/14/94, (PB95-181996, A09, MF-A02).

NCEER-94-0016 "Seismic Study of Building Frames with Added Energy-Absorbing Devices," by W.S. Pong, C.S. Tsai and G.C. Lee, 6/20/94, (PB94-219136, A10, A03).

NCEER-94-0017 "Sliding Mode Control for Seismic-Excited Linear and Nonlinear Civil Engineering Structures," by J. Yang, J. Wu, A. Agrawal and Z. Li, 6/21/94, (PB95-138483, A06, MF-A02).

NCEER-94-0018 "3D-BASIS-TABS Version 2.0: Computer Program for Nonlinear Dynamic Analysis of Three Dimensional Base Isolated Structures," by A.M. Reinhorn, S. Nagarajaiah, M.C. Constantinou, P. Tsopelas and R. Li, 6/22/94, (PB95-182176, A08, MF-A02).

NCEER-94-0019 "Proceedings of the International Workshop on Civil Infrastructure Systems: Application of Intelligent Systems and Advanced Materials on Bridge Systems," Edited by G.C. Lee and K.C. Chang, 7/18/94, (PB95-252474, A20, MF-A04).

NCEER-94-0020 "Study of Seismic Isolation Systems for Computer Floors," by V. Lambrou and M.C. Constantinou, 7/19/94, (PB95-138533, A10, MF-A03).

NCEER-94-0021 "Proceedings of the U.S.-Italian Workshop on Guidelines for Seismic Evaluation and Rehabilitation of Unreinforced Masonry Buildings," Edited by D.P. Abrams and G.M. Calvi, 7/20/94, (PB95-138749, A13, MF-A03).

NCEER-94-0022 "NCEER-Taisei Corporation Research Program on Sliding Seismic Isolation Systems for Bridges: Experimental and Analytical Study of a System Consisting of Lubricated PTFE Sliding Bearings and Mild Steel Dampers," by P. Tsopelas and M.C. Constantinou, 7/22/94, (PB95-182184, A08, MF-A02).

NCEER-94-0023 “Development of Reliability-Based Design Criteria for Buildings Under Seismic Load,” by Y.K. Wen, H. Hwang and M. Shinozuka, 8/1/94, (PB95-211934, A08, MF-A02).

NCEER-94-0024 “Experimental Verification of Acceleration Feedback Control Strategies for an Active Tendon System,” by S.J. Dyke, B.F. Spencer, Jr., P. Quast, M.K. Sain, D.C. Kaspari, Jr. and T.T. Soong, 8/29/94, (PB95-212320, A05, MF-A01).

NCEER-94-0025 “Seismic Retrofitting Manual for Highway Bridges,” Edited by I.G. Buckle and I.F. Friedland, published by the Federal Highway Administration (PB95-212676, A15, MF-A03).

NCEER-94-0026 “Proceedings from the Fifth U.S.-Japan Workshop on Earthquake Resistant Design of Lifeline Facilities and Countermeasures Against Soil Liquefaction,” Edited by T.D. O’Rourke and M. Hamada, 11/7/94, (PB95-220802, A99, MF-E08).

NCEER-95-0001 "Experimental and Analytical Investigation of Seismic Retrofit of Structures with Supplemental Damping: Part 1 - Fluid Viscous Damping Devices," by A.M. Reinhorn, C. Li and M.C. Constantinou, 1/3/95, (PB95-266599, A09, MF-A02).

NCEER-95-0002 "Experimental and Analytical Study of Low-Cycle Fatigue Behavior of Semi-Rigid Top-And-Seat Angle Connections," by G. Pekcan, J.B. Mander and S.S. Chen, 1/5/95, (PB95-220042, A07, MF-A02).

NCEER-95-0003 "NCEER-ATC Joint Study on Fragility of Buildings," by T. Anagnos, C. Rojahn and A.S. Kiremidjian, 1/20/95, (PB95-220026, A06, MF-A02).

NCEER-95-0004 "Nonlinear Control Algorithms for Peak Response Reduction," by Z. Wu, T.T. Soong, V. Gattulli and R.C. Lin, 2/16/95, (PB95-220349, A05, MF-A01).

NCEER-95-0005 "Pipeline Replacement Feasibility Study: A Methodology for Minimizing Seismic and Corrosion Risks to Underground Natural Gas Pipelines," by R.T. Eguchi, H.A. Seligson and D.G. Honegger, 3/2/95, (PB95-252326, A06, MF-A02).

NCEER-95-0006 "Evaluation of Seismic Performance of an 11-Story Frame Building During the 1994 Northridge Earthquake," by F. Naeim, R. DiSulio, K. Benuska, A. Reinhorn and C. Li, to be published.

NCEER-95-0007 "Prioritization of Bridges for Seismic Retrofitting," by N. Basöz and A.S. Kiremidjian, 4/24/95, (PB95-252300, A08, MF-A02).

NCEER-95-0008 "Method for Developing Motion Damage Relationships for Reinforced Concrete Frames," by A. Singhal and A.S. Kiremidjian, 5/11/95, (PB95-266607, A06, MF-A02).

NCEER-95-0009 "Experimental and Analytical Investigation of Seismic Retrofit of Structures with Supplemental Damping: Part II - Friction Devices," by C. Li and A.M. Reinhorn, 7/6/95, (PB96-128087, A11, MF-A03).

NCEER-95-0010 "Experimental Performance and Analytical Study of a Non-Ductile Reinforced Concrete Frame Structure Retrofitted with Elastomeric Spring Dampers," by G. Pekcan, J.B. Mander and S.S. Chen, 7/14/95, (PB96-137161, A08, MF-A02).

NCEER-95-0011 "Development and Experimental Study of Semi-Active Fluid Damping Devices for Seismic Protection of Structures," by M.D. Symans and M.C. Constantinou, 8/3/95, (PB96-136940, A23, MF-A04).

NCEER-95-0012 "Real-Time Structural Parameter Modification (RSPM): Development of Innervated Structures," by Z. Liang, M. Tong and G.C. Lee, 4/11/95, (PB96-137153, A06, MF-A01).

NCEER-95-0013 "Experimental and Analytical Investigation of Seismic Retrofit of Structures with Supplemental Damping: Part III - Viscous Damping Walls," by A.M. Reinhorn and C. Li, 10/1/95, (PB96-176409, A11, MF-A03).

NCEER-95-0014 "Seismic Fragility Analysis of Equipment and Structures in a Memphis Electric Substation," by J-R. Huo and H.H.M. Hwang, 8/10/95, (PB96-128087, A09, MF-A02).

NCEER-95-0015 "The Hanshin-Awaji Earthquake of January 17, 1995: Performance of Lifelines," Edited by M. Shinozuka, 11/3/95, (PB96-176383, A15, MF-A03).

NCEER-95-0016 "Highway Culvert Performance During Earthquakes," by T.L. Youd and C.J. Beckman, available as NCEER-96-0015.

NCEER-95-0017 "The Hanshin-Awaji Earthquake of January 17, 1995: Performance of Highway Bridges," Edited by I.G. Buckle, 12/1/95, to be published.

NCEER-95-0018 "Modeling of Masonry Infill Panels for Structural Analysis," by A.M. Reinhorn, A. Madan, R.E. Valles, Y. Reichmann and J.B. Mander, 12/8/95, (PB97-110886, MF-A01, A06).

NCEER-95-0019 "Optimal Polynomial Control for Linear and Nonlinear Structures," by A.K. Agrawal and J.N. Yang, 12/11/95, (PB96-168737, A07, MF-A02).

NCEER-95-0020 "Retrofit of Non-Ductile Reinforced Concrete Frames Using Friction Dampers," by R.S. Rao, P. Gergely and R.N. White, 12/22/95, (PB97-133508, A10, MF-A02).

NCEER-95-0021 "Parametric Results for Seismic Response of Pile-Supported Bridge Bents," by G. Mylonakis, A. Nikolaou and G. Gazetas, 12/22/95, (PB97-100242, A12, MF-A03).

NCEER-95-0022 "Kinematic Bending Moments in Seismically Stressed Piles," by A. Nikolaou, G. Mylonakis and G. Gazetas, 12/23/95, (PB97-113914, MF-A03, A13).

NCEER-96-0001 "Dynamic Response of Unreinforced Masonry Buildings with Flexible Diaphragms," by A.C. Costley and D.P. Abrams," 10/10/96, (PB97-133573, MF-A03, A15).

NCEER-96-0002 "State of the Art Review: Foundations and Retaining Structures," by I. Po Lam, to be published.

NCEER-96-0003 "Ductility of Rectangular Reinforced Concrete Bridge Columns with Moderate Confinement," by N. Wehbe, M. Saiidi, D. Sanders and B. Douglas, 11/7/96, (PB97-133557, A06, MF-A02).

NCEER-96-0004 "Proceedings of the Long-Span Bridge Seismic Research Workshop," edited by I.G. Buckle and I.M. Friedland, to be published.

NCEER-96-0005 "Establish Representative Pier Types for Comprehensive Study: Eastern United States," by J. Kulicki and Z. Prucz, 5/28/96, (PB98-119217, A07, MF-A02).

NCEER-96-0006 "Establish Representative Pier Types for Comprehensive Study: Western United States," by R. Imbsen, R.A. Schamber and T.A. Osterkamp, 5/28/96, (PB98-118607, A07, MF-A02).

NCEER-96-0007 "Nonlinear Control Techniques for Dynamical Systems with Uncertain Parameters," by R.G. Ghanem and M.I. Bujakov, 5/27/96, (PB97-100259, A17, MF-A03).

NCEER-96-0008 "Seismic Evaluation of a 30-Year Old Non-Ductile Highway Bridge Pier and Its Retrofit," by J.B. Mander, B. Mahmoodzadegan, S. Bhadra and S.S. Chen, 5/31/96, (PB97-110902, MF-A03, A10).

NCEER-96-0009 "Seismic Performance of a Model Reinforced Concrete Bridge Pier Before and After Retrofit," by J.B. Mander, J.H. Kim and C.A. Ligozio, 5/31/96, (PB97-110910, MF-A02, A10).

NCEER-96-0010 "IDARC2D Version 4.0: A Computer Program for the Inelastic Damage Analysis of Buildings," by R.E. Valles, A.M. Reinhorn, S.K. Kunnath, C. Li and A. Madan, 6/3/96, (PB97-100234, A17, MF-A03).

NCEER-96-0011 "Estimation of the Economic Impact of Multiple Lifeline Disruption: Memphis Light, Gas and Water Division Case Study," by S.E. Chang, H.A. Seligson and R.T. Eguchi, 8/16/96, (PB97-133490, A11, MF-A03).

NCEER-96-0012 "Proceedings from the Sixth Japan-U.S. Workshop on Earthquake Resistant Design of Lifeline Facilities and Countermeasures Against Soil Liquefaction, Edited by M. Hamada and T. O'Rourke, 9/11/96, (PB97-133581, A99, MF-A06).

NCEER-96-0013 "Chemical Hazards, Mitigation and Preparedness in Areas of High Seismic Risk: A Methodology for Estimating the Risk of Post-Earthquake Hazardous Materials Release," by H.A. Seligson, R.T. Eguchi, K.J. Tierney and K. Richmond, 11/7/96, (PB97-133565, MF-A02, A08).

NCEER-96-0014 "Response of Steel Bridge Bearings to Reversed Cyclic Loading," by J.B. Mander, D-K. Kim, S.S. Chen and G.J. Premus, 11/13/96, (PB97-140735, A12, MF-A03).

NCEER-96-0015 "Highway Culvert Performance During Past Earthquakes," by T.L. Youd and C.J. Beckman, 11/25/96, (PB97-133532, A06, MF-A01).

NCEER-97-0001 "Evaluation, Prevention and Mitigation of Pounding Effects in Building Structures," by R.E. Valles and A.M. Reinhorn, 2/20/97, (PB97-159552, A14, MF-A03).

NCEER-97-0002 "Seismic Design Criteria for Bridges and Other Highway Structures," by C. Rojahn, R. Mayes, D.G. Anderson, J. Clark, J.H. Hom, R.V. Nutt and M.J. O'Rourke, 4/30/97, (PB97-194658, A06, MF-A03).

NCEER-97-0003 “Proceedings of the U.S.-Italian Workshop on Seismic Evaluation and Retrofit,” Edited by D.P. Abrams and G.M. Calvi, 3/19/97, (PB97-194666, A13, MF-A03).

NCEER-97-0004 "Investigation of Seismic Response of Buildings with Linear and Nonlinear Fluid Viscous Dampers," by A.A. Seleemah and M.C. Constantinou, 5/21/97, (PB98-109002, A15, MF-A03).

NCEER-97-0005 "Proceedings of the Workshop on Earthquake Engineering Frontiers in Transportation Facilities," edited by G.C. Lee and I.M. Friedland, 8/29/97, (PB98-128911, A25, MR-A04).

NCEER-97-0006 "Cumulative Seismic Damage of Reinforced Concrete Bridge Piers," by S.K. Kunnath, A. El-Bahy, A. Taylor and W. Stone, 9/2/97, (PB98-108814, A11, MF-A03).

NCEER-97-0007 "Structural Details to Accommodate Seismic Movements of Highway Bridges and Retaining Walls," by R.A. Imbsen, R.A. Schamber, E. Thorkildsen, A. Kartoum, B.T. Martin, T.N. Rosser and J.M. Kulicki, 9/3/97, (PB98-108996, A09, MF-A02).

NCEER-97-0008 "A Method for Earthquake Motion-Damage Relationships with Application to Reinforced Concrete Frames," by A. Singhal and A.S. Kiremidjian, 9/10/97, (PB98-108988, A13, MF-A03).

NCEER-97-0009 "Seismic Analysis and Design of Bridge Abutments Considering Sliding and Rotation," by K. Fishman and R. Richards, Jr., 9/15/97, (PB98-108897, A06, MF-A02).

NCEER-97-0010 "Proceedings of the FHWA/NCEER Workshop on the National Representation of Seismic Ground Motion for New and Existing Highway Facilities," edited by I.M. Friedland, M.S. Power and R.L. Mayes, 9/22/97, (PB98-128903, A21, MF-A04).

NCEER-97-0011 "Seismic Analysis for Design or Retrofit of Gravity Bridge Abutments," by K.L. Fishman, R. Richards, Jr. and R.C. Divito, 10/2/97, (PB98-128937, A08, MF-A02).

NCEER-97-0012 "Evaluation of Simplified Methods of Analysis for Yielding Structures," by P. Tsopelas, M.C. Constantinou, C.A. Kircher and A.S. Whittaker, 10/31/97, (PB98-128929, A10, MF-A03).

NCEER-97-0013 "Seismic Design of Bridge Columns Based on Control and Repairability of Damage," by C-T. Cheng and J.B. Mander, 12/8/97, (PB98-144249, A11, MF-A03).

NCEER-97-0014 "Seismic Resistance of Bridge Piers Based on Damage Avoidance Design," by J.B. Mander and C-T. Cheng, 12/10/97, (PB98-144223, A09, MF-A02).

NCEER-97-0015 “Seismic Response of Nominally Symmetric Systems with Strength Uncertainty,” by S. Balopoulou and M. Grigoriu, 12/23/97, (PB98-153422, A11, MF-A03).

NCEER-97-0016 “Evaluation of Seismic Retrofit Methods for Reinforced Concrete Bridge Columns,” by T.J. Wipf, F.W. Klaiber and F.M. Russo, 12/28/97, (PB98-144215, A12, MF-A03).

NCEER-97-0017 “Seismic Fragility of Existing Conventional Reinforced Concrete Highway Bridges,” by C.L. Mullen and A.S. Cakmak, 12/30/97, (PB98-153406, A08, MF-A02).

NCEER-97-0018 “Loss Asssessment of Memphis Buildings,” edited by D.P. Abrams and M. Shinozuka, 12/31/97, (PB98-144231, A13, MF-A03).

NCEER-97-0019 “Seismic Evaluation of Frames with Infill Walls Using Quasi-static Experiments,” by K.M. Mosalam, R.N. White and P. Gergely, 12/31/97, (PB98-153455, A07, MF-A02).

NCEER-97-0020 “Seismic Evaluation of Frames with Infill Walls Using Pseudo-dynamic Experiments,” by K.M. Mosalam, R.N. White and P. Gergely, 12/31/97, (PB98-153430, A07, MF-A02).

NCEER-97-0021 “Computational Strategies for Frames with Infill Walls: Discrete and Smeared Crack Analyses and Seismic Fragility,” by K.M. Mosalam, R.N. White and P. Gergely, 12/31/97, (PB98-153414, A10, MF-A02).

NCEER-97-0022 "Proceedings of the NCEER Workshop on Evaluation of Liquefaction Resistance of Soils," edited by T.L. Youd and I.M. Idriss, 12/31/97, (PB98-155617, A15, MF-A03).

MCEER-98-0001 "Extraction of Nonlinear Hysteretic Properties of Seismically Isolated Bridges from Quick-Release Field Tests," by Q. Chen, B.M. Douglas, E.M. Maragakis and I.G. Buckle, 5/26/98, (PB99-118838, A06, MF-A01).

MCEER-98-0002 "Methodologies for Evaluating the Importance of Highway Bridges," by A. Thomas, S. Eshenaur and J. Kulicki, 5/29/98, (PB99-118846, A10, MF-A02).

MCEER-98-0003 "Capacity Design of Bridge Piers and the Analysis of Overstrength," by J.B. Mander, A. Dutta and P. Goel, 6/1/98, (PB99-118853, A09, MF-A02).

MCEER-98-0004 "Evaluation of Bridge Damage Data from the Loma Prieta and Northridge, California Earthquakes," by N. Basoz and A. Kiremidjian, 6/2/98, (PB99-118861, A15, MF-A03).

MCEER-98-0005 "Screening Guide for Rapid Assessment of Liquefaction Hazard at Highway Bridge Sites," by T. L. Youd, 6/16/98, (PB99-118879, A06, not available on microfiche).

MCEER-98-0006 "Structural Steel and Steel/Concrete Interface Details for Bridges," by P. Ritchie, N. Kauhl and J. Kulicki, 7/13/98, (PB99-118945, A06, MF-A01).

MCEER-98-0007 "Capacity Design and Fatigue Analysis of Confined Concrete Columns," by A. Dutta and J.B. Mander, 7/14/98, (PB99-118960, A14, MF-A03).

MCEER-98-0008 "Proceedings of the Workshop on Performance Criteria for Telecommunication Services Under Earthquake Conditions," edited by A.J. Schiff, 7/15/98, (PB99-118952, A08, MF-A02).

MCEER-98-0009 "Fatigue Analysis of Unconfined Concrete Columns," by J.B. Mander, A. Dutta and J.H. Kim, 9/12/98, (PB99-123655, A10, MF-A02).

MCEER-98-0010 "Centrifuge Modeling of Cyclic Lateral Response of Pile-Cap Systems and Seat-Type Abutments in Dry Sands," by A.D. Gadre and R. Dobry, 10/2/98, (PB99-123606, A13, MF-A03).

MCEER-98-0011 "IDARC-BRIDGE: A Computational Platform for Seismic Damage Assessment of Bridge Structures," by A.M. Reinhorn, V. Simeonov, G. Mylonakis and Y. Reichman, 10/2/98, (PB99-162919, A15, MF-A03).

MCEER-98-0012 "Experimental Investigation of the Dynamic Response of Two Bridges Before and After Retrofitting with Elastomeric Bearings," by D.A. Wendichansky, S.S. Chen and J.B. Mander, 10/2/98, (PB99-162927, A15, MF-A03).

MCEER-98-0013 "Design Procedures for Hinge Restrainers and Hinge Sear Width for Multiple-Frame Bridges," by R. Des Roches and G.L. Fenves, 11/3/98, (PB99-140477, A13, MF-A03).

MCEER-98-0014 "Response Modification Factors for Seismically Isolated Bridges," by M.C. Constantinou and J.K. Quarshie, 11/3/98, (PB99-140485, A14, MF-A03).

MCEER-98-0015 "Proceedings of the U.S.-Italy Workshop on Seismic Protective Systems for Bridges," edited by I.M. Friedland and M.C. Constantinou, 11/3/98, (PB2000-101711, A22, MF-A04).

MCEER-98-0016 "Appropriate Seismic Reliability for Critical Equipment Systems: Recommendations Based on Regional Analysis of Financial and Life Loss," by K. Porter, C. Scawthorn, C. Taylor and N. Blais, 11/10/98, (PB99-157265, A08, MF-A02).

MCEER-98-0017 "Proceedings of the U.S. Japan Joint Seminar on Civil Infrastructure Systems Research," edited by M. Shinozuka and A. Rose, 11/12/98, (PB99-156713, A16, MF-A03).

MCEER-98-0018 "Modeling of Pile Footings and Drilled Shafts for Seismic Design," by I. PoLam, M. Kapuskar and D. Chaudhuri, 12/21/98, (PB99-157257, A09, MF-A02).

MCEER-99-0001 "Seismic Evaluation of a Masonry Infilled Reinforced Concrete Frame by Pseudodynamic Testing," by S.G. Buonopane and R.N. White, 2/16/99, (PB99-162851, A09, MF-A02).

MCEER-99-0002 "Response History Analysis of Structures with Seismic Isolation and Energy Dissipation Systems: Verification Examples for Program SAP2000," by J. Scheller and M.C. Constantinou, 2/22/99, (PB99-162869, A08, MF-A02).

MCEER-99-0003 "Experimental Study on the Seismic Design and Retrofit of Bridge Columns Including Axial Load Effects," by A. Dutta, T. Kokorina and J.B. Mander, 2/22/99, (PB99-162877, A09, MF-A02).

MCEER-99-0004 "Experimental Study of Bridge Elastomeric and Other Isolation and Energy Dissipation Systems with Emphasis on Uplift Prevention and High Velocity Near-source Seismic Excitation," by A. Kasalanati and M. C. Constantinou, 2/26/99, (PB99-162885, A12, MF-A03).

MCEER-99-0005 "Truss Modeling of Reinforced Concrete Shear-flexure Behavior," by J.H. Kim and J.B. Mander, 3/8/99, (PB99-163693, A12, MF-A03).

MCEER-99-0006 "Experimental Investigation and Computational Modeling of Seismic Response of a 1:4 Scale Model Steel Structure with a Load Balancing Supplemental Damping System," by G. Pekcan, J.B. Mander and S.S. Chen, 4/2/99, (PB99-162893, A11, MF-A03).

MCEER-99-0007 "Effect of Vertical Ground Motions on the Structural Response of Highway Bridges," by M.R. Button, C.J. Cronin and R.L. Mayes, 4/10/99, (PB2000-101411, A10, MF-A03).

MCEER-99-0008 "Seismic Reliability Assessment of Critical Facilities: A Handbook, Supporting Documentation, and Model Code Provisions," by G.S. Johnson, R.E. Sheppard, M.D. Quilici, S.J. Eder and C.R. Scawthorn, 4/12/99, (PB2000-101701, A18, MF-A04).

MCEER-99-0009 "Impact Assessment of Selected MCEER Highway Project Research on the Seismic Design of Highway Structures," by C. Rojahn, R. Mayes, D.G. Anderson, J.H. Clark, D'Appolonia Engineering, S. Gloyd and R.V. Nutt, 4/14/99, (PB99-162901, A10, MF-A02).

MCEER-99-0010 "Site Factors and Site Categories in Seismic Codes," by R. Dobry, R. Ramos and M.S. Power, 7/19/99, (PB2000-101705, A08, MF-A02).

MCEER-99-0011 "Restrainer Design Procedures for Multi-Span Simply-Supported Bridges," by M.J. Randall, M. Saiidi, E. Maragakis and T. Isakovic, 7/20/99, (PB2000-101702, A10, MF-A02).

MCEER-99-0012 "Property Modification Factors for Seismic Isolation Bearings," by M.C. Constantinou, P. Tsopelas, A. Kasalanati and E. Wolff, 7/20/99, (PB2000-103387, A11, MF-A03).

MCEER-99-0013 "Critical Seismic Issues for Existing Steel Bridges," by P. Ritchie, N. Kauhl and J. Kulicki, 7/20/99, (PB2000-101697, A09, MF-A02).

MCEER-99-0014 "Nonstructural Damage Database," by A. Kao, T.T. Soong and A. Vender, 7/24/99, (PB2000-101407, A06, MF-A01).

MCEER-99-0015 "Guide to Remedial Measures for Liquefaction Mitigation at Existing Highway Bridge Sites," by H.G. Cooke and J. K. Mitchell, 7/26/99, (PB2000-101703, A11, MF-A03).

MCEER-99-0016 "Proceedings of the MCEER Workshop on Ground Motion Methodologies for the Eastern United States," edited by N. Abrahamson and A. Becker, 8/11/99, (PB2000-103385, A07, MF-A02).

MCEER-99-0017 "Quindío, Colombia Earthquake of January 25, 1999: Reconnaissance Report," by A.P. Asfura and P.J. Flores, 10/4/99, (PB2000-106893, A06, MF-A01).

MCEER-99-0018 "Hysteretic Models for Cyclic Behavior of Deteriorating Inelastic Structures," by M.V. Sivaselvan and A.M. Reinhorn, 11/5/99, (PB2000-103386, A08, MF-A02).

MCEER-99-0019 "Proceedings of the 7th U.S.- Japan Workshop on Earthquake Resistant Design of Lifeline Facilities and Countermeasures Against Soil Liquefaction," edited by T.D. O'Rourke, J.P. Bardet and M. Hamada, 11/19/99, (PB2000-103354, A99, MF-A06).

MCEER-99-0020 "Development of Measurement Capability for Micro-Vibration Evaluations with Application to Chip Fabrication Facilities," by G.C. Lee, Z. Liang, J.W. Song, J.D. Shen and W.C. Liu, 12/1/99, (PB2000-105993, A08, MF-A02).

MCEER-99-0021 "Design and Retrofit Methodology for Building Structures with Supplemental Energy Dissipating Systems," by G. Pekcan, J.B. Mander and S.S. Chen, 12/31/99, (PB2000-105994, A11, MF-A03).

MCEER-00-0001 "The Marmara, Turkey Earthquake of August 17, 1999: Reconnaissance Report," edited by C. Scawthorn; with major contributions by M. Bruneau, R. Eguchi, T. Holzer, G. Johnson, J. Mander, J. Mitchell, W. Mitchell, A. Papageorgiou, C. Scaethorn, and G. Webb, 3/23/00, (PB2000-106200, A11, MF-A03).

MCEER-00-0002 "Proceedings of the MCEER Workshop for Seismic Hazard Mitigation of Health Care Facilities," edited by G.C. Lee, M. Ettouney, M. Grigoriu, J. Hauer and J. Nigg, 3/29/00, (PB2000-106892, A08, MF-A02).

MCEER-00-0003 "The Chi-Chi, Taiwan Earthquake of September 21, 1999: Reconnaissance Report," edited by G.C. Lee and C.H. Loh, with major contributions by G.C. Lee, M. Bruneau, I.G. Buckle, S.E. Chang, P.J. Flores, T.D. O'Rourke, M. Shinozuka, T.T. Soong, C-H. Loh, K-C. Chang, Z-J. Chen, J-S. Hwang, M-L. Lin, G-Y. Liu, K-C. Tsai, G.C. Yao and C-L. Yen, 4/30/00, (PB2001-100980, A10, MF-A02).

MCEER-00-0004 "Seismic Retrofit of End-Sway Frames of Steel Deck-Truss Bridges with a Supplemental Tendon System: Experimental and Analytical Investigation," by G. Pekcan, J.B. Mander and S.S. Chen, 7/1/00, (PB2001-100982, A10, MF-A02).

MCEER-00-0005 "Sliding Fragility of Unrestrained Equipment in Critical Facilities," by W.H. Chong and T.T. Soong, 7/5/00, (PB2001-100983, A08, MF-A02).

MCEER-00-0006 "Seismic Response of Reinforced Concrete Bridge Pier Walls in the Weak Direction," by N. Abo-Shadi, M. Saiidi and D. Sanders, 7/17/00, (PB2001-100981, A17, MF-A03).

MCEER-00-0007 "Low-Cycle Fatigue Behavior of Longitudinal Reinforcement in Reinforced Concrete Bridge Columns," by J. Brown and S.K. Kunnath, 7/23/00, (PB2001-104392, A08, MF-A02).

MCEER-00-0008 "Soil Structure Interaction of Bridges for Seismic Analysis," I. PoLam and H. Law, 9/25/00, (PB2001-105397, A08, MF-A02).

MCEER-00-0009 "Proceedings of the First MCEER Workshop on Mitigation of Earthquake Disaster by Advanced Technologies (MEDAT-1), edited by M. Shinozuka, D.J. Inman and T.D. O'Rourke, 11/10/00, (PB2001-105399, A14, MF-A03).

MCEER-00-0010 "Development and Evaluation of Simplified Procedures for Analysis and Design of Buildings with Passive Energy Dissipation Systems, Revision 01," by O.M. Ramirez, M.C. Constantinou, C.A. Kircher, A.S. Whittaker, M.W. Johnson, J.D. Gomez and C. Chrysostomou, 11/16/01, (PB2001-105523, A23, MF-A04).

MCEER-00-0011 "Dynamic Soil-Foundation-Structure Interaction Analyses of Large Caissons," by C-Y. Chang, C-M. Mok, Z-L. Wang, R. Settgast, F. Waggoner, M.A. Ketchum, H.M. Gonnermann and C-C. Chin, 12/30/00, (PB2001-104373, A07, MF-A02).

MCEER-00-0012 "Experimental Evaluation of Seismic Performance of Bridge Restrainers," by A.G. Vlassis, E.M. Maragakis and M. Saiid Saiidi, 12/30/00, (PB2001-104354, A09, MF-A02).

MCEER-00-0013 "Effect of Spatial Variation of Ground Motion on Highway Structures," by M. Shinozuka, V. Saxena and G. Deodatis, 12/31/00, (PB2001-108755, A13, MF-A03).

MCEER-00-0014 "A Risk-Based Methodology for Assessing the Seismic Performance of Highway Systems," by S.D. Werner, C.E. Taylor, J.E. Moore, II, J.S. Walton and S. Cho, 12/31/00, (PB2001-108756, A14, MF-A03).

MCEER-01-0001 "Experimental Investigation of P-Delta Effects to Collapse During Earthquakes," by D. Vian and M. Bruneau, 6/25/01, (PB2002-100534, A17, MF-A03).

MCEER-01-0002 "Proceedings of the Second MCEER Workshop on Mitigation of Earthquake Disaster by Advanced Technologies (MEDAT-2)," edited by M. Bruneau and D.J. Inman, 7/23/01, (PB2002-100434, A16, MF-A03).

MCEER-01-0003 "Sensitivity Analysis of Dynamic Systems Subjected to Seismic Loads," by C. Roth and M. Grigoriu, 9/18/01, (PB2003-100884, A12, MF-A03).

MCEER-01-0004 "Overcoming Obstacles to Implementing Earthquake Hazard Mitigation Policies: Stage 1 Report," by D.J. Alesch and W.J. Petak, 12/17/01, (PB2002-107949, A07, MF-A02).

MCEER-01-0005 "Updating Real-Time Earthquake Loss Estimates: Methods, Problems and Insights," by C.E. Taylor, S.E. Chang and R.T. Eguchi, 12/17/01, (PB2002-107948, A05, MF-A01).

MCEER-01-0006 "Experimental Investigation and Retrofit of Steel Pile Foundations and Pile Bents Under Cyclic Lateral Loadings," by A. Shama, J. Mander, B. Blabac and S. Chen, 12/31/01, (PB2002-107950, A13, MF-A03).

MCEER-02-0001 "Assessment of Performance of Bolu Viaduct in the 1999 Duzce Earthquake in Turkey" by P.C. Roussis, M.C. Constantinou, M. Erdik, E. Durukal and M. Dicleli, 5/8/02, (PB2003-100883, A08, MF-A02).

MCEER-02-0002 "Seismic Behavior of Rail Counterweight Systems of Elevators in Buildings," by M.P. Singh, Rildova and L.E. Suarez, 5/27/02. (PB2003-100882, A11, MF-A03).

MCEER-02-0003 "Development of Analysis and Design Procedures for Spread Footings," by G. Mylonakis, G. Gazetas, S. Nikolaou and A. Chauncey, 10/02/02, (PB2004-101636, A13, MF-A03, CD-A13).

MCEER-02-0004 "Bare-Earth Algorithms for Use with SAR and LIDAR Digital Elevation Models," by C.K. Huyck, R.T. Eguchi and B. Houshmand, 10/16/02, (PB2004-101637, A07, CD-A07).

MCEER-02-0005 "Review of Energy Dissipation of Compression Members in Concentrically Braced Frames," by K.Lee and M. Bruneau, 10/18/02, (PB2004-101638, A10, CD-A10).

MCEER-03-0001 "Experimental Investigation of Light-Gauge Steel Plate Shear Walls for the Seismic Retrofit of Buildings" by J. Berman and M. Bruneau, 5/2/03, (PB2004-101622, A10, MF-A03, CD-A10).

MCEER-03-0002 "Statistical Analysis of Fragility Curves," by M. Shinozuka, M.Q. Feng, H. Kim, T. Uzawa and T. Ueda, 6/16/03, (PB2004-101849, A09, CD-A09).

MCEER-03-0003 "Proceedings of the Eighth U.S.-Japan Workshop on Earthquake Resistant Design f Lifeline Facilities and Countermeasures Against Liquefaction," edited by M. Hamada, J.P. Bardet and T.D. O'Rourke, 6/30/03, (PB2004-104386, A99, CD-A99).

MCEER-03-0004 "Proceedings of the PRC-US Workshop on Seismic Analysis and Design of Special Bridges," edited by L.C. Fan and G.C. Lee, 7/15/03, (PB2004-104387, A14, CD-A14).

MCEER-03-0005 "Urban Disaster Recovery: A Framework and Simulation Model," by S.B. Miles and S.E. Chang, 7/25/03, (PB2004-104388, A07, CD-A07).

MCEER-03-0006 "Behavior of Underground Piping Joints Due to Static and Dynamic Loading," by R.D. Meis, M. Maragakis and R. Siddharthan, 11/17/03, (PB2005-102194, A13, MF-A03, CD-A00).

MCEER-04-0001 "Experimental Study of Seismic Isolation Systems with Emphasis on Secondary System Response and Verification of Accuracy of Dynamic Response History Analysis Methods," by E. Wolff and M. Constantinou, 1/16/04 (PB2005-102195, A99, MF-E08, CD-A00).

MCEER-04-0002 "Tension, Compression and Cyclic Testing of Engineered Cementitious Composite Materials," by K. Kesner and S.L. Billington, 3/1/04, (PB2005-102196, A08, CD-A08).

MCEER-04-0003 "Cyclic Testing of Braces Laterally Restrained by Steel Studs to Enhance Performance During Earthquakes," by O.C. Celik, J.W. Berman and M. Bruneau, 3/16/04, (PB2005-102197, A13, MF-A03, CD-A00).

MCEER-04-0004 "Methodologies for Post Earthquake Building Damage Detection Using SAR and Optical Remote Sensing: Application to the August 17, 1999 Marmara, Turkey Earthquake," by C.K. Huyck, B.J. Adams, S. Cho, R.T. Eguchi, B. Mansouri and B. Houshmand, 6/15/04, (PB2005-104888, A10, CD-A00).

MCEER-04-0005 "Nonlinear Structural Analysis Towards Collapse Simulation: A Dynamical Systems Approach," by M.V. Sivaselvan and A.M. Reinhorn, 6/16/04, (PB2005-104889, A11, MF-A03, CD-A00).

MCEER-04-0006 "Proceedings of the Second PRC-US Workshop on Seismic Analysis and Design of Special Bridges," edited by G.C. Lee and L.C. Fan, 6/25/04, (PB2005-104890, A16, CD-A00).

MCEER-04-0007 "Seismic Vulnerability Evaluation of Axially Loaded Steel Built-up Laced Members," by K. Lee and M. Bruneau, 6/30/04, (PB2005-104891, A16, CD-A00).

MCEER-04-0008 "Evaluation of Accuracy of Simplified Methods of Analysis and Design of Buildings with Damping Systems for Near-Fault and for Soft-Soil Seismic Motions," by E.A. Pavlou and M.C. Constantinou, 8/16/04, (PB2005-104892, A08, MF-A02, CD-A00).

MCEER-04-0009 "Assessment of Geotechnical Issues in Acute Care Facilities in California," by M. Lew, T.D. O'Rourke, R. Dobry and M. Koch, 9/15/04, (PB2005-104893, A08, CD-A00).

MCEER-04-0010 "Scissor-Jack-Damper Energy Dissipation System," by A.N. Sigaher-Boyle and M.C. Constantinou, 12/1/04 (PB2005-108221).

MCEER-04-0011 "Seismic Retrofit of Bridge Steel Truss Piers Using a Controlled Rocking Approach," by M. Pollino and M. Bruneau, 12/20/04 (PB2006-105795).

MCEER-05-0001 "Experimental and Analytical Studies of Structures Seismically Isolated with an Uplift-Restraint Isolation System," by P.C. Roussis and M.C. Constantinou, 1/10/05 (PB2005-108222).

MCEER-05-0002 "A Versatile Experimentation Model for Study of Structures Near Collapse Applied to Seismic Evaluation of Irregular Structures," by D. Kusumastuti, A.M. Reinhorn and A. Rutenberg, 3/31/05 (PB2006-101523).

MCEER-05-0003 "Proceedings of the Third PRC-US Workshop on Seismic Analysis and Design of Special Bridges," edited by L.C. Fan and G.C. Lee, 4/20/05, (PB2006-105796).

MCEER-05-0004 "Approaches for the Seismic Retrofit of Braced Steel Bridge Piers and Proof-of-Concept Testing of an Eccentrically Braced Frame with Tubular Link," by J.W. Berman and M. Bruneau, 4/21/05 (PB2006-101524).

MCEER-05-0005 "Simulation of Strong Ground Motions for Seismic Fragility Evaluation of Nonstructural Components in Hospitals," by A. Wanitkorkul and A. Filiatrault, 5/26/05 (PB2006-500027).

MCEER-05-0006 "Seismic Safety in California Hospitals: Assessing an Attempt to Accelerate the Replacement or Seismic Retrofit of Older Hospital Facilities," by D.J. Alesch, L.A. Arendt and W.J. Petak, 6/6/05 (PB2006-105794).

MCEER-05-0007 "Development of Seismic Strengthening and Retrofit Strategies for Critical Facilities Using Engineered Cementitious Composite Materials," by K. Kesner and S.L. Billington, 8/29/05 (PB2006-111701).

MCEER-05-0008 "Experimental and Analytical Studies of Base Isolation Systems for Seismic Protection of Power Transformers," by N. Murota, M.Q. Feng and G-Y. Liu, 9/30/05 (PB2006-111702).

MCEER-05-0009 "3D-BASIS-ME-MB: Computer Program for Nonlinear Dynamic Analysis of Seismically Isolated Structures," by P.C. Tsopelas, P.C. Roussis, M.C. Constantinou, R. Buchanan and A.M. Reinhorn, 10/3/05 (PB2006-111703).

MCEER-05-0010 "Steel Plate Shear Walls for Seismic Design and Retrofit of Building Structures," by D. Vian and M. Bruneau, 12/15/05 (PB2006-111704).

MCEER-05-0011 "The Performance-Based Design Paradigm," by M.J. Astrella and A. Whittaker, 12/15/05 (PB2006-111705).

MCEER-06-0001 "Seismic Fragility of Suspended Ceiling Systems," H. Badillo-Almaraz, A.S. Whittaker, A.M. Reinhorn and G.P. Cimellaro, 2/4/06 (PB2006-111706).

MCEER-06-0002 "Multi-Dimensional Fragility of Structures," by G.P. Cimellaro, A.M. Reinhorn and M. Bruneau, 3/1/06 (PB2007-106974, A09, MF-A02, CD A00).

MCEER-06-0003 "Built-Up Shear Links as Energy Dissipators for Seismic Protection of Bridges," by P. Dusicka, A.M. Itani and I.G. Buckle, 3/15/06 (PB2006-111708).

MCEER-06-0004 "Analytical Investigation of the Structural Fuse Concept," by R.E. Vargas and M. Bruneau, 3/16/06 (PB2006-111709).

MCEER-06-0005 "Experimental Investigation of the Structural Fuse Concept," by R.E. Vargas and M. Bruneau, 3/17/06 (PB2006-111710).

MCEER-06-0006 "Further Development of Tubular Eccentrically Braced Frame Links for the Seismic Retrofit of Braced Steel Truss Bridge Piers," by J.W. Berman and M. Bruneau, 3/27/06 (PB2007-105147).

MCEER-06-0007 "REDARS Validation Report," by S. Cho, C.K. Huyck, S. Ghosh and R.T. Eguchi, 8/8/06 (PB2007-106983).

MCEER-06-0008 "Review of Current NDE Technologies for Post-Earthquake Assessment of Retrofitted Bridge Columns," by J.W. Song, Z. Liang and G.C. Lee, 8/21/06 (PB2007-106984).

MCEER-06-0009 "Liquefaction Remediation in Silty Soils Using Dynamic Compaction and Stone Columns," by S. Thevanayagam, G.R. Martin, R. Nashed, T. Shenthan, T. Kanagalingam and N. Ecemis, 8/28/06 (PB2007-106985).

MCEER-06-0010 "Conceptual Design and Experimental Investigation of Polymer Matrix Composite Infill Panels for Seismic Retrofitting," by W. Jung, M. Chiewanichakorn and A.J. Aref, 9/21/06 (PB2007-106986).

MCEER-06-0011 "A Study of the Coupled Horizontal-Vertical Behavior of Elastomeric and Lead-Rubber Seismic Isolation Bearings," by G.P. Warn and A.S. Whittaker, 9/22/06 (PB2007-108679).

MCEER-06-0012 "Proceedings of the Fourth PRC-US Workshop on Seismic Analysis and Design of Special Bridges: Advancing Bridge Technologies in Research, Design, Construction and Preservation," Edited by L.C. Fan, G.C. Lee and L. Ziang, 10/12/06 (PB2007-109042).

MCEER-06-0013 "Cyclic Response and Low Cycle Fatigue Characteristics of Plate Steels," by P. Dusicka, A.M. Itani and I.G. Buckle, 11/1/06 06 (PB2007-106987).

MCEER-06-0014 "Proceedings of the Second US-Taiwan Bridge Engineering Workshop," edited by W.P. Yen, J. Shen, J-Y. Chen and M. Wang, 11/15/06 (PB2008-500041).

MCEER-06-0015 "User Manual and Technical Documentation for the REDARS^{TM} Import Wizard," by S. Cho, S. Ghosh, C.K. Huyck and S.D. Werner, 11/30/06 (PB2007-114766).

MCEER-06-0016 "Hazard Mitigation Strategy and Monitoring Technologies for Urban and Infrastructure Public Buildings: Proceedings of the China-US Workshops," edited by X.Y. Zhou, A.L. Zhang, G.C. Lee and M. Tong, 12/12/06 (PB2008-500018).

MCEER-07-0001 "Static and Kinetic Coefficients of Friction for Rigid Blocks," by C. Kafali, S. Fathali, M. Grigoriu and A.S. Whittaker, 3/20/07 (PB2007-114767).

MCEER-07-0002 "Hazard Mitigation Investment Decision Making: Organizational Response to Legislative Mandate," by L.A. Arendt, D.J. Alesch and W.J. Petak, 4/9/07 (PB2007-114768).

MCEER-07-0003 "Seismic Behavior of Bidirectional-Resistant Ductile End Diaphragms with Unbonded Braces in Straight or Skewed Steel Bridges," by O. Celik and M. Bruneau, 4/11/07 (PB2008-105141).

MCEER-07-0004 "Modeling Pile Behavior in Large Pile Groups Under Lateral Loading," by A.M. Dodds and G.R. Martin, 4/16/07(PB2008-105142).

MCEER-07-0005 "Experimental Investigation of Blast Performance of Seismically Resistant Concrete-Filled Steel Tube Bridge Piers," by S. Fujikura, M. Bruneau and D. Lopez-Garcia, 4/20/07 (PB2008-105143).

MCEER-07-0006 "Seismic Analysis of Conventional and Isolated Liquefied Natural Gas Tanks Using Mechanical Analogs," by I.P. Christovasilis and A.S. Whittaker, 5/1/07.

MCEER-07-0007 "Experimental Seismic Performance Evaluation of Isolation/Restraint Systems for Mechanical Equipment – Part 1: Heavy Equipment Study," by S. Fathali and A. Filiatrault, 6/6/07 (PB2008-105144).

MCEER-07-0008 "Seismic Vulnerability of Timber Bridges and Timber Substructures," by A.A. Sharma, J.B. Mander, I.M. Friedland and D.R. Allicock, 6/7/07 (PB2008-105145).

MCEER-07-0009 "Experimental and Analytical Study of the XY-Friction Pendulum (XY-FP) Bearing for Bridge Applications," by C.C. Marin-Artieda, A.S. Whittaker and M.C. Constantinou, 6/7/07 (PB2008-105191).

MCEER-07-0010 "Proceedings of the PRC-US Earthquake Engineering Forum for Young Researchers," Edited by G.C. Lee and X.Z. Qi, 6/8/07 (PB2008-500058).

MCEER-07-0011 "Design Recommendations for Perforated Steel Plate Shear Walls," by R. Purba and M. Bruneau, 6/18/07, (PB2008-105192).

MCEER-07-0012 "Performance of Seismic Isolation Hardware Under Service and Seismic Loading," by M.C. Constantinou, A.S. Whittaker, Y. Kalpakidis, D.M. Fenz and G.P. Warn, 8/27/07, (PB2008-105193).

MCEER-07-0013 "Experimental Evaluation of the Seismic Performance of Hospital Piping Subassemblies," by E.R. Goodwin, E. Maragakis and A.M. Itani, 9/4/07, (PB2008-105194).

MCEER-07-0014 "A Simulation Model of Urban Disaster Recovery and Resilience: Implementation for the 1994 Northridge Earthquake," by S. Miles and S.E. Chang, 9/7/07, (PB2008-106426).

MCEER-07-0015 "Statistical and Mechanistic Fragility Analysis of Concrete Bridges," by M. Shinozuka, S. Banerjee and S-H. Kim, 9/10/07, (PB2008-106427).

MCEER-07-0016 "Three-Dimensional Modeling of Inelastic Buckling in Frame Structures," by M. Schachter and AM. Reinhorn, 9/13/07, (PB2008-108125).

MCEER-07-0017 "Modeling of Seismic Wave Scattering on Pile Groups and Caissons," by I. Po Lam, H. Law and C.T. Yang, 9/17/07 (PB2008-108150).

MCEER-07-0018 "Bridge Foundations: Modeling Large Pile Groups and Caissons for Seismic Design," by I. Po Lam, H. Law and G.R. Martin (Coordinating Author), 12/1/07 (PB2008-111190).

MCEER-07-0019 "Principles and Performance of Roller Seismic Isolation Bearings for Highway Bridges," by G.C. Lee, Y.C. Ou, Z. Liang, T.C. Niu and J. Song, 12/10/07 (PB2009-110466).

MCEER-07-0020 "Centrifuge Modeling of Permeability and Pinning Reinforcement Effects on Pile Response to Lateral Spreading," by L.L Gonzalez-Lagos, T. Abdoun and R. Dobry, 12/10/07 (PB2008-111191).

MCEER-07-0021 "Damage to the Highway System from the Pisco, Perú Earthquake of August 15, 2007," by J.S. O'Connor, L. Mesa and M. Nykamp, 12/10/07, (PB2008-108126).

MCEER-07-0022 "Experimental Seismic Performance Evaluation of Isolation/Restraint Systems for Mechanical Equipment – Part 2: Light Equipment Study," by S. Fathali and A. Filiatrault, 12/13/07 (PB2008-111192).

MCEER-07-0023 "Fragility Considerations in Highway Bridge Design," by M. Shinozuka, S. Banerjee and S.H. Kim, 12/14/07 (PB2008-111193).

MCEER-07-0024 "Performance Estimates for Seismically Isolated Bridges," by G.P. Warn and A.S. Whittaker, 12/30/07 (PB2008-112230).

MCEER-08-0001 "Seismic Performance of Steel Girder Bridge Superstructures with Conventional Cross Frames," by L.P. Carden, A.M. Itani and I.G. Buckle, 1/7/08, (PB2008-112231).

MCEER-08-0002 "Seismic Performance of Steel Girder Bridge Superstructures with Ductile End Cross Frames with Seismic Isolators," by L.P. Carden, A.M. Itani and I.G. Buckle, 1/7/08 (PB2008-112232).

MCEER-08-0003 "Analytical and Experimental Investigation of a Controlled Rocking Approach for Seismic Protection of Bridge Steel Truss Piers," by M. Pollino and M. Bruneau, 1/21/08 (PB2008-112233).

MCEER-08-0004 "Linking Lifeline Infrastructure Performance and Community Disaster Resilience: Models and Multi-Stakeholder Processes," by S.E. Chang, C. Pasion, K. Tatebe and R. Ahmad, 3/3/08 (PB2008-112234).

MCEER-08-0005 "Modal Analysis of Generally Damped Linear Structures Subjected to Seismic Excitations," by J. Song, Y-L. Chu, Z. Liang and G.C. Lee, 3/4/08 (PB2009-102311).

MCEER-08-0006 "System Performance Under Multi-Hazard Environments," by C. Kafali and M. Grigoriu, 3/4/08 (PB2008-112235).

MCEER-08-0007 "Mechanical Behavior of Multi-Spherical Sliding Bearings," by D.M. Fenz and M.C. Constantinou, 3/6/08 (PB2008-112236).

MCEER-08-0008 "Post-Earthquake Restoration of the Los Angeles Water Supply System," by T.H.P. Tabucchi and R.A. Davidson, 3/7/08 (PB2008-112237).

MCEER-08-0009 "Fragility Analysis of Water Supply Systems," by A. Jacobson and M. Grigoriu, 3/10/08 (PB2009-105545).

MCEER-08-0010 "Experimental Investigation of Full-Scale Two-Story Steel Plate Shear Walls with Reduced Beam Section Connections," by B. Qu, M. Bruneau, C-H. Lin and K-C. Tsai, 3/17/08 (PB2009-106368).

MCEER-08-0011 "Seismic Evaluation and Rehabilitation of Critical Components of Electrical Power Systems," S. Ersoy, B. Feizi, A. Ashrafi and M. Ala Saadeghvaziri, 3/17/08 (PB2009-105546).

MCEER-08-0012 "Seismic Behavior and Design of Boundary Frame Members of Steel Plate Shear Walls," by B. Qu and M. Bruneau, 4/26/08 . (PB2009-106744).

MCEER-08-0013 "Development and Appraisal of a Numerical Cyclic Loading Protocol for Quantifying Building System Performance," by A. Filiatrault, A. Wanitkorkul and M. Constantinou, 4/27/08 (PB2009-107906).

MCEER-08-0014 "Structural and Nonstructural Earthquake Design: The Challenge of Integrating Specialty Areas in Designing Complex, Critical Facilities," by W.J. Petak and D.J. Alesch, 4/30/08 (PB2009-107907).

MCEER-08-0015 "Seismic Performance Evaluation of Water Systems," by Y. Wang and T.D. O'Rourke, 5/5/08 (PB2009-107908).

MCEER-08-0016 "Seismic Response Modeling of Water Supply Systems," by P. Shi and T.D. O'Rourke, 5/5/08 (PB2009-107910).

MCEER-08-0017 "Numerical and Experimental Studies of Self-Centering Post-Tensioned Steel Frames," by D. Wang and A. Filiatrault, 5/12/08 (PB2009-110479).

MCEER-08-0018 "Development, Implementation and Verification of Dynamic Analysis Models for Multi-Spherical Sliding Bearings," by D.M. Fenz and M.C. Constantinou, 8/15/08 (PB2009-107911).

MCEER-08-0019 "Performance Assessment of Conventional and Base Isolated Nuclear Power Plants for Earthquake Blast Loadings," by Y.N. Huang, A.S. Whittaker and N. Luco, 10/28/08 (PB2009-107912).

MCEER-08-0020 "Remote Sensing for Resilient Multi-Hazard Disaster Response – Volume I: Introduction to Damage Assessment Methodologies," by B.J. Adams and R.T. Eguchi, 11/17/08 (PB2010-102695).

MCEER-08-0021 "Remote Sensing for Resilient Multi-Hazard Disaster Response – Volume II: Counting the Number of Collapsed Buildings Using an Object-Oriented Analysis: Case Study of the 2003 Bam Earthquake," by L. Gusella, C.K. Huyck and B.J. Adams, 11/17/08 (PB2010-100925).

MCEER-08-0022 "Remote Sensing for Resilient Multi-Hazard Disaster Response – Volume III: Multi-Sensor Image Fusion Techniques for Robust Neighborhood-Scale Urban Damage Assessment," by B.J. Adams and A. McMillan, 11/17/08 (PB2010-100926).

MCEER-08-0023 "Remote Sensing for Resilient Multi-Hazard Disaster Response – Volume IV: A Study of Multi-Temporal and Multi-Resolution SAR Imagery for Post-Katrina Flood Monitoring in New Orleans," by A. McMillan, J.G. Morley, B.J. Adams and S. Chesworth, 11/17/08 (PB2010-100927).

MCEER-08-0024 "Remote Sensing for Resilient Multi-Hazard Disaster Response – Volume V: Integration of Remote Sensing Imagery and VIEWS^{TM} Field Data for Post-Hurricane Charley Building Damage Assessment," by J.A. Womble, K. Mehta and B.J. Adams, 11/17/08 (PB2009-115532).

MCEER-08-0025 "Building Inventory Compilation for Disaster Management: Application of Remote Sensing and Statistical Modeling," by P. Sarabandi, A.S. Kiremidjian, R.T. Eguchi and B. J. Adams, 11/20/08 (PB2009-110484).

MCEER-08-0026 "New Experimental Capabilities and Loading Protocols for Seismic Qualification and Fragility Assessment of Nonstructural Systems," by R. Retamales, G. Mosqueda, A. Filiatrault and A. Reinhorn, 11/24/08 (PB2009-110485).

MCEER-08-0027 "Effects of Heating and Load History on the Behavior of Lead-Rubber Bearings," by I.V. Kalpakidis and M.C. Constantinou, 12/1/08 (PB2009-115533).

MCEER-08-0028 "Experimental and Analytical Investigation of Blast Performance of Seismically Resistant Bridge Piers," by S.Fujikura and M. Bruneau, 12/8/08 (PB2009-115534).

MCEER-08-0029 "Evolutionary Methodology for Aseismic Decision Support," by Y. Hu and G. Dargush, 12/15/08.

MCEER-08-0030 "Development of a Steel Plate Shear Wall Bridge Pier System Conceived from a Multi-Hazard Perspective," by D. Keller and M. Bruneau, 12/19/08 (PB2010-102696).

MCEER-09-0001 "Modal Analysis of Arbitrarily Damped Three-Dimensional Linear Structures Subjected to Seismic Excitations," by Y.L. Chu, J. Song and G.C. Lee, 1/31/09 (PB2010-100922).

MCEER-09-0002 "Air-Blast Effects on Structural Shapes," by G. Ballantyne, A.S. Whittaker, A.J. Aref and G.F. Dargush, 2/2/09 (PB2010-102697).

MCEER-09-0003 "Water Supply Performance During Earthquakes and Extreme Events," by A.L. Bonneau and T.D. O'Rourke, 2/16/09 (PB2010-100923).

MCEER-09-0004 "Generalized Linear (Mixed) Models of Post-Earthquake Ignitions," by R.A. Davidson, 7/20/09 (PB2010-102698).

MCEER-09-0005 "Seismic Testing of a Full-Scale Two-Story Light-Frame Wood Building: NEESWood Benchmark Test," by I.P. Christovasilis, A. Filiatrault and A. Wanitkorkul, 7/22/09 (PB2012-102401).

MCEER-09-0006 "IDARC2D Version 7.0: A Program for the Inelastic Damage Analysis of Structures," by A.M. Reinhorn, H. Roh, M. Sivaselvan, S.K. Kunnath, R.E. Valles, A. Madan, C. Li, R. Lobo and Y.J. Park, 7/28/09 (PB2010-103199).

MCEER-09-0007 "Enhancements to Hospital Resiliency: Improving Emergency Planning for and Response to Hurricanes," by D.B. Hess and L.A. Arendt, 7/30/09 (PB2010-100924).

MCEER-09-0008 "Assessment of Base-Isolated Nuclear Structures for Design and Beyond-Design Basis Earthquake Shaking," by Y.N. Huang, A.S. Whittaker, R.P. Kennedy and R.L. Mayes, 8/20/09 (PB2010-102699).

MCEER-09-0009 "Quantification of Disaster Resilience of Health Care Facilities," by G.P. Cimellaro, C. Fumo, A.M Reinhorn and M. Bruneau, 9/14/09 (PB2010-105384).

MCEER-09-0010 "Performance-Based Assessment and Design of Squat Reinforced Concrete Shear Walls," by C.K. Gulec and A.S. Whittaker, 9/15/09 (PB2010-102700).

MCEER-09-0011 "Proceedings of the Fourth US-Taiwan Bridge Engineering Workshop," edited by W.P. Yen, J.J. Shen, T.M. Lee and R.B. Zheng, 10/27/09 (PB2010-500009).

MCEER-09-0012 "Proceedings of the Special International Workshop on Seismic Connection Details for Segmental Bridge Construction," edited by W. Phillip Yen and George C. Lee, 12/21/09 (PB2012-102402).

MCEER-10-0001 "Direct Displacement Procedure for Performance-Based Seismic Design of Multistory Woodframe Structures," by W. Pang and D. Rosowsky, 4/26/10 (PB2012-102403).

MCEER-10-0002 "Simplified Direct Displacement Design of Six-Story NEESWood Capstone Building and Pre-Test Seismic Performance Assessment," by W. Pang, D. Rosowsky, J. van de Lindt and S. Pei, 5/28/10 (PB2012-102404).

MCEER-10-0003 "Integration of Seismic Protection Systems in Performance-Based Seismic Design of Woodframed Structures," by J.K. Shinde and M.D. Symans, 6/18/10 (PB2012-102405).

MCEER-10-0004 "Modeling and Seismic Evaluation of Nonstructural Components: Testing Frame for Experimental Evaluation of Suspended Ceiling Systems," by A.M. Reinhorn, K.P. Ryu and G. Maddaloni, 6/30/10 (PB2012-102406).

MCEER-10-0005 "Analytical Development and Experimental Validation of a Structural-Fuse Bridge Pier Concept," by S. El-Bahey and M. Bruneau, 10/1/10 (PB2012-102407).

MCEER-10-0006 "A Framework for Defining and Measuring Resilience at the Community Scale: The PEOPLES Resilience Framework," by C.S. Renschler, A.E. Frazier, L.A. Arendt, G.P. Cimellaro, A.M. Reinhorn and M. Bruneau, 10/8/10 (PB2012-102408).

MCEER-10-0007 "Impact of Horizontal Boundary Elements Design on Seismic Behavior of Steel Plate Shear Walls," by R. Purba and M. Bruneau, 11/14/10 (PB2012-102409).

MCEER-10-0008 "Seismic Testing of a Full-Scale Mid-Rise Building: The NEESWood Capstone Test," by S. Pei, J.W. van de Lindt, S.E. Pryor, H. Shimizu, H. Isoda and D.R. Rammer, 12/1/10 (PB2012-102410).

MCEER-10-0009 "Modeling the Effects of Detonations of High Explosives to Inform Blast-Resistant Design," by P. Sherkar, A.S. Whittaker and A.J. Aref, 12/1/10 (PB2012-102411).

MCEER-10-0010 "L'Aquila Earthquake of April 6, 2009 in Italy: Rebuilding a Resilient City to Withstand Multiple Hazards," by G.P. Cimellaro, I.P. Christovasilis, A.M. Reinhorn, A. De Stefano and T. Kirova, 12/29/10.

MCEER-11-0001 "Numerical and Experimental Investigation of the Seismic Response of Light-Frame Wood Structures," by I.P. Christovasilis and A. Filiatrault, 8/8/11 (PB2012-102412).

MCEER-11-0002 "Seismic Design and Analysis of Precast Segmental Concrete Bridge Model," by M. Anagnostopoulou, A. Filiatrault and A. Aref, 9/15/11.

MCEER-11-0003 'Proceedings of the Workshop on Improving Earthquake Response of Substation Equipment," Edited by A.M. Reinhorn, 9/19/11 (PB2012-102413).

MCEER-11-0004 "LRFD-Based Analysis and Design Procedures for Bridge Bearings and Seismic Isolators," by M.C. Constantinou, I. Kalpakidis, A. Filiatrault and R.A. Ecker Lay, 9/26/11.

MCEER-11-0005 “Experimental Seismic Evaluation, Model Parameterization, and Effects of Cold-Formed Steel-Framed Gypsum Partition Walls on the Seismic Performance of an Essential Facility,” by R. Davies, R. Retamales, G. Mosqueda and A. Filiatrault, 10/12/11.

MCEER

EARTHQUAKE ENGINEERING TO EXTREME EVENTS

University at Buffalo, The State University of New York

Red Jacket Quadrangle ▪ Buffalo, New York 14261

Phone: (716) 645-3391 ▪ Fax: (716) 645-3399

E-mail: *mceer@buffalo.edu* ▪ WWW Site *http://mceer.buffalo.edu*

University at Buffalo *The State University of New York*

ISSN 1520-295X